A STUDY OF THE INTERACTIONS OF METAL CARBONYL PHOTOFRAGMENTS WITH BOTH MONOMERIC AND POLYMERIC LIGANDS

A Thesis presented for the degree of Doctor of Philosophy

at

by

Gerard Farrell BSc.

under the supervision of Dr. Conor Long

School of Chemical Sciences

May 1992

To
My Parents
and
Sinéad

WIZARD of ID

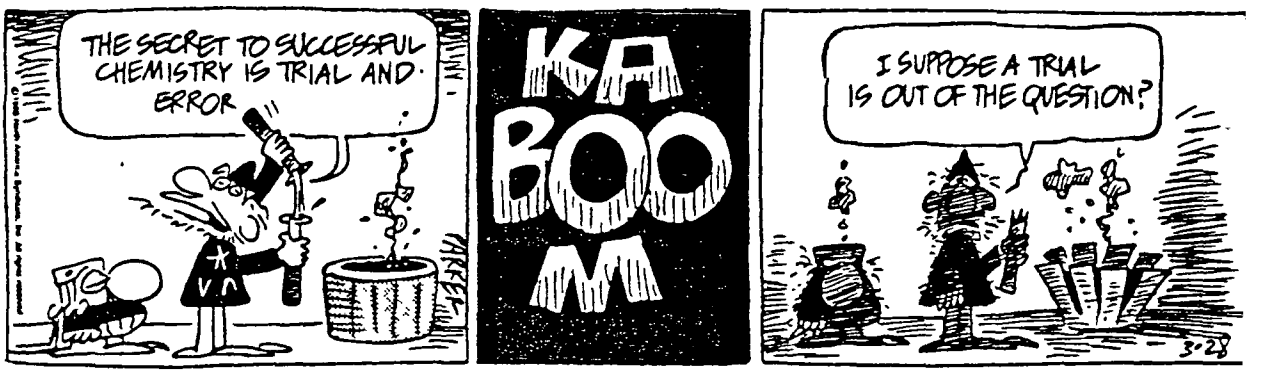
THE SECRET TO SUCCESSFUL CHEMISTRY IS TRIAL AND ERROR
KA BOO M
I SUPPOSE A TRIAL IS OUT OF THE QUESTION?

Acknowledgements

I would like to express my sincere thanks to Dr. Conor Long for his supervision and encouragement over the last three and "a bit" years. I thank my fellow postgrads., the academic, and technical staff for their help and friendship during my time at Dublin City University.

I especially thank my great friend and "socialising partner" Barry "The Football Brain" Crocock.

Also John "Redzer-Sky News" Curley, Alan "Happy" Clarke, and Conor "Friend of the People" Tonra. My thanks to the past and present members of the CLRG, namely Bernie, Graham, Irene, Celia, Maureen, Mick, and Mary, as well as Albert's boys who also live in AG07. I must also acknowledge football in the form of DCU FC, Dynamo Benzene, and Howard Wilkinson for many hours of enjoyment.

Most importantly I thank my parents for their unquestioning support over my extended educational career.

Finally I would like to thank my girlfnend Sinéad for putting up with my various and changing moods during the course of my research in particular while writing this thesis.

Declaration

I, the undersigned, declare that this thesis represents the sole work of the author carried out at Dublin City University under the supervision of Dr. Conor Long

Gerard Farrell

Table of Contents

Chapter 2

Photolysis of $MeCpMn(CO)_3$, $ArCr(CO)_3$, and $Cr(CO)_6$ in Low Temperature Polymer Films

Chapter 3

Flash Photolysis of $MeCpMn(CO)_3$, $ArCr(CO)_3$, and $Cr(CO)_6$ in Toluene

Abstract

The photochemistry of $MeCpMn(CO)_3$ dispersed in polymer films at low temperatures was investigated using infrared or UV/visible detection. The photolysis of the isoelectronic $ArCr(CO)_3$ complex in low temperature polymer films was then studied for comparison purposes and because the parent tricarbonyl bands were obscuring some of the bands arising from the photoproducts in the manganese system. As the higher energy infrared bands arising from the photoproducts in both tricarbonyl systems were masked the photochemistry of $Cr(CO)_6$ dispersed in polystyrene at low temperatures was examined.

The solution photochemistry of the $MeCpMn(CO)_3$ and $ArCr(CO)_3$ complexes in ambient temperature toluene was investigated by laser flash photolysis, 355 nm excitation, with UV/vis detection. The mechanism and kinetics of the reaction of the primary photoproducts with both monomeric and polymeric pyridine ligands was then examined. As different trends were observed for the manganese and chromium tricarbonyl systems, the interaction of the $Cr(CO)_5$(toluene) fragment with the various pyridine ligands was investigated.

A polymer-anchored chromium tricarbonyl complex was prepared and its photochemistry was studied by laser flash photolysis. The kinetics of the reaction of the polymer-bound primary photoproduct with pyridine ligands was then examined.

Chapter 1

Introduction

1 Introduction

Iron pentacarbonyl was synthesised in 1890 independently by L. Mond in England and M. Berthelot in France. Since then metal carbonyls have been a widely studied area in transition metal organometallic chemistry. Metal carbonyl derivatives of at least one type are known for each of the transition metals. Table 1.1 lists the elements known to form photoreactive metal carbonyl complexes [1].

The drain on the world's natural supplies of coal, oil, gas, and rubber was recognised earlier in this century and the search for alternative sources of these materials began in earnest. This impetus for new process technology came during a period of rapid development in the organic chemistry of the transition metals. Fischer, Wilkinson, Ziegler, and Natta developed catalytic systems that won them Nobel prizes in chemistry. Industry has built on their fundamental discoveries to create about two dozen major processes that are catalysed by soluble transition metal complexes. In most of these industrial processes the transition metal complexes are used to convert the simple molecules of methane, carbon dioxide, water, and hydrogen to industrially useful organic molecules or polymers. The most favourable characteristic of homogeneous catalysis that has led to its widespread adoption by industry is selectivity, the ability to produce pure products in high yield. This characteristic is especially important in the production of pure pharmaceuticals and polymer intermediates. The most impressive example of this selectivity is the hydrogenation of prochiral olefins to produce single optical isomers in more than 90% yield. This process is used commercially to produce L-dopa which is used in the treatment of Parkinson's disease [2]. In the synthesis of L-dopa a substituted cinamic acid is the prochiral olefin and a rhodium(I) complex bearing an optically active phosphine ligand is the catalyst.

Table 1.1: Photoreactive metal carbonyl complexes

Group V	Group VI	Group VII		GroupVIII	
$[V(CO)_6]^-$	$Cr(CO)_6$	$Mn_2(CO)_{10}$	$Fe(CO)_5$	$Co_4(CO)_{12}$	$Ni(CO)_4$
$[Nb(CO)_6]^-$	$Mo(CO)_6$	$Tc_2(CO)_{10}$	$Ru(CO)_5$	$Rh_4(CO)_{12}$	
$[Ta(CO)_6]^-$	$W(CO)_6$	$Re_2(CO)_{10}$	$Os(CO)_5$	$Ir_4(CO)_{12}$	

The application of homogeneous catalysts to industrial processes has led to extensive studies of the reaction mechanisms involved One of the first catalytic processes developed was the "oxo" process. In this process a cobalt carbonyl is used as the catalyst in the hydroformylation of alkenes (Reaction 1 1). About 500 million tonnes of aldehydes and aldehyde derivatives are produced annually using this method

$$CH_2{=}CH_2 \longrightarrow HCO{-}CH_2{-}CH_3 \qquad 1.1$$

One of the most important catalytic processes developed has been the synthesis gas reaction. Synthesis gas (CO / H_2 mixture) can be produced from coal and organic wastes, as well as from hydrocarbon feedstocks Hence chemistry based on synthesis gas is relatively independent of the source The synthesis gas-based chemistry is versatile in its applications and uses homogeneous catalysis to good advantage. The presence of water in the synthesis gas mixture can lead to the production of hydrogen *via* the water gas shift reaction (Reaction 1 2)

$$CO + H_2O \rightleftharpoons CO_2 + H_2 \qquad 1.2$$

An industrial method for the low pressure polymerisation of ethylene or propylene was developed by Zeigler and Natta using transition metal salts Wilkinson [3] developed a method for the reduction of olefins using reversible *cis*- dihydro catalysts (Scheme 1.1).

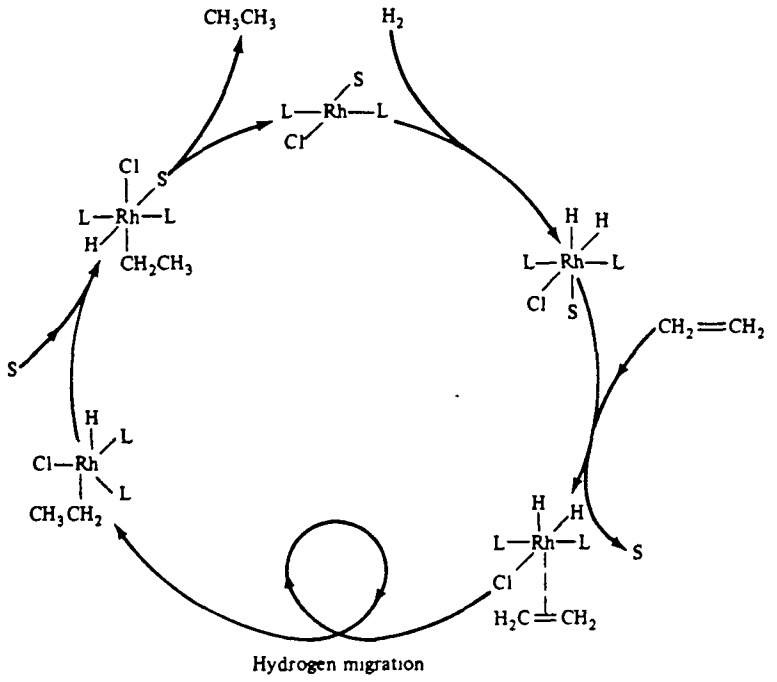

Scheme 1.1

These homogeneous catalysts have in some cases being "heterogenised" by anchoring them to polymer supports [4]. Haag and Whitehurst [5] were the first to introduce the idea of binding known homogeneous catalysts to solid phase supports. They investigated the catalytic use of salts of $Pt(NH_3)_4^{2+}$ with polymeric sulfonate counterions and later the catalytic applications of heterogeneous species obtained by the co-ordination of $RhCl_3$ to polymers containing pendant phosphine units. Since then there has been intensive research in this area [4] The catalyst functions mechanistically as if it were in solution, but physically it operates as a separate immobile phase which

eases catalyst recovery. In the binding of the metal complexes to the polymer supports, the desirable characteristics of homogeneous catalysts are maintained, such as catalyst recovery and high selectivity under mild reaction conditions The activity and selectivity of these catalysts may be controlled by attaching different ligands to the metal or varying the solvent. Enhanced activity has also been reported for polymer bound systems. Grubbs and Kroll [6], in their investigation of the reduction of olefins with a polymer supported rhodium catalyst, showed that the activity was greatly increased over a surface reduction reaction with $RhCl(PPh_3)_3$ and that the specificity for the polymer supported rhodium catalyst was much greater than for its unsupported analogue.

The applications of metal containing polymers are not just confined to organometallic catalysts. Areas of application currently under investigation [7] range from antifungal agents and insecticides to the biomedical field where they may be used as tumour detectors or as carriers for controlled-release drugs.

The mechanisms of many of these catalytic processes are still unclear, but in many instances the initial step appears to be the generation of a vacant co-ordination site at the metal centre Further reactions are then initiated at this vacant site. A site of coordinative unsaturation is perhaps the single most important property of a homogeneous catalyst [8]. However it is now widely recognised that, in many cases, the species produced in predominant concentration after metal-ligand bond fission are not co-ordinatively unsaturated but are specifically solvated $Cr(CO)_6$ has served as a model for studies of solvation in coordinatively unsaturated intermediates. It has been found that upon Cr–CO bond fission in $Cr(CO)_6$, the $Cr(CO)_5$ species produced reacts very rapidly with solvent to give the $Cr(CO)_5$(solvent) species in which the solvent molecule occupies a position in the inner coordination sphere of $Cr(CO)_5$ and forms a coordinate covalent bond with the metal atom [9]

The generation of a vacant coordination site by photolysis and the subsequent reaction of polymeric or monomeric ligands at these sites is the basis of this thesis

The reactivity of metal carbonyl complexes cannot be explained without understanding the nature of the metal carbonyl bond. The bonding between CO and a metal comprises a combination of both σ– and π-bonding interactions [10] The overlap of a filled carbon σ-orbital with an orbital of appropriate symmetry on the metal (Figure 1.1(a)) leads to a higher concentration of electron density on metals in their low oxidation states. The metal therefore reduces this charge density by off-loading electrons back to the ligand This is only possible if the ligand has suitable acceptor orbitals, such as those on the CO ligand (carbon monoxide is among the most important and extensively studied π-acceptor ligands). This results in a delocalisation of the d-π electrons from the metal into the π^* CO orbital which gives rise to π-back-bonding (Figure 1 1(b)). As the extent of back donation from the metal to the CO ligand increases, the metal to carbon bond becomes stronger and the carbon to oxygen bond becomes weaker Thus the multiple bonding can be exemplified by shorter M-C and longer C-O bonds as compared to M-C single bonds and C-O triple bonds respectively. As a result the carbonyl stretching frequencies in the infrared are shifted to lower values.

Figure 1.1: Schematic diagram of bonding between CO and a metal

(a)

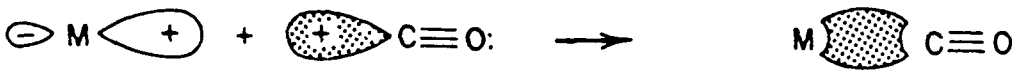

(b)

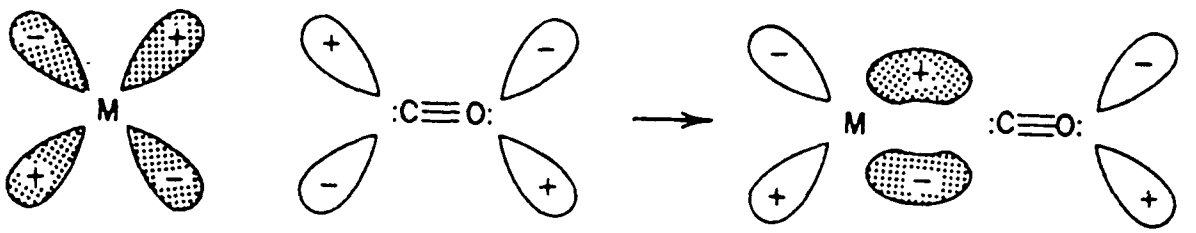

1.1 Photolysis of Metal Carbonyl Complexes

Since the use of light as a synthetic tool became important in the late 1950's, the photochemical reactions of metal carbonyl compounds have found wide application in a variety of syntheses. The first substantial review on the photochemistry of metal carbonyls appeared in 1969 [11] From then on research into the photochemistry of metal carbonyl compounds has expanded, mainly because of the importance of such compounds as catalysts in several organic transformations Photodecarbonylation can be used to investigate the primary photoreactions of metal carbonyls and the reactivity of their photoproducts.

In general the primary photoinduced reaction of metal carbonyls involves the monodecarbonylation process as shown in Reaction 1.1 1.

$$M(CO)_x \xrightarrow{h\nu} M(CO)_{x-1} + CO \qquad 1.1.1$$

One important feature of this reaction is its high quantum efficiency and also the reactive nature of the decarbonylated complex. The high quantum efficiency can be explained by examining the molecular orbital diagram of the bonding between the metal and the carbon monoxide ligand (Figure 1.1.1). From the diagram it can be seen that the highest occupied orbital subset are the metal based t_{2g} orbitals, while the lowest unoccupied orbitals are the σ^*, i e those orbitals which are strongly antibonding with respect to the σ–interaction of the carbonyls The photoinduced promotion of an electron from the t_{2g} orbital subset to the σ^* orbital removes electron density from those orbitals contributing to the back-bonding interaction and populates an orbital which is strongly anti-bonding with respect to the carbonyl σ–interaction The result of this is efficient labilisation of a carbonyl ligand

Figure 1.1.1: Simplified molecular orbital diagram showing the interaction of a CO molecule with a d^6 metal

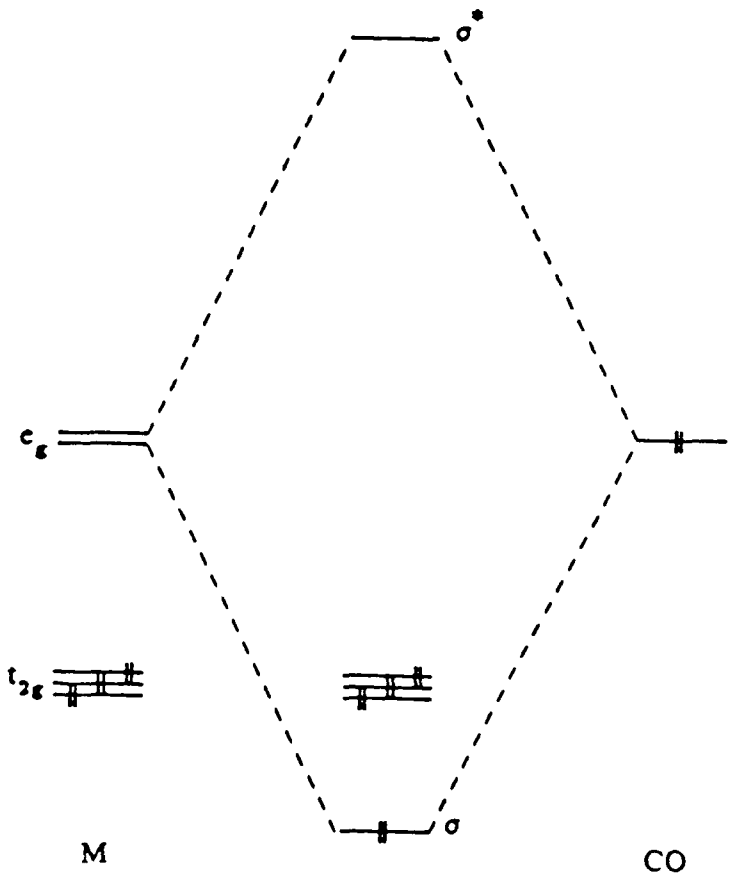

Chemistry involving ligand exchange and substitution dominates the excited state processes of $M(CO)_6$ complexes The photochemical formation of $M(CO)_5L$ is achieved by the sequence outlined in Reactions 1.1.2 and 1.1.4.

$$M(CO)_6 \xrightarrow{h\nu} M(CO)_5 + CO \qquad 1.1.2$$

$$M(CO)_5 + CO \longrightarrow M(CO)_6 \qquad 1.1.3$$

$$M(CO)_5 + L \longrightarrow M(CO)_5L \qquad 1.1.4$$

The importance of Reaction 1.1.4 lies in the high quantum efficiency (Φ) of the process (see Figure 1.1.1). Initially the reaction was so efficient Φ was thought to be close to unity [12], however subsequently Φ was calculated to be 0.67 [13].

The photochemistry of monosubstituted derivatives of the group 6 hexacarbonyls is influenced by the nature of the unique ligand. In compounds such as $M(CO)_5L$ (L = pyridine), the pyridine has poor π-acceptor ability, although the lowest energy transition has some metal to ligand charge transfer character (MLCT). Since the pyridine is a poor π-acceptor, the back donation to the CO *trans* to it increases with a resultant increase in the metal-carbon bond order. Thus on photolysis, the pyridine is lost preferentially. In the case of a good π-acceptor (L = PPh_3) where the lowest energy transition is principally a ligand field transition, photoexpulsion of CO rather than PPh_3 occurs. This occurs because PPh_3 is a better π-acceptor than pyridine and as a result the metal to phosphine bond is stronger.

The primary photoreaction of $M(CO)_nL_x$ complexes, therefore involves ligand substitution of either L or CO (Reaction 1.1.5 or 1.1.6).

$$M(CO)_nL_x \xrightarrow{h\nu} M(CO)_{n-1}YL_x + CO \qquad 1.1.5$$

$$M(CO)_nL_x \xrightarrow{h\nu} M(CO)_nL_{x-1}Y + L \qquad 1.1.6$$

1.1.1 Matrix Isolation

The development of matrix isolation techniques by George Pimentel [14] greatly enhanced the study of reactive fragments generated on the photolysis of a stable molecule. The reactive or unstable photofragment is trapped in a rigid, chemically inert solid at low temperatures, its lifetime may be extended almost indefinitely It is unable to diffuse through the solid matrix if the matrix is rigid enough and the temperature sufficiently low It will not, therefore, react with other species in the matrix, although the photofragment can interact with the "inert" matrix material. The only other possible decay pathway, unimolecular decomposition, may be blocked if the temperature is sufficiently low.

The matrix isolation method has proved to be a particularly productive area in the photolysis of metal carbonyl compounds [15]. The spectroscopic characteristics of the carbonyl ligand are useful in elucidating the structure of transition metal carbonyl complexes Such vibrations in the infrared spectrum between 2000 and 1750 cm^{-1} are very intense and the matrices (i e noble gases, N_2 and polymers) usually have a spectral window in this region.

The metal carbonyls also have intense-charge transfer electronic absorption bands in the UV region Although these bands are of secondary interest from the point of view of structure determination, the photolysis products may be readily studied by the combination of UV/vis and ir spectroscopy. The sharpness and simplicity of matrix spectra have led to the extension of matrix isolation to the study of stable molecules in an environment free of intermolecular perturbations in which only ground electronic and vibrational states are populated

Sheline and coworkers [16] were the first to persent infrared evidence for the generation of the coordinatively unsaturated intermediate $M(CO)_5$ (M = Cr, Mo, or W) The infrared spectra were obtained after photolysis of $M(CO)_6$ at 77 K in methylcyclohexane glasses. These workers stated that the photofragment had a substantial lifetime, but it is now universally accepted that what was observed was the formation of the $M(CO)_5$–(methylcyclohexane) complex. The spectra obtained supported the assignment of a C_{4v} structure to the $M(CO)_5$ species. Later Turner [17] photolysed the group 6 hexacarbonyls in low temperature matrices (pure argon and argon doped with CO). This work also supported the assignment of a C_{4v} symmetry to the pentacarbonyl fragments produced by photolysis of the $M(CO)_6$ species.

The visible spectra of photoproduced $M(CO)_5$ have been shown to be very senstive to the nature of the matrix media [18]. The differences in visible band maxima are shown in Table 1.1 1 1 [18]. This variation in the visible band maxima is a result of the interaction of the matrix material in the vacant coordination site on the $M(CO)_5$ fragment.

Since the diffusion of the CO molecule away from the metal atom is unlikely, on photolysis the photoproduct undergoes a rearrangement so as to lie in a position from which rapid CO recombination will not occur (Scheme 1 1.1 1) [19] The excited pentacarbonyl fragment rearranges and is frozen in a spatial onentation such that there is a matrix molecule and not a CO molecule in the sixth coordination site of the metal On visible photolysis of the pentacarbonyl a photochemical rearrangement is possible to reestablish the original spatial position of the ligands relative to the photoejected CO such that thermal recombination is possible (Reaction 1.1 1.1) [19].

The implication that the carbonyl fragment and CO share the same matrix cage is supported by the observation of spectral features which indicate perturbation by CO.

Table 1.2: Variation in visible band with various matrix media

Matrix	Band Maxima		
	$Cr(CO)_5$	$Mo(CO)_5$	$W(CO)_5$
	nm	nm	nm
Ne	624		
SF_6	560	450	461
CF_4	547		
Ar	533	429	437
Kr	518		
Xe	492	413	417
CH_4	489	411	413

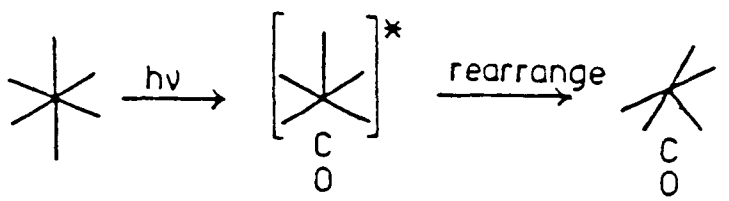

Scheme 1.1.1.1

$$M(CO)_x \rightleftharpoons M(CO)_{x-1} + CO \qquad 1.1.1.1$$

Matrix isolation also has some limitations: firstly it cannot easily be used for charged species, secondly very little kinetic information can be obtained because of the restricted temperature range and limited diffusion. Finally the solid matrix cage can effectively block pathways in photochemical reactions. Despite these limitations, matrix isolation has been used to generate a large number of transition metal fragments containing carbonyl groups. The frequencies of their IR absorption bands have been measured and this data forms a "spectral library" which has played a central role in the interpretation of time resolved infrared experiments

Liquified noble gases have proved to be very useful solvents for stabilising thermally reactive fragments. The noble gases have also helped in the investigation of metal carbonyl systems Studies by Simpson *et al.* [20] on the UV photolysis of $Cr(CO)_6$ dissolved in liquid Xe, or liquified Kr doped with Xe, resulted in the production of a relatively long lived species ($t_{1/2}$ = 2 s at 193 K) identified as $Cr(CO)_5(Xe)$ Jackson *et al.* [21] produced thermally labile metal carbonyl compounds coordinated to an alkene and either N_2 or D_2 in liquid Kr or Xe doped with N_2 or D_2 Liquified noble gases allow studies of the activation parameters of reactive metal carbonyl compounds and therefore offer a great advantage over matrix isolation techniques

1.1.2 Polymer Films

Low temperature matrices such as inert gases, methane, or N_2 and liquified noble gases require the use of very expensive low-temperature equipment and high-vacuum systems One way to study the photochemical reactions of a carbonyl complex without the necessity of the expensive cryogenic and vacuum equipment is to use glassy materials such as isopentane and methylcyclohexane [19] or polymer films [22] A

solution of the stable parent carbonyl is made in the case of isopentane and methylcyclohexane, they are rapidly frozen to a glass at liquid nitrogen temperature between two sapphire windows in a suitable cold cell In the case of polymers, a film of the polymer with the metal carbonyl dispersed within can be cast on a sapphire disk and then cooled to liquid nitrogen temperature These techniques have some limitations, firstly the infrared bands of the photofragments are usually broad which reduces their value for structural characterisation since overlapping bands make assignments difficult Secondly there is evidence that these glassy materials are not "inert" matrices and may interact in a significant way with the carbonyl fragment However, in our case this is not a limitation as we are interested in the interaction between the photofragment and its environment When the polymer films are cast from solvent, some solvent may remain in the film and interact with the photofragment Also studies involving isotopic enrichment are impossible Finally the polymeric materials may contain large cavities at low temperatures and diffusion of photoejected CO away from the photolysis site occurs relatively easily

Polymer films have provided a means of trapping unstable intermediates resulting from photolysis In one of the first studies Massey and Orgel [23] found that a methylmethacrylate polymer containing a small amount of $M(CO)_6$ (M = Cr, Mo, or W) assumed a yellow colour when irradiated at room temperature with UV light They proposed that the $M(CO)_5$ fragment had been formed. On leaving the irradiated matrix in the dark the parent hexacarbonyl slowly reformed, but when the polymer was cooled by liquid nitrogen the pentacarbonyl species remained trapped in the polymer matrix Later, McIntyre [24] reported that the thermal back reaction (Reaction 1.1 2.1) following flash photolysis of $Cr(CO)_6$ in a polystyrene film occured at a much slower rate than in solution.

$$Cr(CO)_5 + CO \longrightarrow Cr(CO)_6 \qquad 1.1.2.1$$

$k_{cyclohexane} = 317\ dm^3mol^{-1}s^{-1}$

$k_{polystyrene} = 0.25\ dm^3mol^{-1}s^{-1}$

Since then metal carbonyl photofragments have also been generated by photolysis of the parent molecules in frozen glasses, matrices, and polymer films. De Paoli and his coworkers [22] reported studies of the photochemical reactions of pentacarbonyliron with olefins in a PTFE (polytetrafluoroethylene) room temperature matrix. The reaction with the dienes, butadiene, and isoprene in the matrix produced not only dienetricarbonyl but also bis(diene) monocarbonyliron compounds. With ethylene and acetylene they observed the formation of ethylenetetracarbonyliron and acetylenetetracarbonyliron.

Hitam *et al.* [25] used films of polyvinylchloride to investigate the photochemical reactions of $(Cp)Mo(CO)_3(CH_3)$ at temperatures in the range 10-293 K. On irradiation they observed the formation of $(Cp)Mo(CO)_2(CH_3)$ as the primary photoproduct and $(Cp)Mo(CO)_3^*$ as a second primary photoproduct. Further irradiation produced the $(Cp)Mo(CO)_3Cl$ species. The photolysis scheme is sumarised in Scheme 1.1.2.1.

Hooker and Rest [26] studied the reactions of the metal hexacarbonyls $M(CO)_6$ (M = Cr, Mo, or W) in polyvinylchloride film matrices over the temperature range 12- 298 K. The photoreactions observed are summarised in Scheme 1.1.2.2. These workers also carried out a comparative study with hydrocarbon glass and paraffin wax matrices and proposed the following advantages of solvent cast polymer film matrices. It is possible to isolate at cryogenic temperatures, unstable species which may also be studied in frozen gas matrices, thermal reactions of such species may be monitored over a wide temperature range and these species may be related to mechanisms of reactions in

solution which are also observed in the polymer films at room temperature

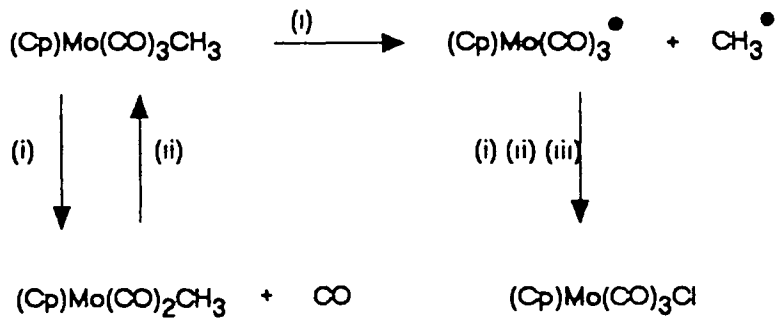

(i) hν $300 < \lambda < 370$ (ii) warming up (iii) Cl radicals in PVC

Scheme 1.1.2.1

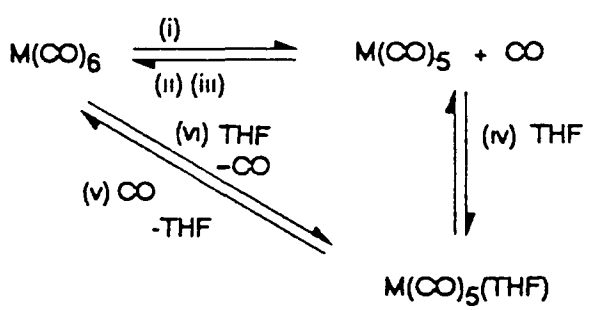

(i) hν (λ<350nm) at 12 K (ii) hν (λ>400nm) at 12 K (iii) Warming to 200 K (iv) Warming between 100 and 200 K (v) thermal rxn above 200 K (vi) hν (λ<350nm) at 298 K (reaction observed in solution)

Scheme 1.1.2.2

Hooker and Rest [27] have also carried out photolysis of methyl- and acetyl- dicarbonyl (η^5-cyclopentadienyl)iron complexes in PVC film matrices at 12 - 200 K (η^5-cyclopentadienly = Cp) The photoinduced decarbonylation of $(Cp)Fe(CO)_2(COCH_3)$ was observed to be thermally reversible, and the photolysis of $(Cp)Fe(CO)_2(CH_3)$ leads to the reversible formation of the new species $(Cp)Fe(CO)(CH_3)$ The decarbonylated species could not be generated in frozen gas matrices even under vigorous irradiation conditions They suggested that this was because of a rapid back reaction in the closely confined gas matrix environment Polymer films provide a more cavernous medium [19] where the photofragments can diffuse apart as a result the "cage effect" is less important

The photoreactions of $(Cp)M(CO)_3(CH_3)$ and $(Cp)M(CO)_3(C_2H_5)$ (M = Mo or W) in PVC film matrices over a wide temperature range (12-200 K) have been studied [28] It was found that on photolysis ($\lambda > 300$ nm) at 298 K the methyl complexes undergo homolytic cleavage of the $M\text{-}CH_3$ bond to form $(Cp)Mo(CO)_3Cl$ In the molybdenum complex cleavage of the $M\text{-}CH_3$ bond also occurs at 12 K and the complexes $(Cp)Mo(CO)_3Cl$ and $CpMo(CO)_3H$ are generated on warming the matrices [28] Photolysis of the equivalent ethylene complexes at 12 K leads to loss of CO. The photoproduct rearranges photochemically or thermally to form *trans* -$(Cp)M(CO)_2(C_2H_4)H$ Photolysis of the tungsten-ethylene complex at 298 K leads directly to the *trans*-$(Cp)W(CO)_2(C_2H_4)H$ The main product from photolysis of the molybdenum complex at 298 K is $Mo(CO)_6$

One of the prime objectives of applying the matrix isolation technique to metal carbonyl complexes is to learn something of the intermediates in solution photochemical reactions. This can be seen from the fact that most of the publications compare the matrix results with similar experiments carried out in solution [18]

1.1.3. Laser Flash Photolysis

The technique of flash photolysis was developed in the 1950's by Norrish and Porter [29] as an attempt to identify the reactive intermediates present in photochemical systems. When the flash is of sufficient intensity the concentration of the transient intermediates can be followed by their absorption spectra, and kinetic data may be obtained. The mechanisms of many photochemical reactions have been studied and determined from the information given by flash photolysis experiments. Transition metal carbonyls are well suited to flash photolysis techniques because they are moderately soluble in non-polar solvents, have reasonably high UV/vis and ir extinction coefficients and have high quantum yields for their photochemical reactions (Reaction 1.1.3.1).

$$M(CO)_6 \longrightarrow M(CO)_5 + CO \quad \phi = 0.67 \qquad 1.1.3.1$$

The pentacarbonyls of group 6 are among the most widely studied intermediate species [30]. It is generally accepted that the primary decay of photolytically excited $M(CO)_6$ (M = Cr, Mo, or W) is the photodissociation of CO to form the intermediate $M(CO)_5$ species (Reaction 1.1.3.1). $M(CO)_5$ is a 16 valence electron coordinatively unsaturated species which reacts with normally inert substances such as Xe or N_2. As a result, in the presence of a coordinating ligand or solvent molecule, the substitution product $M(CO)_5L$ is formed. Nasielski *et al* [30a] were the first to report the formation of this transient species. They observed the presence of two transient species having absorptions in the visible region. Kelly *et al* [30b] later assigned the first observable species on flash photolysis of $Cr(CO)_6$ in cyclohexane as a $Cr(CO)_5$ complex. In further studies the first observable species was identified as the solvent coordinated pentacarbonyl fragment [30c]. Later Simon and Peters [9a] examined the primary photoproduct of $Cr(CO)_6$ in both neat and mixtures of THF and cyclohexane. The primary intermediate they observed was the

solvated pentacarbonyl complex in which one solvent molecule occupies the coordination site created by the elimination of CO. The rate of exchange of cyclohexane from (cyclohexane)$Cr(CO)_5$ by THF to form (THF)$Cr(CO)_5$ was found to be bimolecular (k = (4±1) x 10^7 $dm^3mol^{-1}s^{-1}$). The transient absorption spectrum, observed 25 ps after photolysis, was assigned to a solvent coordinated $Cr(CO)_5(S)$ (S = solvent complex) No evidence for uncoordinated $Cr(CO)_5$ was obtained in the solution phase photolysis of $Cr(CO)_6$ Since then work has centred on the initial reactivity of the photogenerated species with the solvent molecule Simon and Xie investigated the flash photolysis of $Cr(CO)_6$ in cyclohexane and methanol solutions [9b] The rise time in MeOH solution was longer than in cyclohexane (2 5 ps compared to t < 0.8 ps) It was concluded that the longer nse time in MeOH was a result of solvent reorganisation, resulting in the coordination of a solvent molecule to the vacant site of the reactive $Cr(CO)_5$ intermediate. Thus any excited state processes or vibrational relaxation of the photofragment must occur on a faster timescale in cyclohexane than in methanol. These workers also investigated the effect of solvent structure on the photogenerated species [9c,d] $Cr(CO)_6$ was photolysed in pentanol because of the availability of both hydroxyl and alkyl groups for coordination to the reactive intermediate [9c]. 50% of the photofragments are initially occupied by the hydroxyl group of the alcohol. Rearrangement of the initially formed alkyl complex to the more stable hydroxyl complex occurs during the first nanosecond following photolysis (Scheme 1.1.3 1). This rearrangement process was considerably faster in 2-propanol than in 1-propanol a nse time of 100 ps as compared to 400 ps [9d] Rearrangement in 2-propanol occurs by a unimolecular displacement process, as coordination of any of the alkane groups results in a metal-solvent bond which is in close proximity to the hydroxyl group of the molecule.

Nelson and Joly [32] using femtosecond time resolution have demonstrated that cleavage of the Cr-CO bond in the photodissociation of $Cr(CO)_6$ occurs in less than 250 fs.

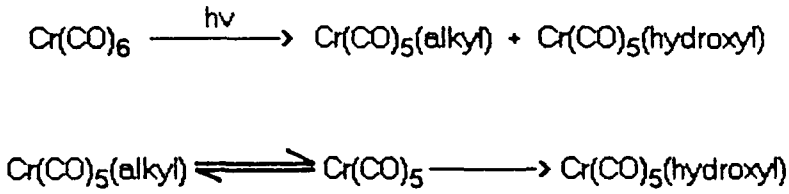

Scheme 1.1.3.1

There are some limitations with UV/vis spectroscopy used for determining intermediates generated by laser flash photolysis. These arise from the general broadness and lack of resolvable fine structure in the electronic absorptions of most organometallic species The use of time resolved infrared detection, in addition to kinetic data, gives valuable structural information from the frequency and intensity of the infrared bands associated with a particular transient species This is especially true of the metal carbonyls as the absorptions in the CO stretching region are a direct indication of the geometry of the molecule [30,33].

1.2 References

1 M S. Wrighton, *Chem. Revs.* 74, 401, (1974).

2 G.W. Parshall, "Homogeneous Catalysis", Wiley Interscience, New York, (1980)

3 J.A. Osborne, F.H. Jardine, J.F Young, and G. Wilkinson, *J Chem Soc A* 1711, (1966)

4 For example see: C.U. Pittman Jr. in "Comprehensive Organometallic Chemistry", eds Wilkinson, Stone, and Abel, Pergamon Press, Oxford, Ch. 55, 553, (1982)

5 W Haag and D D. Whitehurst Belg Pat 721,686, (1969)

6 R.H Grubbs and L C Kroll, *J Amer Chem Soc.* 93, 3062, (1971)

7 C U. Pittman Jr and C E. Carraher Jr., *Appl. Polym* (Proc Amer. Chem Soc Symp O.A. Battista. Appl. Polym. Sci), 113, (1988)

8 J P Collman, *Acc. Chem. Res.* 1, 136, (1968).

9 (a) J D Simon and K S. Peters, *Chem Phys Lett.* 98, 53, (1983).

(b) J.D. Simon and X. Xie, *J. Phys. Chem.* 90, 6751, (1986)

(c) J.D. Simon and X. Xie, *J. Phys. Chem.* 91, 5538, (1987).

(d) J D. Simon and X. Xie, *J Phys Chem.* 93, 291, (1989).

10 F.A. Cotton and G. Wilkinson, "Advanced Inorganic Chemistry", 5th ed., Interscience, New York, (1988).

11 E Koerner von Gustorf and F.W. Grevels, *Fortschr Chem. Forsh.* 13, 366, (1969).

12 W Strohmeier and D. von Hobe, *Chem Ber.* 94, 761, (1961).

13 J. Nasielski and A. Colas, *J. Organomet Chem.* 101, 215, (1975).

14 (a) E. Whittle, D.A. Dows, and G.C. Pimentel, *J Chem Phys.* 22, 1943, (1954)

(b) J D. Baldeschwieler and G C. Pimentel, *J Chem. Phys.* 33, 1008, (1960)

15 R.N. Perutz, *Annu Rep Prog. Chem.* Sect C, 157, (1985).

16 (a) I W. Stolz, G.R. Dobson, and R.K. Sheline, *J Amer Chem. Soc.* 84, 3889, (1962).

(b) I.W. Stolz, G.R. Dobson, and R.K. Sheline, *J. Amer Chem Soc.* 85, 1013, (1963).

17 M.A. Graham, M. Poliakoff, and J J Turner, *J. Chem Soc* A., 2939, (1971).

18 R.N. Perutz and J J Turner, *J Amer Chem Soc.* 97, 4791, (1975).

19 J K. Burdett, *Coordination Chemistry Reviews* 27, 1, (1978)

20 M B Simpson, M. Poliakoff, J J Turner, W.B. Mier, and J.G. McLaughlin, *J. Chem Soc. Chem. Commun.* 1355, (1983).

21 S.A. Jackson, R.K. Upmacis, M. Poliakoff, J J Turner, J.K. Burdett, and F.W Grevels, *J Chem. Soc. Chem Commun.* 678, (1987)

22 M.A. De Paoli, S M. De Oliveira, and F Galembeck, *J Organomet Chem* 193, 105, (1980).

23 A.G. Massey and L E Orgel, *Nature* 191, 1089, (1962).

24 J.A. McIntyre, *J Phys. Chem.* 74, 11, (1970).

25 H B. Hitam, R.H. Hooker, K.A. Mahmoud, R. Naraganaswamy, and A.J. Rest, *J. Organomet Chem.* 222, C9, (1981).

26 R.H Hooker and A.J. Rest, *J Organomet Chem.* 249, 137, (1983)

27 R.H Hooker, A.J. Rest, and I Whitwell, *J Organomet Chem.* 266, C27, (1984)

28 R.H. Hooker and A.J. Rest, *J. Chem. Soc. Dalton Trans.* 761, (1984)

29 R.P. Wanye, "Principles and Applications of Photochemistry", Oxford Science Publications, Ch. 7, (1988)

30 For example (a) J. Nasielski, P. Kirsh, and L. Wipulte-Steiner, *J Organomet Chem.* 29, 269, (1971)

(b) J M Kelly, H Herman, and E K. von Gustorf, *J. Chem. Soc. Chem Commun.* 105, (1973).

(c) A.J. Lees and A.W. Adamson, *Inorg. Chem.* 20, 4381, (1981).

(d) J.M. Kelly, C. Long, and R. Bonneau, *J Phys. Chem.* 87, 3344, (1983)

(e) S.P Church, F.W. Grevels, H. Herman, and K. Schnaffer, *Inorg. Chem.* 24, 418, (1985).

(f) S. Oishi, *Organometallics* 7, 363, (1988)

31 J M Kelly, D.V. Brent, H. Hermann, D. Schulte-Frohlinde, and E K. von Gustorf, *J Organomet Chem.* 69, 259, (1974).

32 A.G Joly and K.A. Nelson, *J Phys Chem.* 93, 2976, (1989)

33 S P. Church, F.W Grevels, H. Hermann, and K. Schnaffer, *Inorg. Chem.* 23, 3830, (1984).

Chapter 2

Photolysis of $MeCpMn(CO)_3$, $ArCr(CO)_3$, and $Cr(CO)_6$ in Low Temperature Polymer Films

2.1 Photolytic studies of $CpMn(CO)_3$, $MeCpMn(CO)_3$ in low temperature matrices

The $CpMn(CO)_3$ (Cp = η^5-cycopentadienyl) complexes are stable and have the d^6 electronic configuration which is inert to thermal substitution because the t_{2g} orbital subset is filled and the next available orbital is the σ^* antibonding orbital. The carbon monoxide ligand can be replaced photochemically as described earlier (Figure 1.1.1). The primary photoreaction of $CpMn(CO)_3$ is loss of CO which leads to monosubstituted products (Reaction 2.1.1).

$$CpMn(CO)_3 \xrightarrow[L]{h\nu} CpMn(CO)_2L + CO \qquad 2.1.1$$

It is likely that Reaction 2.1.1 will proceed for any L having any nucleophilic character. This fact is demonstrated by the large number of examples in Table 2.1.1 [1-8]. Further loss of CO from $CpMn(CO)_2L$ has been observed in several cases notably for L = π-acceptor ligand as can be seen from examples given in Table 2.1.1. Complete decarbonylation has been observed in the formation of CpMn(benzene) [8]. The $CpMn(CO)_2$ moiety functions like a vice or clamp for the capture and stabilisation of L [9].

While oxidative addition to photogenerated coordinatively unsaturated intermediates is common, there appears to be no definitive data to show that either photooxidation or photoreduction of the metal is a primary photoprocess upon UV or visible excitation. However the coordinatively unsaturated intermediate $CpMn(CO)_2$ is susceptible to oxidative addition as shown in Reaction 2.1.2 [10]. The resulting product is a distorted square pyramid and formally seven coordinate.

Table 2.1.1: Photosubstitution reactions of $CpMn(CO)_3$ [10]

Entenng group, L	Products	Ref
Tetrahydrofuran	$CpMn(CO)_2L$	1
$(Ph_2PCH_2CH_2)_3N$	$CpMn(CO)L$	2
Pyridine	$CpMn(CO)_2L$	3
Piperidine	$CpMn(CO)_2L$	4
SO_2	$CpMn(CO)_2L$	5
PPh_3	$CpMn(CO)_2L$	6
	$CpMn(CO)L_2$	
1,3-Butadiene	$CpMn(CO)L$	7
Benzene	$CpMnL$	8

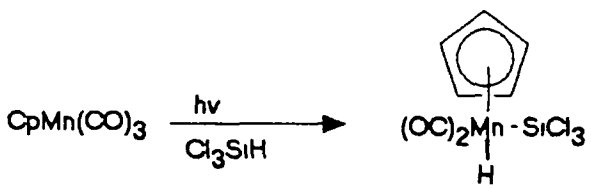

2.1.2

A number of low temperature studies have been carried out on $CpMn(CO)_3$ and related complexes. Rest *et al* [11] presented evidence for the formation of the coordinatively unsaturated species $ML(CO)_2$ {ML = $Cr(\eta^6C_6H_6)$, $Mn(\eta^6C_5H_5)$, $Fe(\eta^4C_4H_4)$} on the UV photolysis of $ML(CO)_3$ complexes in argon and methane matrices, and dinitrogen

complexes $ML(CO)_2(N_2)$ in nitrogen matrices at 12 K. The principal substitution process is outlined in Scheme 2.1.1.

$$ML(CO)_3 \xrightarrow{h\nu} [ML(CO)_3]^* \xrightarrow[-CO]{} ML(CO)_2 \xrightarrow{L'} ML(L')(CO)_2$$

Scheme 2.1.1

Braterman and Black [12] photolysed $CpMn(CO)_3$ in a 3:1 methyl cyclohexane/nujol mixture at 80 K because of solubility problems in isopentane/methylcyclohexane glasses. They reported the disappearance of the parent tricarbonyl peaks at 2061 and 1938 cm^{-1} simultaneously with the appearance of two peaks at 1955 and 1886 cm^{-1} which were assigned to the dicarbonyl species $CpMn(CO)_2$. In the presence of diethylether (ether) they observed the formation of $CpMn(CO)_2(ether)$ and $CpMn(CO)(ether)_2$ [12b]. $MeCpMn(CO)_3$ was reported to behave similarly (MeCp = methylcyclopentadienyl).

Photolysis of $CpMn(CO)_3$, $CpCr(CO)_2(NO)$, and $CpV(CO)(NO)_2$ in either low temperature matrices or ambient temperature solutions (hexane, tetrahydrofuran, cyclooctene) was carried out by Herberhold *et al.* [13]. These workers observed the elimination of CO as the primary photoreaction. The photogenerated species were characterised by their I.R. absorptions and by their secondary reactions in "reactive" matrices such as ^{13}CO, N_2, or coordinating solvents.

Later Hill and Wrighton carried out a study on the photochemistry of $CpMn(CO)_3$ in hydrocarbon glasses at 12 K [14]. They reported the primary photoproduct to be the dicarbonyl species with concomitant production of free carbon monoxide From the quantitative measurement of increase in CO absorption and decrease in the absorptions of $CpMn(CO)_3$, they measured a net loss of one CO molecule for each molecule of $CpMn(CO)_3$ consumed (Reaction 2.1 3)

$$CpMn(CO)_3 \xrightarrow{h\nu} CpMn(CO)_2 + CO \qquad 2.1.3$$

These workers also determined the rates of reaction and activation parameters for the reaction of the dicarbonyl complex with trisubstituted silanes. The dicarbonyl species reacts with the R_3SiH species, which is doped in the frozen matrix upon warming the glass

The methyl derivative, $MeCpMn(CO)_3$, which is used in this study has been reported to behave in a similar manner to the $CpMn(CO)_3$ species [12b,15]. The greater general availability and lower cost of $MeCpMn(CO)_3$, an anti-knock agent used in automobile fuel, has led to its use in many studies [9]

2.2 Photolytic studies of $ArCr(CO)_3$ in low temperature matrices

The earliest observations of the photoreactivity of $ArCr(CO)_3$ (Ar = η^6-arene) were made by Strohmeier and von Hobe who proposed the reaction mechanism shown in Scheme 2.2 1 [16].

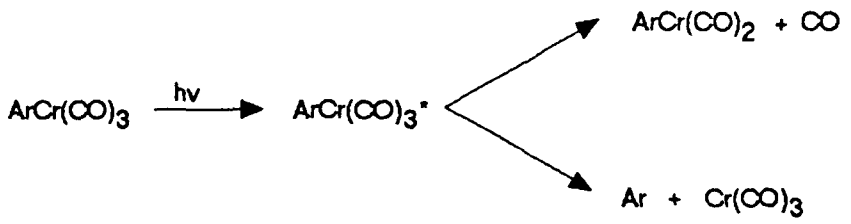

Scheme 2.2.1

This scheme was based on experiments in which the $ArCr(CO)_3$ complex was irradiated in the presence of ^{14}CO and ^{14}C-labelled arene. Incorporation of the labelled species was observed for both the arene and CO.

Rest *et al* [11] investigated the photochemistry of $ArCr(CO)_3$ in frozen gas matrices (argon, CH_4 or N_2) at 12 K. Photolysis of $ArCr(CO)_3$ in argon and methane matrices gives rise to bands in the infrared region which can be attributed to CO and the unsaturated $ArCr(CO)_2$(matrix) species. There was a slight variation in the bands between the two matrices. Photolysis of the parent tricarbonyl species in N_2 matrices resulted in the formation of the $ArCr(CO)_2(N_2)$ complex. The dinitrogen complex, unlike the $CbFe(CO)_2(N_2)$, did not undergo photoreversal upon irradiation at longer wavelengths. There was no evidence for photoejection of the arene ligand even when $ArCr(CO)_3$ was photolysed in a CO matrix.

Hill and Wrighton [14] studied the thermal reactivity of trisubstituted silanes with the coordinatively unsaturated species $ArCr(CO)_2$, produced at low temperatures by photolysis. Photolysis of $ArCr(CO)_3$ at low temperatures (85-157 K) in inert organic solvents leads to dissociative loss of CO to form the 16 valence-electron dicarbonyl species. The unsaturated $ArCr(CO)_2$ species was characterised by means of infrared

spectroscopy On warming the matrix, doped with R_3SiH, the dicarbonyl species reacts to form the 18 valence-electron oxidative addition product $ArCr(CO)_2H(SiR_3)$

2.3 Results and Discussion

Initially it had been hoped to microencapsulate the metal carbonyl in a polymer surround Microencapsulation would have been an ideal way to study the photochemistry of these species By microencapsulating the metal carbonyl the environment in which the photofragments exist can be controlled. Thus any photochemical reaction that occurs could be easily followed It was hoped to observe the formation of the dinuclear species (Reaction 2 3 1-2 3.2), which Creaven *et al.* [17] detected on laser flash photolysis, by photolysis of microencapsulated $MeCpMn(CO)_3$, and to develop a possible method for its synthesis and ultimate isolation.

$$MeCpMn(CO)_3 \xrightarrow{h\nu} MeCpMn(CO)_2 + CO \qquad 2.3.1$$

$$MeCpMn(CO)_2S + MeCpMn(CO)_3 \longrightarrow (MeCp)_2Mn_2(CO)_5 \qquad 2.3.2$$

A film of the microcapsules was cast on a sapphire disk. The disk was then exposed to broad band radiation from a short arc mercury lamp for 5 second exposures and the change in the spectrum was recorded (Figure 2 3 1) A decrease in the parent tricarbonyl bands (2011 and 1914 cm^{-1}) was observed until after a period of 30 seconds irradiation the bands had completely disappeared. No new bands were observed

Before photolysis the film was viewed under a microscope (mag. x 40) and microcapsules were observed However on viewing after photolysis there appeared to be a breakdown in the microcapsules on the film. A second film was prepared, this time photolysis was carried out using light of $\lambda > 390$ nm Similar results were obtained except over a longer timescale (980 secs compared to 30 secs as seen previously)

On photolysis it appears that the microcapsule is being broken down with subsequent release of the $MeCpMn(CO)_3$ species This is confirmed by the fact that there is a decrease in the parent bands and there is no new species formed Also the microscopic evidence shows an apparent breakdown of the microcapsule.

The microcapsulation process proved to be difficult and irreproducible as a result no further experiments were undertaken with the microcapsules.

Figure 2.3.1: Infrared spectra of the encapsulated $MeCpMn(CO)_3$ complex before photolysis (A) and after photolysis (B)

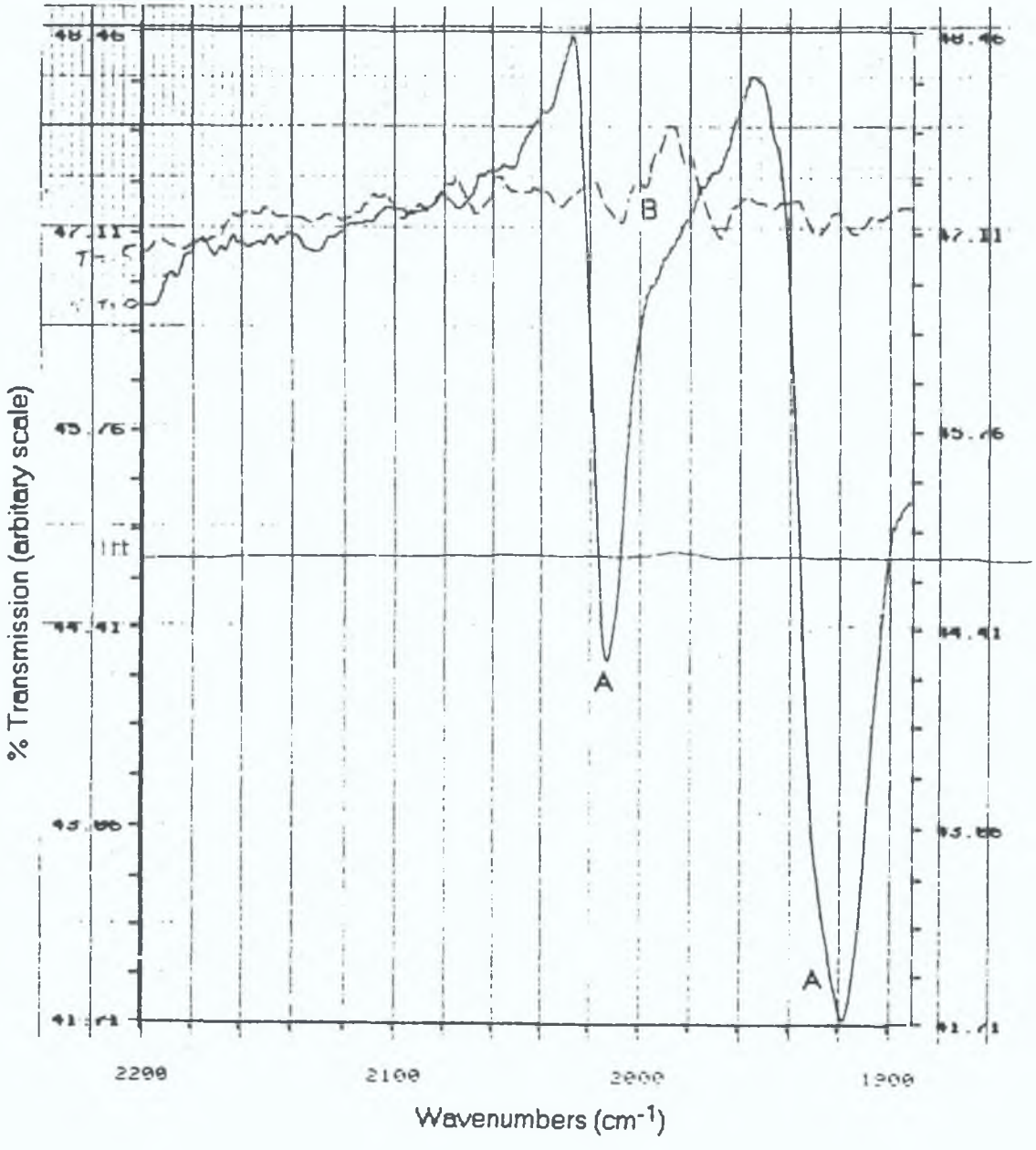

2.3.1 Photolysis of $MeCpMn(CO)_3$ in Polymer Films

As a result of the irreproducible nature of the microencapsulation process it was decided to disperse the metal carbonyl species in a polymer film and to expose the resulting polymer to UV irradiation at low temperature (120 K) The photoproducts were detected using ir spectroscopy. By using low temperatures any reactive intermediate formed will be stabilised in the frozen matrix, thus were the dinuclear species to be formed it would have a substantial lifetime.

Table 2 3.1.1 shows the stretching frequencies observed by Braterman and Black [12a] for $CpMn(CO)_3$ and $CpMn(CO)_2$ in low temperature hydrocarbon glasses

Table 2.3.1

Compound	νCO cm $^{-1}$	
	symmetric	antisymmetric
$CpMn(CO)_3$	2026	1938
$CpMn(CO)_2$	1955	1886

Photolysis of the tricarbonyl complex in polymethylmethacrylate (PMMA) films (Figure 2.3.1.1) resulted in the production of matrix isolated CO (band at 2132 cm^{-1}) and a band at 1848 cm^{-1} which has been assigned to the dicarbonyl species During the course of these experiments there is a concomitant decrease in the parent tricarbonyl bands at 2015 and 1930 cm^{-1} What is probably been observed is the depletion of the parent complex to form the dicarbonyl polymer species (Reaction 2 3 1 1)

$$MeCpMn(CO)_3 \longrightarrow MeCpMn(CO)_2(PMMA) + CO \qquad 2.3.1.1$$

The higher energy band of the dicarbonyl complex in the infrared spectrum is obscured by the bands arising from the parent complex. As a result the assignment of the band at 1848 cm^{-1} to the dicarbonyl complex cannot be taken as absolute

A dispersion of the metal carbonyl in a styrene-co-4-vinyl pyridine (5 1) polymer film was then photolysed using broad band radiation in order to observe the photochemical reactions in the absence of the C=O groups on the PMMA polymer backbone (Figure 2 3.1.2). Also the coodinatively unsaturated species has been shown to be sensitive to the matrix occupying the vacant coordination site [18] Therefore by changing the polymer matrix there may be a shift in the infrared bands arising from the dicarbonyl polymer complex. On photolysis the production of matrix isolated CO was again observed (band at 2128 cm^{-1}), and bands at 1875 and 1845 cm^{-1}appeared These bands continue to grow until a photolysis time of 17 minutes has elapsed when the the band at 1875 cm^{-1} begins to decrease in intensity while the intensity of the band at 1845 cm^{-1} remains constant. The polymer was then warmed to room temperatutre (Figure 2.3.1.3), and the CO band and the band at 1872 cm^{-1} disappeared, giving partial regeneration of the parent tricarbonyl compound (Reaction 2.3 1.1) The band at 1872 cm^{-1} is again probably the result of the formation of the dicarbonyl polymer complex. Only partial regeneration of the parent species was observed as most of the CO boils off on warming the polymer film (Reaction 2 3.1.1).

$$MeCpMn(CO)_2(copol) + CO \longrightarrow MeCpMn(CO)_3 + copol + CO \qquad 2.3.1.1$$

copol = poly(styrene-co-4-vinylpyridine)

The complexation of the dicarbonyl species with the pendant nitrogen on the polymer backbone (Complex 2 3 1.1) gives rise to the band at 1845 cm^{-1} This was verified by carrying out the photolysis in polystyrene on which there is no pendant nitrogen (Figure 2.3 1.4)

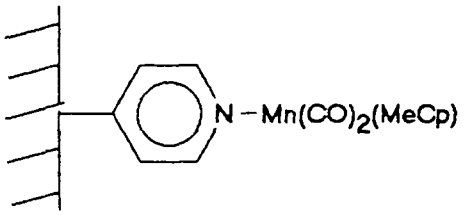

2.3.1.1

The observed CO stretching frequencies for this complex are at 1928 and 1863 cm^{-1} [19] The band at 1928 cm^{-1} is obscured by the parent tricarbonyl bands and the shift in the second band from 1845 to 1863 cm^{-1} is possibly a result of the effects of the low temperature and the polymer matrix.

Figure 2.3.1.1: Changes observed in the carbonyl region of the infrared on photolysis of $MeCpMn(CO)_3$ in a PMMA film at 120 K.

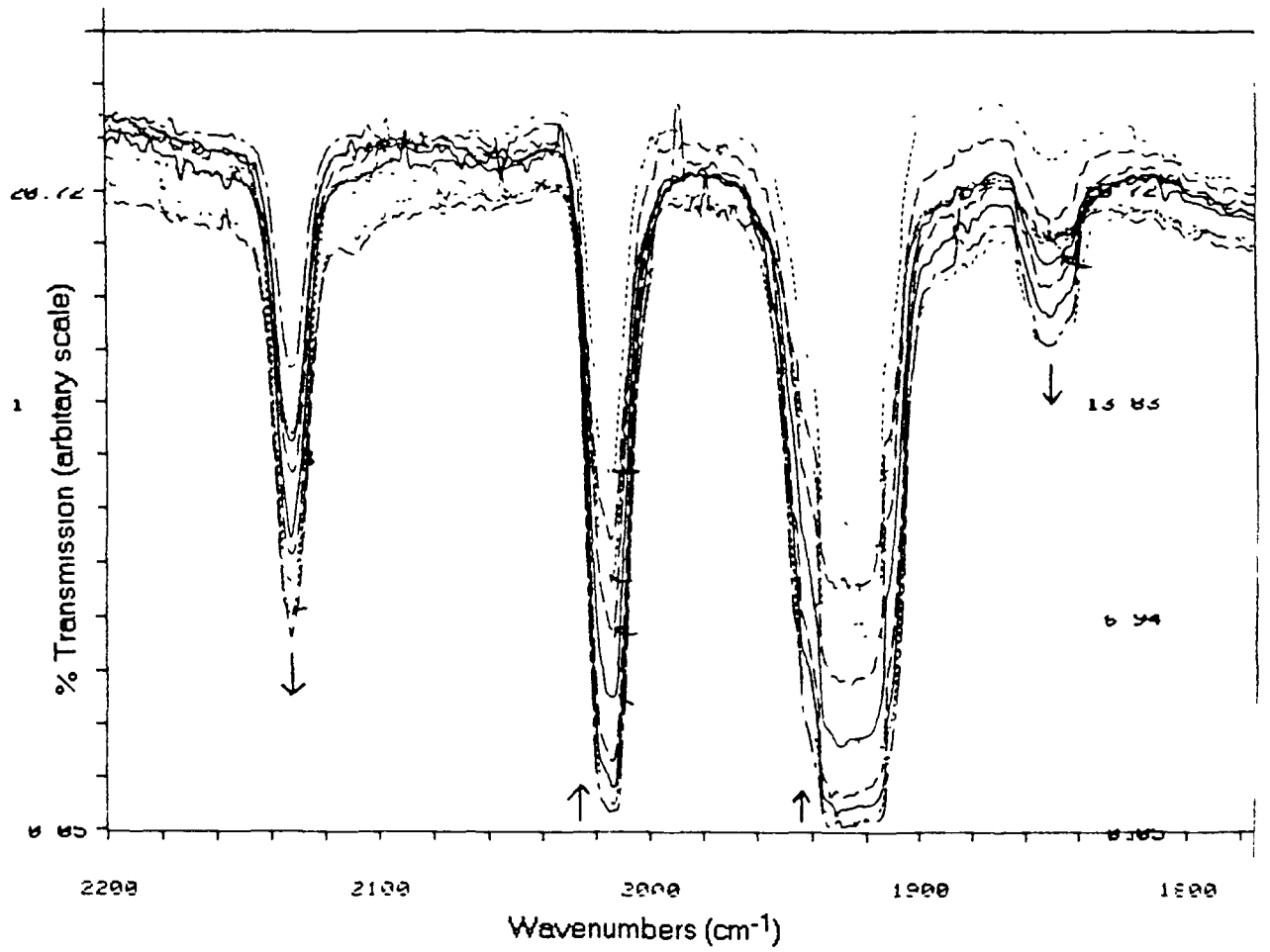

Figure 2.3.1.2: Changes observed in the carbonyl region of the infrared during the photolysis of $MeCpMn(CO)_3$ in a styrene-4-vinyl pyridine copolymer at 120 K

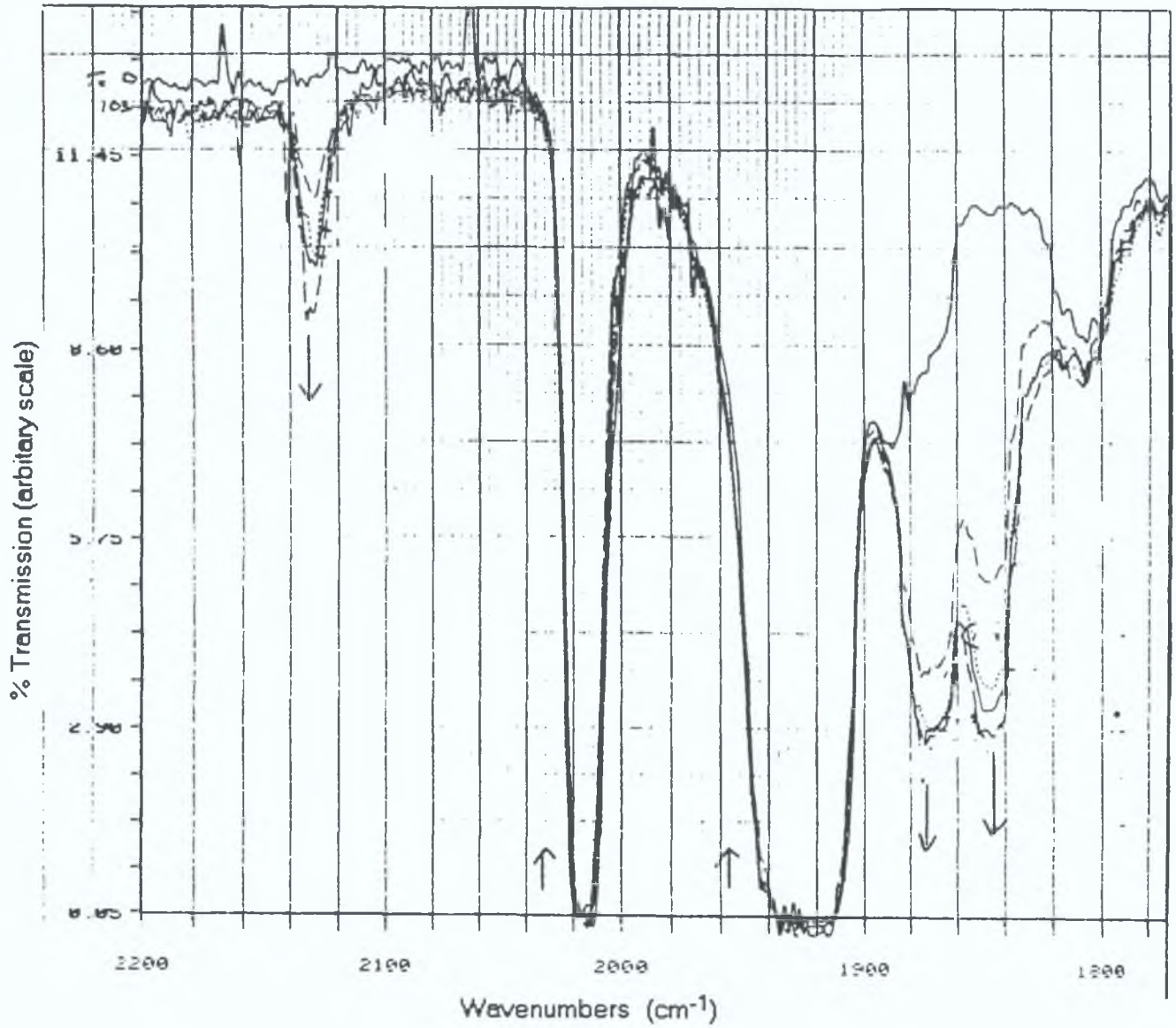

Figure 2.3.1.3: Changes observed in the infrared spectrum on warming the copolymer film from 120 K to room temperature.

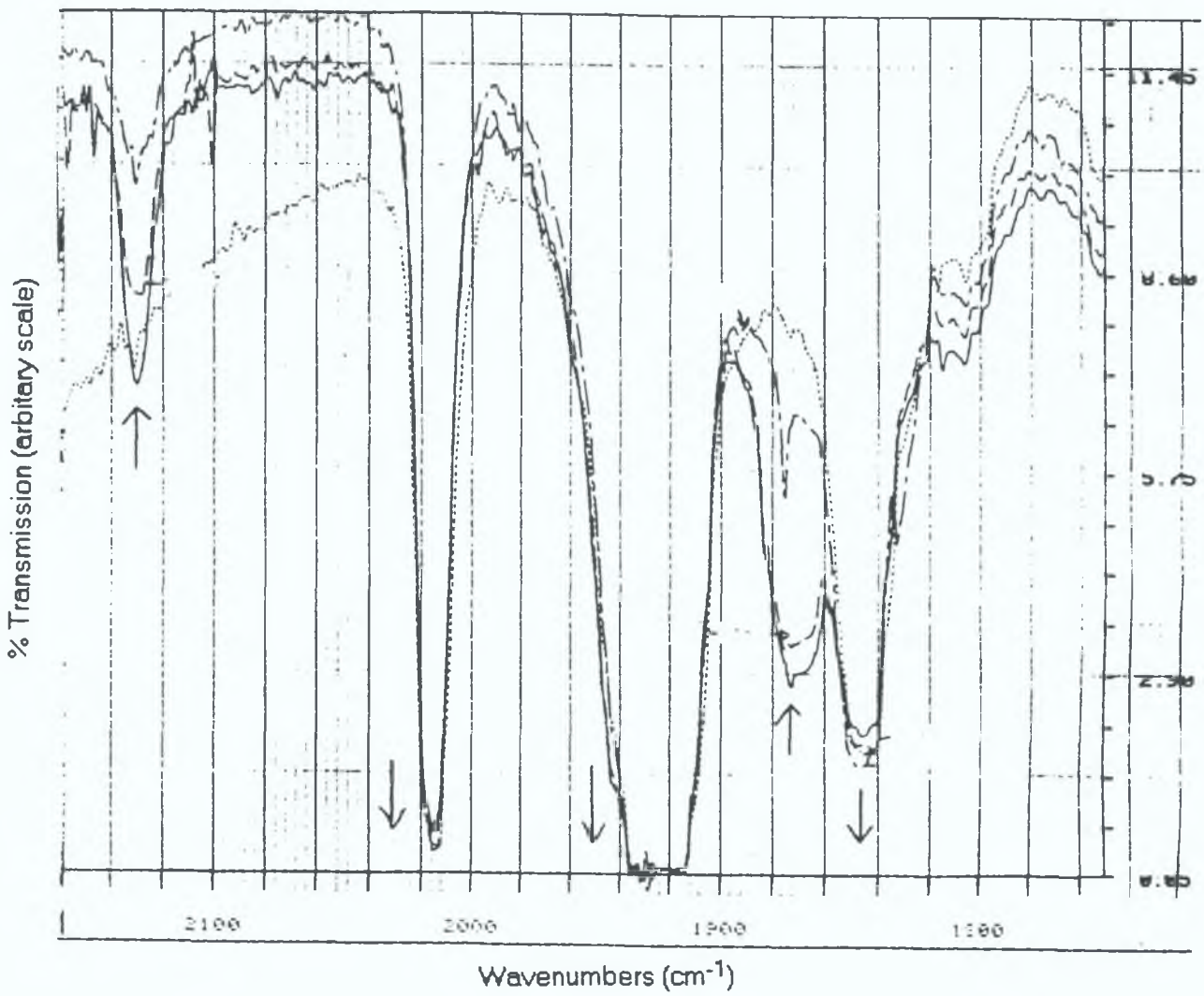

Figure 2.3.1.4: IR spectrum of the photolysis of $MeCpMn(CO)_3$ in a polystyrene film at 120 K

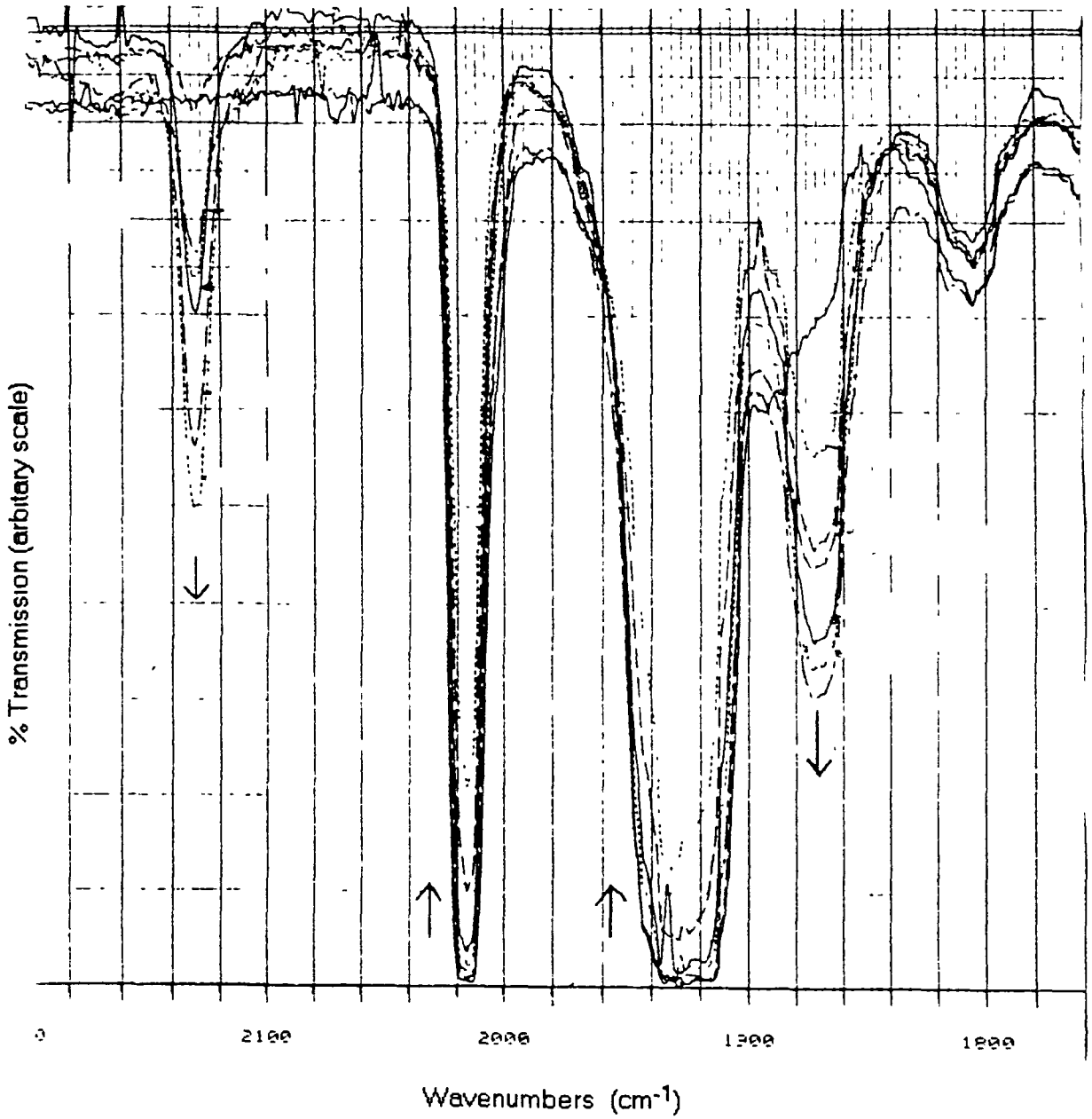

A film of the $MeCpMn(CO)_3$ complex dispersed in polystyrene was cast and the results of the photolysis were recorded using the absorbance mode on the infrared spectrophotometer (Table 2 3 1 2) The absorbances were recorded to see if there was a relationship between the intensity of the free CO band and that at 1873 cm^{-1}

Table 2.3.2: The absorbance recorded at the relevant wavenumbers in A U at various photolysis times at T = 120 K and then the absorbances recorded on warming the film.

	νCO (cm^{-1})			
Time	2128	2018	1933	1873
0 s	–	1 7178	1 7683	–
10 s	0 7725	1 6851	1 7825	1 0407
20 s	0 7274	1 6317	1 7033	1 1358
120 s.	0 7853	1 3920	1.5143	1 1484
Warming				
173 K	0 7603	1 4237	1.5302	1 1258
223 K	0 7400	1 5107	1 5884	0 8923
273 K	–	1.7747	1 8027	–

As the photolysis time increases the intensity of the CO band (2128 cm^{-1}) and the band of the species at 1873 cm^{-1} increase At the same time the bands of the tricarbonyl species decrease in intensity On warming the film the CO is released from the matrix, the species at 1873 cm^{-1} disappears and there is partial regeneration of the parent tricarbonyl There

is a ten-fold difference in their rates of decay, the band at 1873 cm^{-1} having the faster decay rate.

From the infrared data obtained the complex giving rise to the band at 1873 cm^{-1} is probably the $MeCpMn(CO)_2$ polymer species. The higher energy carbonyl band is unfortunately obscured by the parent bands [12a,20].

In order to obtain more information UV/vis detection was used in conjunction with the infrared detection The λ_{max} of $MeCpMn(CO)_3$ in polystyrene was found at 324 nm On photolysis a band appears at 504 nm (Figure 2 3 1 5) This band continues to grow until a photolysis time of 120 secs has elapsed On warming the film from 120 K to 273 K (Figure 2 3.1 6) there was a shift in the observed bands (324 and 504 nm) to shorter wavelengths. On reaching 273 K the spectrum returned to its pre-photolysis form. The broad band centred at 504 nm is thought to be a result of the weak interaction between the $MeCpMn(CO)_2$ species, generated on photolysis, and the aromatic units on the polymer matrix (Reaction 2 3.1 3)

$$MeCpMn(CO)_3 \xrightarrow[\lambda_{max} = 504\ nm]{h\nu} MeCpMn(CO)_2(PS) + CO \qquad 2.3.1.3$$

Figure 2.3.1.5: UV/vis spectra of the photolysis of $MeCpMn(CO)_3$ in polystyrene at 120 K

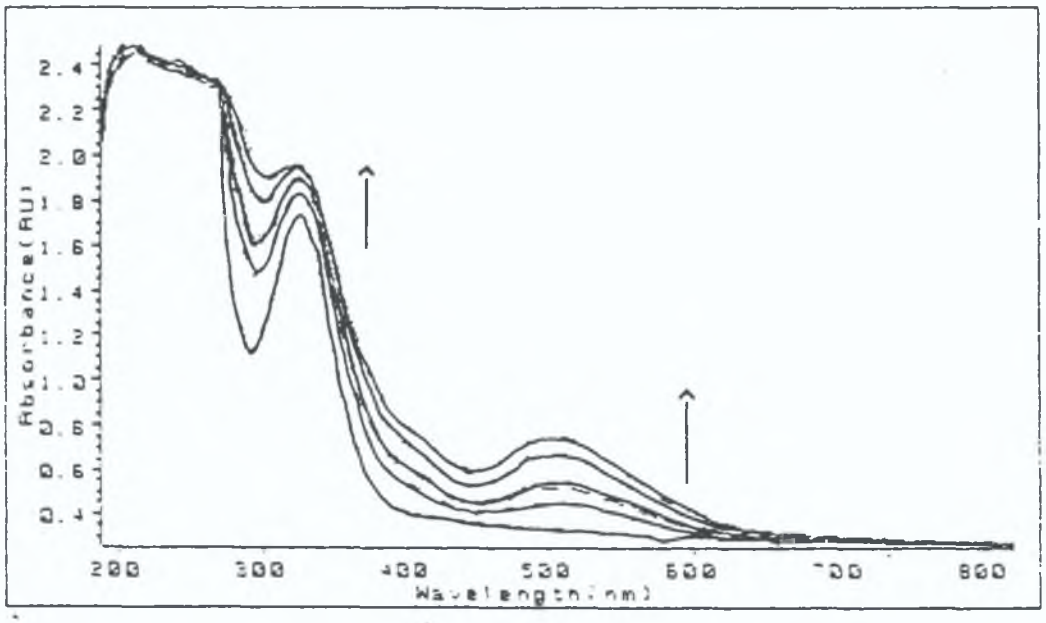

Figure 2.3.6: UV/vis spectra obtained on warming film from Figure 2.3.1.5 to 273 K.

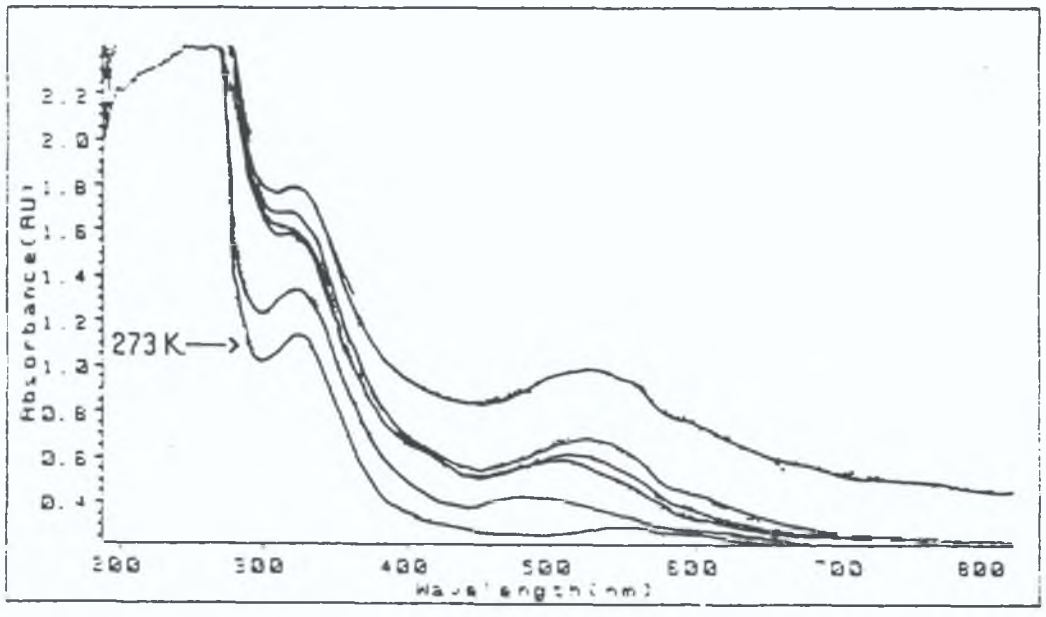

2 3 2 Photolysis of $ArCr(CO)_3$ in Polymer Films

As the parent bands of the $MeCpMn(CO)_3$ species were obscuring bands arising from the photoproducts it was decided to use a different tricarbonyl system, in the hope that the photoproduct bands could be more readily distinguished Arene chromium tricarbonyl was photolysed in a polystyrene film at 120 K infrared or UV/vis detection were used The chromium species was photolysed for comparison with the manganese tricarbonyl system and to see if any information could be obtained which would help in the elucidation of the latter system

On photolysis (Figure 2 3 2 1) there is a decrease in the tricarbonyl parent species (1970 cm^{-1} and 1886 cm^{-1}) with subsequent appearance of CO at 2130 cm^{-1} and the species at 1847 cm^{-1} The latter species has shifted from 1872 cm^{-1} in the $MeCpMn(CO)_3$ experiment this is because of the fact that there is a higher electron density on the metal in the chromium system

On warming (Figure 2 3 2 2) the CO band and the band at 1847 cm^{-1} disappear A new species is also observed with a νCO at 2083 cm^{-1} which is stable as it remains after warming to 273 K The parent tricarbonyl species is also partially regenerated. The film was recooled to 120 K and a second photolysis was carried out The species with a band at 2083 cm^{-1} disappeared, there was generation of CO and the species at 1847 cm^{-1} with a concomitant decrease in the tricarbonyl species. On reheating again the CO is released from the matrix and the species at 1847 cm^{-1} disappears with partial regeneration of the parent tricarbonyl species, as well as the appearance of the band at 2083 cm^{-1}.

The photochemically generated species giving rise to the band at 1847 cm^{-1} is probably the dicarbonyl $ArCr(CO)_2$(polymer) complex (Reaction 2.3 4) the higher frequency band being obscured by the parent tricarbonyl bands The species giving rise to the band at 2083 cm^{-1} is possibly a result of an interaction between the parent and photoproduct as they are released from the matrix on warming the film (Reaction 3 2 2 2).

$$ArCr(CO)_3 \xrightarrow{h\nu} ArCr(CO)_2(polymer) \qquad 2.3.2.1$$

$$ArCr(CO)_2 + ArCr(CO)_3 \longrightarrow Ar_2Cr_2(CO)_5 \qquad 2.3.2.2$$

The UV/vis spectra reveal very little information as the bands from the arene complex are very broad What is probably being observed is the formation of the dicarbonyl polymer complex (Figure 2 3 2 3, Reaction 2 3 2 1)

Figure 2.3.2.1: Changes observed in the infrared spectrum of $ArCr(CO)_3$ upon photolysis at 120 K.

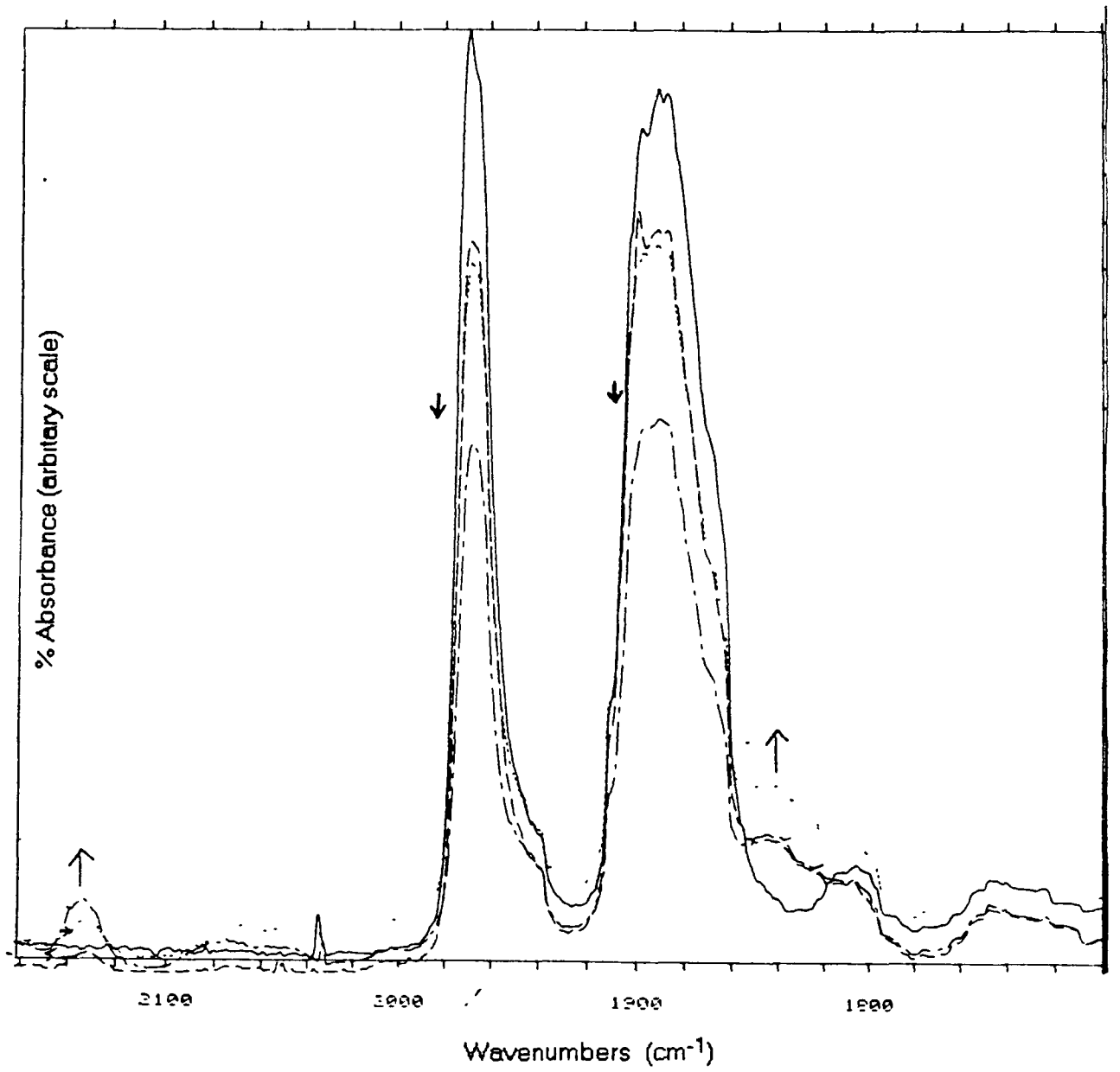

Figure 2.3.2.2: IR spectrum on warming the chromium system after photolysis

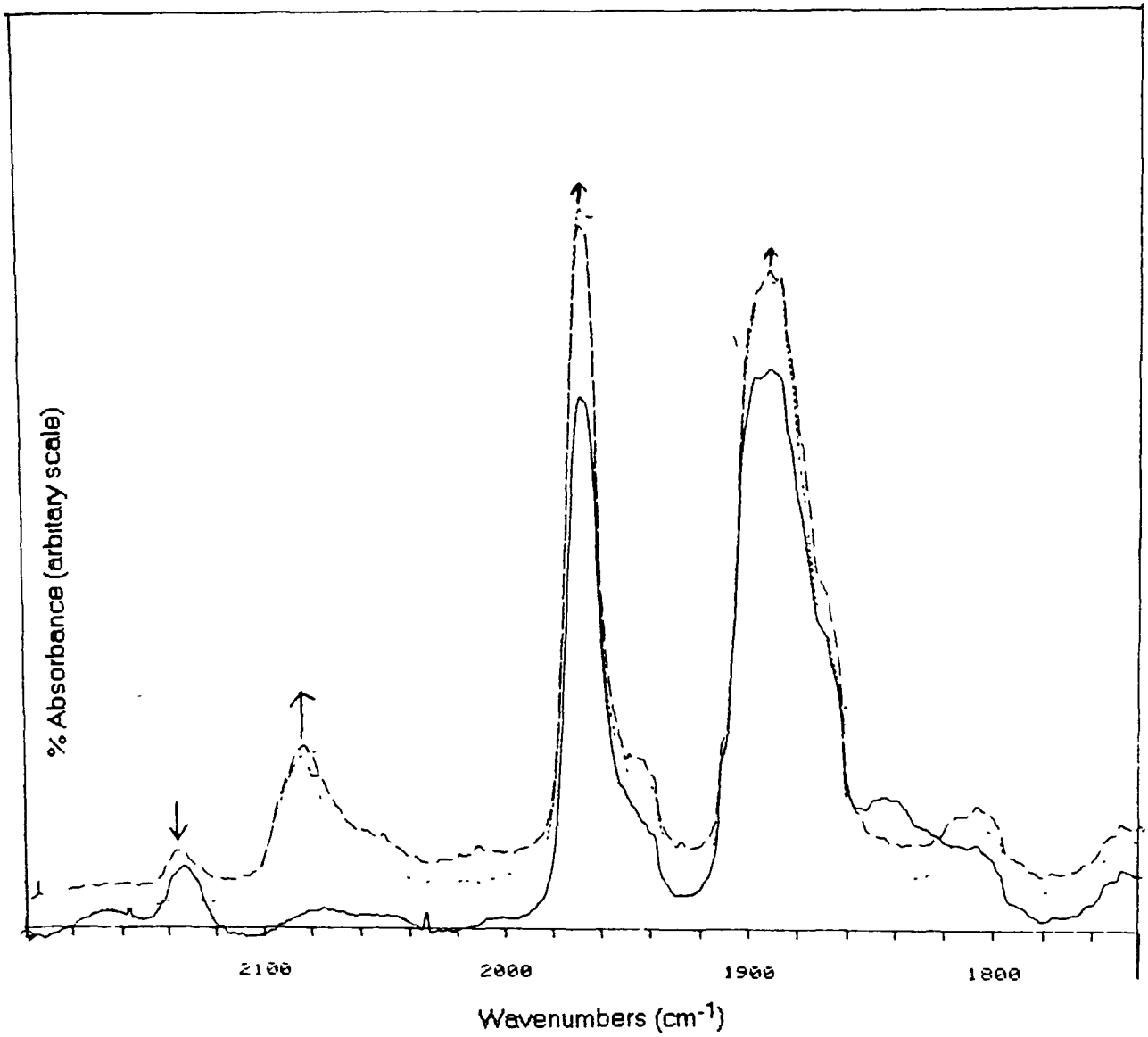

Figure 2.3.9: Changes observed in the UV/vis spectrum during the photolysis of the arene chromium system at 120 K.

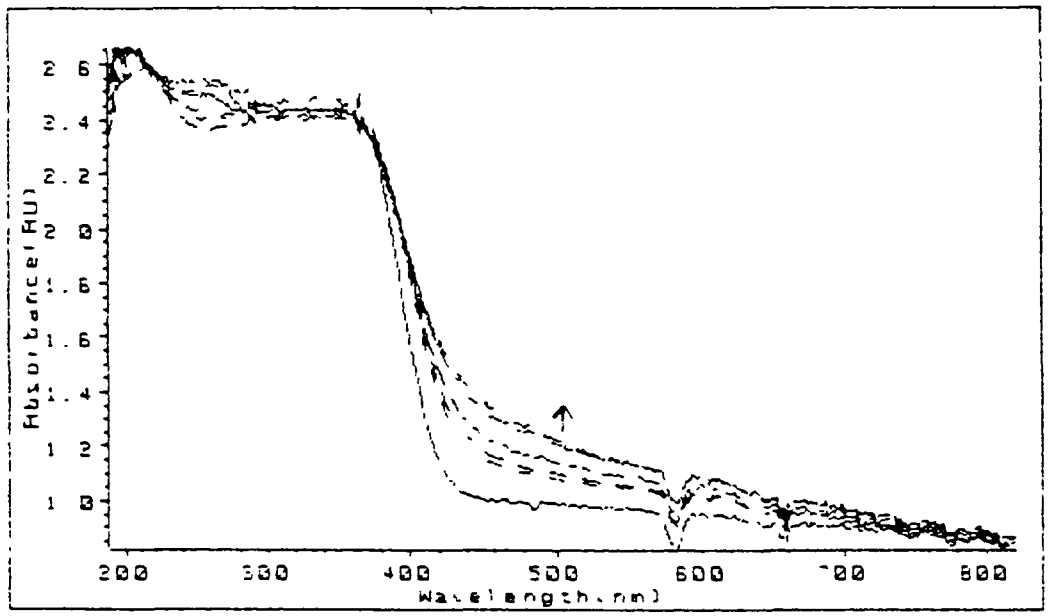

2.3.3 Photolysis of $Cr(CO)_6$ in Polymer Films

As some bands arising from the photoproducts were obscured in both tricarbonyl systems studied it was decided to use the $Cr(CO)_6$ complex, since this system has been widely studied and is well understood. A film of $Cr(CO)_6$ in polystyrene was cast from THF and photolysed at 120 K for comparison purposes in particular with work carried out by Rest *et al* [21]. On photolysis there is a decrease in the parent $Cr(CO)_6$ complex (2020 and 1975 cm^{-1}) with the formation of CO (2130 cm^{-1}) and pentacarbonyl fragments at 2070, 1945, and 1920 (sh) cm^{-1} (Figure 2.3.9.1). On reheating to 123 K partial regeneration of the hexacarbonyl species is observed with a resultant decrease in the CO and pentacarbonyl fragments.

The UV/vis spectrum (Figure 2 3 3 2) shows the appearance of a band at 460 nm. This band can be assigned to the interaction of the $Cr(CO)_5$ fragment with the polymer matrix when compared with the bands recorded by Rest and his coworkers [21] for a similar interaction (i e 2080, 1949, and 1922 (sh) cm^{-1}, UV/vis 420 nm) Rest also found evidence for the existance of $Cr(CO)_5THF$ as the films used were soaked in THF prior to photolysis. Whereas the films used in this experiment were cast from THF solution.

Figure 2.3..3.1: Infrared spectra of the photolysis of $Cr(CO)_6$ in a polystyrene film at 120K

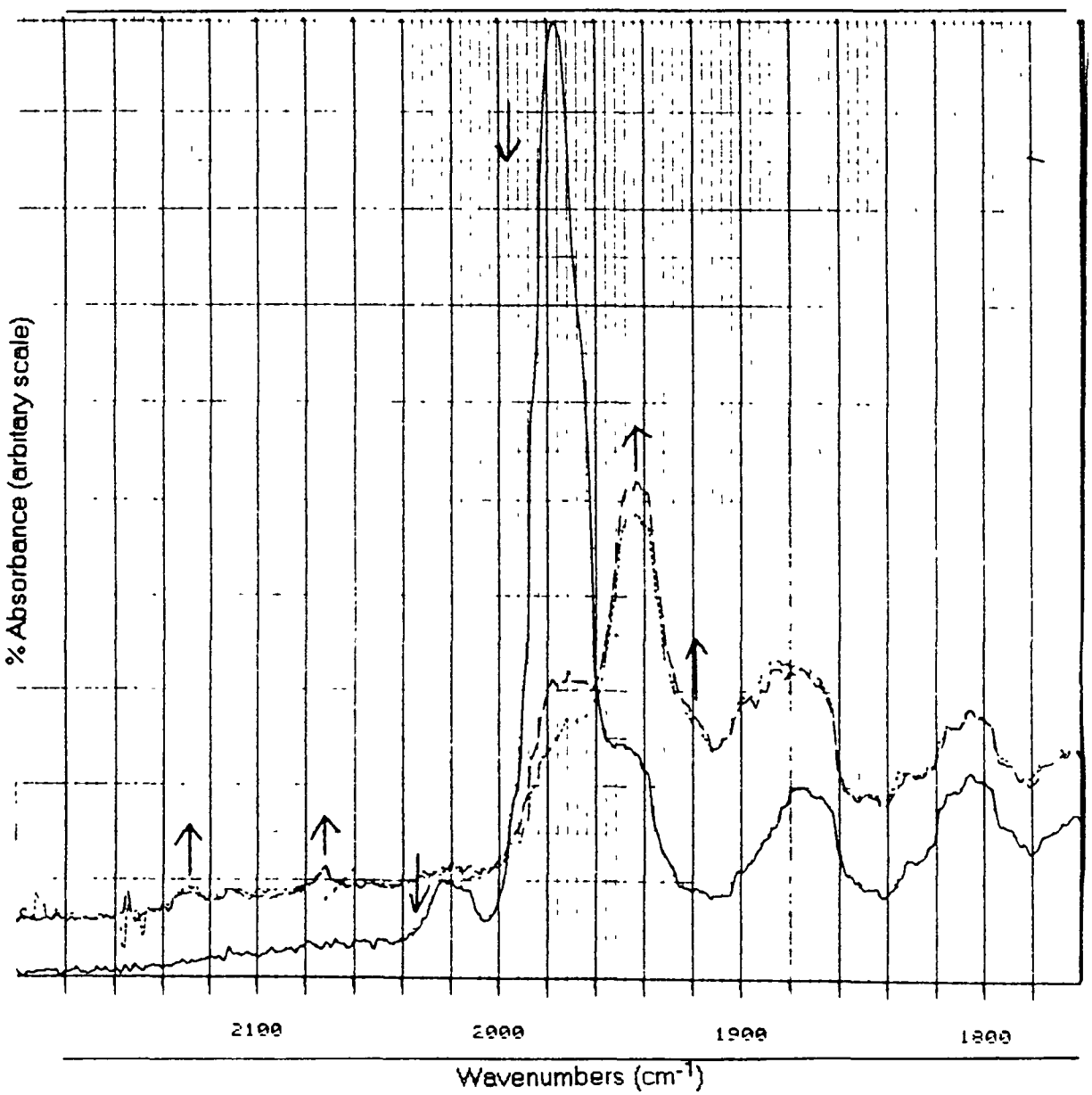

Figure 2.3.11: UV/vis spectrum of photolysis of $Cr(CO)_6$ in polystyrene at 120K.

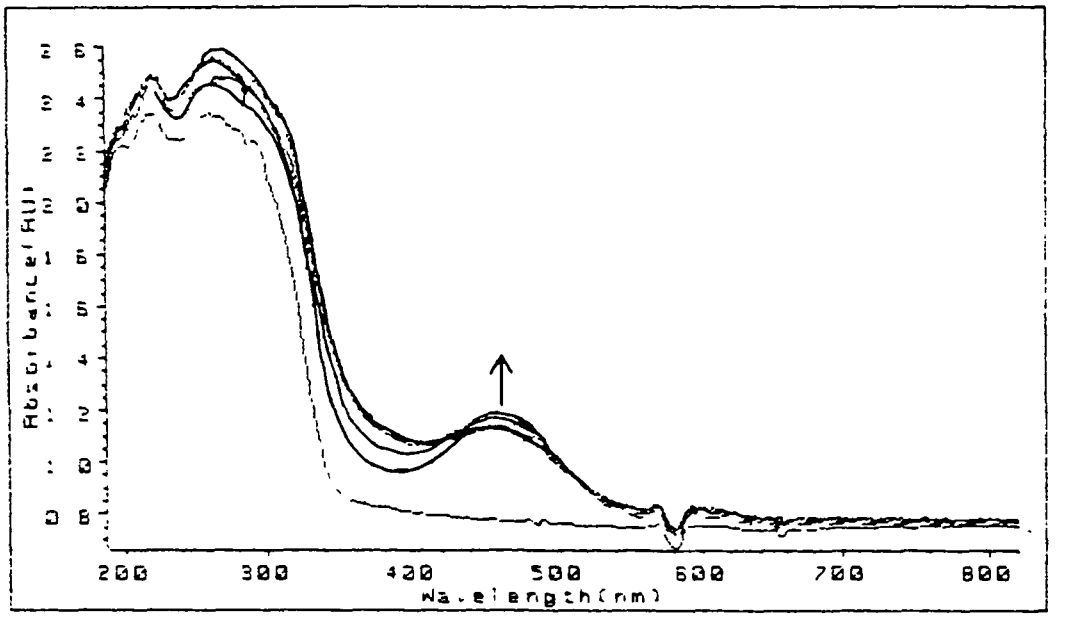

The position of the visible absorption band of $Cr(CO)_5$ is extremely sensitive to the matrix. It has been reported to vary from 624 nm for Ne to 490 nm for Xe [18]. In this work the absorption band of the $Cr(CO)_5$ species in polystyrene was found at 460 nm (Figure 2.3.3.2). This shift in the visible absorption band in different matrices is a result of the stereospecific interaction between $Cr(CO)_5$ and the species occupying the sixth coordination site.

2.3.4 Conclusion

Photolysis of the microencapsulated metal carbonyl complex resulted in the breakdown of the polymer surround with the release of the $MeCpMn(CO)_3$ species.

Studies on the photolysis of $CpMn(CO)_3$ and $ArCr(CO)_3$ in low temperature matrices have shown the formation of the dicarbonyl complex as the primary photoproduct [11-15] This complex is then stabilised by the interaction of a matrix molecule in the vacant coordination site. The results of our studies on the photolysis of $MeCpMn(CO)_3$ dispersed in low temperature polymer films also indicate the formation of the dicarbonyl complex as the primary photoproduct. The primary photoreaction is therefore loss of CO with the resulting formation of a polymer complex (Reaction 2 3 4 1)

$$MeCpMn(CO)_3 \xrightarrow{h\nu} MeCpMn(CO)_2(polymer) + CO \qquad 2.3.4.1$$

In the polymethylmethacrylate film the pendant oxygen on the polymer backbone interacts with the dicarbonyl complex. Whereas in the poly(styrene-co-4-vinylpyridine) the dicarbonyl fragment can either interact with the pendant nitrogen atoms or the aromatic units on the polymer backbone Unfortunately the infrared bands of the parent tricarbonyl species mask the higher energy bands of the dicarbonyl complexes that are formed

Photolysis of $ArCr(CO)_3$ dispersed in polystyrene at 120 K resulted in the formation of the polystyrene dicarbonyl complex (Reaction 2.3 4 2)

$$ArCr(CO)_3 \xrightarrow{h\nu} ArCr(CO)_2(PS) + CO \qquad 2.3.4.2$$

On warming the film containing the arene chromium species to room temperature a second species was observed. This species is possibly a dinuclear complex formed from the interaction of the parent and photoproduct as they are released from the matrix on warming the film (Reaction 2 3.4 3) . Rest and his coworkers [22] have recently

reported the formation of this dinuclear species (Reaction 2.3.4.3) on the photolysis of $ArCr(CO)_3$ in Nujol mulls at 77 K.

$$ArCr(CO)_2 + ArCr(CO)_3 \longrightarrow Ar_2Cr_2(CO)_5 \qquad 2.3.4.3$$

Again as in the $MeCpMn(CO)_3$ system some of the infrared bands are masked by those arising from the parent complex. As a result identifying the products formed is difficult, therefore laser flash photolysis of these complexes in toluene was used to help in the elucidation of their photoproducts.

Investigation of the photolysis of $Cr(CO)_6$ dispersed in low temperature polystyrene films, resulted in the formation of the pentacarbonyl polymer complex as reported by Rest *et al.* [21] (Reaction 2.3.4.4).

$$Cr(CO)_6 \xrightarrow{h\nu} Cr(CO)_5(PS) + CO \qquad 2.3.4.4$$

The visible absorption band of $Cr(CO)_5$ is extremely sensitive to the matrix [18] In the photolysis of $Cr(CO)_6$ carried out in polystyrene the band for $Cr(CO)_5$ was found at 460 nm.

2.4 References

1 J.K. Ruff, *Inorg.Chem.*, **10**, 409, (1971).

2 R.B. King, R.N. Kapoor, M.S. Suran, and P.N. Kapoor, *Inorg. Chem.*, **10**, 1851, (1971).

3 W. Strohmeier and K. Gerlach, *Z. Naturforsch.*, **15b**, 675, (1960)

4 W Strohmeier, J.F Guttenberger, and H Hellman, *Z Naturforsch.*, **19b**, 353, (1964)

5 W. Strohmeier and J K. Guttenberger, *Chem. Ber.*, **97**, 1871, (1964)

6 W Strohmeier and C Barbeau, *Z Naturforsch.*, **17b**, 848, (1962)

7 M L. Ziegler and R.K. Sheline, *Inorg. Chem.*, **4**, 1230, (1965)

8 E O Fischer and M Herberhold, *Experimentia Suppl.*, **9**, 259, (1964)

9 K.G Caulton, *Cord Chem. Revs.*, **38**, 1, (1981)

10 M S Wrighton, *Chem Revs.*, **74**, 401, (1974)

11 A.J Rest, J R. Sodeau, and D J Taylor, *J. Chem Soc., Dalton Trans.*, 651, (1978)

12 (a) P S. Braterman and J D Black, *J Organomet Chem.*, **39**, C3, (1972).
(b) J D Black, M J Boylan, and P S. Braterman, *J Chem Soc., Dalton Trans.*, 673, (1981)

13 M Herberhold, W. Kremnitz, H Trampisch, R.B. Hitam, A.J. Rest, and D.J. Taylor, *J Chem Soc., Dalton Trans.*, 1261, (1982)

14 R.H Hill and M S Wrighton, *Organometallics*, **6**, 632, (1987).

15 W. Jetz and W.A.G Graham, *Inorg Chem.*, **10**, 4, (1971)

16 W Srohmeier and D von Hobe, *Z. Naturforsch.*, **18b**, 981, (1963)

17 B S. Creaven, A.J Dixon, J M Kelly, C Long, and M. Poliakoff, *Organometallics*, **6**, 2600, (1987).

18 R.N Perutz and J J Turner, *J Amer. Chem Soc.*, **97**, 4791, (1975)

19 J M. Kelly and C. Long, *J. Organomet Chem.*, **231**, C9, (1982)

20 R.H Hooker and A.J. Rest, *J Chem. Soc., Dalton Trans.*, 761, (1984)

21 R.H Hooker and A.J. Rest, *J Organomet Chem.*, **249**, 137, (1983).

22 T.E Bitterwolf, K.A Lott, A.J. Rest and J. Mascetti, *J. Organomet Chem.*, **419**, 113, (1991).

Chapter 3

Flash Photolysis of $MeCpMn(CO)_3$, $ArCr(CO)_3$, and $Cr(CO)_6$ in Toluene Solution

3.1 Solution photolysis studies of $CpMn(CO)_3$, $MeCpMn(CO)_3$

Photolysis of $CpMn(CO)_3$ in solution is known to result in photosubstitution of CO to yield substituted derivatives in the presence of an entering nucleophillic group [1-8] (Table 2 1 1) (Reaction 3 1 1)

$$CpMn(CO)_3 + L \xrightarrow{h\nu} CpMn(CO)_2L + CO \qquad 3.1.1$$

The addition Reaction 3.1 1 was reported to occur with a quantum efficiency of unity for the replacement of a CO ligand by diphenylacetylene [9]. The quantum efficiency for the replacement of a CO ligand by pyridine was later calculated to be 0 65 [10].

Herberhold and his coworkers [11] investigated the photochemistry of the half sandwich carbonyl complexes of manganese, vanadium, and chromium in ambient temperature solutions (hexane, tetrahydrofuran (THF), cyclooctene). Photolysis of $CpMn(CO)_3$ in hexane which is an inert solvent, led to photodecomposition and loss of all CO ligands, whereas photolysis in the donor solvent THF leads to stabilisation of the $CpMn(CO)_2$ fragment in the form of the wine red complex $CpMn(CO)_2(THF)$ Irradiation of the tricarbonyl species in cyclooctene also resulted in the formation of the monosubstituted derivative.

The production of the $CpMn(CO)_2$ species as a photochemical intermediate has been suggested in many studies because the quantum yield of formation of $CpMn(CO)_2L$ (L = nucleophillic ligand) is independent of the concentration of L [10]. The photosubstitution reactions with triphenylphosphine (PEt_3) as an entering ligand were studied by Herberhold *et al.* [11] They reported the rate of disappearance of $CpMn(CO)_3$ upon photolysis in solution is not significantly influenced by the concentration of PEt_3, although

the ratio of mono and di-substituted products depends on the concentration of ligand. No evidence was recorded for the ejection of a cyclopentadienyl ligand

The results recorded by these workers [10,11] are characteristic of the photochemical substitution reactions of metal carbonyls in solution They generally proceed with high quantum efficiency and are independent of the nature and concentration of the incoming ligand. The primary photochemical reaction involves the dissociative loss of CO (Reaction 3.1.2).

$$CpMn(CO)_3 \xrightarrow{h\nu} CpMn(CO)_2 + CO \qquad 3.1.2$$

The flash photolysis of $CpMn(CO)_3$ in alkane solution has been studied by Creaven *et al.* [12]. Two transient species were observed, the first was identified as $CpMn(CO)_2S$ (S = cyclohexane or n-heptane). This solvent complex reacts with CO, N_2, and PPh_3 with similar rate constants to the corresponding group 6 pentacarbonyls in cyclohexane The second species was identified as $Cp_2Mn_2(CO)_5$ formed by the reaction of $CpMn(CO)_2S$ with unphotolysed $CpMn(CO)_3$ (Reactions 3 1.3-3.1.4)

$$CpMn(CO)_3 \xrightarrow{h\nu} CpMn(CO)_2S \qquad 3.1.3$$

$$CpMn(CO)_2S + CpMn(CO)_3 \longrightarrow (Cp)_2Mn_2(CO)_5 \qquad 3.1.4$$

Recent work on the $CpMn(CO)_3$ complex has centred on the metal-ligand bond dissociation energies in $CpMn(CO)_2L$ complexes Klassen *et al.* [13], in an effort to understand why $CpMn(CO)_3$ readily undergoes photochemical ligand substitution but is inert to thermal substitution, examined the Mn-L bond dissociation energies in a number of manganese complexes. They found the strength of the Mn-CO bond in $CpMn(CO)_3$ to

be remarkably high when compared to other known metal-CO bonds, but consistent with the observed reluctance of this complex to undergo thermal CO substitution reactions

3.2 Solution photolysis studies of $ArCr(CO)_3$

Strohmeier and von Hobe [14] were one of the first to investigate the photochemistry of the $ArCr(CO)_3$ complex Upon photolysis they found that $ArCr(CO)_3$ will undergo carbon monoxide or benzene exchange processes (Scheme 2.2.1).

Yaroskii *et al* [15] and Trembovler *et al* [16] have described spectral changes which occurred during irradiation of $ArCr(CO)_3$ in cyclohexane solution It was concluded that the spectral data are compatible with the formation of free arene and chromium hexacarbonyl during the reaction.Trembovler and coworkers [16] also determined the quantum yield of photodecomposition as a function of light intensity and proposed the simultaneous occurrence of three photodecay processes, with different dependencies on light intensity However no conclusions about the detailed photolytic reactions were drawn.

An extensive range of carbonyl substituted compounds of the form $ArCr(CO)_2L$ can be prepared by the UV photolysis of $ArCr(CO)_3$ in hydrocarbon solvents in the presence of suitable nucleophiles [17]. Wrighton and Ginley [18] investigated the mechanisms of photosubstitution They found that the quantum efficiency for the formation of $ArCr(CO)_2$(pyridine) from $ArCr(CO)_3$ and pyridine was independent of the irradiating wavelength (ϕ = 0.72 +/- 0 007 at 313, 366, or 436 nm) and of the concentration of pyridine. The quantum yield for the photosubstitution of a CO ligand in $(1,3,5\text{-}Me_3C_6H_3)Cr(CO)_3$ by N-dodecylmaleimide was calculated to be 0 9 +/- 0 09 at 313 nm and no evidence was found for the photolabilisation of the mesitylene ligand [19] Photolysis of $ArCr(CO)_3$ like

the photolysis of the analgous $CpMn(CO)_3$ complex in general leads to loss of only the carbonyl ligand Disubstituted $LM(CO)L_2$ (LM = ArCr or CpMn) complexes only seem to result from photolysis of $LM(CO)_2L$ when L is a reasonable π-acceptor ligand i e PPh_3 [20].

Wrighton and Haverty [21] investigated the efficiency of photosubstitution of $ArCr(CO)_3$ according to Reaction 3 2.3.

$$ArCr(CO)_3 \xrightarrow{h\nu} ArCr(CO)_2L + CO \qquad 3.2.3$$

(Ar = benzene or mesitylene, L = pyridine)

The results observed were consistant with dissociative loss of CO as the primary photoreaction Also, the nearly quantitative chemical yield (0 72 +/- 0 07) of $ArCr(CO)_2$(pyridine) implied that if arene group exchange occurred at all under these conditions it was a very minor part of the photochemistry

Exchange of the arene ligands was believed to proceed *via* the one step dissociation of the excited molecule to give $Cr(CO)_3$ and arene. However studies by Gilbert *et al* [22] in cyclohexane with 313 nm irradiation have shown that benzene exchange is inefficient (ϕ_{C6H6} = 0 12) compared with carbonyl exchange (ϕ_{CO} = 0.72) This value is in accordance with that reported by Wrighton and Haverty [21] Competition experiments suggest that the species $ArCr(CO)_2$ may be the precursor in the exchange of the benzene ligand as well as the CO exchange [22]. On flash photolysis in cyclohexane solution a weakly absorbing transient species was recorded, which they considered to be the primary species $ArCr(CO)_2$. This species reacted further within one millisecond to form a second transient species The formation of both transients was quenched if the

solution was saturated with CO at one atmosphere pressure so they concluded that exchange with benzene involves the primary species as an intermediate and does not occur through a one step dissociation of the excited molecule [22]

Bamford *et al.* [23] reported results of the photolysis of $ArCr(CO)_3$ in isooctane and methyl methacrylate solutions which were consistant with the findings of Wrighton and Haverty [21] and Gilbert *et al.* [22].

Although both the arene and carbonyl ligands can be replaced by nucleophiles, thermal conditions generally favour arene displacement while photolysis usually leads to CO loss Strohmeier and Stancco [24] carried out initial work on the exchange of various substituted arene ligands with the arene moiety in the $ArCr(CO)_3$ complex. These exchange reactions were determined to be equilibrium processes and were carried out at high temperatures in sealed tubes. Addition of donor solvents such as THF or benzonitrile catalyses the arene exchange after allowing equilibrium to occur at reasonable rates and temperatures (at 140^{o}C or below)

More recently Traylor *et al.* [25] investigated the thermal exchange of arene ligands. They carried out a kinetic study of the displacement of benzene or substituted benzenes from their chromium carbonyl complexes by other substituted benzenes. The reactions were carried out at 170^{o}C in vacuum sealed NMR tubes They stated that the exchange process occurs *via* a η^6 to η^4 hapticity change at the arene ligand resulting in a simple stepwise displacement of the arene (Scheme 3 2 1). The catalytic ligand L can be any two electron Lewis base, including ketones, nitriles, carbonyl groups (M-C≡O), alkenes or even another molecule of arene

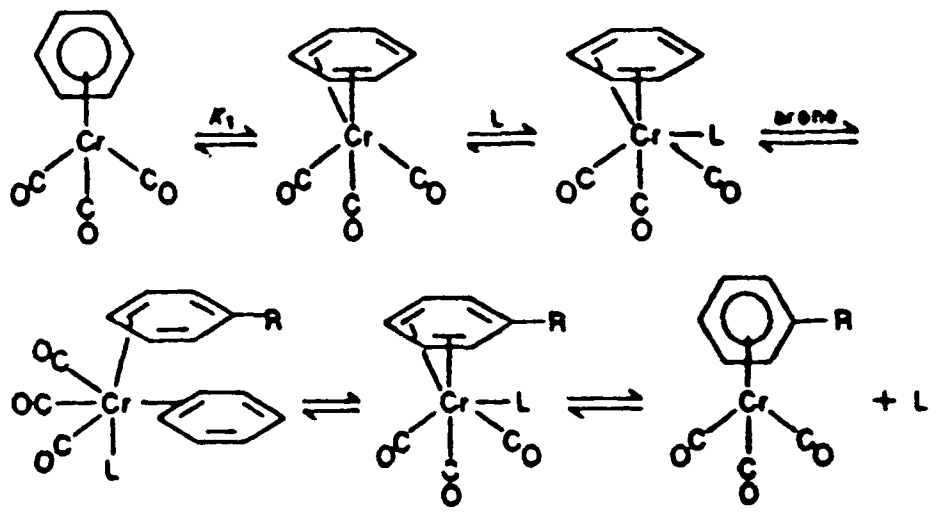

Scheme 3.2.1

3.3 Results and Discussion

3.3.1 Laser flash photolysis of $MeCpMn(CO)_3$ in toluene solution

Laser flash photolysis experiments of $MeCpMn(CO)_3$ were carried out at room temperature in toluene solution, the excitation wavelength was 355 nm Toluene was chosen as the solvent because of its aromatic character and its ability to solvate the polymeric ligands. The interaction of the photofragments with toluene could then be compared to the photochemical reactions in the aromatic polymer film (i e polystyrene, discussed in Chapter 2).

The UV\vis spectrum of $MeCpMn(CO)_3$ in toluene is shown in Figure 3.3.1.1. The extinction coefficient of $MeCpMn(CO)_3$ in toluene was calculated to be 628.54 $dm^3mol^{-1}cm^{-1}$ at 354 nm.

The spectrum of the only observed species recorded at the time of flash and 1.5 s after the flash is shown in Figure 3.3.1.2. Its λ_{max} is centred at 360 nm. This species was formed immmediately in the flash and its risetime is too rapid to be detected with the equipment available. The decay of this complex was investigated.

Figure 3.3.1.1: UV\vis spectrum of $MeCpMn(CO)_3$ in toluene

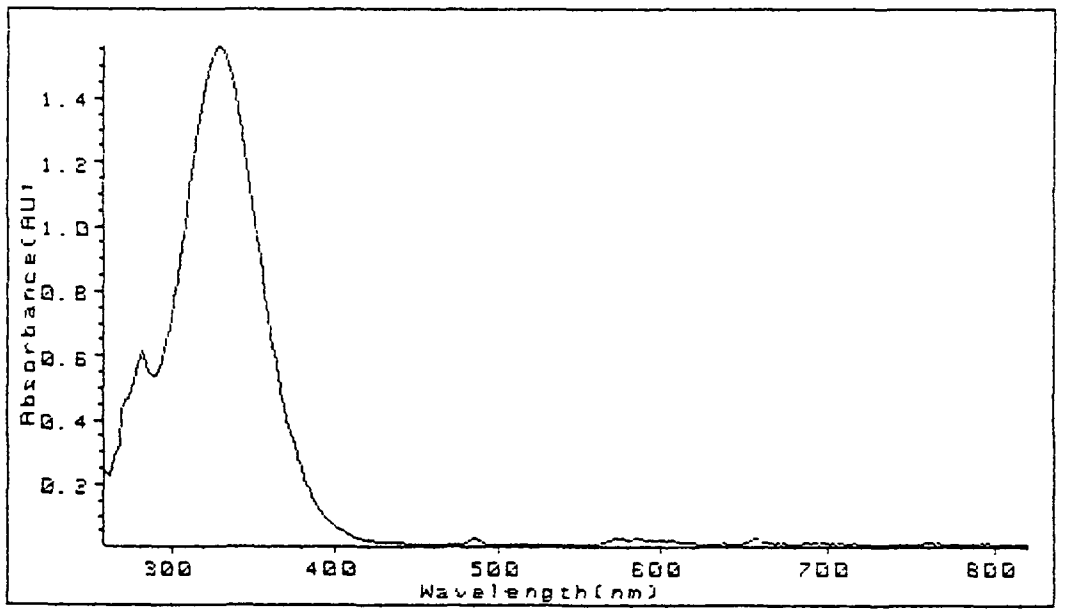

Figure 3.3.1.2: UV/vis difference spectrum observed following the flash photolysis of $MeCpMn(CO)_3$ in toluene solution under an Ar atmosphere

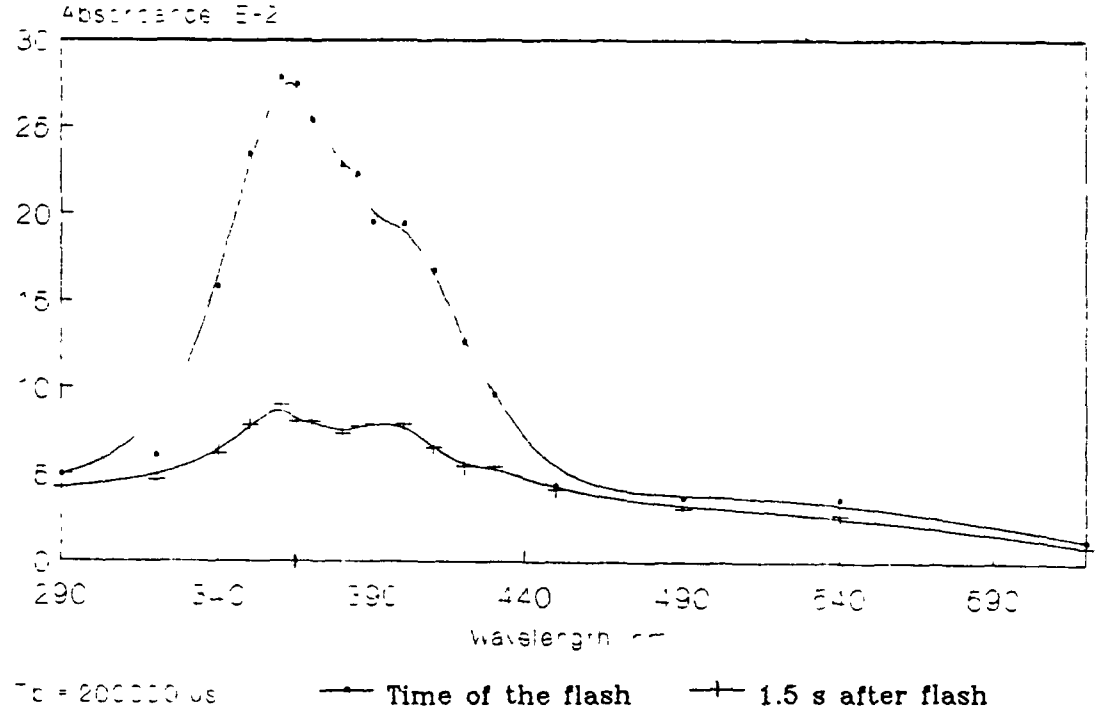

The $MeCpMn(CO)_3$ system in toluene is not fully reversible under an Argon atmosphere. As can be seen from Figure 3.3.1.3 there is some depletion of the parent tricarbonyl during the course of the experiment.

Figure 3.3.1.3: UV/vis spectra of $MeCpMn(CO)_3$ in toluene recorded before and after the flash photolysis experiment.

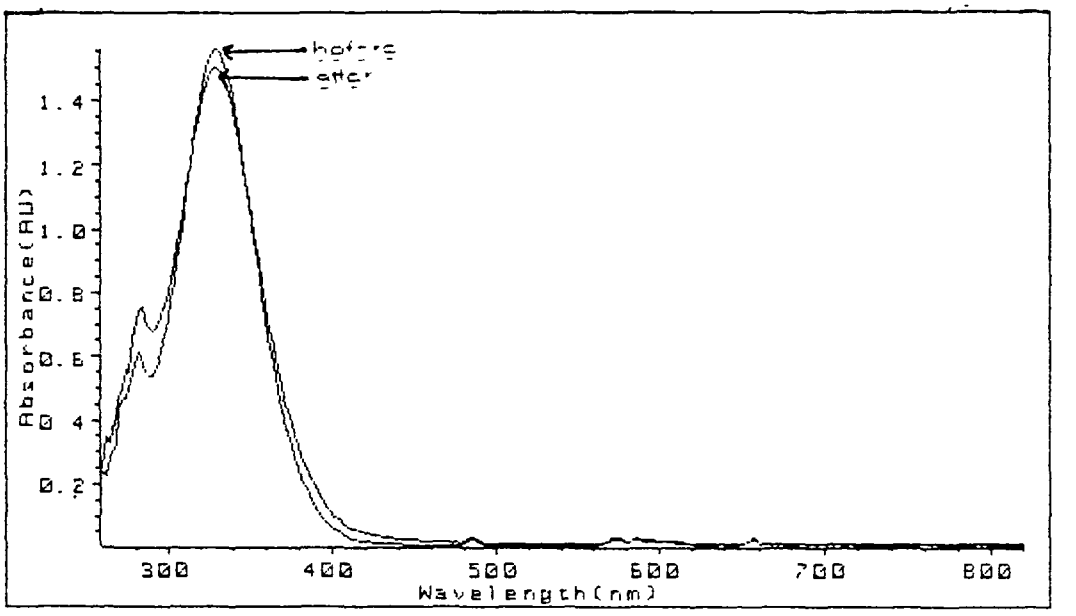

3.3.1.1 Primary Photoproduct

The effect of saturating the solvent with CO was investigated. Under a CO atmosphere the system was found to be completely reversible as would be expected if the primary photoprocess involves CO loss. The UV/vis difference spectrum of the transient species recorded under a CO atmosphere is shown in Figure 3.3.1.4.

Figure 3.3.1.4: UV/vis difference spectrum of $MeCpMn(CO)_2$(toluene) recorded under 1 0 atm CO

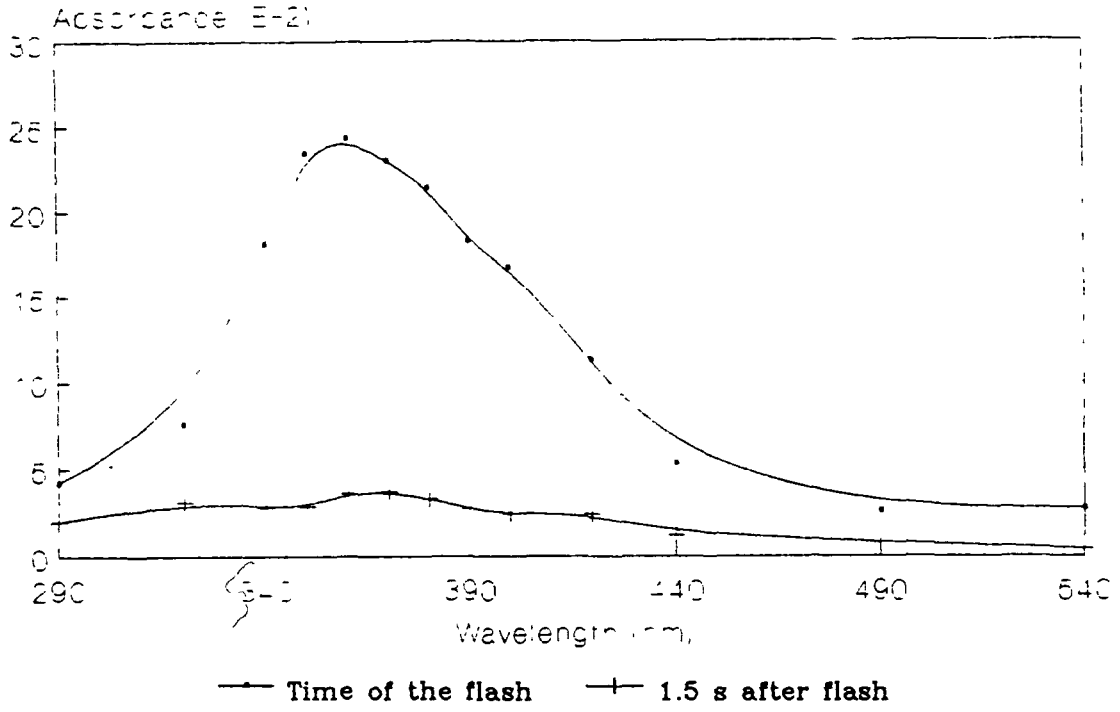

The lifetime of the transient species was decreased upon addition of CO to the system, whereas its yield was unaffected Figure 3.3 1 5 shows the decay of the observed transient species under both argon and carbon monoxide atmospheres

If the primary photoreaction is loss of CO then the yield of the primary photoproduct would be unaffected by the addition of CO This is because the formation of the primary photoproduct is a result of the photophysical processes. Secondly the presence of CO in solution ensures that the backreaction of the photolytically formed species proceeds

efficiently. As both of these conditions are satisfied (Figure 3 3 1 5) the primary photochemical reaction is given by Reaction 3 3 1 1

$$MeCpMn(CO)_3 \longrightarrow MeCpMn(CO)_2 + CO \qquad 3.3.1.1$$

Figure 3.3.1.5: Decay of the observed transient species under (a) argon and (b) CO atmospheres (see Section 5 2 1 for explanation of axes)

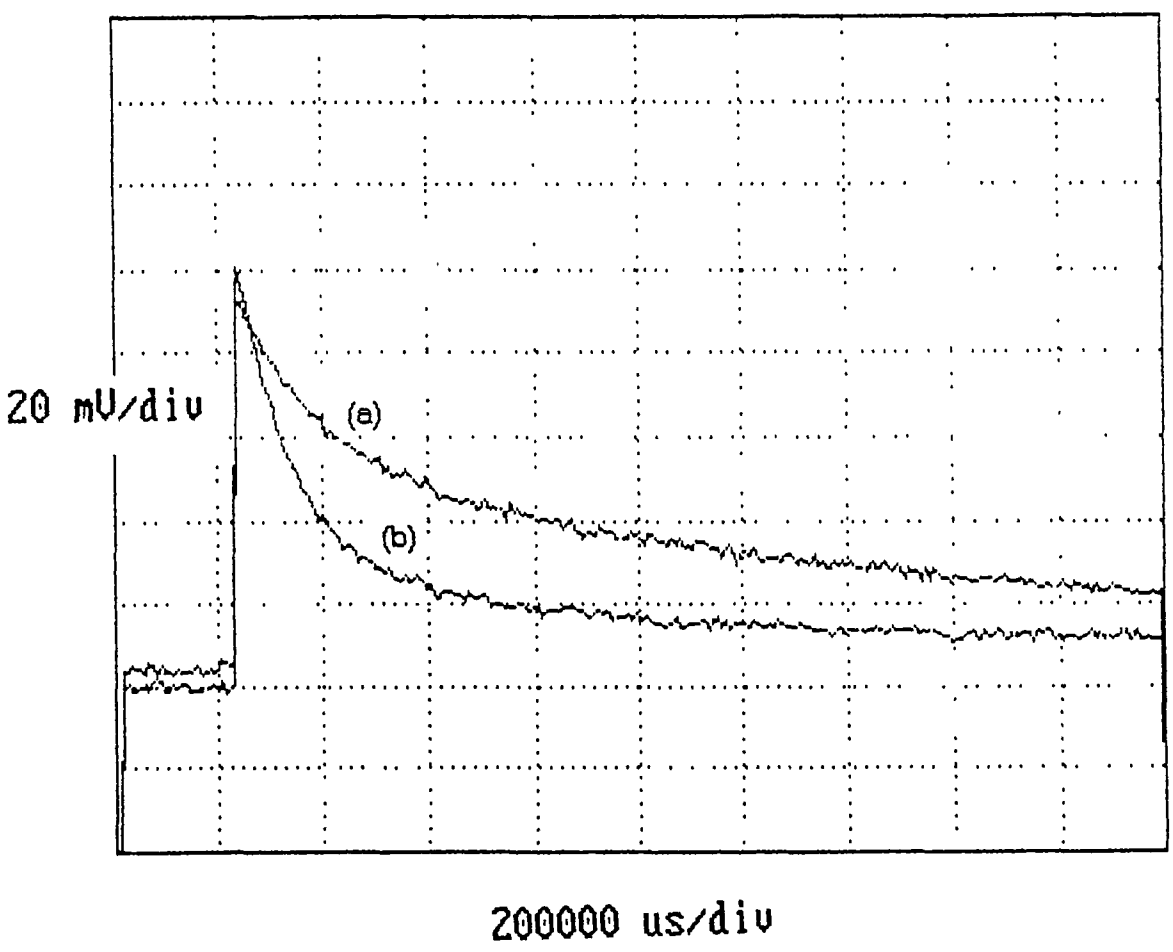

The $MeCpMn(CO)_2$ species upon formation coordinates to a solvent molecule acting as a token ligand. This fact has been reported by several workers for other systems Perutz and Turner reported the variation in the UV/vis maximum of the pentacarbonyl fragment was due to the interaction of the coordinatively unsaturated species with varying solvents [26]. Simon *et al.* investigating the photochemical reactions of $Cr(CO)_6$ in methanol, found that the risetime of 2.5 ps was due to the coordination of the pentacarbonyl by methanol [27] Creaven *et al* [12] observed the formation of the $CpMn(CO)_2S$ species as the primary photoproduct on the photolysis of $CpMn(CO)_3$ in cyclohexane solution. Several studies in low temperature matrices have also identified the $CpMn(CO)_2S$ (S = matrix species) as the primary photoproduct [11,28,29,30]

Thus from the experimental results obtained and the observations stated in the literature it can be concluded that the transient species observed is the dicarbonyl toluene complex (Reactions 3.3.1.1 and 3.3.1.2)

$$MeCpMn(CO)_2 + \text{toluene} \longrightarrow MeCpMn(CO)_2(\text{toluene}) \qquad 3.3.1.2$$

The lifetime of the primary photoproduct at a given concentration of $MeCpMn(CO)_3$ was determined before and after the addition of carbon monoxide and the difference was used to calculate the rate constant for the reaction of the species with carbon monoxide. The concentration of carbon monoxide in toluene was determined from its solubility at various pressures of CO [31] (see experimental section for detailed calculations). The rate constant for the reaction was calculated to be 1.18×10^3 $dm^3mol^{-1}s^{-1}$ (Table 3.3.1.1 and Figure 3.3.1.6) This is two orders of magnitude slower for the equivalent reaction in cyclohexane (3.2×10^5 $dm^3mol^{-1}s^{-1}$) [12] This is because the Mn-solvent bond is much stronger in toluene than cyclohexane

Table 3.3.1.1: The effect of CO on the lifetime of the primary photoproduct

[$MeCpMn(CO)_3$] = 1 63 x 10^{-3} M (k_{obs} = 1st order decay of primary photoproduct)

[CO] x10^{-3} M	k_{obs} - (k_{obs} Ar)
1 88	2 35 s^{-1}
3 77	4 33 s^{-1}
5 65	6 50 s^{-1}
7 53	9 04 s^{-1}

Slope = 1181 ± 48 43 $dm^3mol^{-1}s^{-1}$, Intercept = -4 64 ± 0.2 s^{-1};

Correlation coefficient = 0 99832

Figure 3.3.1 6: Plot for second order rate constant for $MeCpMn(CO)_2$(toluene) + CO

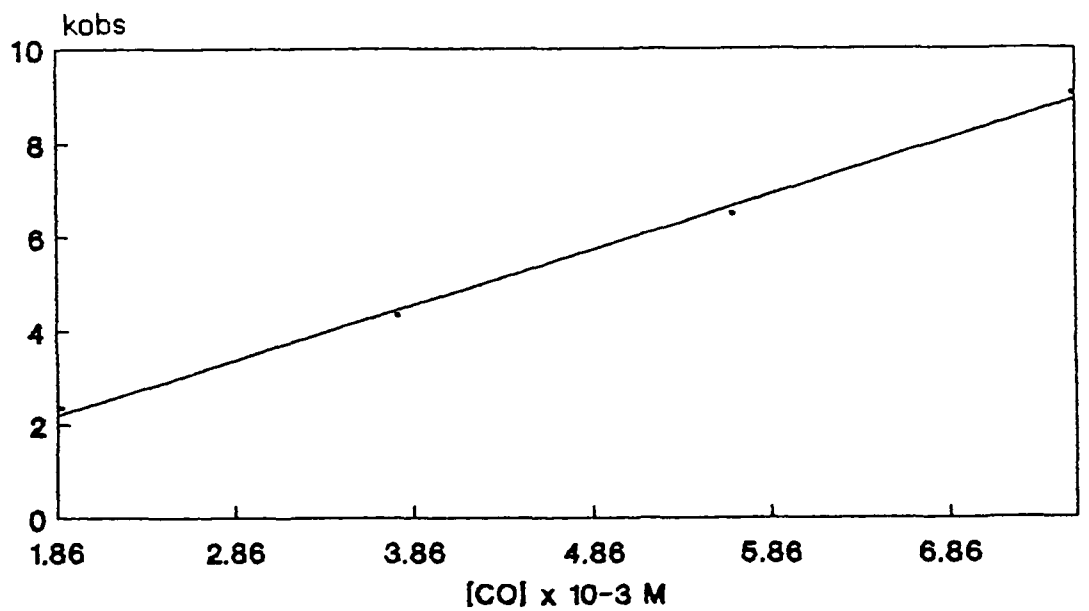

3.3.1.2 Effect of Power of Laser on Concentration of Primary Photoproduct

In order to confirm that the formation of the $MeCpMn(CO)_2$ species was a result of a single photon event, an experiment was carried out in which the intensity of the laser pulse was varied. The absorbance of the primary photoproduct should vary linearly with the power of the laser. This was found to be the case, as can be seen from Figure 3.3.7 where the relative power of the laser was plotted against the absorbance of primary photoproduct formed.

Figure 3.3.1.7: Plot showing the variation in the absorbance of the $MeCpMn(CO)_2$(toluene) species with relative laser power

---

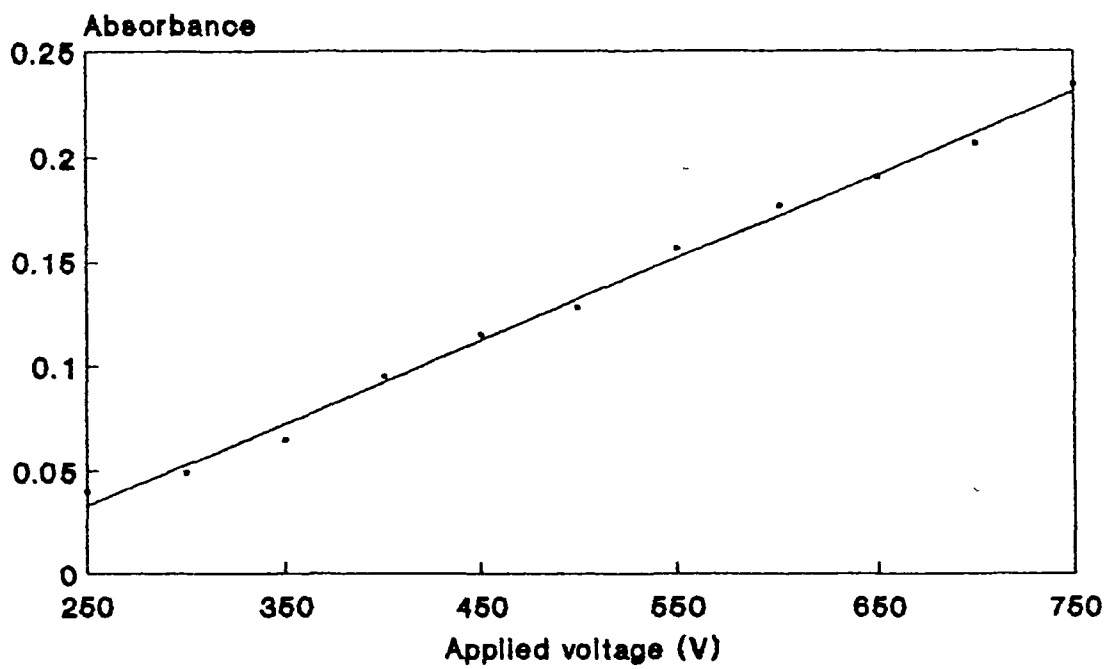

---

3 3.1.3 Effect of Parent Concentration on Primary Photoproduct

Increasing the parent concentration ($MeCpMn(CO)_3$) under an argon atmosphere results in an increase in the amount of primary photoproduct ($MeCpMn(CO)_2$(toluene)) formed in the flash. The rate of decay of the $MeCpMn(CO)_2$(toluene) species is unaffected by the parent concentration as shown in Table 3 3 1.2. All the decay rates are within experimental error of each other. This indicates that the primary photoproduct does not react with the parent to form a dinuclear species as observed in cyclohexane (Reaction 3 3.1 3) [12]

$$CpMn(CO)_2(cyclohexane) + CpMn(CO)_3 \longrightarrow Cp_2Mn_2(CO)_5 \qquad 3.3.1.3$$

Table 3.3.2: Effect of parent concentration on the lifetime of the primary photoproduct

$[MeCpMn(CO)_3]$ 10^{-3} M	k_{obs} for decay of Primary Photopdt
0 92	3 20
1 07	4 65
1.21	3.17
1 65	4 32

3.3.1.4 Activation parameters for the reaction of CO with $MeCpMn(CO)_2$(toluene)

The activation parameters were determined using the Arrhenius and Eyring equations (Section 5.3.8) k_2 was used instead of k_{obs} for the reaction of $MeCpMn(CO)_2$(toluene) with CO. $k_2 = k_{obs}/[CO]$. The parameters are listed in Table 3.3.1.3. The experimental data is summarised in Table 3.3.1.4 and shown graphically in Figures 3.3.1.8.

Table 3.3.3: Activation parameters for reaction of $MeCpMn(CO)_2$(toluene) with CO

E_{act} = 44.12 $kJmol^{-1}$

$\Delta H^{\ddagger}$ = 41.55 $kJmol^{-1}$

$\Delta S^{\ddagger}$ = -42.93 $Jmol^{-1}K^{-1}$

$\Delta G^{\ddagger}$ = 54.34 $kJmol^{-1}$

$\Delta G^{\ddagger}$ was estimated at 298 K

From the data we can see that the activation energy for the reaction is relatively low and the activation entropy implies an associative process. Thus the reaction of $MeCpMn(CO)_2$(toluene) with CO involves a transition state in which the CO molecule binds to the dicarbonyl complex before displacing the toluene molecule (Scheme 3.3.1.1). The activation energy determined for the reaction of $MeCpMn(CO)_2$(toluene) with CO is slightly higher than that determined in other systems. Creaven calculated the activation energy to be 30 ± 4 $kJmol^{-1}$ for the reaction of $CpMn(CO)_2(S)$ with various ligands including CO in alkane solvents [32]. Wrighton reported a similar value (33 ± 4 $kJmol^{-1}$) for the oxidative addition of a range of R_3SiH compounds to $CpMn(CO)_2$ in low

temperature matrices [30]. This slight difference in the activation energies is probably a result of the stronger Mn-S bond in toluene compared to alkane solvents [32] and the Mn-matrix interaction [30]

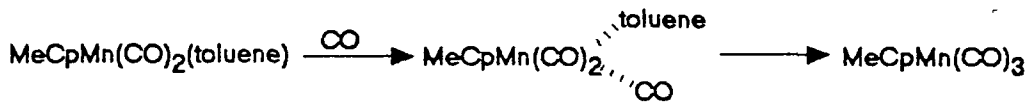

Scheme 3.3.1.1

Table 3.3.1.4: Experimental data for the determination of the activation parameters for the reaction of $MeCpMn(CO)_2$(toluene) with CO

T K	1/T K 10^{-3}	k_2	Ln k_2	Ln (k_2/T)
287	3 48	933 60	6 84	1 18
293	3 41	1431 61	7 27	1 59
299	3 34	1760 96	7 47	1 77
303	3 30	2803 45	7 94	2 22
308	3 25	3407 70	8 13	2 40
318	3 14	5867 20	8 68	2 92
323	3.10	6848 61	8 83	3 05

Arrhenius Plot

Slope = -5306 ± 265

Intercept = 25 33 ± 0 09

Correlation coefficient = 0 99381

E_{act} = 44 12 ± 2 1 kJmol^{-1}

Eyring Plot

Slope = -4997 ± 260

Intercept = 18 60 ± 0 09

Correlation coefficient = 0 99325

$\Delta H^{\ddagger}$ = 41.55 ± 2 2 kJmol^{-1}

$\Delta S^{\ddagger}$ = -42 93 ± 0 75 Jmol^{-1}K^{-1}

Figure 3.3.1.8: Arrhenius plot (a) and Eyring plots (b) for the reaction of $MeCpMn(CO)_2$(toluene) with CO.

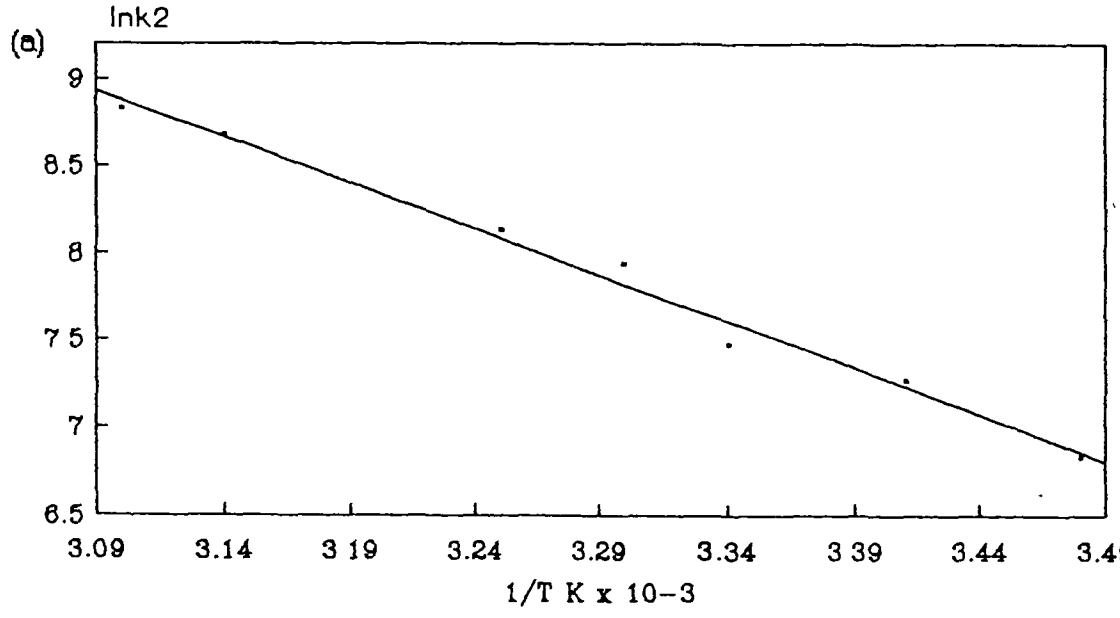

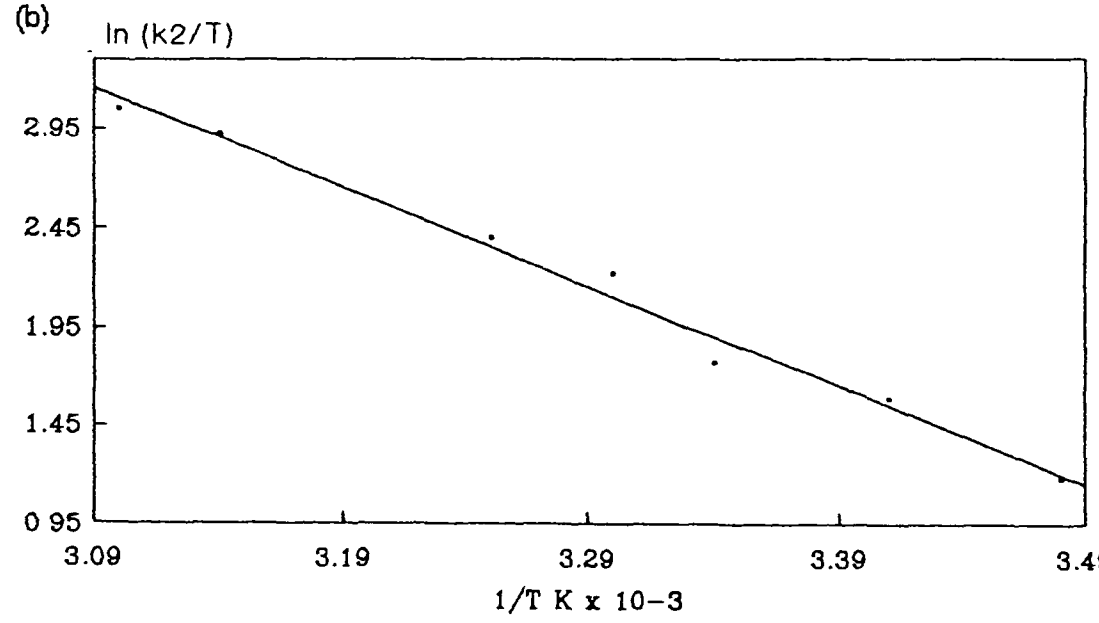

3.3.1.5. Laser flash photolysis of $MeCpMn(CO)_3$ in toluene in the presence of pyridine

The aim of this work was to compare the reaction of monomeric and polymeric pyridine ligands with the dicarbonyl toluene species. The pyridine in solution displaces the toluene from the primary photoproduct to form the pyridine dicarbonyl complex (Reactions 3.3.1.4 and 3.3.1.5). The $MeCpMn(CO)_2$(pyridine) complex formed is red-orange in colour.

$$MeCpMn(CO)_3 \xrightarrow{h\nu} MeCpMn(CO)_2(toluene) \qquad 3.3.1.4$$

$$MeCpMn(CO)_2(toluene) + pyridine \longrightarrow MeCpMn(CO)_2(pyridine) \qquad 3.3.1.5$$

The growth of the band at 430 nm in the UV/vis spectrum (Figure 3.3.1.10) indicates the formation of the pyridine complex during the course of the experiment. This is confirmed by referring to work carried out by Giordano and Wrighton on the photosubstitution of CO by pyridine in $CpMn(CO)_3$ and related complexes [10].

The rates of reaction of monomeric and polymeric pyridine with the dicarbonyl toluene complex were then investigated (Table 3.3.1.5). The activation parameters for this reaction (Reaction 3.3.1.5) were also determined. The polymeric pyridine was in the form of poly(styrene-co-4-vinylpyridine). The mole ratio of styrene to 4-vinylpyridine was varied to form polymers of different loadings of binding sites (pendant nitrogen atoms).

Figure 3.3.10: Changes observed in the UV/vis spectrum of $MeCpMn(CO)_3$ during the course of a flash photolysis experiment in the presence of pyridine

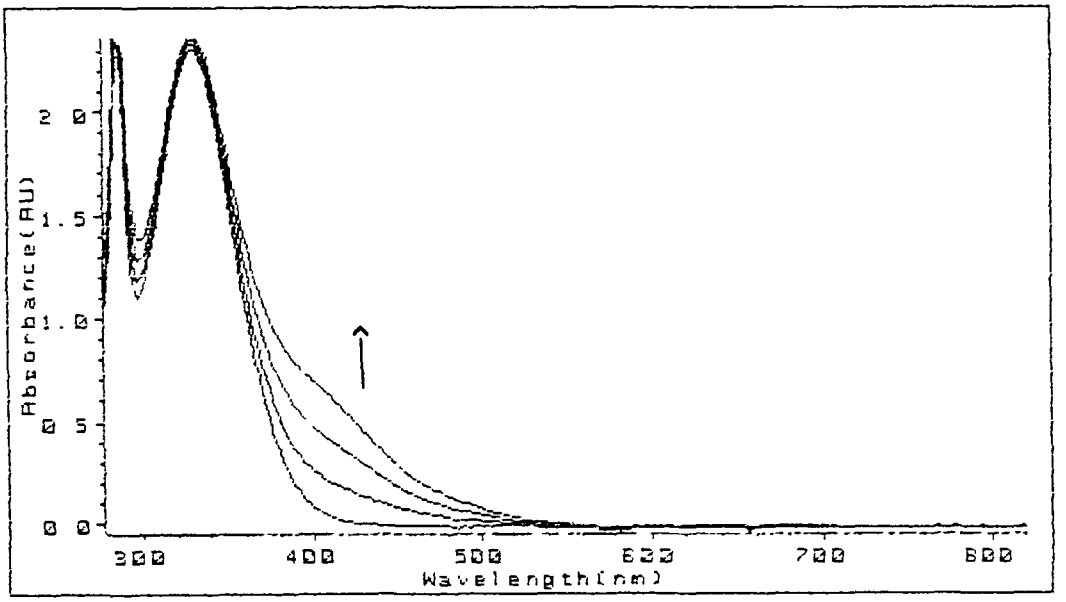

As can be seen from the second order rate constants determined (Table 3.3.1.5), the rates of reaction are higher for the copolymers than for free pyridine in toluene solution. The second order rate constants also increase within the polymeric ligands as the loading of nitrogen on the polymer backbone decreases. One would have expected the polymeric ligands to have lower rate constants because of diffusion constraints posed by the polymer coils in solution, especially in the case of the lower loading polymers where the amount of polymer in solution is increased to maintain pyridine concentration. Initially it was thought that the difference in rates may be a result of a difference in the Gibbs free energy of activation ($\Delta G^{\ddagger}$) or the activation energy itself (E_{act}) for the reaction

Therefore the activation parameters for the reaction of the dicarbonyl toluene complex with the monomeric and polymeric ligands were determined.

Table 3.3.1.5: The second order rate constants determined for the reaction of $MeCpMn(CO)_2$(toluene) with both monomeric and polymeric pyridine ligands.

Ligand	k_2 ($dm^3mol^{-1}s^{-1}$)
Pyridine	0.93×10^3
5:1 copol	1.96×10^3
10:1 copol	2.54×10^3
20:1copol	2.61×10^3
30:1 copol	2.89×10^3

copol = poly(styrene-co-4-vinylpyridine)

Tables 3.3.1.6 to 3.3.1.10 and Figures 3.3.1.10 to 3.3.1.15 give the experimental data and graphical representations of the second order rate constants

Table 3.3.1.6 and Figure 3.3.1.10: Second order rate constant for the reaction of $MeCpMn(CO)_2$(toluene) with pyridine

[Pyr]M x 10^{-2}	k_{obs} s^{-1}
0.62	14.2
1.23	22.11
1.85	26.8
2.47	31.83

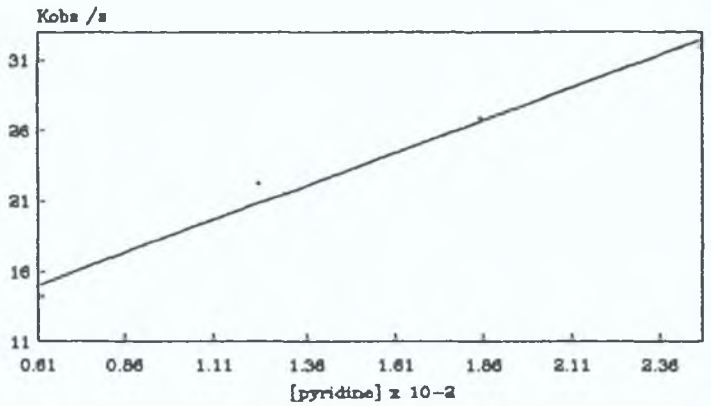

Slope = 931.93 ± 86.33 $dm^3mol^{-1}s^{-1}$

Intercept = 9.36 ± 1.2 s^{-1}

Correlation coefficient = 0.99153

Table 3.3.1.7 and Figure 3.3.1.11: Second order rate constant for the reaction of $MeCpMn(CO)_2$(toluene) with 5:1 copol

[Pyr]M x10^{-2}	k_{obs} s^{-1}
0.80	17.87
1.24	26.84
1.84	37.77
2.33	48.31

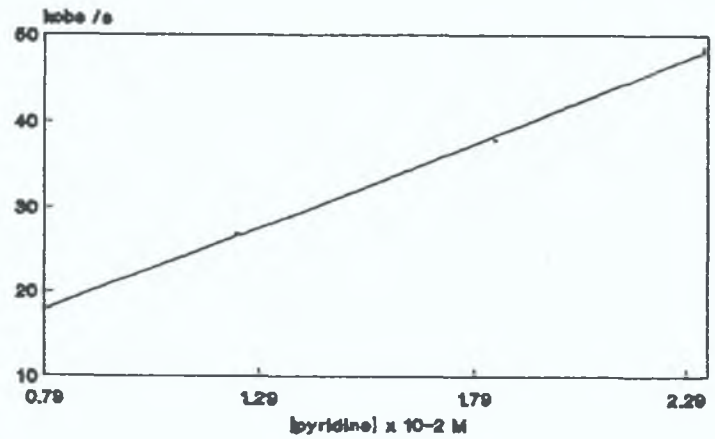

Slope = 1959.9 ± 47.01 $dm^3mol^{-1}s^{-1}$

Intercept = 2.26 ± 0.55 s^{-1}

Correlation coefficient = 0.99943

Table 3.3.1.8 and Figure 3.3.1.12: Second order rate constant for the reaction of $MeCpMn(CO)_2$(toluene) with 10:1 copol.

[Pyr]M x10^{-2}	k_{obs} s^{-1}
0.58	11.14
1.12	23.47
1.69	30.80
2.89	66.63
3.99	96.73

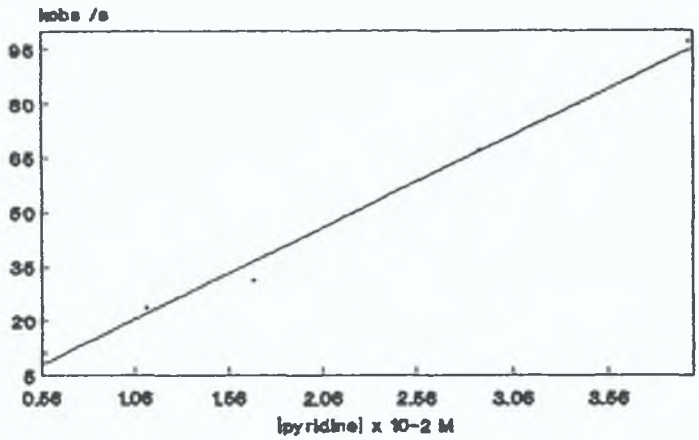

Slope = 2537.3 ± 141.64 $dm^3mol^{-1}s^{-1}$

Intercept = -6.37 ± 3.91 s^{-1}

Correlation coefficient = 0.99536

Table 3.3.1.9 and Figure 3.3.1.13: Second order rate constant for the reaction of MeCpMn(CO)2(toluene) with 20:1 copol.

[Pyr]M x10^{-2}	k_{obs} s^{-1}
0.84	8.68
1.73	27.45
2.46	47.06
3.37	73.03
4.03	90.55

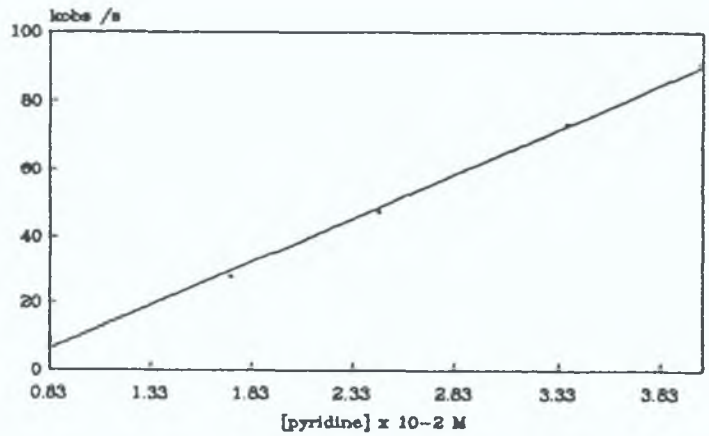

Slope = 2610.3 ± 82.88 $dm^3mol^{-1}s^{-1}$

Intercept = -15.56 ± 2.10 s^{-1}

Correlation coefficient = 0.99849

Table 3.3.1.10 and Figure 3.3.1.14: Second order rate constant for the reaction of $MeCpMn(CO)_2$(toluene) with 30.1 copol

[Pyr]M x10^{-2}	k_{obs} s^{-1}
2 78	17.94
2 98	23 25
3 14	27 50
3.34	33 50
3 57	40 83

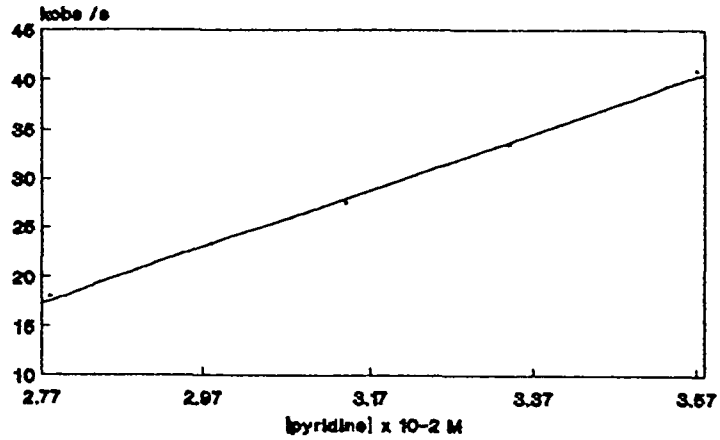

Slope = 2894.4 ± 73 93 $dm^3mol^{-1}s^{-1}$

Intercept = -62.92 ± 0 45 s^{-1}

Correlation coefficient = 0 99902

3.3.1.6 Activation parameters for the reaction of $MeCpMn(CO)_2$(toluene) with pyridine ligands

The activation parameters determined for the reaction of the dicarbonyl complex with both monomeric and polymeric pyridine are summarised in Table 3 3 1.11

In the case of the reaction of free pyridine with the dicarbonyl complex, the activation parameters are based on k_2 ($k_2 = k_{obs}/[pyr]$). In the case of the polymeric ligands it was decided to use k_{obs} for the calculations, k_{obs} was used because it appeared that the rates of reaction observed were not dependent on pyridine concentration alone but were also affected by the concentration of polymer in solution Because in the lower loading polymers, which had the higher rates of reaction, the amount of polymer in solution had to be increased to maintain the concentration of pyridine in solution Therefore in the case of pyridine $k_{obs} = k_2$[pyridine], for polymeric ligands it may be possible that kobs = k_2([polymer] + [pyr])

Table 3.3.1.11: Activation parameters for the formation of $MeCpMn(CO)_2$(pyridine) on flash photolysis of $MeCpMn(CO)_3$ in the presence of pyridine ligands in toluene solution

Ligand	E_{act} kJmol^{-1}	$\Delta H^{\ddagger}$ kJmol^{-1}	$\Delta S^{\ddagger}$ Jmol^{-1}K^{-1}	$\Delta G^{\ddagger}$ kJmol^{-1}
Pyridine	53 60	51 12	-3 33	52.11
5 1 copol	49 96	47 42	-51 93	62 89
10:1 copol	53 83	51 30	-44 30	64 50
20 1 copol	46 23	43 99	-64 02	63 07
30:1 copol	41.64	39.08	-85.26	64 49

The activation energies for the monomeric and polymeric pyridine ligands are essentially the same with the two lower loading polymers (20.1,30 1) having the lowest activation energy This corresponds to the second order reaction rates for the reactions If two reactions of similiar activation energies proceed with different rates, there should be a difference in their entropy of activation. As can be seen from Table 3 3 11 the negative value of $\Delta S^{\ddagger}$ for the polymeric ligands indicates the associative nature of the transition state In the case of monomenc pyridine the low negative value would seem to indicate that the reaction is not associative. Although the values of $\Delta S^{\ddagger}$ for the polymeric ligands are within experimental error of each other there is a definite trend as the loading of nitrogen on the polymer backbone is decreased (except for the 10·1 copolymer) The lower loading polymers being involved in a more associative process. The values of the Gibbs free energy of activation are practically the same (monomeric pyridine being slightly lower), so there is no difference in the spontaneity of the process regardless of whether the pyridine is monomeric or polymeric in nature These results would imply that the differences in k_{obs} with the polymenc ligands is not the result of a difference in reaction mechanisms for these processes

As the trend in k_{obs} can not be attributed to a difference in the $\Delta G^{\ddagger}$ for the reactions, it is probably the result of a polymer effect in solution. One possibility could be that the parent tricarbonyl diffuses into the polymer coils and then on photolysis the concentration of pyridine close to the reaction is high because of polymer coiling.

However the most likely explanation is that after formation of the $MeCpMn(CO)_2$(toluene) complex, the toluene is displaced by pyridine and there is also some interaction between the dicarbonyl complex and the polymer backbone. Possibly the aromatic units on the polystyrene backbone interact with the dicarbonyl complex. However this would

require that the dicarbonyl complex be able to distinguish between the solvent toluene and polystyrene.

Table 3.3.1.12: Experimental data for the determination of the activation parameters for the formation of $MeCpMn(CO)_2(pyridine)$ for 1.24×10^{-2} M pyridine in toluene

---

T K	$1/T\ K \times 10^{-3}$	$k_2\ s^{-1}$	$Ln\ k_2$	$Ln(k_2/T)$
292	3.42	3141.94	8.05	2.38
299	3.34	4908.06	8.50	2.80
303	3.30	6218.55	8.74	3.02
307	3.26	8916.94	9.10	3.37
314	3.18	14354.03	9.57	3.82
318	3.14	15879.84	9.67	3.91
323	3.09	28391.13	10.25	4.48

Arrhenius Plot

Slope = -6447.1 ± 317.73

Intercept = 30.06 ± 0.09

Correlation coefficient = 0.99398

E_{act} = 53.60 ± 2.7 kJmol^{-1}

Eyring Plot

Slope = -6148.5 ± 324.27

Intercept = 23.36 ± 0.09

Correlation coefficient = 0.99312

$\Delta H^{\ddagger}$ = 51.12 ± 2.2 kJmol^{-1}

$\Delta S^{\ddagger}$ = -3.33 ± 0.6 Jmol^{-1}K^{-1}

Figure 3.3.1.15: Arrhenius (a) and Eyring (b) plots for the formation of $MeCpMn(CO)_2$(pyridine)

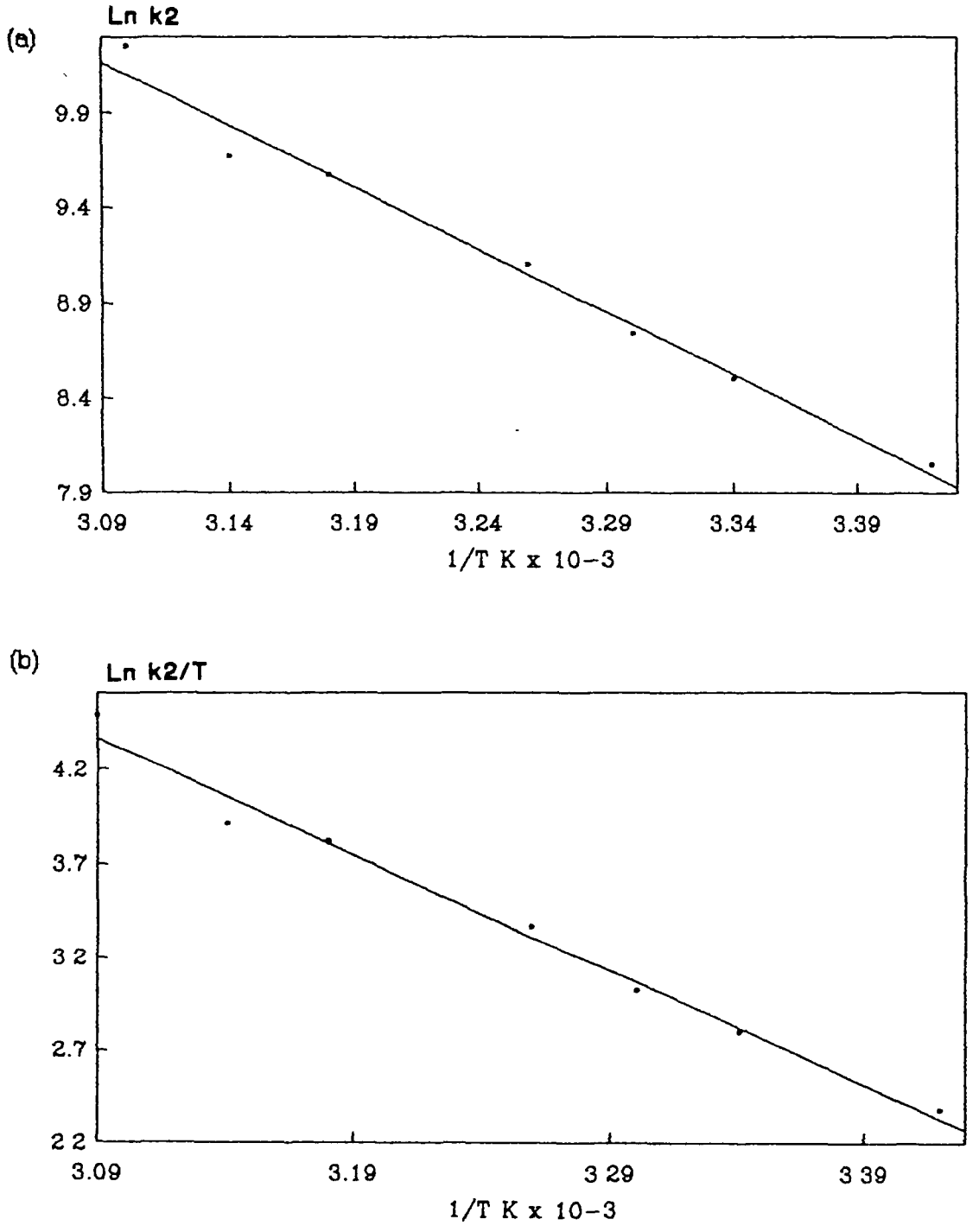

Table 3.3.1.13: Experimental data for the determination of the activation parameters for the reaction of $MeCpMn(CO)_2$(toluene) with 5 1 copolymer of styrene and 4-vinylpyridine.

[pyridine] = 1.64×10^{-2} M

T K	$1/T\ K \times 10^{-3}$	$k_{obs}\ s^{-1}$	Ln k_{obs}	Ln (k_{obs}/T)
290	3 45	35 09	3 56	-2 11
298	3 36	53 83	3 99	-1 71
303	3 30	82 32	4 41	-1 30
309	3 24	110 34	4.70	-1.03
313	3 19	181 89	5 20	-0 54
318	3 14	212 95	5 36	-0 40
323	3 10	261 07	5 56	-0 21

Arrhenius Plot

Slope = -6009 3 ± 327 31

Intercept = 24 24 ± 0.10

Correlation coefficient= 0 99265

E_{act} = 49 96 ± 2 7 kJmol^{-1}

Eyring Plot

Slope = -5703 8 ± 327 77

Intercept = 17 51 ± 0.1

Correlation coefficient = 0 99185

$\Delta H^{\ddagger}$ = 47 42 ± 2 7 kJmol^{-1}

$\Delta S^{\ddagger}$ = -51 93 ± 0.8 Jmol^{-1}K^{-1}

Figure 3.3.1.16: Arrhenius (a) and Eyring (b) plots for the formation of MeCpMn(CO)$_2$(5 1 copol)

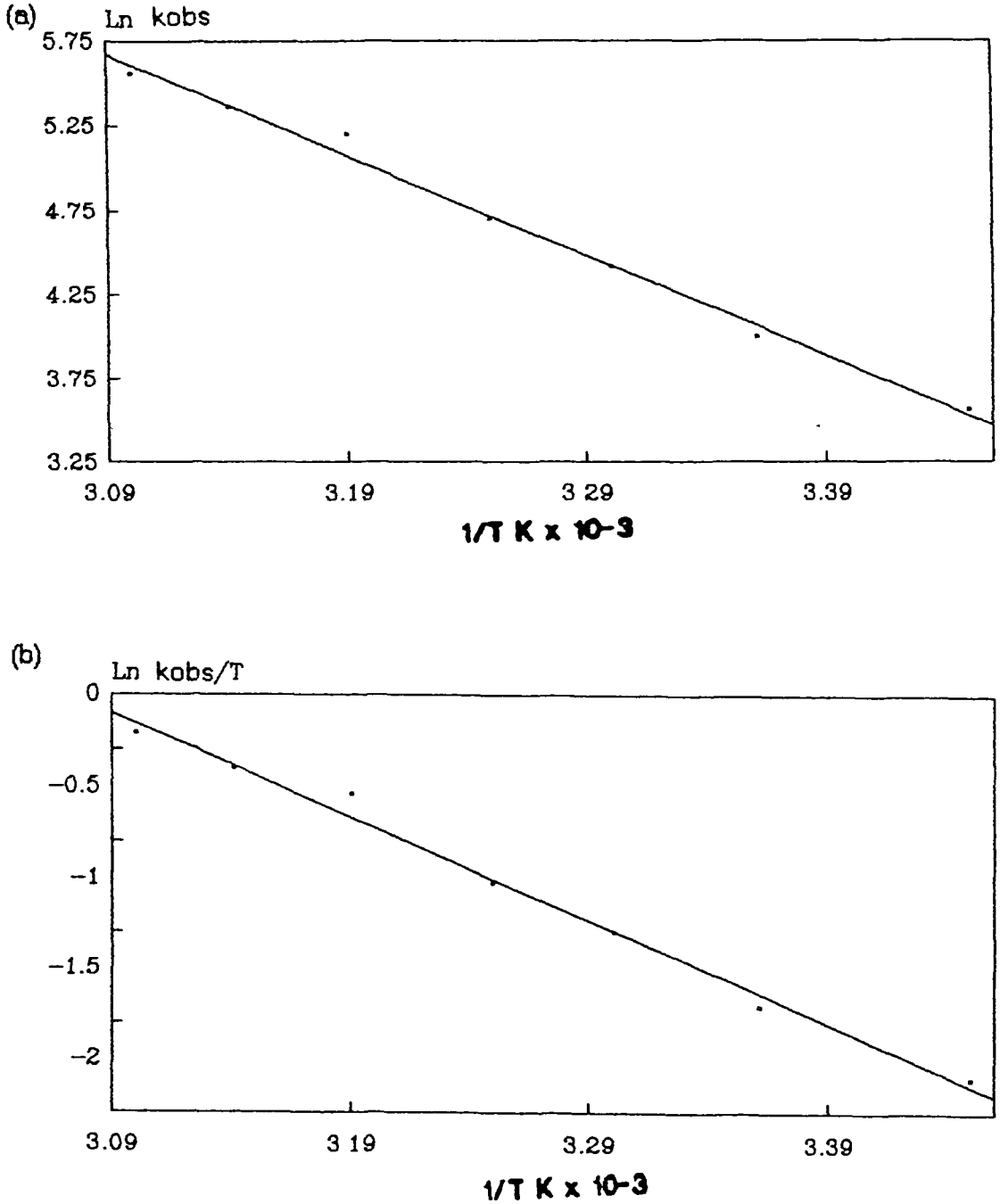

Table 3.3.1.14: Experimental data for the determination of the activation parameters for the formation of $MeCpMn(CO)_2$(pyridine) on the photolysis of $MeCpMn(CO)_3$ in the presence of a 10 1 copolymer of styrene 4-vinylpyridine in toluene solution [pyridine] = 1.68×10^{-2} M

T K	$1/T\ K \times 10^{-3}$	k_{obs}	Ln k_{obs}	Ln (k_{obs}/T)
288	3 47	12.75	2 55	-3 12
293	3 41	22.45	3.11	-2 57
299	3 34	33 89	3 52	-2.18
308	3 25	72 76	4 29	-1 44
313	3 19	89 76	4 50	-1 25
318	3 14	111 48	4 71	-1 05
323	3 10	154.69	5 04	-0 74

Arrhenius Plot

Slope = -6475 2 ± 304 89

Intercept = 25 15 ± 0.11

Correlation coefficient = 0 9945

E_{act} = 53.85 ± 2 5 kJmol^{-1}

Eyring Plot

Slope -6169 9 ± 306 26

Intercept = 18.43 ± 0.10

Correlation coefficient = 0 9939

$\Delta H^{\ddagger}$ = 51 30 ± 2.5 kJmol^{-1}

$\Delta S^{\ddagger}$ = -44 30 ± 0 88 Jmol^{-1}K^{-1}

Figure 3.3.1.17: Arrhenius (a) and Eyring (b) plots for the formation of $MeCpMn(CO)_2$(10 1 copol)

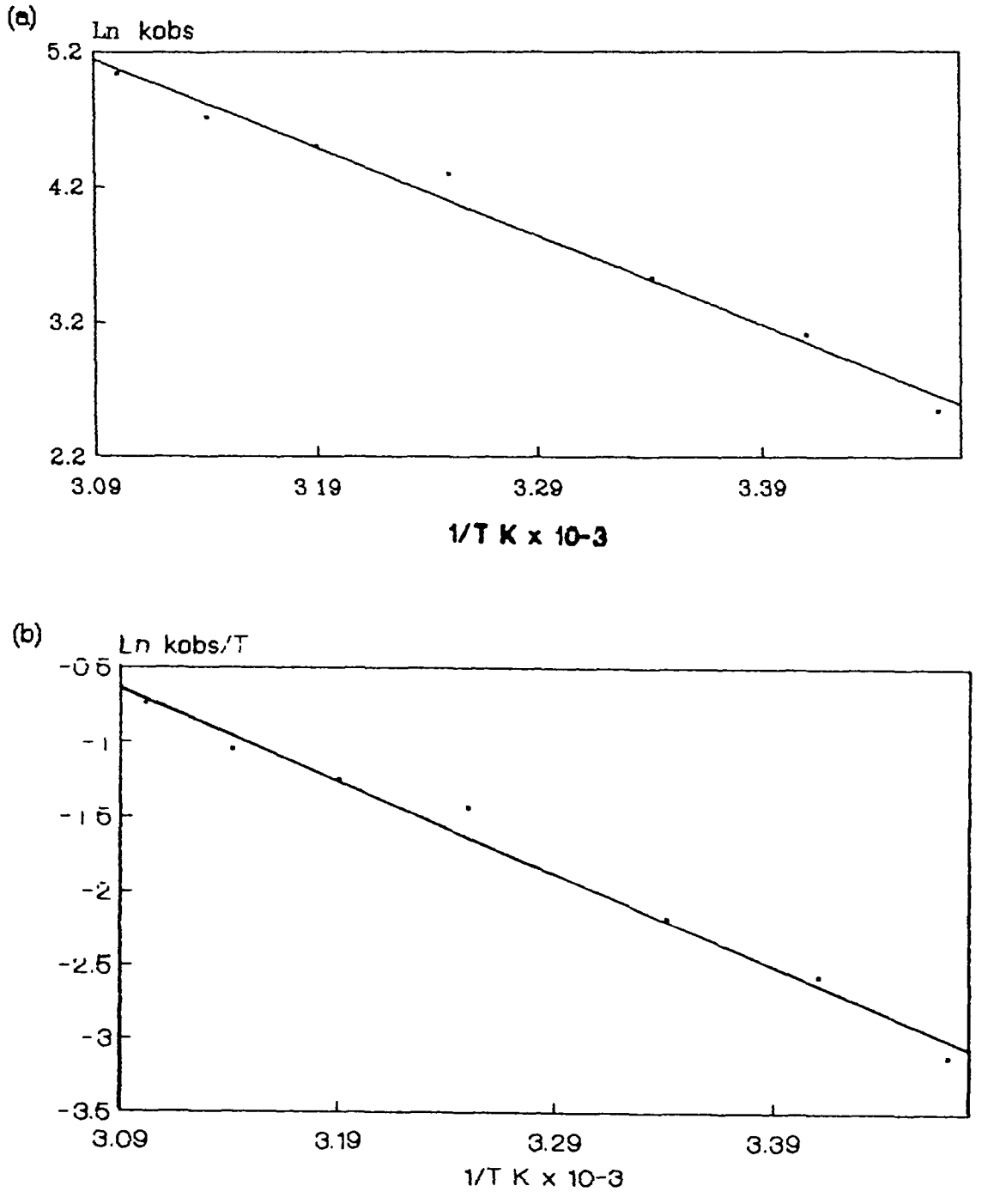

Table 3.3.1.15: Experimental data for the determination of the activation parameters for the formation of $MeCpMn(CO)_2$(copol) on the photolysis of $MeCpMn(CO)_3$ in the presence of a 20.1 copolymer of styrene-co-4-vinylpyridine [pyridine] = 2.30×10^{-2} M

T K	$1/T\ K \times 10^{-3}$	k_{obs}	Ln k_{obs}	Ln (k_{obs}/T)
294	3 40	40 37	3 70	-1 99
298	3 36	58.68	4 07	-1 63
303	3 30	69 06	4 24	-1 48
308	3 25	110 57	4 71	-1 02
313	3 19	134 29	4 90	-0 85
318	3 14	179 47	5 19	-0 57
323	3.10	228 93	5 43	-0 34

Arrhenius Plot

Slope = -5560.7 ± 288 88

Intercept = 22.67 ± 0 08

Correlation coefficient = 0.99332

E_{act} = 46 23 ± 2 4 kJmol^{-1}

Eyring Plot

Slope = -5291 3 ± 293 17

Intercept = 16.06 ± 0 08

Correlation coefficient = 0 99241

$\Delta H^{\ddagger}$ = 43 99 ± 2.4 kJmol^{-1}

$\Delta S^{\ddagger}$ = -64.02 ± 0 6 Jmol^{-1}K^{-1}

Figure 3.3.1.18: Arrhenius (a) and Eunng (b) plots for the reaction of $MeCpMn(CO)_2$(toluene) with 20.1 copolymer of styrene-co-4-vinylpyndine in toluene

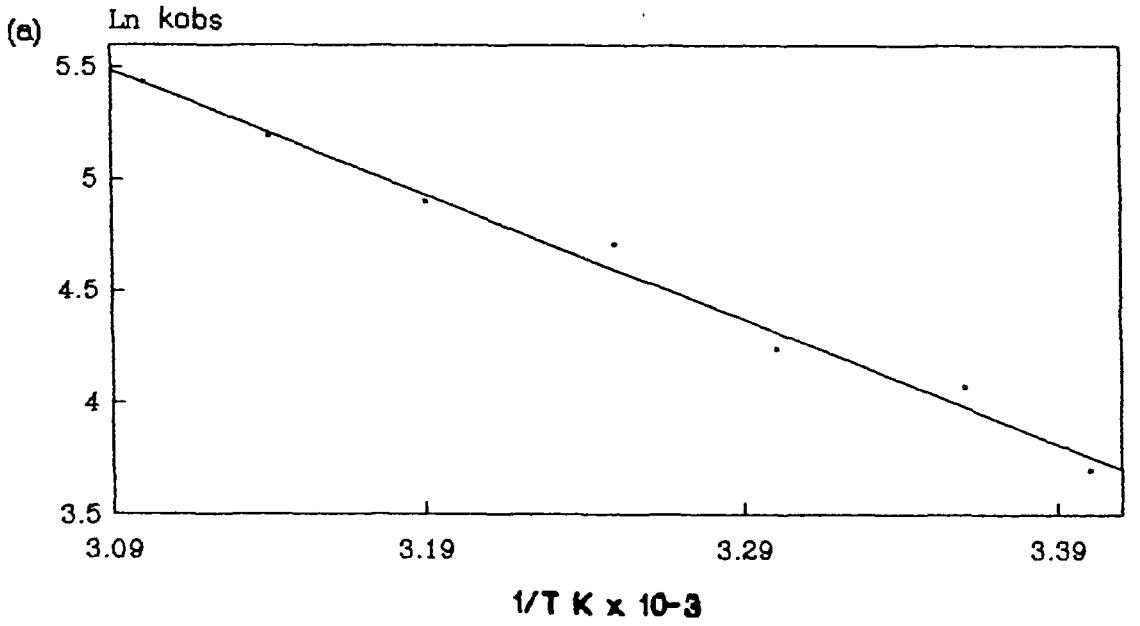

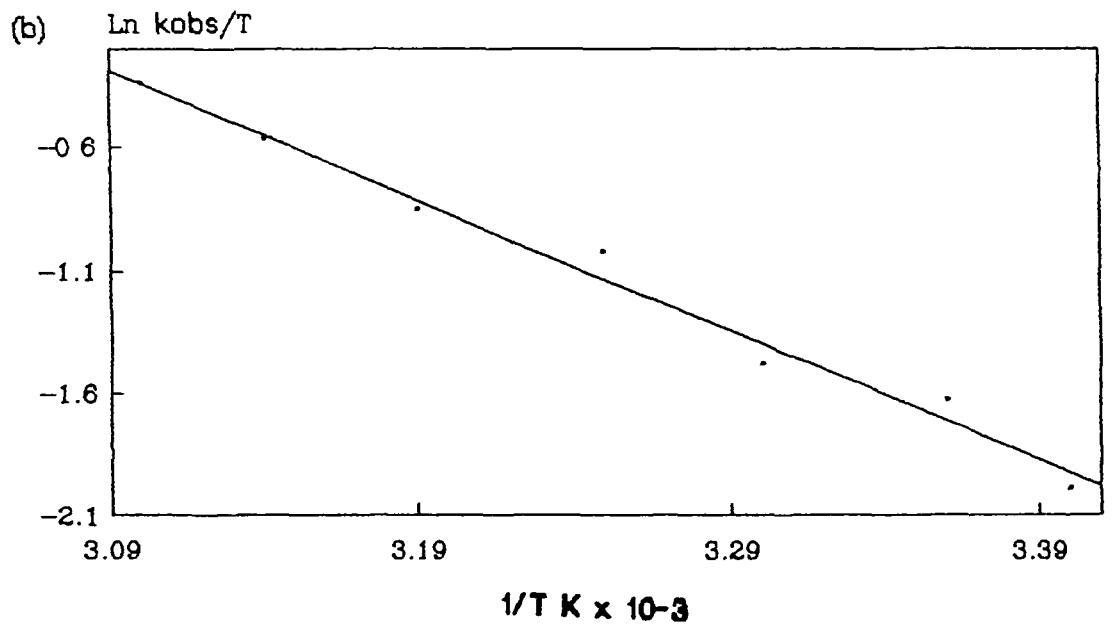

Table 3.3.1.16: Experimental data for the determination of the activation parameters for the formation of $MeCpMn(CO)_2$(copolymer) on the photolysis of $MeCpMn(CO)_3$ in the presence of a 30 1 copolymer of styrene-co-4-vinylpyridine in toluene solution [pyridine] = 2.10×10^{-2} M

T K	$1/T\ K \times 10^{-3}$	k_{obs}	Ln k_{obs}	Ln(k_{obs}/T)
294	3 40	25 50	3 24	-2 45
298	3 36	28 65	3 36	-2 34
308	3 25	50 19	3.92	-1 81
313	3 19	81 11	4.40	-1 35
322	3 11	100 30	4 61	-1 17

Arrhenius Plot

Slope = -5008 ± 492 37

Intercept = 20 23 ± 0 12

Correlation coefficient = 0 98581

E_{act} = 41 64 ± 4 0 kJmol^{-1}

Eyring Plot

Slope = -4700 8 ± 492.85

Intercept = 13 51 ± 0 12

Correlation coefficient = 0 98391

$\Delta H^{\ddagger}$ = 39 08 ± 4.1 kJmol^{-1}

$\Delta S^{\ddagger}$ = -85 26 ± 1 0 Jmol^{-1}K^{-1}

Figure 3.3.1.19: Arrhenius (a) and Eyring (b) plots for the reaction of $MeCpMn(CO)_2$(toluene) with 30.1 copolymer of styrene-co-4-vinylpyridine

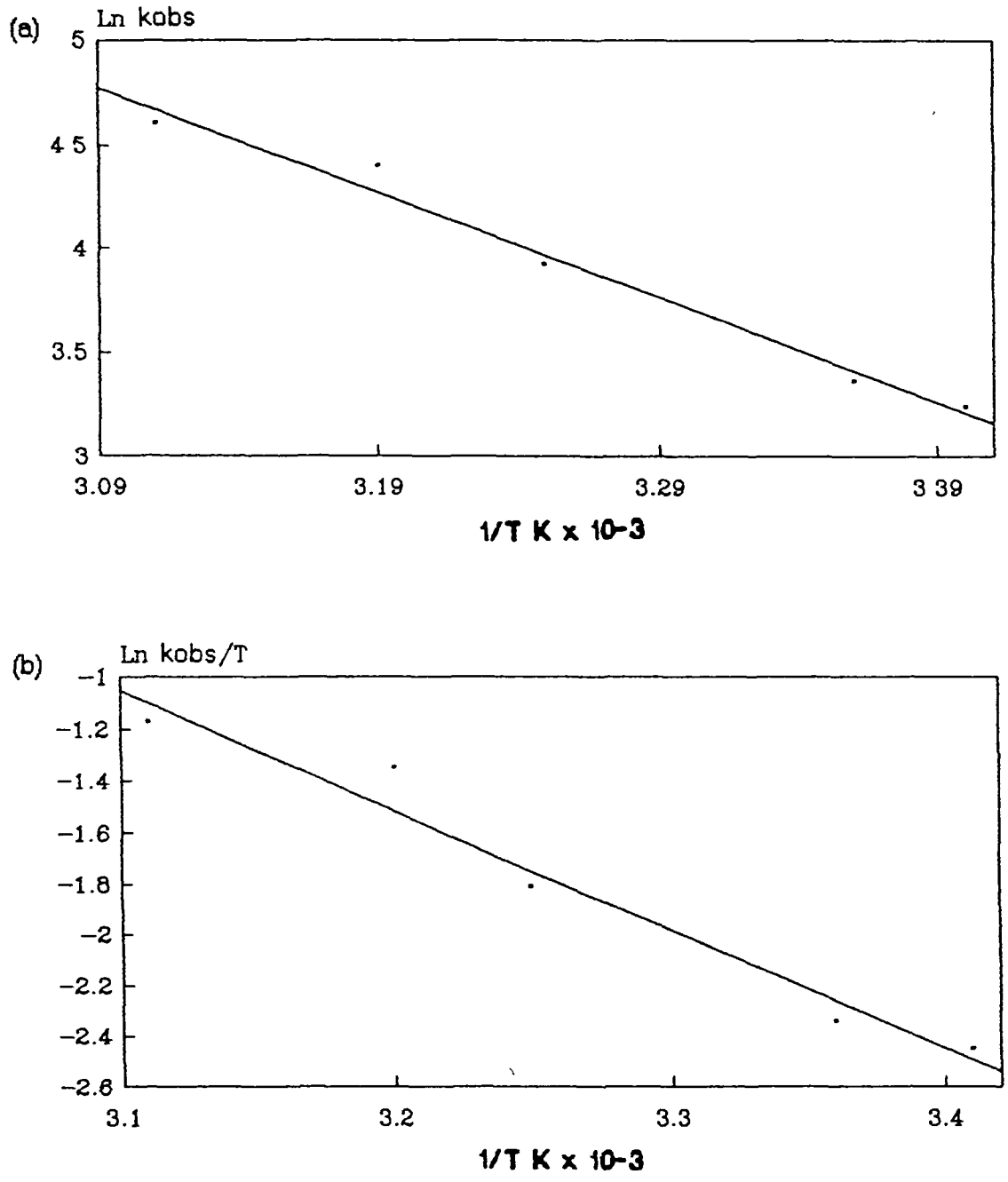

3.3.1.7 Flash photolysis of $MeCpMn(CO)_3$ in toluene in the presence of Methylpyridine.

Because of the trend observed (i e polymer bound pyridine reacting quicker than the monomeric pyridine) it was decided to investigate the reaction of the $MeCpMn(CO)_2$(toluene) with a substituted pyridine (i e. 4-methyl pyridine) The electronic nature of the pyridine ligand is changed by its substituents These changes have a substantial effect on the order of the low lying energy states in these complexes As the pyridine substituent becomes more electron withdrawing the MLCT transition shifts to longer wavelength [33,34] Thus by comparing the second order rate constants determined for the reaction of 4-methyl pyridine with the toluene complex to the rates determined for the monomenc and polymeric pyridine ligands One could determine if the change in the electronic nature of the pyridine ligand due to polymensation was giving nse to the enhanced reaction rates observed for the polymeric ligands

The rate of reaction of $MeCpMn(CO)_2$(toluene) with 4-methylpyridine was calculated to be 1.29×10^3 $dm^3mol^{-1}s^{-1}$. This reaction rate is quite similar to the rate determined for pyridine but is slower than all the rates determined for the polymeric ligands (Table 3 3 1.17).

From Table 3.3 1.17 it could be concluded that the trend observed is not a result of some change in the electronic nature of the pyridine ligands brought about by the polymensation process As the rates for the monomeric pyridine ligands (pyridine and 4-methylpyridine) are quite similar when compared to the rates for the polymeric ligands

Table 3.3.1.17: Second order rate constants for the reaction of $MeCpMn(CO)_2$(toluene) with pyridine ligands

Ligand	k_2 $dm^3mol^{-1}s^{-1}$
Pyridine	0.9×10^3
Methylpyridine	1.29×10^3
5:1 copol	1.96×10^3
10:1 copol	2.54×10^3
20:1 copol	2.61×10^3
30:1 copol	2.89×10^3

Table 3.3.1.18 and Figure 3.3.1.20: Determination of second order rate constant for the reaction of $MeCpMn(CO)_2$(toluene) with 4-methylpyridine

[pyridine] M	k_{obs} s^{-1}
1.39×10^2	29.14
2.04×10^2	40.84
3.54×10^2	62.51
4.06×10^2	59.34
6.02×10^2	91.50

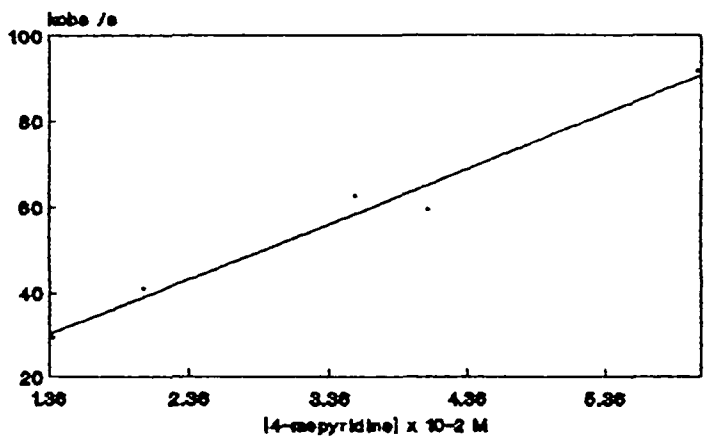

Slope = 1292.3 ± 119.83 $dm^3mol^{-1}s^{-1}$

Intercept = 12.60 ± 4.4 s^{-1}

Correlation coefficient = 0.98735

The activation parameters for the reaction of $MeCpMn(CO)_2$(toluene) with 4-methylpyridine were calculated as shown in Table 3 3 19 As in the case of pyridine k_2 was used in the determination of the activation parameters for the reaction of 4-methylpyridine with the toluene complex ($k_2 = k_{obs}/[pyridine]$)

Table 3.3.1.19: Activation parameters for the reaction of $MeCpMn(CO)_2$(toluene) with 4-methylpyridine

---

E_{act} = 66.51 $kJmol^{-1}$

$\Delta H^{\ddagger}$ = 64 16 $kJmol^{-1}$

$\Delta S^{\ddagger}$ = +35 50 $Jmol^{-1}K^{-1}$

$\Delta G^{\ddagger}$ = 55 58 $kJmol^{-1}$

Table 3.3.1.20: Comparsion of the activation parameters determined for pyridine and 4-methyl pyridine

---

Ligand	E_{act} $kJmol^{-1}$	$\Delta H^{\ddagger}$ $kJmol^{-1}$	$\Delta S^{\ddagger}$ $Jmol^{-1}K^{-1}$	$\Delta G^{\ddagger}$ $kJmol^{-1}$
Pyridine	53 60	51 22	-3 33	52.11
Mepyridine	66.51	64 16	+35 50	55 58

Mepyridine = 4-Methylpyridine

From Table 3 3 1 20 we can see that the $\Delta G^{\ddagger}$ values are the same 55 58 kJmol^{-1} for 4-methylpyridine compared to 52 11 kJmol^{-1} for pyridine therefore the two reactions proceed at similar rates, although there is a slight difference in values of E_{act} The only major difference is in the $\Delta S^{\ddagger}$ values, for pyridine it was -3 33 Jmol^{-1}K^{-1} such a low negative value cannot be cassified definitely as associative or dissociative it is probably an interchange process Whereas for 4-methylpyridine $\Delta S^{\ddagger}$ was determined to be +35 50 Jmol^{-1}K^{-1}, this value indicates a dissociative mechanism Therefore the reaction of MeCpMn(CO)$_2$(toluene) with 4-methylpyridine is a dissociative process whereas the same reaction with pyridine cannot be classified definitely either way

Table 3.3.1.21: Experimental data for the determination of the activation parameters for the formation of $MeCpMn(CO)_2$(4-methylpyridine) on the photolysis of $MeCpMn(CO)_3$ in the presence of methylpyridine in toluene solution [pyridine] = 1.91×10^{-2} M

T K	$1/T\ K \times 10^{-3}$	k_2	Ln k_2	Ln k_2/T
293	3.41	1538.22	7.34	1.66
298	3.36	2343.43	7.76	2.06
303	3.30	4173.82	8.34	2.62
308	3.25	6508.90	8.78	3.05
314	3.18	10482.20	9.26	3.51
318	3.14	12812.57	9.46	3.70
323	3.10	19416.75	9.87	4.10

Arrhenius Plot

Slope = -7999.3 ± 270.57

Intercept = 34.67 ± 0.07

Correlation coefficient = 0.99715

E_{act} = 66.51 ± 2.18 kJmol^{-1}

Eyring Plot

Slope = -7716.9 ± 265.02

Intercept = 28.03 ± 0.07

Correlation coefficient = 0.99706

$\Delta H^{\ddagger}$ = 64.16 ± 2.13 kJmol^{-1}

$\Delta S^{\ddagger}$ = +35.50 Jmol^{-1}K^{-1}

Figure 3.3.27: Arrhenius (a) and Eyring (b) plots for the reaction of $MeCpMn(CO)_2$(toluene) with methylpyridine

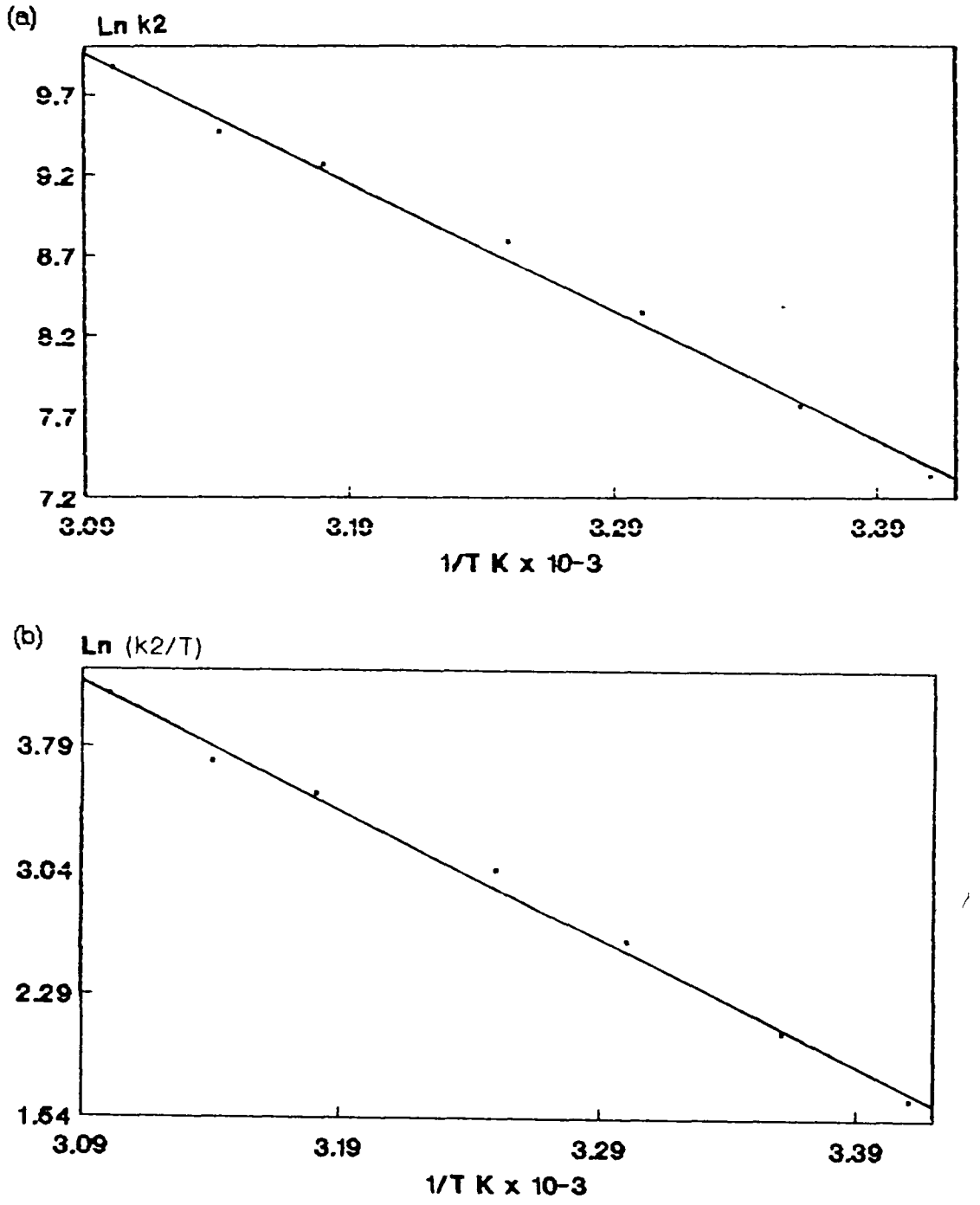

3.3.1.8: Photolysis of $MeCpMn(CO)_3$ and pyridine in the presence of polystyrene in toluene solution

From the second order rate constants and the activation parameters determined for the monomeric and polymeric pyridine ligands, it appeared that the enhanced rate constants were not a result of a change in the Gibbs free energy of activation or the electronic nature of the pyridine ligand. Therefore it was then decided to investigate the effect of adding polystyrene to the solution prior to the flash photolysis experiment. This experiment was carried out because it appeared the amount of polymer in solution was affecting the rates of reaction (i.e. lower loading copolymers with more polymer in solution were reacting quicker).

The second order rate constants for the reaction of $MeCpMn(CO)_2$(toluene) with both free and polymer bound pyridine were determined in the presence of polystyrene (1% w/v polystyrene in toluene) (Table 3.3.1.22).

Table 3.3.1.22: Second order rate constants determined for the reaction of $MeCpMn(CO)_2$(toluene) with pyridine ligands in a 1% w/v polystyrene solution in toluene.

Ligand	k_2 $dm^3mol^{-1}s^{-1}$
Pyridine	2.82×10^{-3}
5:1 copol	3.12×10^{-3}
10:1 copol	3.28×10^{-3}
30:1 copol	6.22×10^{-3}

Table 3.3.1.23: Comparison of the second order rate constants determined in toluene solution and in 1% w/v polystyrene in toluene solution for the reaction of $MeCpMn(CO)_2$(toluene) with the pyridine ligands.

	k_2 $dm^3mol^{-1}s^{-1}$	
Ligand	Toluene[1]	Polystyrene[2]
Pyridine	0.93×10^3	2.82×10^3
5:1 copol	1.96×10^3	3.12×10^3
10:1 copol	2.54×10^3	3.28×10^3
30:1 copol	2.89×10^3	6.22×10^3

1 = ligand in toluene solution, 2 = ligand + 1% polystyrene in toluene solution

From Table 3.3.1.23 it can be seen that the rate of reaction in a solution containing 1% polystyrene increases dramatically. This would seem to imply that the primary photoproduct as well as reacting with the pyridine ligand also interacts in some way with the polymer backbone, possibly with the aromatic units on the polymer backbone. Surprisingly, from the results obtained it appears that $MeCpMn(CO)_2$(toluene) can distinguish between toluene and polystyrene.

The experiment was repeated for pyridine using a 5% w/v solution of polystyrene in toluene. The second order rate constant was determined again for the reaction of $MeCpMn(CO)_2$(toluene) with pyridine in the 5% solution. The rate constant was found to be 3.24×10^3 $dm^3mol^{-1}s^{-1}$.

The value determined was greater than that for the reaction of $MeCpMn(CO)_2$(toluene) with pyridine in toluene solution and in a 1% polystyrene solution (Table 3 3 1 24) Thus even in a 5% polymer solution the reaction rates are quicker than in a toluene solution this would seem to confirm that the primary photoproduct interacts with the polymer molecules in solution as well as reacting with the pyridine ligands

---

Table 3.3.1.24: Comparison of the reaction rates for the reaction of $MeCpMn(CO)_2$(toluene) with pyridine in toluene and polystyrene solutions.

Solution	k_2 $dm^3mol^{-1}s^{-1}$
Toluene	0.93×10^3
1% PS	2.82×10^3
5% PS	3.24×10^3

PS = w/v polystyrene in toluene

Tables 3.3 1 25 - 3.3.1 29 and Figures 3 3.1 22 - 3.3.1 26 give the experimental data for determining the second order rate constants in polystyrene solution.

Table 3.3.1.25 and Figure 3.3.1.22: Second order rate constant for $MeCpMn(CO)_2$(toluene) + pyridine in 1% polystyrene solution

[pyridine]	k_{obs} s^{-1}
1.14×10^{-2} M	23 63
$1\ 77 \times 10^{-2}$ M	44 50
$4\ 30 \times 10^{-2}$ M	117.45
$5\ 82 \times 10^{-2}$ M	155 75

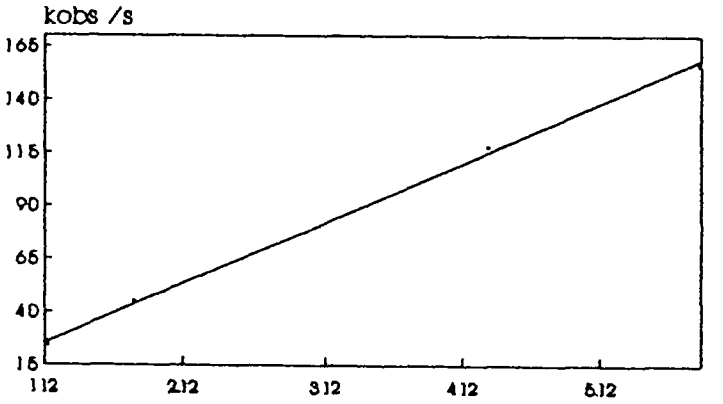

Slope = 2824 6 ± 74 59 $dm^3mol^{-1}s^{-1}$

Intercept = -6 68 ± 2 8 s^{-1}

Correlation coefficient = 0 9993

Table 3.3.1.26 and Figure 3.3.1.23: Second order rate constant for the reaction of $MeCpMn(CO)_2$(toluene) with 5·1 copol in 1% polystyrene solution

[pyridine]	k_{obs} s^{-1}
2.38×10^{-2} M	38 25
$3\ 13 \times 10^{-2}$ M	60 09
$3\ 32 \times 10^{-2}$ M	65 22
$4\ 26 \times 10^{-2}$ M	96.83

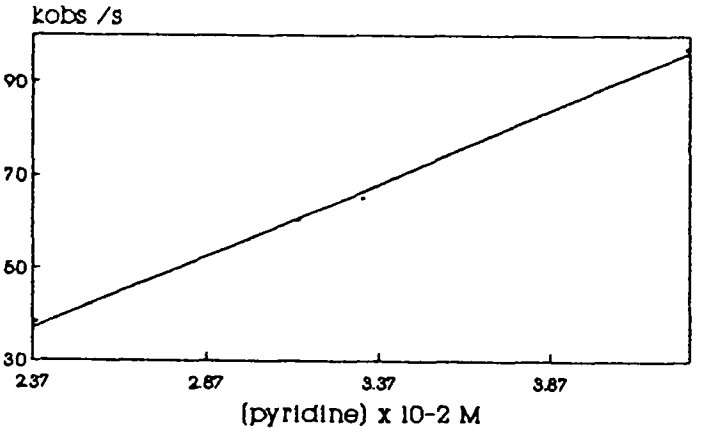

Slope = 3122 ± 105 72 $dm^3mol^{-1}s^{-1}$

Intercept = -37 07 ± 1 42 s^{-1}

Correlation coefficient = 0 99886

Table 3.3.1.27 and Figure 3 3.1.24: Second order rate constant for the reaction of $MeCpMn(CO)_2$(toluene) with 10.1 copol in 1% polystyrene solution.

[pyridine]	k_{obs} s^{-1}
1 24 x 10^{-2} M	30 34
1 51 x 10^{-2} M	41 51
1 90 x 10^{-2} M	51 93
2 16 x 10^{-2} M	61 99
2 46 x 10^{-2} M	70 90

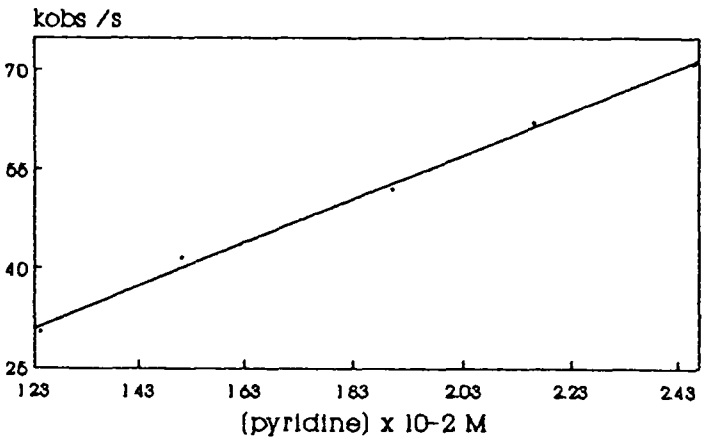

Slope = 3278.1 ± 120 48 $dm^3mol^{-1}s^{-1}$

Intercept = -9.44 ± 1.18 s^{-1}

Correlation coefficient = 0 99798

Table 3 3.1.28 and Figure 3.3 1.25: Second order rate constant for the reaction of $MeCpMn(CO)_2$(toluene) with 30 1 copol in 1% polystyrene solution.

[pyridine]	k_{obs} s^{-1}
1.13 x 10^{-2} M	68.90
1.55 x 10^{-2} M	82 06
1 87 x 10^{-2} M	115.33
2.15 x 10^{-2} M	128 02
2.45 x 10^{-2} M	147.30

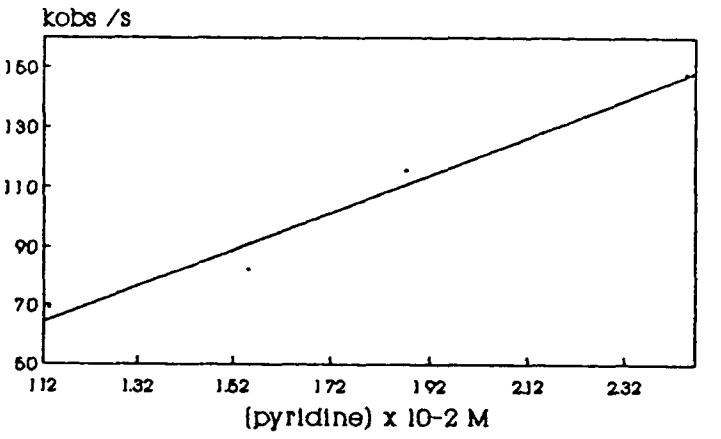

Slope = 6216 8 ± 604 5 $dm^3mol^{-1}s^{-1}$

Intercept = -5.44 ± 6.2 s^{-1}

Correlation coefficient = 0 98611

Table 3.3.1.29 and Figure 3.3.1.26. Second order rate constant for the reaction of $MeCpMn(CO)_2$(toluene) with pyridine in 5% polystyrene solution

[pyridine]	k_{obs} s^{-1}
1 01 x 10^{-2} M	37 89
1 77 x 10^{-2} M	58 53
2.91 x 10^{-2} M	93 26
4 05 x 10^{-2} M	124 13
5 44 x 10^{-2} M	184 18

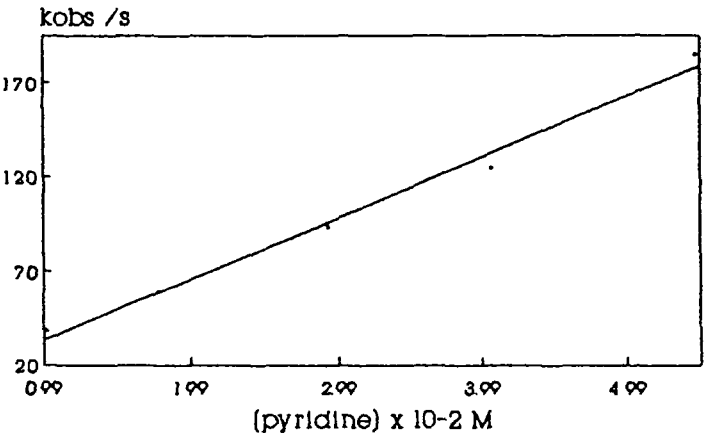

Slope = 3240 2 ± 189 23 $dm^3mol^{-1}s^{-1}$

Intercept = 1 23 ± 6 69 s^{-1}

Correlation coefficient = 0 99492

3.3.1.9 Flash photolysis of $MeCpMn(CO)_3$ and pyridine in a 15% w/v of polystyrene in toluene

An experiment was carried out to see how much polystyrene could be added before the second order rate constant failed to increase or if it continued to increase as the concentration of polymer in solution was increased. Perhaps it could be possible to use a high concentration of polymer in solution to stabilise the photofragment at room temperature in a similar way to polymer films at low temperatures.

As can be seen from the data recorded (Table 3.3.1.30 and Figure 3.3.1.27) the rate of reaction recorded in the 15% polystyrene solution is slower than the rates recorded for the less concentrated polystyrene solutions. This is probably because of diffusion constraints posed by the polymer coils in solution. The large concentration of polymer coils in solution hinder the pyridine ligand in gaining access to the primary photoproduct thus slowing the rate of displacement of the toluene molecule and formation of the dicarbonyl pyridine complex.

Table 3.3.1.30 and Figure 3.3.1.27: Rates of reaction of $MeCpMn(CO)_2$(toluene) with pyridine in 15% w/v polystyrene solution in toluene.

[pyridine]	$k_{obs}s^{-1}$
2.15×10^{-2} M	106.16
3.03×10^{-2} M	111.97
4.55×10^{-2} M	146.26
5.18×10^{-2} M	218.40

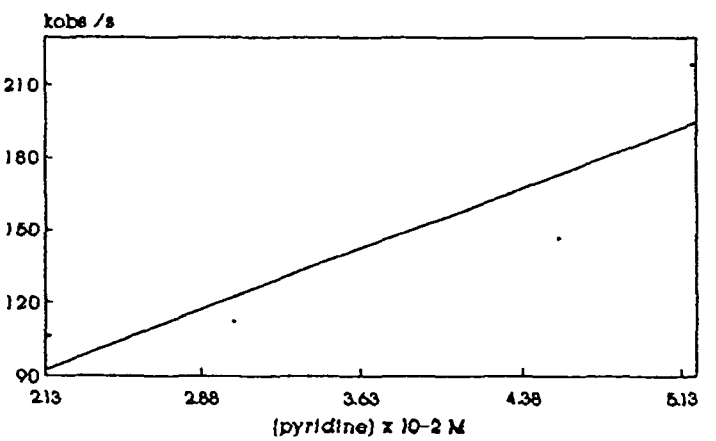

3.3.1.10 Summary

Photolysis of $CpMn(CO)_3$ in low temperature argon and methane matrices [11,28,29] and in alkane solution [12] have shown loss of CO as the primary photoprocess In our studies on the solution photochemistry of $MeCpMn(CO)_3$ in toluene at ambient temperatures, loss of CO was also observed as the primary photoprocess to generate an unsaturated $MeCpMn(CO)_2$ species which was coordinated to a solvent molecule This primary photoproduct was not observed to react further unlike photolysis in alkane solution [12] which results in the formation of a dinuclear species by the reaction of the primary photoproduct with the parent complex (Reaction 3 3.1.6).

$$CpMn(CO)_2S + CpMn(CO)_3 \longrightarrow Cp_2Mn_2(CO)_5 \qquad 3.3.1.6$$

The reaction kinetics of $MeCpMn(CO)_3$ with monomeric and polymenc pyridine ligands were investigated using flash photolysis in ambient temperature toluene solutions The primary photoproduct $MeCpMn(CO)_2$(toluene) was observed to react faster with the polymeric ligands In the case of the copolymers the rate increases as the loading of 4-vinylpyridine on the polymer backbone decreases (as the loading of 4-vinylpyridine decreases the amount of polymer in solution is increased to maintain the concentration of pyridine). The activation parameters were determined and showed that this effect was not a result of a difference in the Gibbs free energy of activation, as the $\Delta G^{\ddagger}$ values determined for all the reactions were within expenmental error of each other It was then thought that the electronic nature of the pyridine may be affected by the polymerisation and this may be the reason for the increase in reaction rates. This was discounted by using substituted pyridine ligands (i e 4-methyl pyridine).

One possible explanation for this observed increase in reaction rates for the polymeric ligands is that the $MeCpMn(CO)_2$(toluene) species can react with a pendant nitrogen or an aromatic centre on the polymer backbone This interaction with the polymer backbone was confirmed by carrying out the flash photolysis of $MeCpMn(CO)_3$ and pyridine in a 1% solution of polystyrene, which resulted in an observed increase in the rate of reaction for pyridine with the $MeCpMn(CO)_2$(toluene) complex. These results imply that the $MeCpMn(CO)_2$ species can distinguish between toluene and polystyrene A possible reaction mechanism for this process is shown in Scheme 3 3.1.2 The interaction with the polymer backbone has a stabilising effect on the dicarbonyl species for a short period possibly similar to the reactions in low temperature polymer films and matrices but on a much shorter timescale The polymer is then displaced by a pendant nitrogen from the polymer backbone.

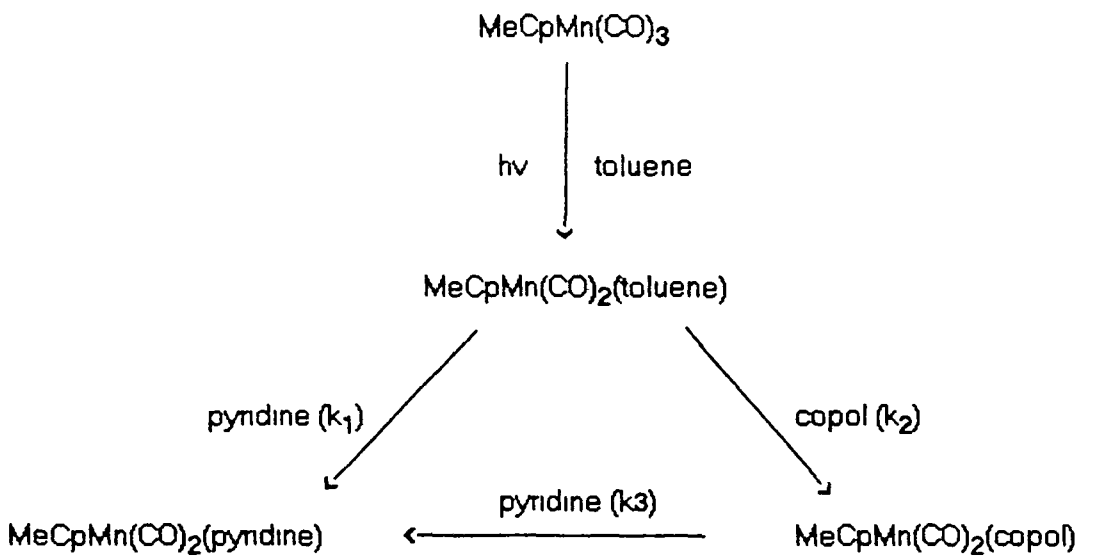

copol = poly(styrene-co-4-vinylpyridine), pyridine = pendant nitrogen on copolymer backbone

Scheme 3.3.1

Assuming a steady-state concentration of $MeCpMn(CO)_2$(copolymer), the rate law corresponding to the mechanism in Scheme 3 3 1 2 is,

$$d[MeCpMn(CO)_2(pyridine)]/dt = [MeCpMn(CO)_2(toluene)](k_1[pyridine] + k_2[copol])$$

In terms of the pseudo-first-order rate constant, k_{obs}, this equation may be written as,

$$k_{obs} = (k_1[pyridine] + k_2[polymer])$$

This would account for the increase in the reaction rates as the amount of polymer in solution was increased This effect has also been seen in other systems, the reaction of $W(CO)_5$ with polymeric pyridine ligands was observed to be faster than the reaction with free pyridine [35] This trend was also observed for the reaction of $M(CO)_5$ (M = Cr, W, or Mo) with both monomeric and polymeric triphenylphosphine ligands [36]

3.3.2 Laser Flash Photolysis of $ArCr(CO)_3$ in Toluene

It was decided to further investigate the reactions of the monomeric and polymeric ligands, by studying the photochemical reactions of the $ArCr(CO)_3$ complex in the presence of such ligands First one had study the $ArCr(CO)_3$ complex, which is isoelectronic to the manganese system. The experiments were conducted in toluene at ambient temperatures and are similar to those already described for the $MeCpMn(CO)_3$ system.

Figure 3321 shows the UV/vis spectrum of $ArCr(CO)_3$ in toluene The extinction coefficient of $ArCr(CO)_3$ in toluene was calculated to be 3016 4 $dm^3mol^{-1}cm^{-1}$ at 354 nm.

Figure 3.3.2.1: The UV/vis spectrum of $ArCr(CO)_3$ in toluene

---

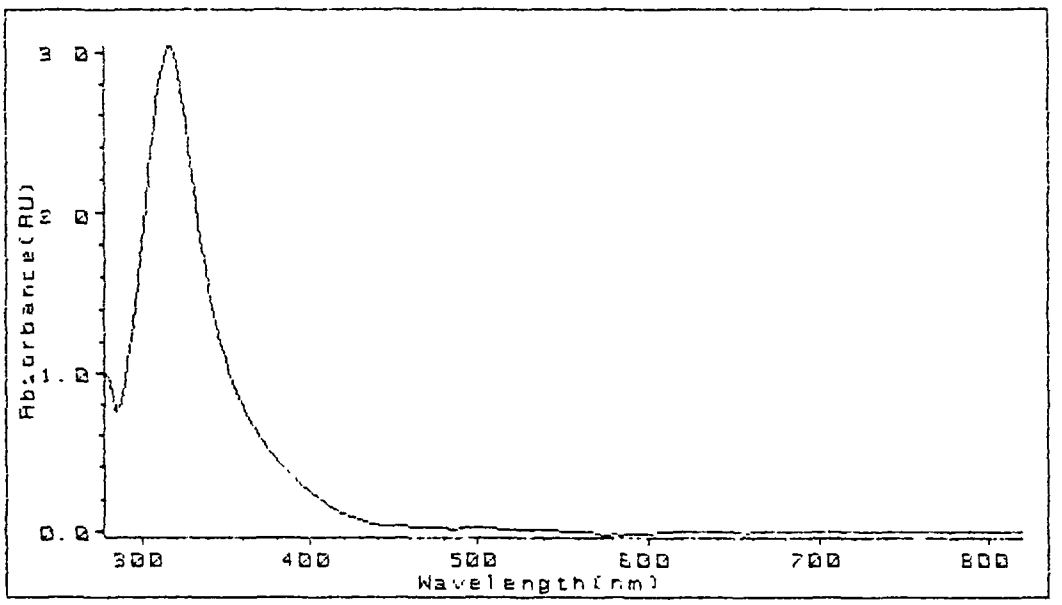

---

3 3 2.1 Primary Photproduct

The UV/vis difference spectrum of the first observed species upon flash photolysis of $ArCr(CO)_3$ in toluene is shown in Figure 3 3 2 2 The spectra were recorded at the time of the flash and 600 μs after the flash The λ_{max} of this species is at 400 nm, the other significant feature in the transient spectrum is the negative band centred at 355nm This negative band can be assigned to depletion of the parent tricarbonyl complex From the spectrum (Figure 3 3.2 2) one can also see a second species (a) growing in around 500 nm.

Figure 3.3.2.2: Transient UV/vis difference spectrum of the first and second observed species

---

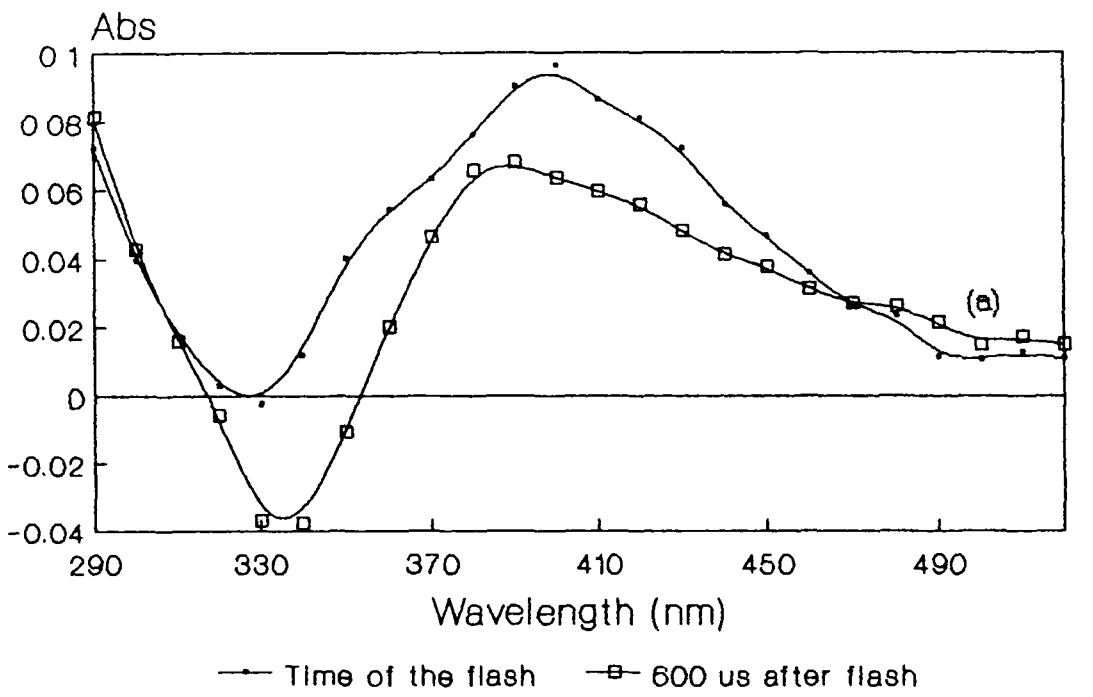

The effect of saturating the $ArCr(CO)_3$ toluene solution with CO was then investigated The UV/vis difference spectrum of the transient species recorded under a CO atmosphere is shown in Figure 3 3 2 3 As can be seen from the spectra (when compared to those recorded under an argon atmosphere Figure 3 3 2 2) the formation of the second species is inhibited (a) Figure 3 3 2 4 shows the effect of CO on the transient species, as can be seen from the traces recorded the lifetime of the transient species is decreased upon addition of CO to the system, whereas the yield is unaffected

Figure 3.3.2.3: UV/vis difference spectrum of first observed species recorded under CO

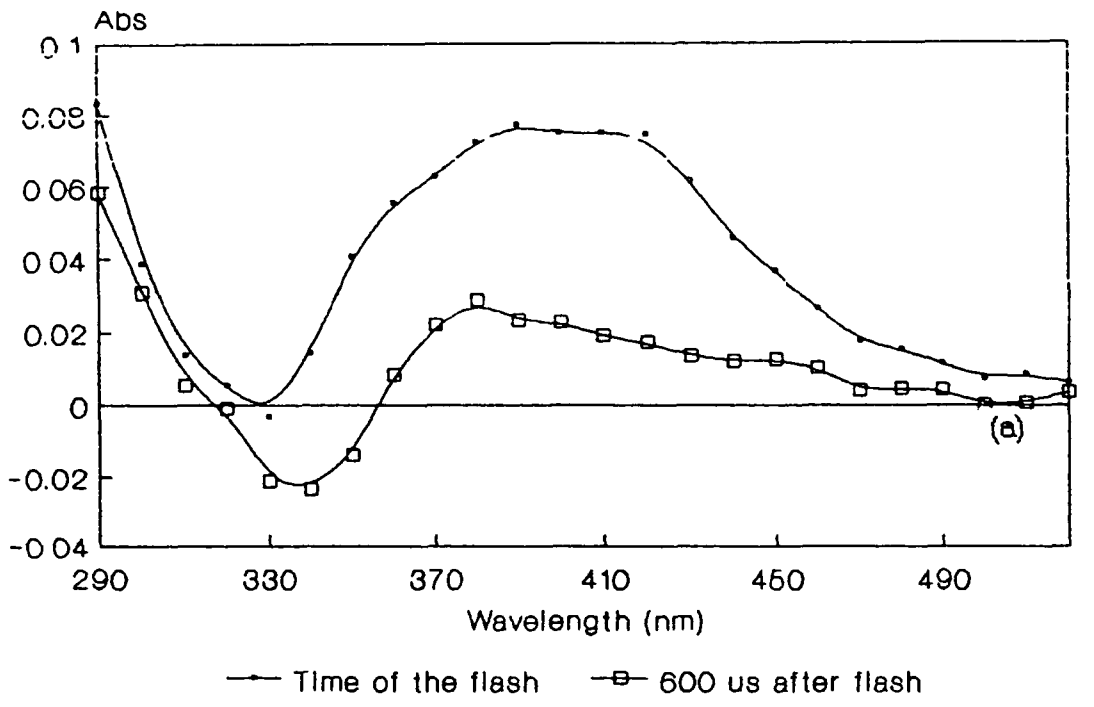

Figure 3.3.2.4: The decay of the first observed species under (a) argon and (b) CO atmospheres (see Section 5 2 1 for explanation of axes)

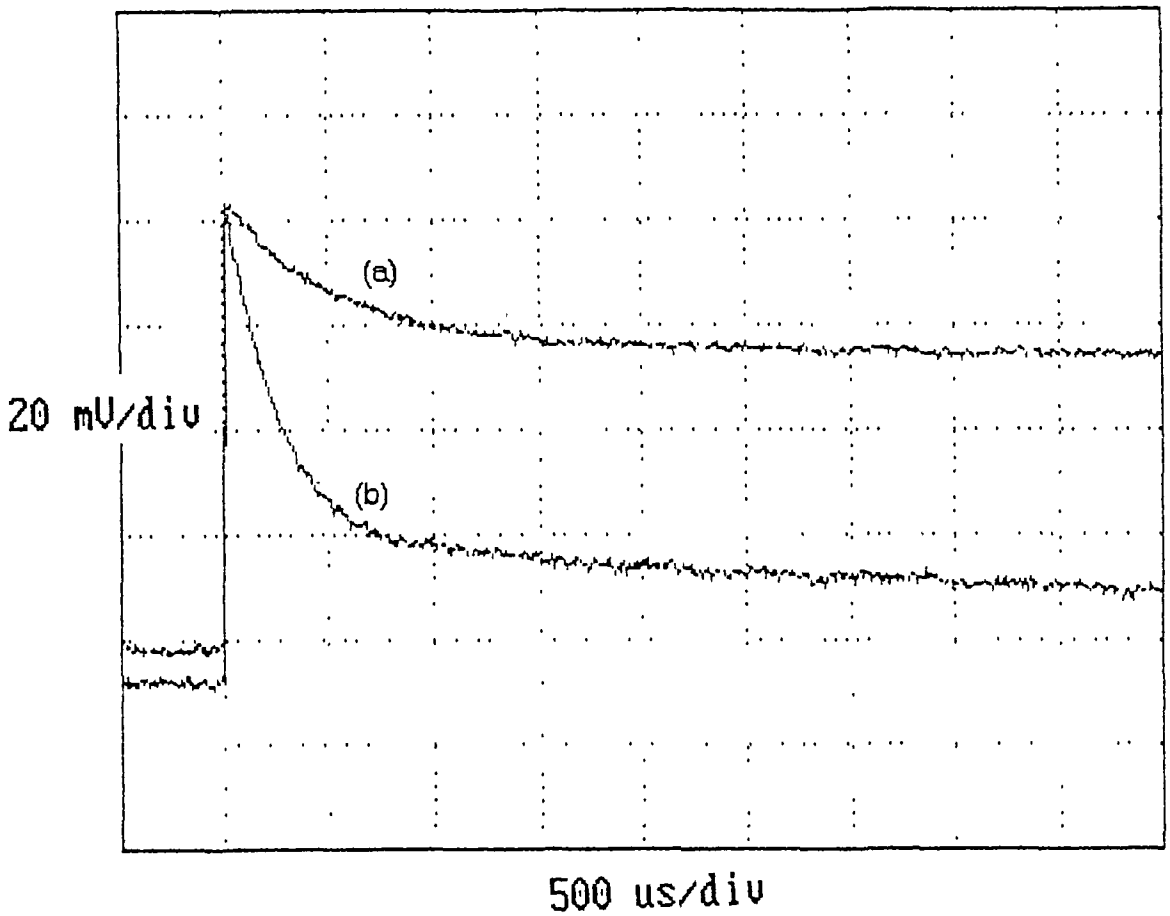

If the primary photoreaction is loss of CO then the yield of the primary photoproduct would be unaffected by the addition of CO This is because the formation of the primary photoproduct is a result of a photophysical process. The lifetime of the primary photoproduct is decreased because the back reaction of the photolytically formed species is favoured by the presence of CO in solution. As in the $MeCpMn(CO)_3$ system,

both of these conditions are satisfied (Figure 3 3 2 4) the primary photochemical reaction is therefore given by Reaction 3 3 2 1

$$ArCr(CO)_3 \xrightarrow{h\nu} ArCr(CO)_2 + CO \qquad 3.3.2.1$$

As with the $MeCpMn(CO)_2$ species, the $ArCr(CO)_2$ complex coordinates to a solvent molecule The solvent molecule occupies the vacant coordination site as a bound ligand. Work carried out by several workers in low temperature matrices have indicated that loss of CO to form $ArCr(CO)_2$(matrix) complex is the primary photoreaction [11,28,30]. Thus from our experimental results for both the manganese and chromium systems and from results in the literature, it can be concluded that the first observed species is the primary photoproduct $ArCr(CO)_2$(toluene) (Reactions 3.3 2.1-3 3 2 2)

$$ArCr(CO)_2 + \text{toluene} \longrightarrow ArCr(CO)_2(\text{toluene}) \qquad 3.3.2.2$$

The rate of the back reaction of the photolytically formed species (Reaction 3 3 2 3) was determined by measuring the rate of decay of the primary photoproduct in the presence and absence of CO and using the difference to determine the rate constant

$$ArCr(CO)_2 + CO \longrightarrow ArCr(CO)_3 \qquad 3.3.2.3$$

Which was determined to be 3.71×10^5 $dm^3mol^{-1}s^{-1}$ Table 3 3.2 1 shows the experimental data and it is represented graphically in Figure 3 3 2 5

Table 3.3.2.1 and Figure 3.3.2.5: Second order rate constant for the reaction of $ArCr(CO)_2$(toluene) with CO

$[CO] \times 10^{-3}$ dm^3mol^{-1}	$k_{obs}(CO) - k_{obs}(Ar)$
1 88	356 4 s^{-1}
3 77	1337 6 s^{-1}
5 65	1724 5 s^{-1}
7 53	2552 4 s^{-1}

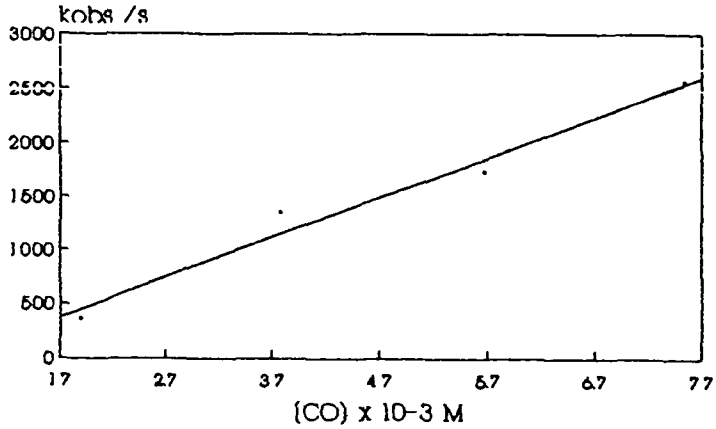

Slope = (3 71 ± 0 41) x 10^5 $dm^3mol^{-1}s^{-1}$

Intercept = -253 19 ± 171.67 s^{-1}

Correlation coefficient = 0 98814

3.3.2.2: Activation parameters for the reaction of $ArCr(CO)_2$(toluene) with CO

The activation parameters were determined from the Arrhenius and Eyring equations [37] The equations are shown in detail in Section 5 3 8 E_{act} was determined from a plot of Ln k_2 versus 1/T $\Delta H^{\ddagger}$ and $\Delta S^{\ddagger}$ were determined from a plot of Ln (k_2/T) versus 1/T (k_2 = k_{obs}/[CO])

The parameters calculated are listed in Table 3 3 2 2 The experimental data is summarised in Table 3 3 2 3 and shown graphically in Figures 3.3 2 6

Table 3.3.2.2: Activation parameters for the reaction of $ArCr(CO)_2$(toluene) with CO

E_{act} = 44 21 kJmol^{-1}

$\Delta H^{\ddagger}$ = 41 79 kJmol^{-1}

$\Delta S^{\ddagger}$ = +17 08 Jmol^{-1}K^{-1}

$\Delta G^{\ddagger}$ = 46 88 kJmol^{-1}

From the data in Table 3 3.2 2 we can see that the activation energy for the reaction is low and is quite similiar to that determined for the same reaction in the $MeCpMn(CO)_3$ system. The positive value for the activation entropy implies a dissociative process However as the value for $\Delta S^{\ddagger}$ is small and because of the concentration of toluene in the reaction vessel an interchange mechanism is more likely (Scheme 3 3 2 1)

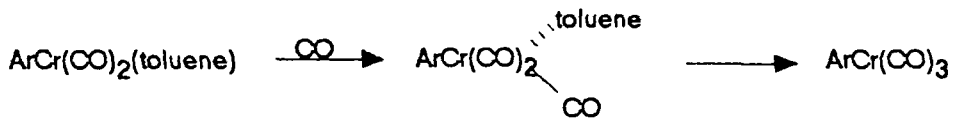

Scheme 3.3.2.1

Table 3.3 2.3: Experimental data for the determination of the activation parameters for the reaction of $ArCr(CO)_2$(toluene) with CO [CO] = $7\ 53 \times 10^{-2}$ M

T K	$1/T \times 10^{-3}$	$k_2 \times 10^6$	Lnk_2	Lnk_2/T
293	3 41	1 71	14 35	8 67
298	3 36	2.49	14 73	9 02
308	3.25	3 68	15 12	9 39
313	3 19	4 82	15 39	9 64
318	3 14	7 66	15 85	10 09
323	3 10	9 73	16 09	10 31

Arrhenius Plot

Slope = -5317.1 ± 400.15

Intercept = 32 49 ± 0 11

Correlation coefficient = 0.9888

E_{act} = 44 21 ± 3 42 kJmol^{-1}

Eyring Plot

Slope = -5026 3 ± 389 61

Intercept = 25 81 ± 0 11

Correlation coefficient = 0 9888

$\Delta H^{\ddagger}$ = 41 79 ± 3 31 kJmol^{-1}

$\Delta S^{\ddagger}$ = +17 08 ± 0 8 Jmol^{-1}K^{-1}

Figure 3.3.2.6. Arrhenius (a) and Eyring (b) plots for the reaction of $ArCr(CO)_2$(toluene) with CO

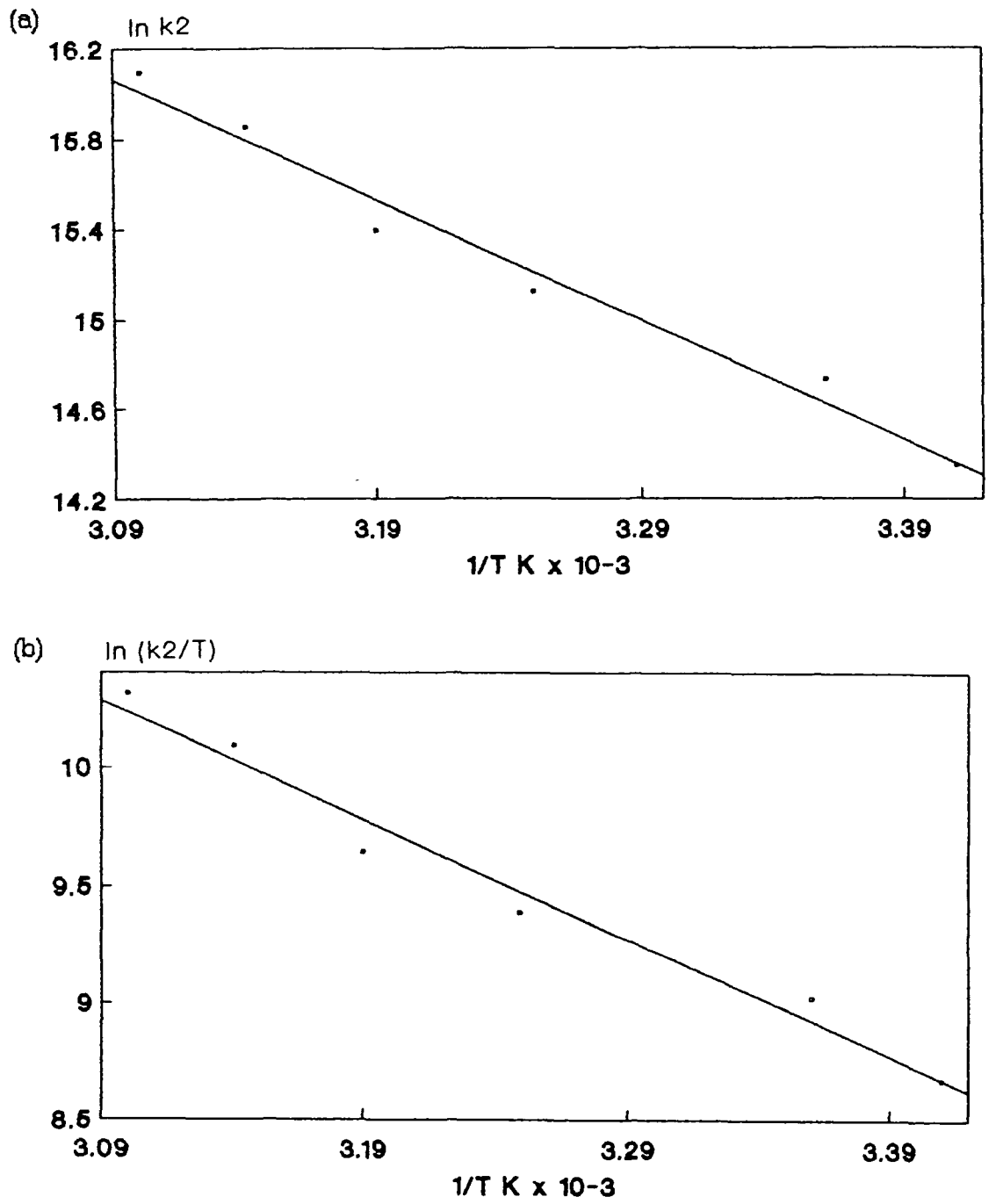

3.3.2.3 Effect of power of laser on concentration of primary photoproduct

Confirmation that the $ArCr(CO)_2$(toluene) species is formed as a result of a single photon excitation of the parent tricarbonyl complex, was obtained in a similar way to that for the $MeCpMn(CO)_3$ system (Section 3.3.1.2). As with the manganese system, a plot of the absorbance of the primary photoproduct ($ArCr(CO)_2$(toluene) varied linearly as the laser power was varied. The results are shown graphically in Figure 3.3.2.7.

Figure 3.3.42: Plot of relative power of the laser versus the absorbance of the primary photoproduct.

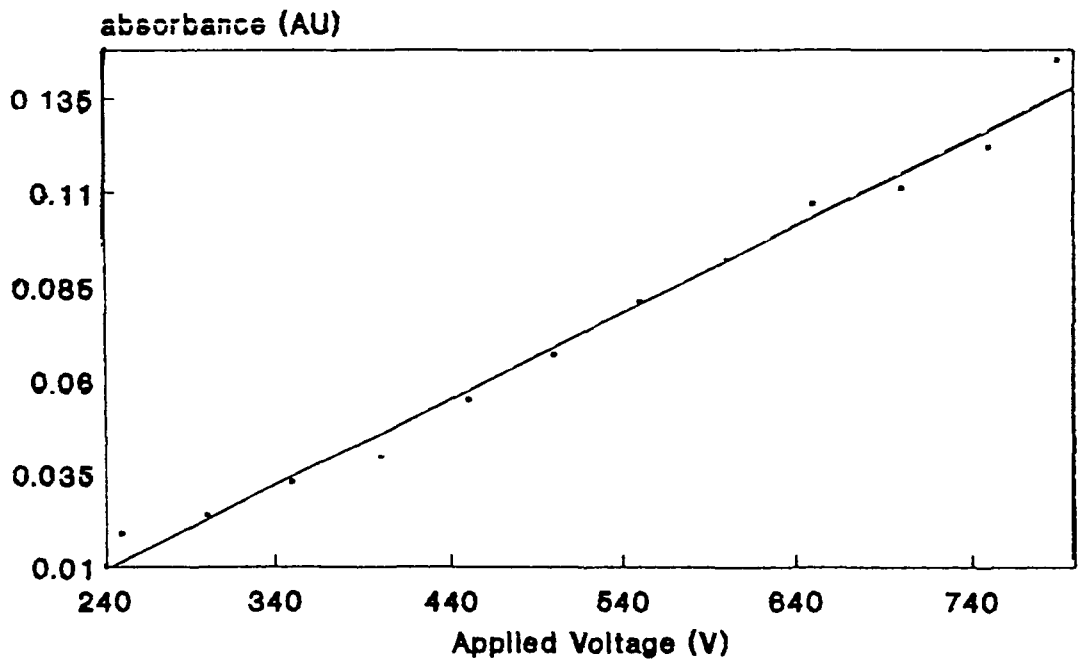

---

3 3 2.4 Formation of the second species

A second species was observed growing in on the same timescale as the decay of the primary photoproduct. In the transient UV/vis difference spectrum (Figure 3 3 2 2) this species can be seen best at 500 nm. Figure 3 3 2 7 shows the oscilloscope trace recorded for the formation of this second species.

Figure 3.3.2.7: Trace recorded for the formation of the second species (see Section 5 2 1 for explanation of axes)

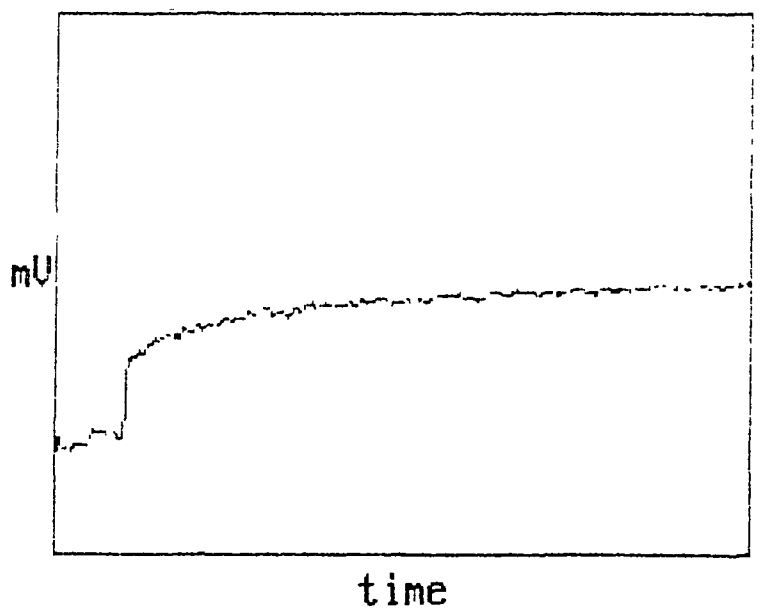

---

3 3.2.5 Effect of parent concentration and CO on the formation of the second species.

The observed rate constants for the formation of this second transient species were recorded as the concentration of $ArCr(CO)_3$ in solution was varied. They are given in Table 3 3 2 4 and shown graphically in Figure 3 3 2 8 It can be seen from the data recorded that the rate constant increased linearly with the concentration of $ArCr(CO)_3$

Table 3.3.2.4: Values of k_{obs} for the formation of the second species at varying concentrations of $ArCr(CO)_3$

$[ArCr(CO)_3]$	k_{obs}
$2\ 23 \times 10^{-4}$ M	248 63
$2\ 32 \times 10^{-4}$ M	273 43
$3\ 99 \times 10^{-4}$ M	452.41
4.97×10^{-4} M	468.04
6.48×10^{-4} M	627 67

Slope = $9\ 25 \pm 1\ 54 \times 10^5$ $dm^3mol^{-1}s^{-1}$

Intercept = $25.80 \pm 49\ 77$ s^{-1}

Correlation coefficient = 0 9610

Figure 3.3.2.8. Plot showing the variation in k_{obs} for the formation of the second species with varying concentration of $ArCr(CO)_3$

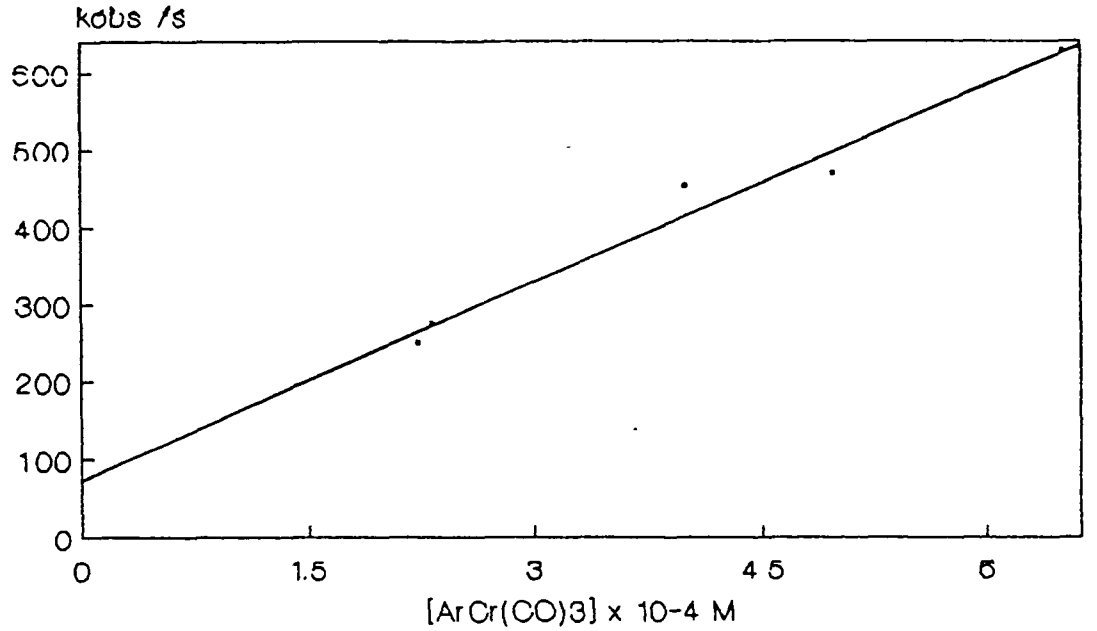

The effect of CO on the formation of this species was also investigated. The flash photolysis experiments were carried out in argon and CO saturated solutions. The overlaid traces in Figure 3.3.2.9 show that the formation of the second transient species is suppressed in CO saturated solution. This would imply that the second transient species is formed *via* the $ArCr(CO)_2$(toluene) species. Therefore it was concluded that this second species is a dinuclear complex formed from the reaction of the dicarbonyl fragment with the parent tricarbonyl, as was observed on the photolysis of $ArCr(CO)_3$ in cyclohexane solution (Reaction 3.3.2.4).

$$ArCr(CO)_2(toluene) + ArCr(CO)_3 \longrightarrow Ar_2Cr_2(CO)_5 \qquad 3.3.2.4$$

Figure 3.3.2.9:Trace (a) shows the formation of the dinuclear species and (b) is the trace recorded under a CO atmosphere (see section 5 2 1 for explanation of axes)

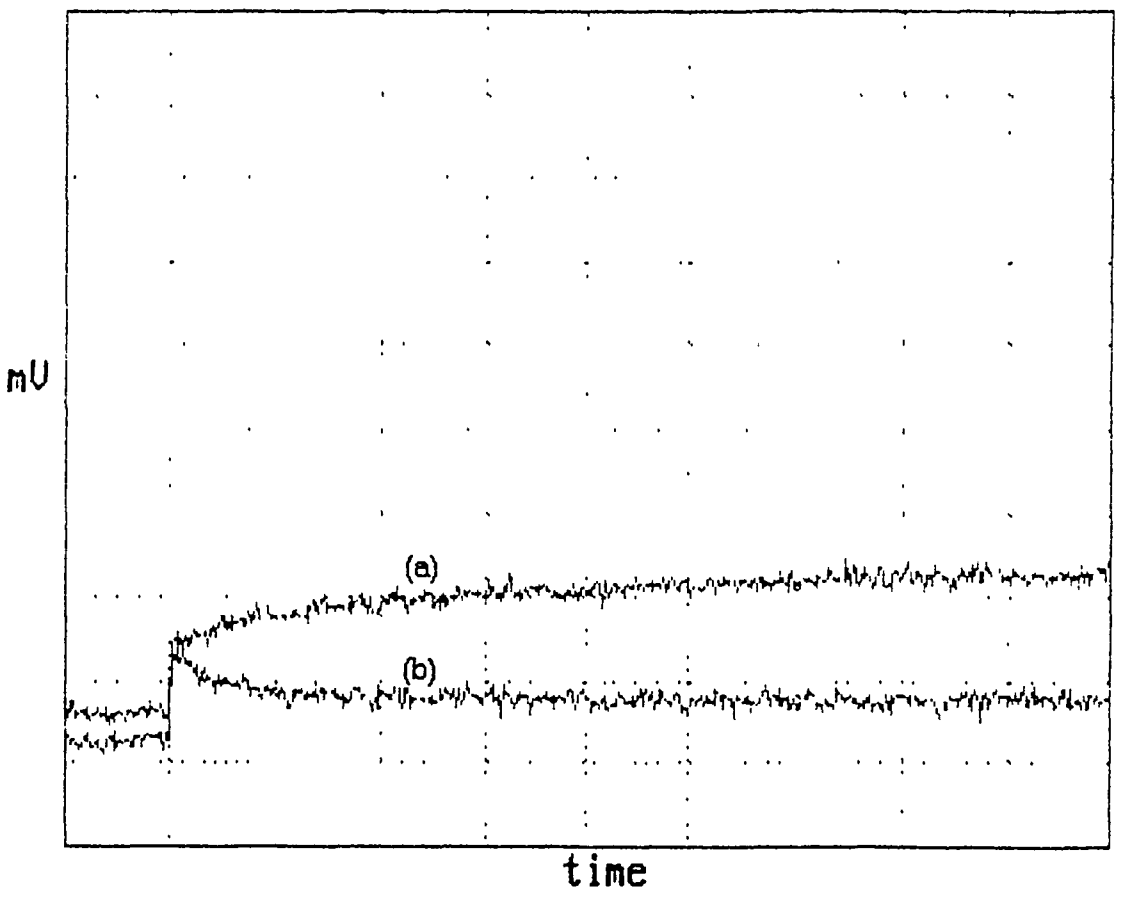

3.3 2.6 Activation parameters for the formation of the dinuclear species

The activation parameters for the formation of the dinuclear species were determined from the Arrhenius and Eyring equations They are listed in Table 3 3 2 6, the experimental data is given in Table 3 3 2 6 and Figure 3 3 2 9

Table 3.3.2.5: Activation parameters for the formation of the dinuclear species

---

E_{act} = 34 32 kJmol^{-1}

$\Delta H^{\neq}$ = 31 76 kJmol^{-1}

$\Delta S^{\neq}$ = -20 79 Jmol^{-1}K^{-1}

$\Delta G^{\neq}$ = 37 96 kJmol^{-1}

The activation energy of the reaction is low at 34 32 kJmol^{-1}. The negative value of $\Delta S^{\neq}$ implies an associative process, which supports the idea of a dinuclear species The $\Delta G^{\neq}$ for the reaction is similar to the value recorded for the reaction of the $ArCr(CO)_2$(toluene) complex with CO and pyridine ligands.

Table 3.3 2.6: Experimental data for the determination of the activation parameters for the formation of the dinuclear species $[ArCr(CO)_3] = 2.93 \times 10^{-4}$ M

T K	$1/T\ K \times 10^{-3}$	$k_2 \times 10^6$	Ln k_2	Ln k_2/T
293	3.41	1.15	13.96	8.28
298	3.36	1.51	14.23	8.53
303	3.30	1.61	14.29	8.58
308	3.25	1.82	14.41	8.68
314	3.18	2.63	14.78	9.03
318	3.14	3.43	15.05	9.29
323	3.10	4.50	15.32	9.54

Arrhenius Plot

Slope = -4127.8 ± 420.9

Intercept = 27.99 ± 0.1

Correlation coefficient = 0.9745

E_{act} = 34.32 ± 3.5 kJmol^{-1}

Eyring Plot

Slope = -3820.4 ± 413.5

Intercept = 21.26 ± 0.12

Correlation coefficient = 0.9719

$\Delta H^{\ddagger}$ = 31.76 ± 3.4 kJmol^{-1}

$\Delta S^{\ddagger}$ = -20.79 ± Jmol^{-1}K^{-1}

Figure 3.3 2.9 Arrhenius (a) and Eyring (b) plots for the formation of the dinuclear species.

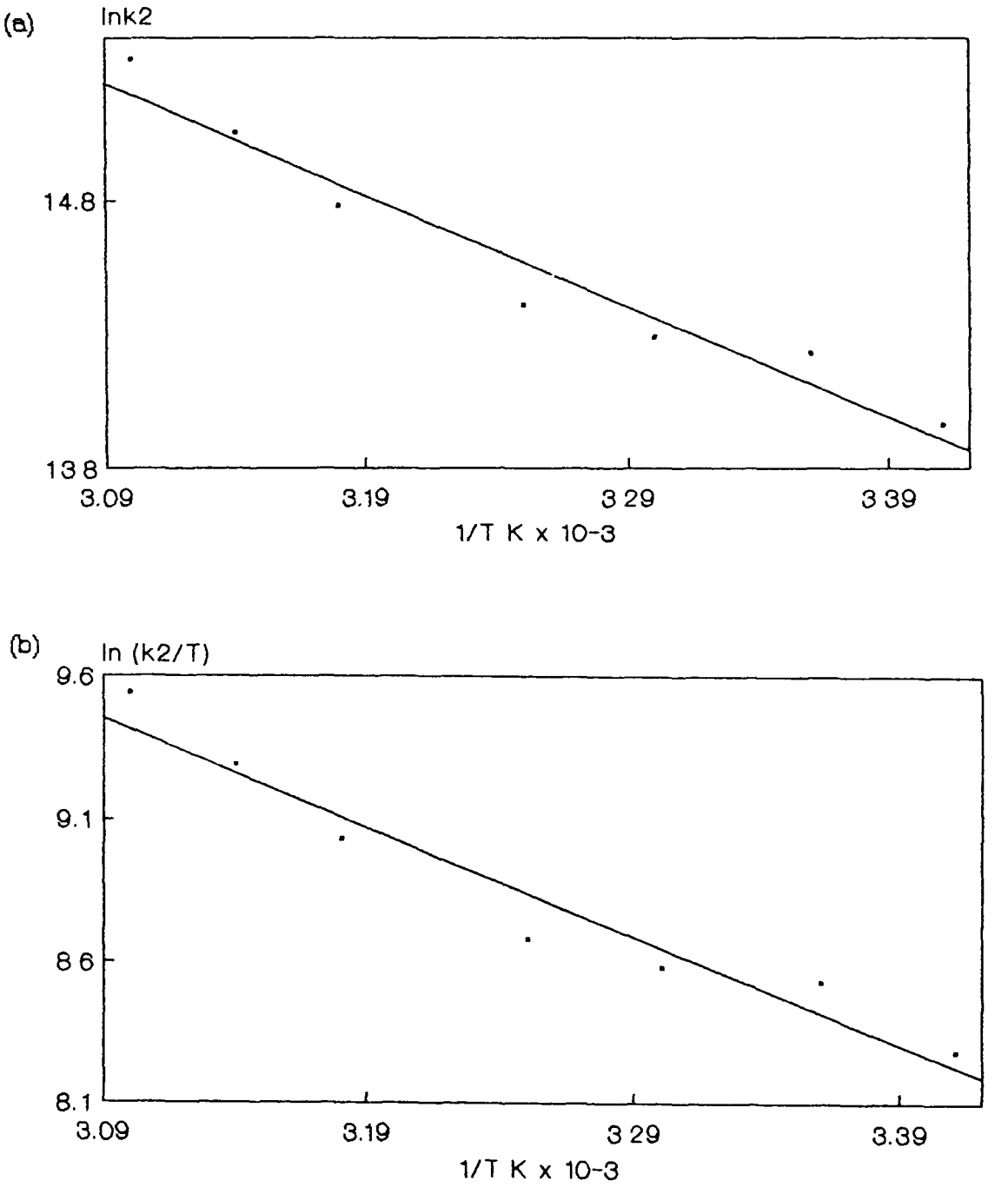

3.3.2 7: Formation of the third species

Following the decay of the primary photoproduct a third transient species was observed on a longer timescale. The trace recorded for the formation of this species is shown in Figure 3.3.2.10, the initial part of the trace shows depletion of the parent complex this is followed by a return to the baseline absorbance recorded for the parent complex. This implies that either the parent tricarbonyl is being reformed or a species with a similar UV absorbance spectrum is being formed. Reformation of the parent complex would take place on a faster timescale which would match the decay of the dicarbonyl toluene fragment. It is possible that the arene exchange product (toluene)$Cr(CO)_3$ is being formed as the UV/vis spectrum of (toluene)$Cr(CO)_3$ in toluene (Figure 3.3.2.11) is identical to the spectrum of $ArCr(CO)_3$ in toluene (Figure 3.3.2.1), this would explain the return to baseline absorbance recorded for the parent complex. In studies on the photolysis products of $ArCr(CO)_3$ loss of the arene group has been reported as a primary photoreaction [14]. Gilbert *et al* [22] reported that the arene exchange product was formed *via* the dicarbonyl species as the addition of carbon monoxide to the system considerably suppressed the exchange process.

Figure 3.3.2.10: Oscilloscope trace recorded for the formation of the third species (see section 5 2 1 for explanation of axes)

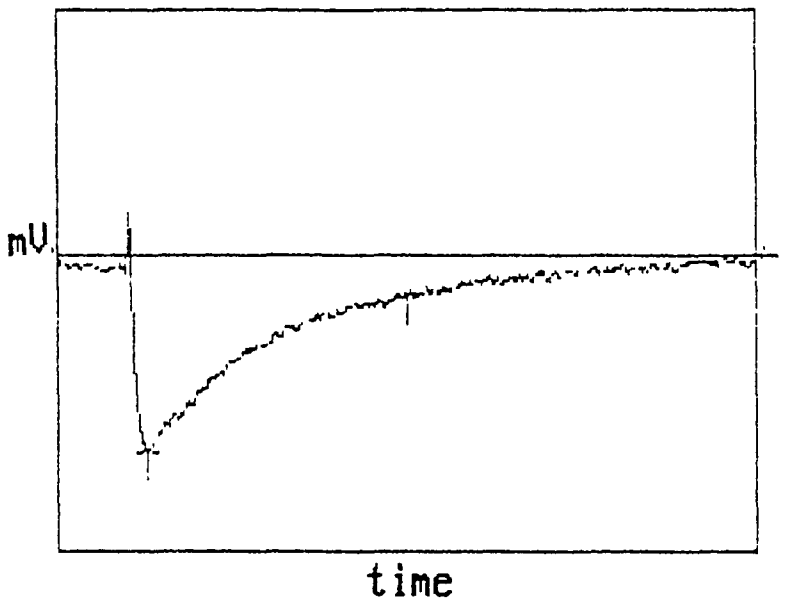

Figure 3.3.2.11: UV/vis spectrum of (toluene)$Cr(CO)_3$ in toluene

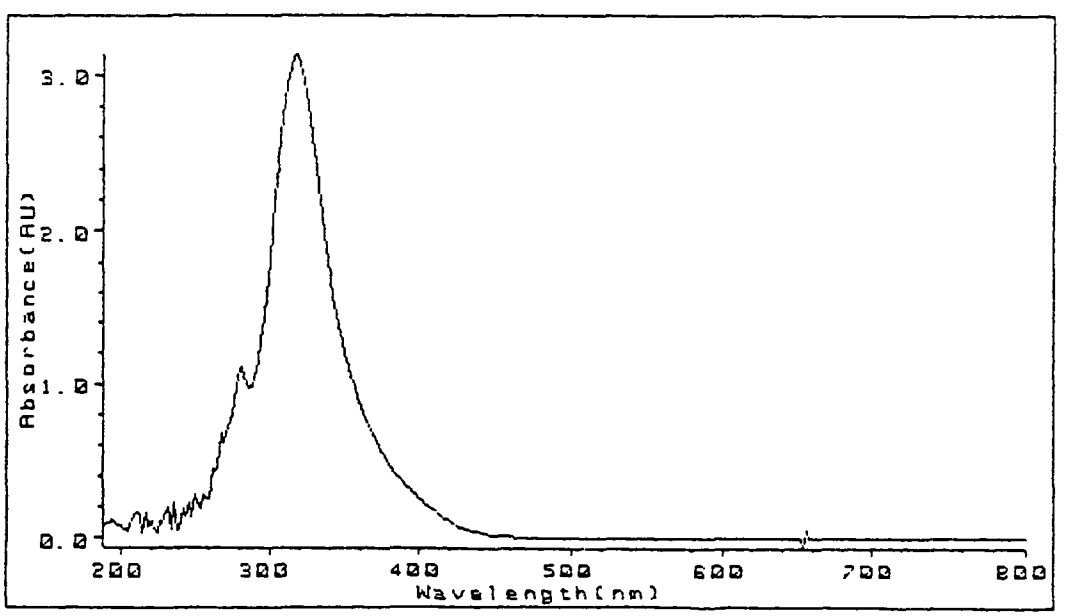

3.3.2.8 Effect of parent concentration and CO on the formation of the arene exchange product

The effect of varying the concentration of $ArCr(CO)_3$ in solution on the rate of formation of the arene exchange product was investigated (Table 3 3 2 7). As can be seen from Table 3 3 2 7 increasing the parent concentration in solution has no effect on the rate of formation of this complex. Therefore it would appear that the reaction mechanism does not involve the parent tricarbonyl

Table 3.3.2.7: Effect of parent concentartion on the rate of formation of the arene exchange product

$[ArCr(CO)_3]$ M	$k_{obs}s^{-1}$
$1\ 88 \times 10^{-4}$	62 99
$1\ 97 \times 10^{-4}$	104 72
$2\ 58 \times 10^{-4}$	130 16
$2\ 93 \times 10^{-4}$	106 84
$3\ 08 \times 10^{-4}$	106 34
$3\ 32 \times 10^{-4}$	108 37

The formation of this arene exchange product was also investigated in a CO saturated solution Figure 3 3 2 12 shows the effect of CO on the formation of the arene exchange product.

Figure 3.3.2.12: (a) Formation of the arene exchange product under argon (b) similar trace recorded under a carbon monoxide atmosphere (see Section 5 2 1 for explanation of axes).

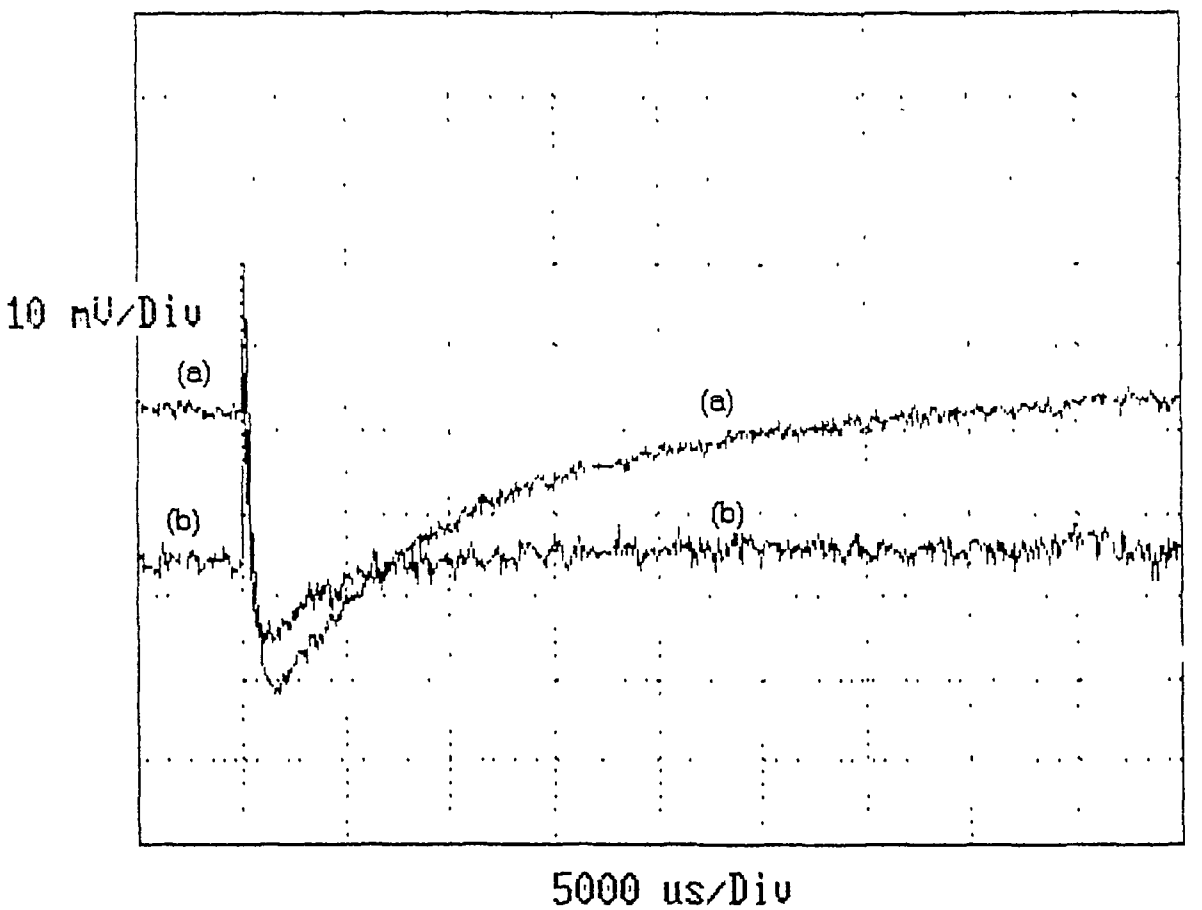

From the trace obtained under an Ar atmosphere (Figure 3 3 2 12) one can see that there is depletion of the parent complex followed by a return to the baseline absorbance Under a CO atmosphere the depletion of the parent complex is greatly reduced , from this reduced depletion there is also a return to the baseline absorbance This would seem to imply that the arene exchange process occurs *via* the dicarbonyl solvent complex as proposed by Gilbert *et al* [22] (Scheme 3 3 2 2)

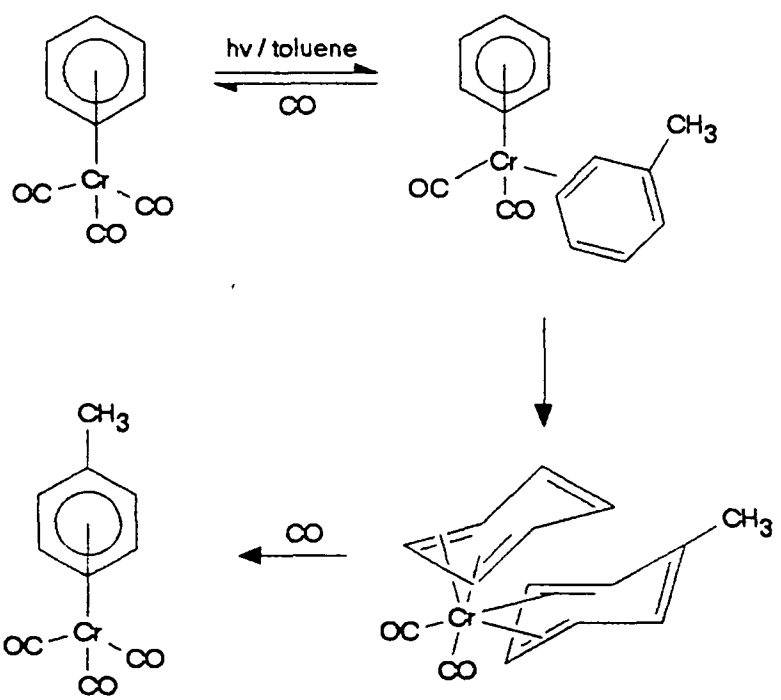

Scheme 3.3 2.2

These workers [22] proposed that from the dicarbonyl solvent complex ring slippage occurs to form two η^4 interactions with the metal centre The arene ring is then displaced, a CO molecule is captured from solution and the toluene forms an η^6 interaction to give the (toluene)$Cr(CO)_3$ complex One problem with this mechanism is that the concentration

of CO in solution is so low (i e the only CO in solution are those knocked off on photolysis of the parent complex) Therefore the final stage of the reaction going from the η^4 to η^6 complex is going to be very inefficient Yet the trace recorded for the formation of this species (Figure 3 3 2.10) appears to show a relatively efficient process.

It may be possible, that as well as seeing the solvent complex as the primary photoproduct there is a second primary photoproduct which is not detected i.e. an η^4 tricarbonyl solvent complex the arene exchange product is then formed from this species (Scheme 3 3 2 3) In a CO saturated solution this η^4 species may pick up a CO molecule to form an η^4 tetracarbonyl complex which can then reform the parent tricarbonyl (Scheme 3 3 2 4) This would account for the reduction in the arene exchange process under a carbon monoxide atmosphere.

The primary photoreaction of the $ArW(CO)_3$ complex which has a similar electronic spectrum to $ArCr(CO)_3$ does not involve photoinduced exchange of CO and has been reported to be possibly isomerisation of the η^6-arene bonding to a η^4-arene bonding [14,38] The photochemistry of the $M(CO)_6$ complexes (M= Cr, W, or Mo) have all been reported to be similar Therefore it is proposed that the arene exchange process occurs via a η^4 complex rather than the dicarbonyl solvent fragment.

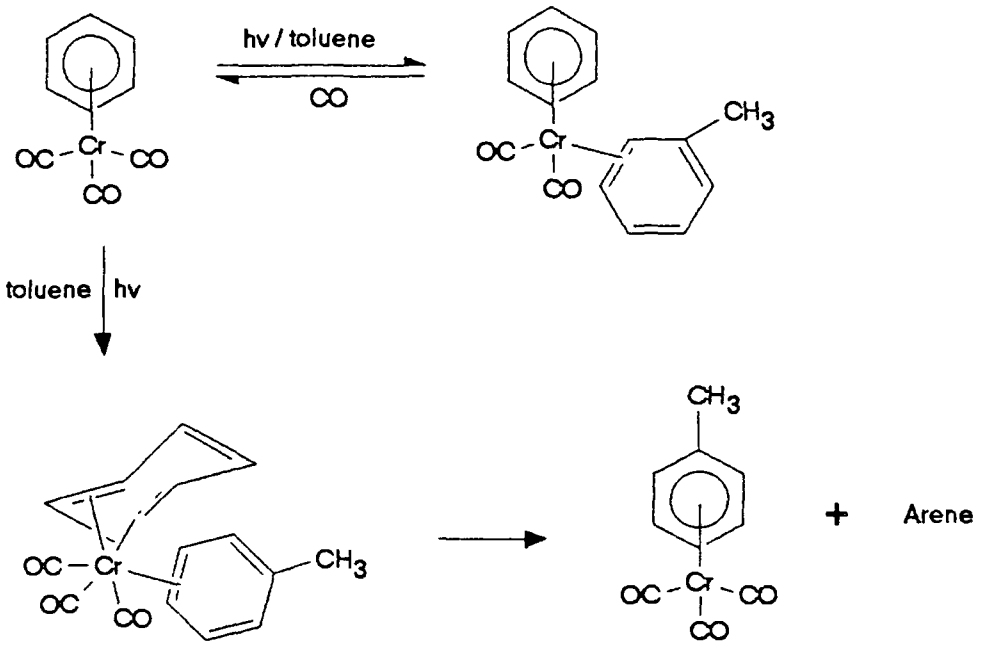

Scheme 3.3.2.3

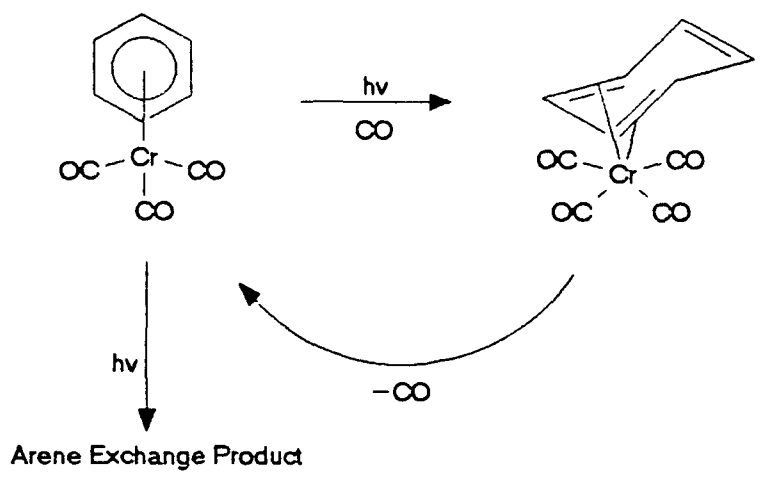

Scheme 3.3.2.4

3 3 2.9 Flash photolysis of $ArCr(CO)_3$ in toluene in the presence of pyridine

The interactions of the monomeric and polymeric pyridine ligands were further investigated by comparing the results obtained for the manganese system with a second system. Therefore the reaction of the $ArCr(CO)_2$(toluene) complex with pyridine ligands was investigated to see if the trend observed in the manganese system was observed with the chromium tricarbonyl complex.

The solvent complex reacts with the pyridine in solution to form the $ArCr(CO)_2$(pyridine) complex (Reactions 3 3 2 5-3 3 2 6)

$$ArCr(CO)_3 \xrightarrow{h\nu} ArCr(CO)_2(\text{toluene}) + CO \qquad 3.3.2.5$$

$$ArCr(CO)_2(\text{toluene}) + \text{pyridine} \longrightarrow ArCr(CO)_2(\text{pyridine}) \qquad 3.3.2.6$$

This complex appears to be stable and as can be seen from Figure 3 3 2 13 all of the parent tricarbonyl is converted to the $ArCr(CO)_2$(pyridine) complex during the course of the experiment to yield a red-orange colour product. Figure 3 3 2 14 shows the decay of the $ArCr(CO)_2$(toluene) complex followed by the formation of the $ArCr(CO)_2$(pyridine) species.

In Figure 3 3 2 13 it is noteworthy that the isosbestic point at 350 nm is preserved to very high fractional conversions. This rules out any further net photoreaction of the $ArCr(CO)_2$(pyridine) complex on the same timescale.

Figure 3.3.2.13: Changes observed in the UV/vis spectrum of $ArCr(CO)_3$ during the course of a flash photolysis experiment in the presence of pyridine in toluene

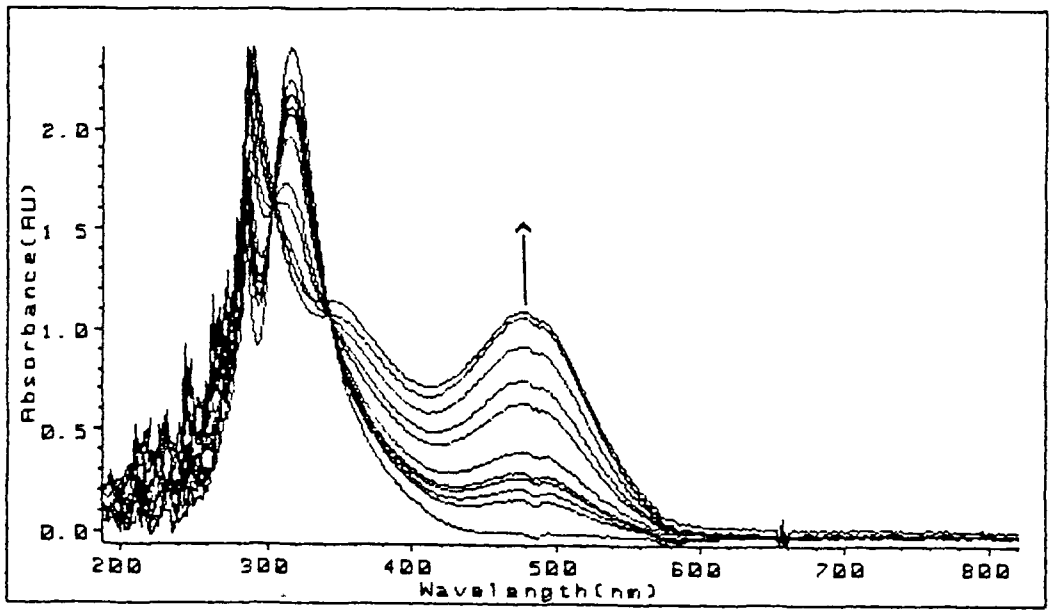

There was no evidence to suggest that arene group exchange occurs in the presence of pyridine Wrighton and Haverty [21] reported a nearly quantitative chemical yield of $ArCr(CO)_2$(pyridine) which implies that if arene exchange takes place it is a minor component of the photochemistry

Figure 3 3.2.14: Shows (a) the decay of the $ArCr(CO)_2$(toluene) complex followed by (b) the formation of the $ArCr(CO)_2$(pyridine) complex (see section 5 2 1 for explanation of axes)

(a)

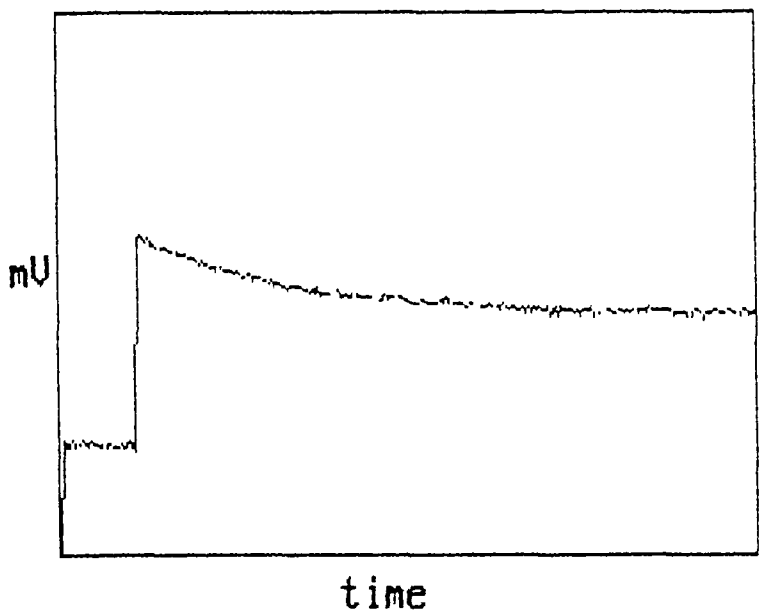

(b)

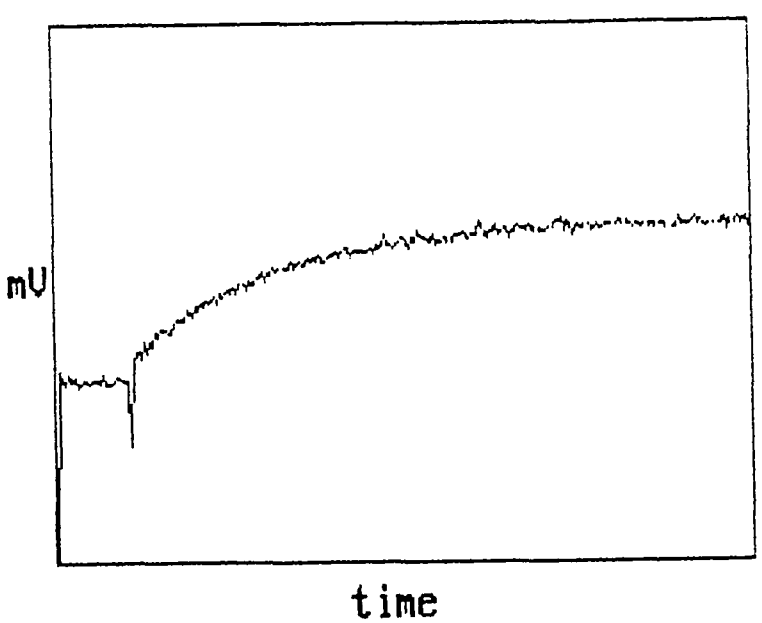

The rates of reaction of monomeric and polymeric pyridine ligands were investigated (Table 3 3 2 8) The activation parameters for Reaction 3 3 2 6 were also determined As in the manganese system the polymeric pyridine ligands were in the form of poly(styrene-co-4-vinylpyridine) with the mole ratio of styrene to 4-vinylpyridine varied The interaction of a substituted pyridine with the $ArCr(CO)_2$(toluene) complex was also investigated to see the effect if any of a change in the electronic nature of the pyridine ligand

---

Table 3.3.2.8: Second order rate constants for the reaction of pyridine ligands with the $ArCr(CO)_2$(toluene) complex.

Ligand	k_2 ($dm^3mol^{-1}s^{-1}$)
pyridine	8.33×10^5
mepyridine	8.30×10^5
5.1 copol	5.93×10^5
10 1 copol	4.92×10^5
30 1 copol	6.50×10^5
40.1 copol	12.12×10^5

mepyridine = 4-methylpyridine, copol = poly(styrene-co-4-vinylpyridine)

From the second order rate constants calculated one can see that the free pyridine complexes react with similiar rates, which in general are quicker than the polymeric ligands The trend that was observed in the manganese system where the lower loading polymers complexed with the dicarbonyl species at higher rates is not apparent

Although the two lowest loadings have faster formation rates than the high loading polymer and only the lowest loading copolymer has a higher rate of formation than the free pyridine complexes

The experimental data for the determination of the second order rate constants is given in Tables 3 3 2 9-3.3 2.14 and shown graphically in Figures 3 3 2 15-3 3.2 20

Table 3.3.2.9 and Figure 3.3.2.15: Second order rate constant for the reaction of $ArCr(CO)_2$(toluene) with pyridine

---

[pyridine]	k_{obs} s^{-1}
1 39 x 10^{-2}M	13930
2 28 x 10^{-2}M	19960
3 03 x 10^{-2}M	29606
4 68 x 10^{-2}M	39742
5 56 x 10^{-2}M	49220

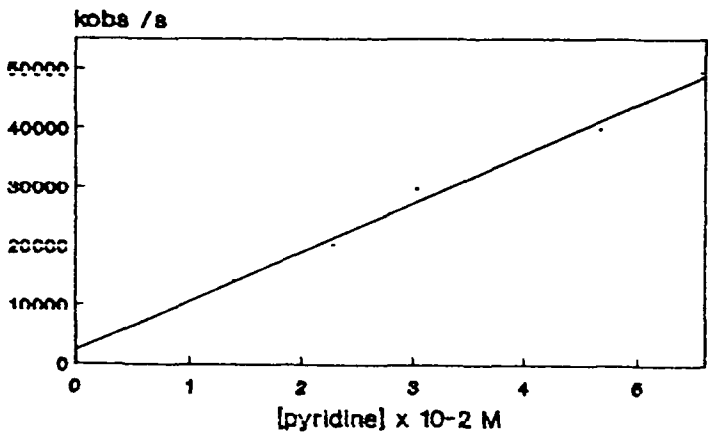

Slope = 8 33 ± 0 5 x 10^5 $dm^3mol^{-1}s^{-1}$

Intercept = 2282.3 ± 17711.6 s^{-1}

Correlation coefficient = 0.99464

Table 3.3.2.10 and Figure 3.3.2.16. Second order rate constant for the reaction of $ArCr(CO)_2$(toluene) with 5 1 poly(styrene-co-4-vinylpyridine)

[pyridine]	$k_{obs}s^{-1}$
1 77 x 10^{-2} M	7476 5
2 07 10^{-2} M	8657 8
2 61 10^{-2} M	12126
3 03 10^{-2} M	15134
3 39 10^{-2} M	16619

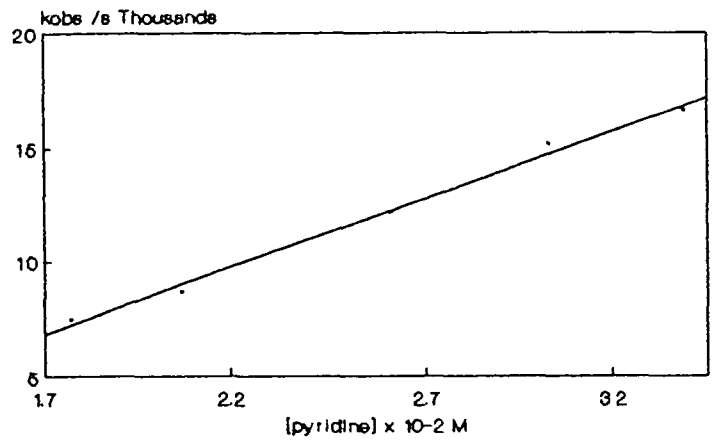

Slope = 5 93 ± 0 3 x 10^5 $dm^3mol^{-1}s^{-1}$

Intercept = -3254.4 ± 376 67 s^{-1}

Correlation coefficient = 0 99661

Table 3.3.2.11 and Figure 3 3 2 17: Second order rate constant for the reaction of $ArCr(CO)_2$(toluene) with 10 1 poly(styrene-co-4-vinylpyridine)

[pyridine]	$k_{obs}s^{-1}$
1 23 x 10^{-2} M	8330 5
1 51 10^{-2} M	9754.9
1 82 10^{-2} M	11744
2 11 10^{-2} M	12277
2 36 10^{-2} M	14106

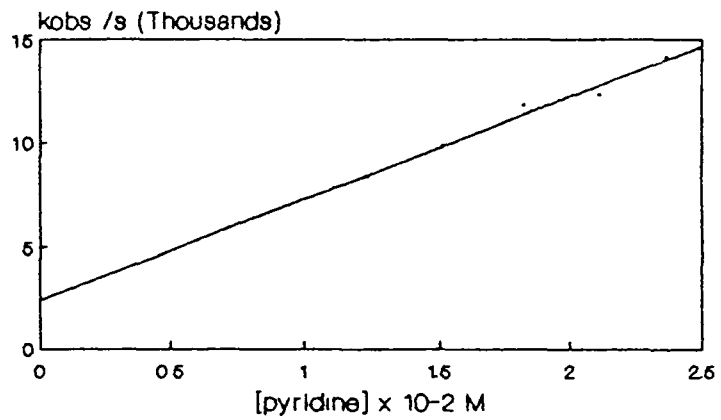

Slope = 4 92 ± 0 4 x 10^5 $dm^3mol^{-1}s^{-1}$

Intercept = 2364 8 ± 376 78 s^{-1}

Correlation coefficient = 0 98941

Table 3.3 2.12 and Figure 3 3.2 18. Second order rate constant for the reaction of $ArCr(CO)_2$(toluene) with 30 1 poly(styrene-co-4-vinylpyridine)

[pyridine]	$k_{obs}s^{-1}$
1 70 x 10^{-2} M	9777 7
2 42 10^{-2} M	13513
2 90 10^{-2} M	17622
3 23 10^{-2} M	19914
3 77 10^{-2} M	22756

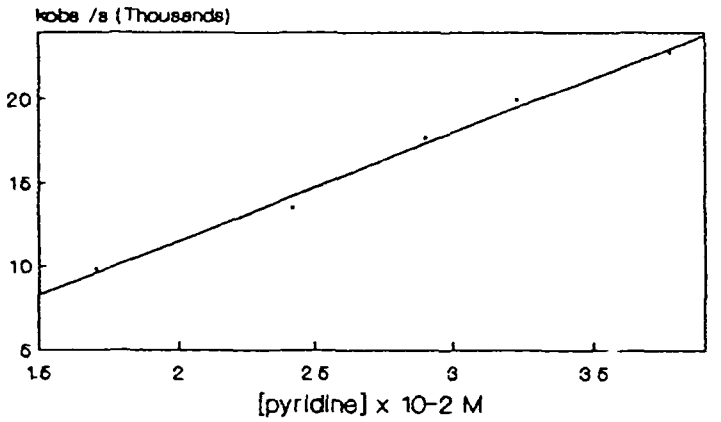

Slope = 6 50 ± 0.34 x 10^5 $dm^3mol^{-1}s^{-1}$

Intercept = -1496 ± 540 s^{-1}

Correlation coefficient = 0 99585

Table 3.3.2.13 and Figure 3.3 2.19: Second order rate constant for the reaction of $ArCr(CO)_2$(toluene) with 40 1 poly(s tyrene-co-4-vinylpyridine)

[pyridine]	$k_{obs}s^{-1}$
6 60 x 10^{-3} M	10101
8 04 x 10^{-3} M	11489
9.40 x 10^{-3} M	12457
1 10 x 10^{-2} M	15087
1 25 x 10^{-2} M	17215

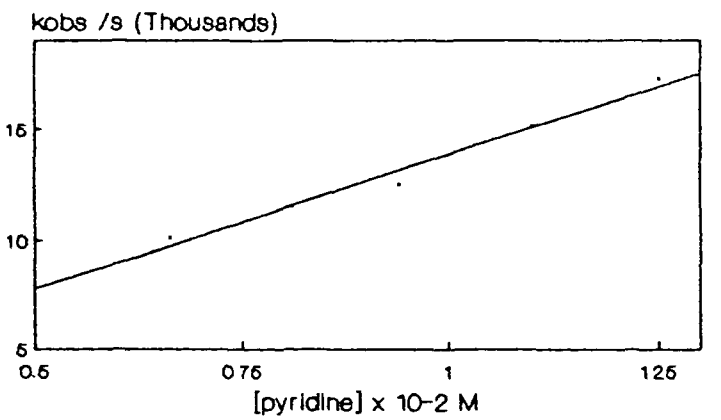

Slope = 1.21 ± 0 1 x 10^6 $dm^3mol^{-1}s^{-1}$

Intercept = 1742 2 ± 80 s^{-1}

Correlation coefficient = 0 98936

Table 3.3.2.14 and Figure 3 3 2.20. Second order rate constant for the reaction of $ArCr(CO)_2$(toluene) with 4-methylpyridine

[mepyr]	$k_{obs}s^{-1}$
9 66 x 10^{-3} M	10350
2 04 x 10-2 M	17159
3 33 10-2 M	29157
4 08 10-2 M	36768
5 80 10-2 M	49283

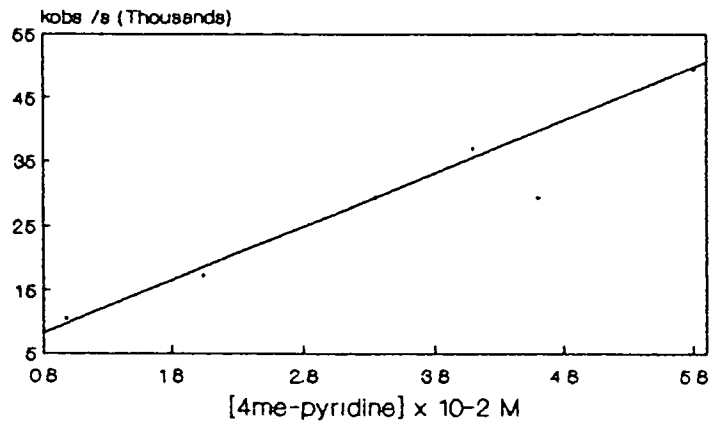

Slope = 8 29 ± 0 32 x 10^5 $dm^3mol^{-1}s^{-1}$

Intercept = 1648 2 ± 1202 1 s^{-1}

Correlation coefficient = 0 99774

3 3.2 10 Activation parameters for the reaction of $ArCr(CO)_2$(toluene) with the pyridine ligands

The activation parameters for Reaction 3 3 2 6 were determined using the Arrhenius and Eyring equations as described in Section 5 3 8 As in the manganese system, in determining the activation parameters k_2 was used for the free pyridine while k_{obs} was used in the calculations for the polymeric ligands ($k_2 = k_{obs}$/[pyridine]) The parameters determined are summarised in Table 3 3 2 15 The experimental data is given in Tables 3 3 2 16-3 3 2 21 and shown graphically in Figures 3 3 2 21-3 3 2 23

Table 3.3.2.15: Activation parameters determined for the reaction of $ArCr(CO)_2$(toluene) with pyridine ligands

Ligand	E_{act} kJmol^{-1}	$\Delta H^{\ddagger}$ kJmol^{-1}	$\Delta S^{\ddagger}$ Jmol^{-1}K^{-1}	$\Delta G^{\ddagger}$ kJmol^{-1}
Pyridine	35 61	32 98	-18 15	38 39
Mepyr	41 08	38 49	-1 91	39 06
5 1 copol	35 04	32 72	-52 60	48 38
10 1 copol	30 42	27 95	-72 14	49 45
30 1 copol	30 67	28 18	-72 69	49 84
40 1 copol	30 54	27 98	-69 09	48 57

As in the manganese system the activation energies (E_{act}) determined for the reaction of the monomeric and polymeric ligands with the dicarbonyl complex are essentially the same with the higher loading polymers having the lower values. The entropy of activation ($\Delta S^{\ddagger}$) varies from the monomeric to polymeric ligands. As can be seen from Table 3.3.2.15 the large negative value of $\Delta S^{\ddagger}$ for the reaction of the polymeric ligands indicates the associative nature of the transition state. The low negative value of $\Delta S^{\ddagger}$ for the monomeric pyridine ligands implies a less associative process than for the polymeric ligands. The values of the Gibbs free energy of activation ($\Delta G^{\ddagger}$) for the polymeric ligands are practically the same which are higher than the monomeric ligands. The lower value of $\Delta G^{\ddagger}$ for the free pyridine ligands implies a more spontaneous process. This compares to the second order rate constants which are higher for the monomeric ligands.

Table 3 3 2 16. Experimental data for determining the activation parameters for the reaction of the $ArCr(CO)_2$(toluene) complex with pyridine [pyridine] = 1 31 x 10^{-2} M

T K	1/T K x 10^{-3}	k_2 x 10^6	Ln k_2	Ln k_2/T
288	3 47	0 75	13 53	7 87
293	3 41	0 89	13 70	8 02
298	3 36	1 17	13 97	8 28
302	3 31	1 26	14 05	8 34
308	3 25	1 92	14 47	8.74
312	3 21	2 13	14 57	8 83
318	3 14	2 62	14 78	9 02
323	3 10	3 87	15 17	9 39

Arrhenius Plot

Slope = -4283 ± 248

Intercept = 28 33 ± 0 09

Correlation coefficient = 0 9906

E_{act} = 35 61 ± 2 07 kJmol^{-1}

Eyring Plot

Slope = -3966 7 ± 244 21

Intercept = 21 58 ± 0 08

Correlation coefficient = 0 9882

$\Delta H^{\ddagger}$ = 32 98 ± 2 07 kJmol^{-1}

$\Delta S^{\ddagger}$ = -18 15 ± 0 71 Jmol^{-1}K^{-1}

Figure 3 3 2.21. Arrhenius (a) and Eyring (b) plots for the reaction of $ArCr(CO)_2$(toluene) with pyridine

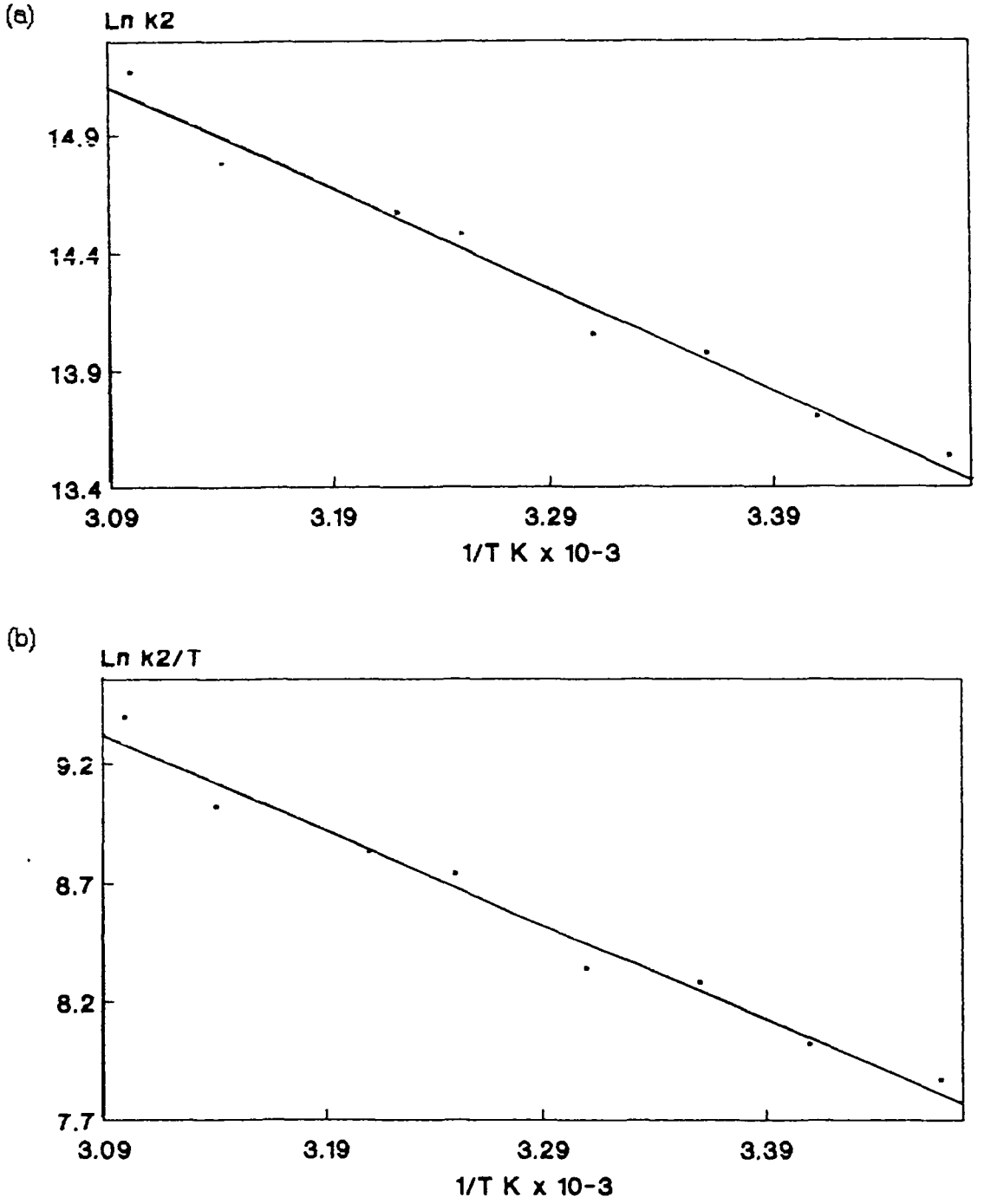

Table 3.3.2.17 Experimental data for determining the activation parameters for the reaction of $ArCr(CO)_2$(toluene) with 5 1 poly(styrene-co-4-vinylpyridine) in toluene [pyridine] = $3\ 03 \times 10^{-2}$ M

T K	$1/T\ K \times 10^{-3}$	$k_{obs} \times 10^4$	Ln k_{obs}	Lnk_{obs}/T
288	3 47	1 21	9 40	3 73
293	3 41	1 62	9 69	4 01
299	3 34	2 26	10 03	4 32
303	3 30	2 59	10 16	4 45
308	3 25	3 18	10 37	4 64
312	3 21	4 02	10 60	4 86
318	3 14	4 71	10 75	5 00

Arrhenius Plot

Slope = -4214 8 ± 178 45

Intercept = 24 07 ± 0 05

Correlation coefficient = 0 99555

E_{act} = 35 04 ± 1 48 kJmol^{-1}

Eyring Plot

Slope = -3936 9 ± 177 3

Intercept = 17.43 ± 0 05

Correlation coefficient = 0 99497

$\Delta H^{\ddagger}$ = 32 72 ± 1 47 kJmol^{-1}

$\Delta S^{\ddagger}$ = -52.60 ± 0 41 Jmol^{-1}K^{-1}

Figure 3 3.2 22 Arrhenius (a) and Eyring (b) plots for the reaction of $ArCr(CO)_2$(toluene) with 5 1 poly(styrene-co-4-vinylpyridine)

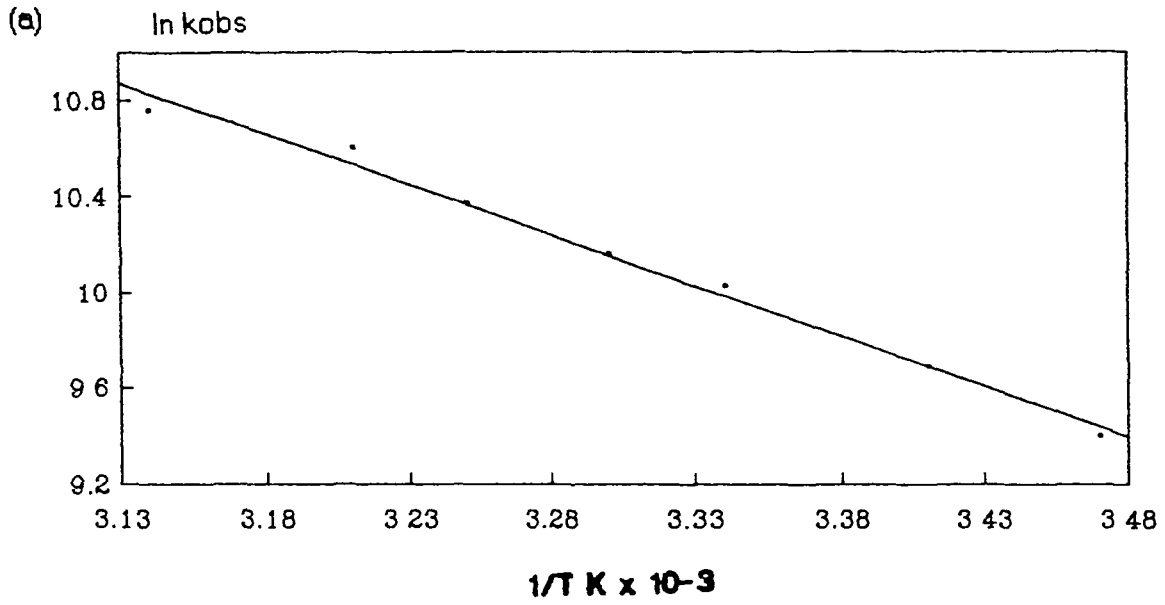

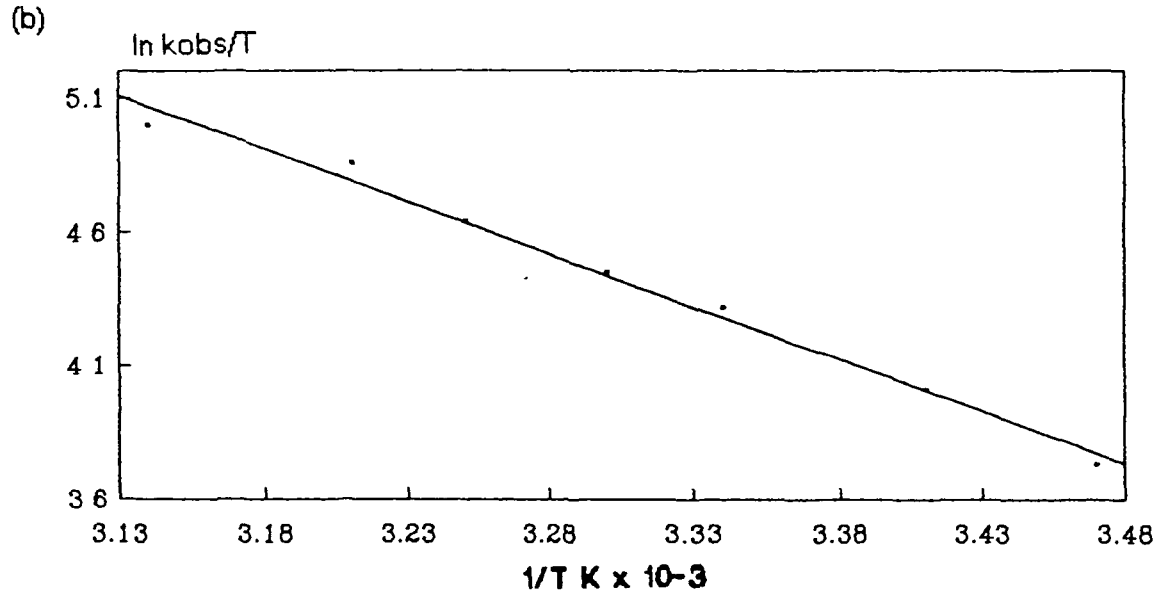

Table 3.3.2 18: Experimental data for the determination of the activation parameters for the reaction of $ArCr(CO)_2$(toluene) with 10 1 poly(styrene-co-4-vinylpyridine) in toluene [pyridine] = 1 23 x 10^{-2} M

T K	1/T K x 10^{-3}	k_{obs} x 10^4	Ln k_{obs}	Ln k_{obs}/T
291	3 44	0 99	9 20	3 53
299	3 34	1 30	9 48	3 78
303	3 30	1 64	9 70	3 99
308	3 25	2 16	9 98	4 25
313	3 19	2 48	10 12	4 37
320	3 13	2 78	10 23	4 47
323	3 10	3 54	10 47	4 70

Arrhenius Plot

Slope = -3659 4 ± 240 54

Intercept = 21 78 ± 0 07

Correlation coefficient = 0 98937

E_{act} = 30 42 ± 2 0 kJmol^{-1}

Eyring Plot

Slope = -3362 4 ± 235 2

Intercept = 15 08 ± 0 07

Correlation coefficient = 0 98799

$\Delta H^{\ddagger}$ = 27 95 ± 1 95 kJmol^{-1}

$\Delta S^{\ddagger}$ = -72 14 ± 0 58 Jmol^{-1}K^{-1}

Figure 3 3.2.23: Arrhenius (a) and Eyring (b) plots for the reaction of $ArCr(CO)_2$(toluene) with 10 1 poly(styrene-co-4-vinylpyridine)

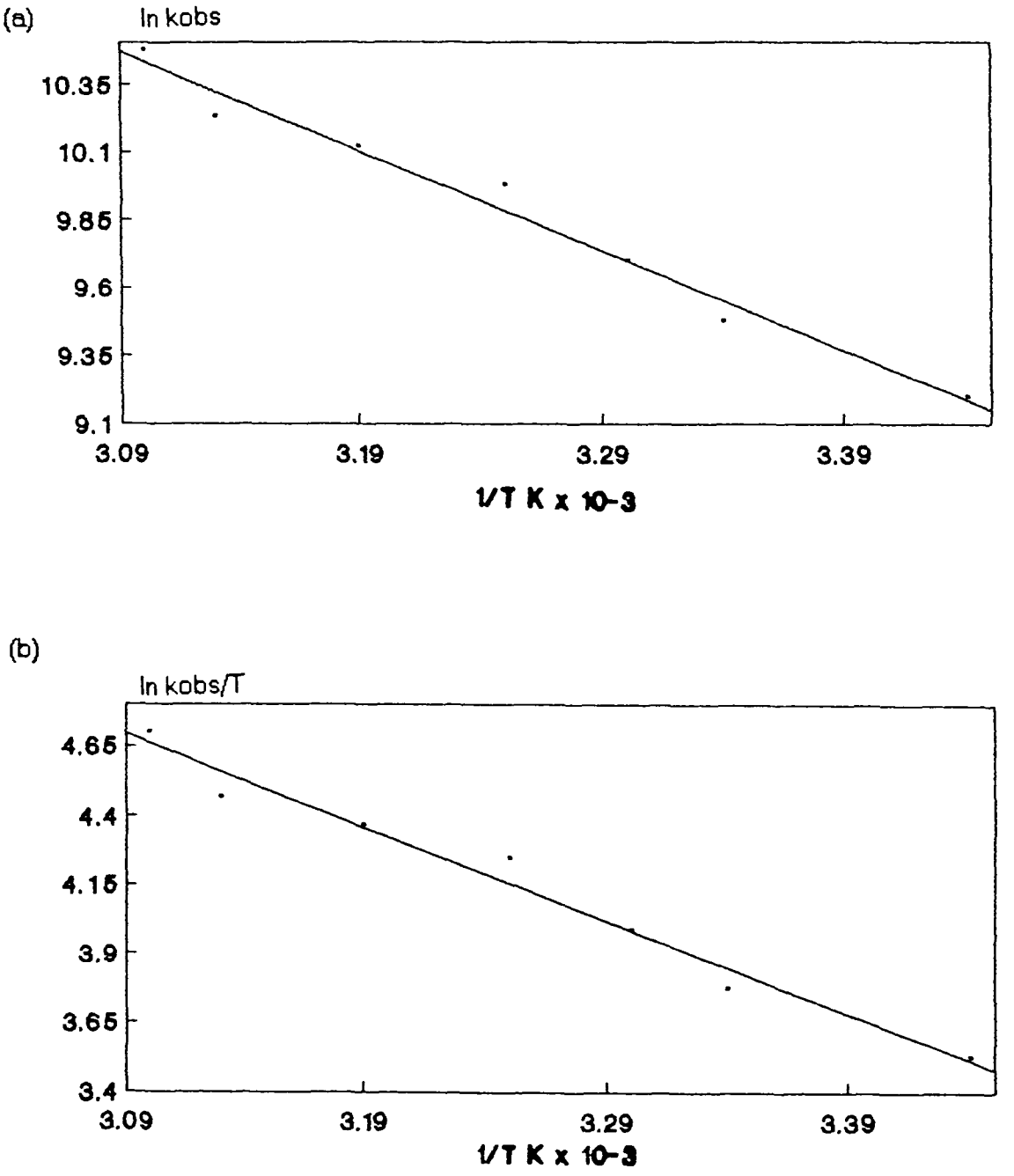

Table 3.3.2 19: Experimental data for the determination of the activation parameters for the reaction of $ArCr(CO)_2$(toluene) with 30 1 poly(styrene-co-4-vinylpyridine) [pyridine] = 1 20 x 10^{-2} M

T K	1/T K x 10^{-3}	k_{obs} x 10^4	Ln k_{obs}	Lnk_{obs}/T
293	3 41	0 90	9 11	3 43
298	3 36	1 09	9 30	3 60
302	3 31	1 49	9 61	3 90
308	3 25	1 52	9 63	3 90
312	3 21	2 16	9 98	4 24
318	3 14	2 51	10 13	4 37
324	3 09	2 95	10 29	4 51

Arrhenius Plot

Slope = -3689 1 ± 286 94

Intercept = 21 72 ± 0 08

Correlation coefficient = 0 98521

E_{act} = 30 67 ± 2 4 kJmol^{-1}

Eyring Plot

Slope = -3389 ± 290 89

Intercept = 15 02 ± 0 08

Correlation coefficient = 0 98206

$\Delta H^{\ddagger}$ = 28 18 ± 2 42 kJmol^{-1}

$\Delta S^{\ddagger}$ = -72.69 ± 0 67 Jmol^{-1}K^{-1}

Figure 3 3 2.24: Arrhenius (a) and Eyring (b) plots for the reaction of $ArCr(CO)_2$(toluene) with 30 1 poly(styrene-co-4-vinylpyridine)

(a)

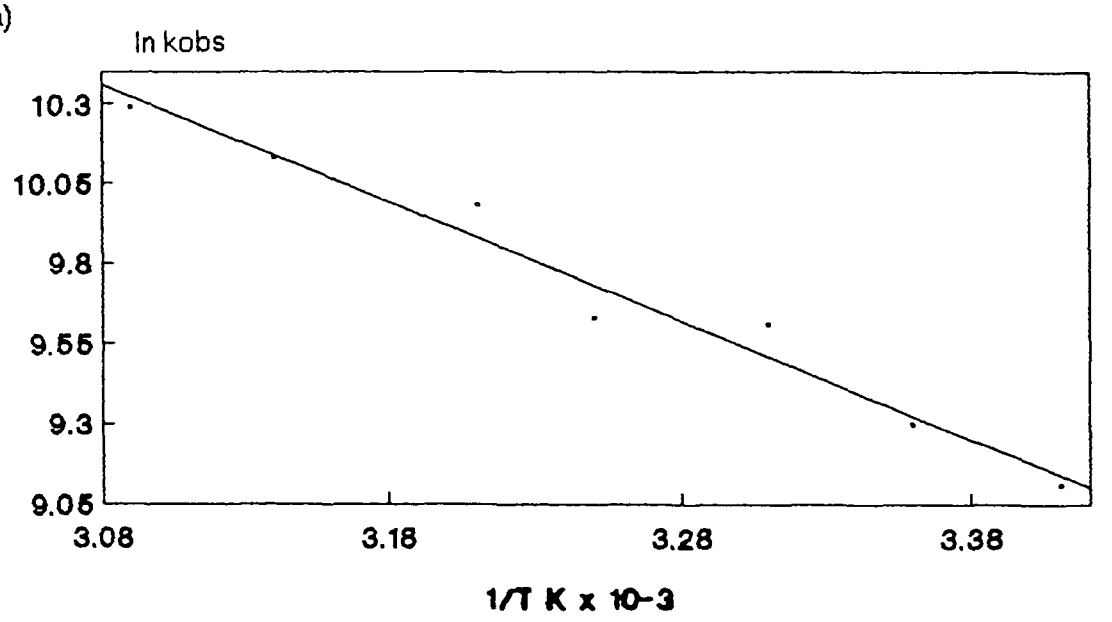

(b)

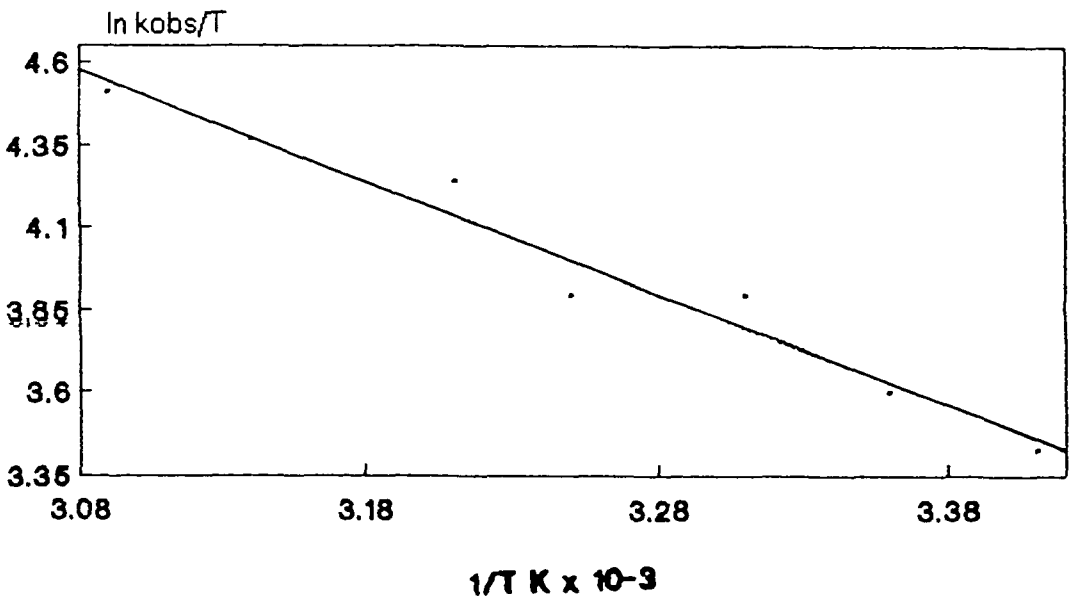

Table 3.3 2 20: Experimental data for the determination of the activation parameters for the reaction of $ArCr(CO)_2$(toluene) with 40 1 poly(styrene-co-4-vinylpyridine) [pyridine] = 0 91 x 10^{-2} M

T K	1/T K x 10^{-3}	k_{obs} x 10^4	Ln k_{obs}	Ln k_{obs}/T
291	3 44	1 44	9 58	3 90
297	3 37	1 84	9 82	4 13
303	3 30	2 18	9 99	4 28
309	3 24	2 92	10 28	4 55
313	3 19	3 54	10 48	4 73
318	3 14	4 10	10 62	4 86
325	3 08	5 46	10 91	5 12

Arrhenius Plot

Slope = -3673 ± 136 69

Intercept = 22 18 ± 0 04

Correlation coefficient = 0 99656

E_{act} = 30 54 ± 1 1 kJmol-1

Eyring Plot

Slope = -3365 9 ± 122 2

Intercept = 15 45 ± 0 03

Correlation coefficient = 0 99672

$\Delta H^{\ddagger}$ = 27 98 ± 1 0 kJmol^{-1}

$\Delta S^{\ddagger}$ = -69 09 ± 0 25 Jmol^{-1}K^{-1}

Figure 3.3 2.25: Arrhenius (a) and Eyring (b) plots for the reaction of $ArCr(CO)_2$(toluene) with 40 1 poly(styrene-co-4-vinylpyridine)

(a)

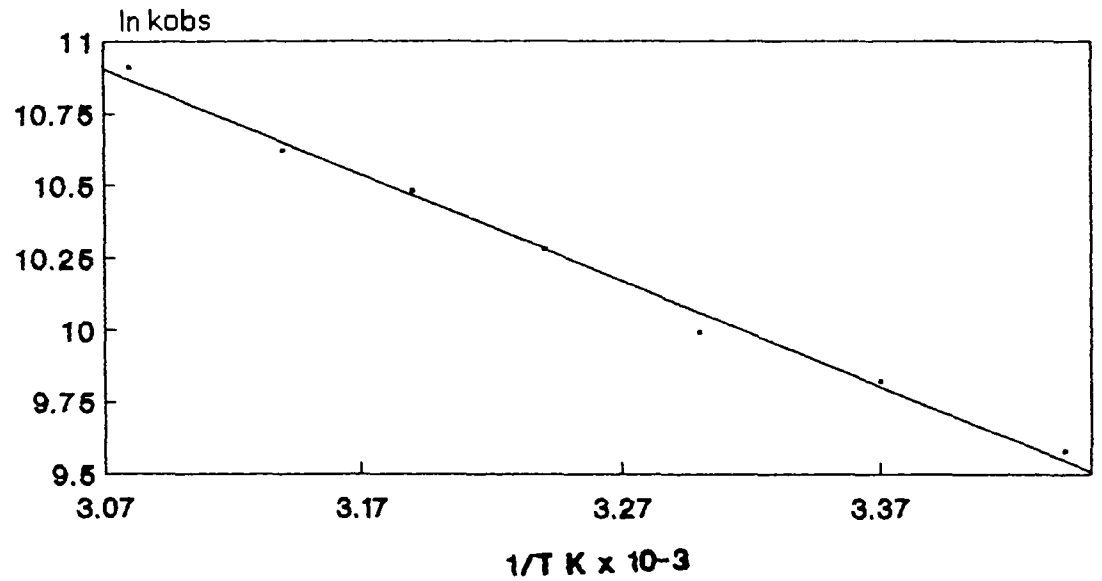

(b)

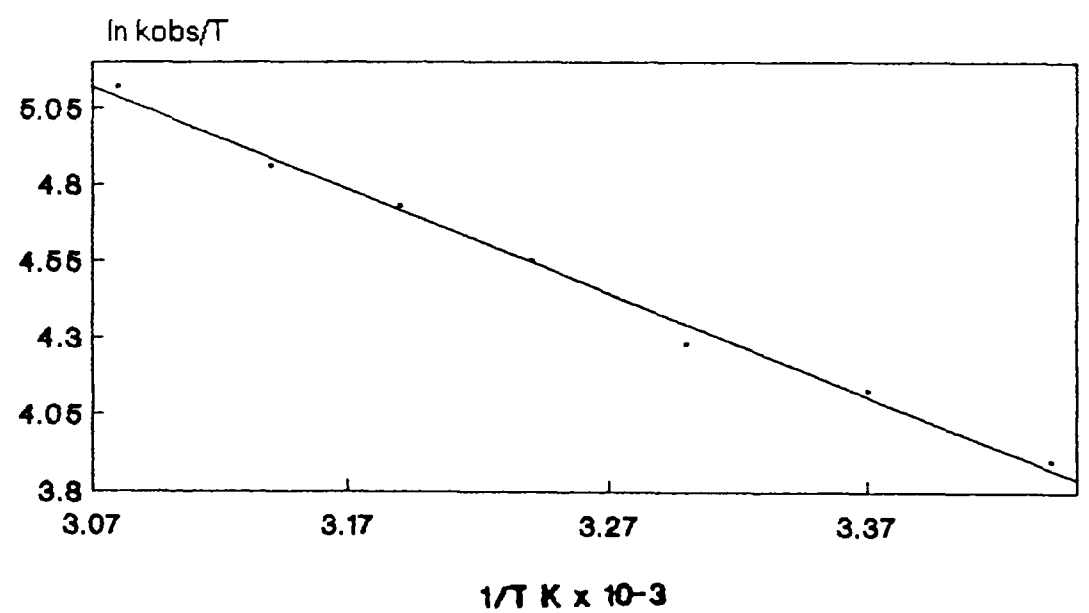

Table 3.3.2 21. Experimental data for the determination of the activation parameters for the reaction of $ArCr(CO)_2$(toluene) with 4-methylpyridine [methylpyridine] = 0 44 M

T	$1/T\ K \times 10^{-3}$	$k_2 \times 10^5$	$Ln\ k_2$	Lnk_2/T
287	3 48	5 16	13 15	7.49
293	3 41	6 69	13 41	7 73
298	3 36	8 34	13 63	7 94
303	3 30	1 16	13 96	8 25
309	3 24	1 44	14 18	8 45
315	3 17	2 06	14 54	8 79
323	3 10	3 51	15 07	9 29

Arrhenius Plot

Slope = -4940 8 ± 242 86

Intercept = 30 27 ± 0 08

Correlation coefficient = 0 99401

E_{act} = 41 08 ± 2 02 kJmol^{-1}

Eyring Plot

Slope = -4629 6 ± 233

Intercept = 23 53 ± 0 08

Correlation coefficient = 0 99373

$\Delta H^{\ddagger}$ = 38 49 ± 1 91 kJmol^{-1}

$\Delta S^{\ddagger}$ = -1 91 ± 0 67 Jmol^{-1}K^{-1}

Figure 3.3.2 26. Arrhenius (a) and Eyring (b) plots for the reaction of $ArCr(CO)_2$(toluene) with 4-methylpyridine

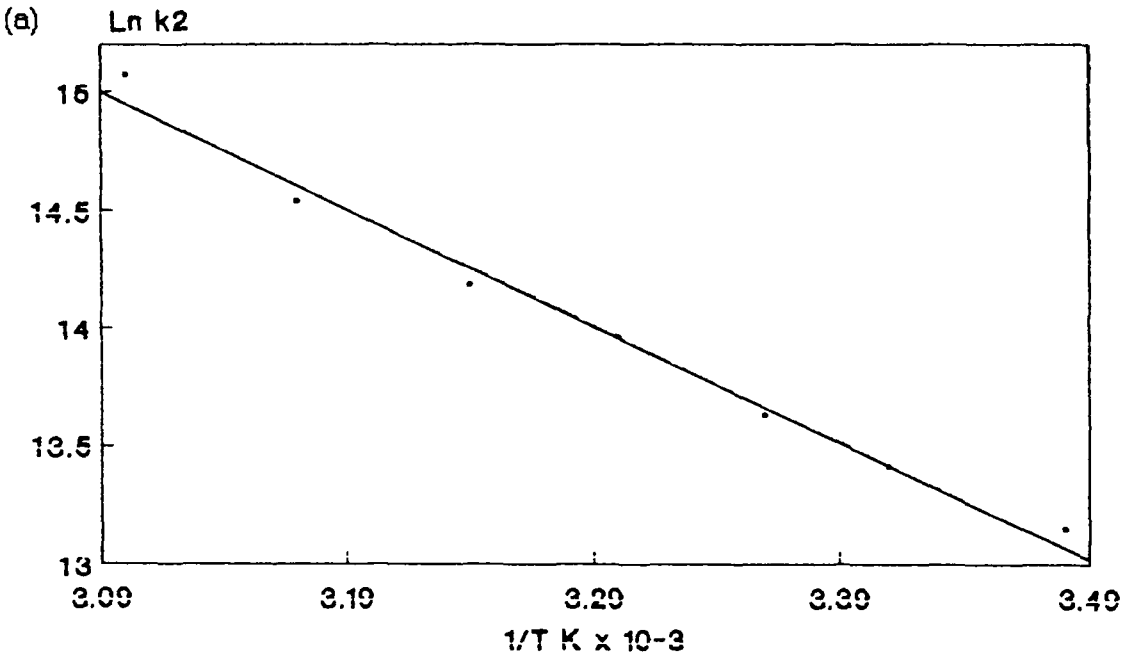

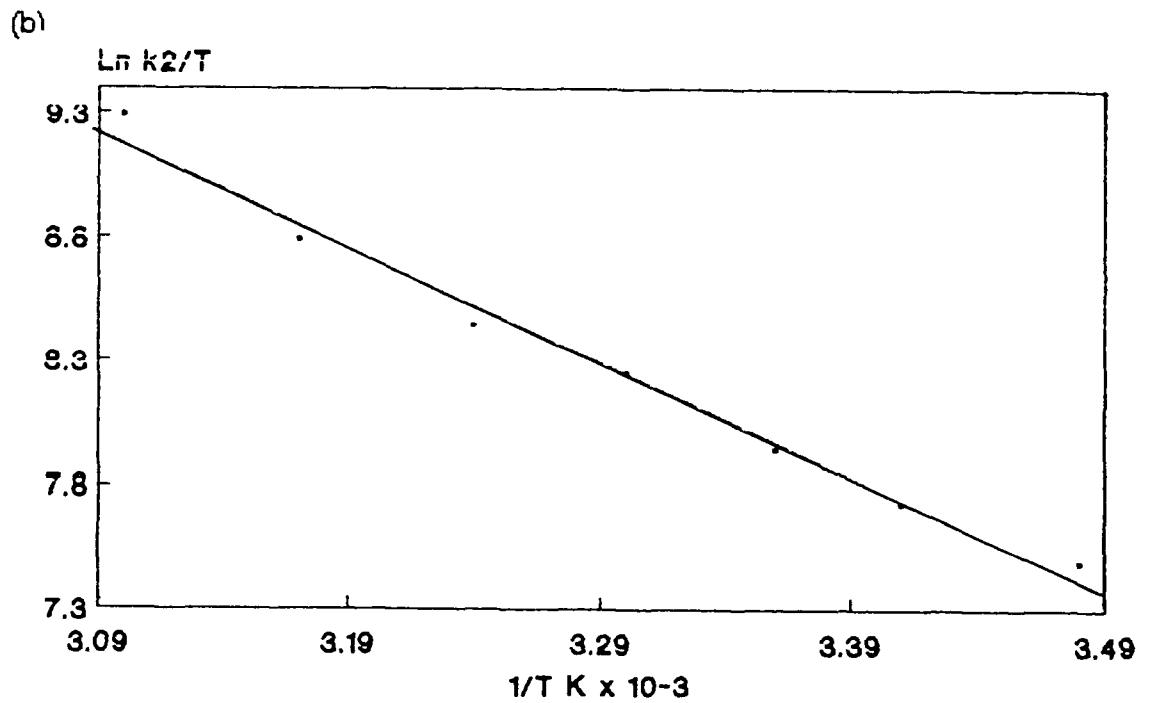

3 3.2.11 Flash photolysis of $ArCr(CO)_3$ in the presence of pyridine in 1% w/v polystyrene in toluene

From the second order rate constants determined for the reaction of the various pyridine ligands with the $ArCr(CO)_2$(toluene) complex, it appeared that the polymer in solution was not enhancing the reaction rates as was observed in the manganese system. To confirm this and to observe the effect of polymer molecules in solution on the reaction rates it was decided to carry out the flash photolysis experiment in a 1% w/v polystyrene in toluene solution

Table 3 3 2 22 compares the second order rate constants determined for the reaction of the $ArCr(CO)_2$(toluene) complex with pyridine in both toluene and polystyrene in toluene solutions

Table 3.3 2.22: Comparison of second order rate constants

Ligand	Solution	k_2 $dm^3mol^{-1}s^{-1}$
pyridine	toluene	8.33×10^5
pyridine	1% PS	6.89×10^5
5 1 copol	toluene	5.93×10^5

1% PS = 1% w/v solution of polystyrene in toluene

5 1 copol = 5 1 poly(styrene-co-4-vinylpyridine)

As can be seen from Table 3 3 2 22 the rate of reaction of $ArCr(CO)_2$(toluene) with pyridine in polystyrene solution was determined to be 6 89 x 10^5 $dm^3mol^{-1}s^{-1}$ This value is slower than that determined for the monomeric pyridine ligand in toluene solution but is faster than the similiar reaction with the polymeric pyridine ligand These results are completely different to those determined for the manganese system, where all the second order rate constants determined in polystyrene solution were quicker than those determined in toluene solution

Table 3 3 2 23 details the data recorded for the flash photolysis experiment carried out in polystyrene solution, the data is shown graphically in Figure 3 3 2 27

Table 3.3.2.23 and Figure 3.3 2.27: Experimental data for the determination of the second order rate constant for the reaction of $ArCr(CO)_2$(toluene) with pyridine in 1% w/v solution of polystyrene in toluene

---

[pyridine]	$k_{obs}s^{-1}$
2 24x10^{-2}	1 91 x10^4
4 10 10^{-2}	3 63x10^4
6 83 10^{-2}	4 92x10^4
8 60 10^{-2}	6 30x10^4
9 47 10^{-2}	7 21x10^4

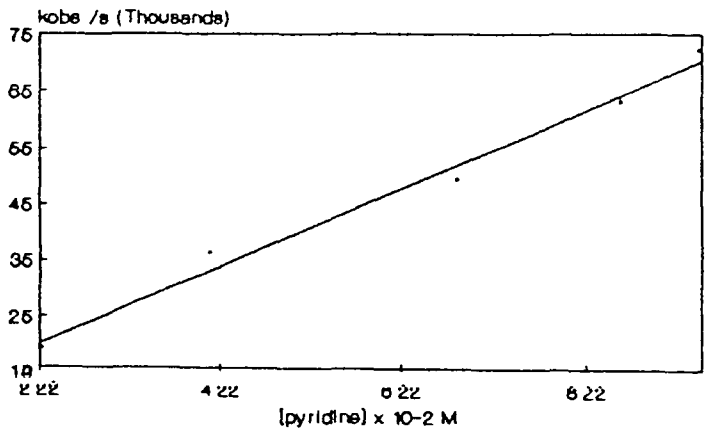

Slope = 6 89 ± 0 47 x 10^5 $dm^3mol^{-1}s^{-1}$

Intercept = 4863 ± 2858 6 s^{-1}

Correlation coefficient = 0 99309

---

3 3.2.12 Summary

The flash photolysis of $ArCr(CO)_3$ in toluene resulted in the formation of three transient species The primary photoreaction was loss of CO to generate the coordinatively unsaturated species $ArCr(CO)_2$, which was coordinated to a solvent molecule The primary photoproduct $ArCr(CO)_2$(toluene) was then obseved to react with an unphotolysed parent complex to form the dinuclear species $Ar_2Cr_2(CO)_5$ (Reaction 3 3 2 7) An arene exchange process was also recorded to yield the (toluene)$Cr(CO)_3$ moiety (Reaction 3 3 2 8).

$$ArCr(CO)_2(\text{toluene}) + ArCr(CO)_3 \longrightarrow Ar_2Cr_2(CO)_5 \qquad 3\ 3.2.7$$

$$ArCr(CO)_3 \xrightarrow{h\nu} (\text{toluene})Cr(CO)_3 + Ar \qquad 3.3.2.8$$

The reaction kinetics of $ArCr(CO)_3$ in the presence of both momomenc and polymeric pyridine ligands were investigated using flash photolysis in ambient temperature toluene solution These experiments were carried out in an attempt to further investigate the trend observed in the manganese system where the rates of reaction increased as a result of polymer concentration in solution

Unlike the manganese system, the monomenc pyridine ligands were observed to react quicker than the copolymer complexes with the primary photoproduct $ArCr(CO)_2$(toluene) The copolymers react slower than the free pyridine except for the 40 1 poly(styrene-co-4-vinylpyridine) complex which has the fastest rate of reaction The cause of the enhanced reaction rates in the manganese system is probably a result of

an interaction between the polymer backbone and the dicarbonyl complex. This interaction does not appear to be occuring in the $ArCr(CO)_3$ system as the reaction rates determined for the polymeric ligands are slower than those for the free pyridine complexes and the rates determined in polystyrene solutions are slower than in toluene solutions

A possible explanation for the different trends observed between the $MeCpMn(CO)_3$ and $ArCr(CO)_3$ could be that the steric effect of the larger arene ring system, compared to the cyclopentadienyl system, hinders the polymer in gaining access to the metal centre Therefore in the chromium system the reaction scheme (Scheme 3 3 2 4) does not involve the formation of a polymer complex with the $ArCr(CO)_2$(toluene) species as was observed in the manganese system (Scheme 3 3 1 2, Section 3 3 1 10) There is only formation of the dicarbonyl nitrogen complex whether free pyridine or polymeric pyridine ligands are in solution

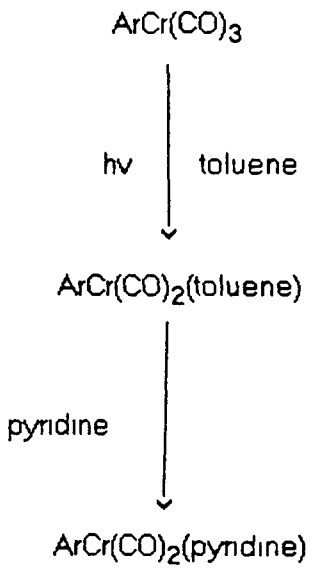

pyridine = monomeric or polymeric pyridine ligands as described earlier

Scheme 3 3.2.4

3.3.3 Flash photolysis of $Cr(CO)_6$ in the presence of monomeric and polymeric pyridine ligands

It was thought that the different trends observed for the reactions of the monomeric and polymeric ligands between the metal systems may be a result of the nature of the metal as well as possible steric hindrance Therefore it was decided to investigate the reactions of the $Cr(CO)_6$ complex in the presence of pyridine ligands in toluene solution at room temperature The photochemistry of the $Cr(CO)_6$ system has been widely studied and reported in the literature [27,39] as a result only the interaction of the pentacarbonyl fragment with the pyridine ligands was studied here

Previous research by our group [35] on the $W(CO)_6$ system in the presence of pyridine ligands in toluene followed a similiar trend to that obseved in the manganese system in this work. The $W(CO)_5$ fragment was observed to react quicker with the polymeric pyridine ligands than the free pyridine entities

The UV/vis spectrum of $Cr(CO)_6$ is shown in Figure 3 3 3 1 and the changes that occur in the spectrum upon the formation of the pentacarbonyl pyridine complex during the course of the flash photolysis experiment can be seen

Figure 3 3.3 1: Changes observed in the UV/vis spectrum on the flash photolysis of $Cr(CO)_6$ in the presence of pyridine in toluene

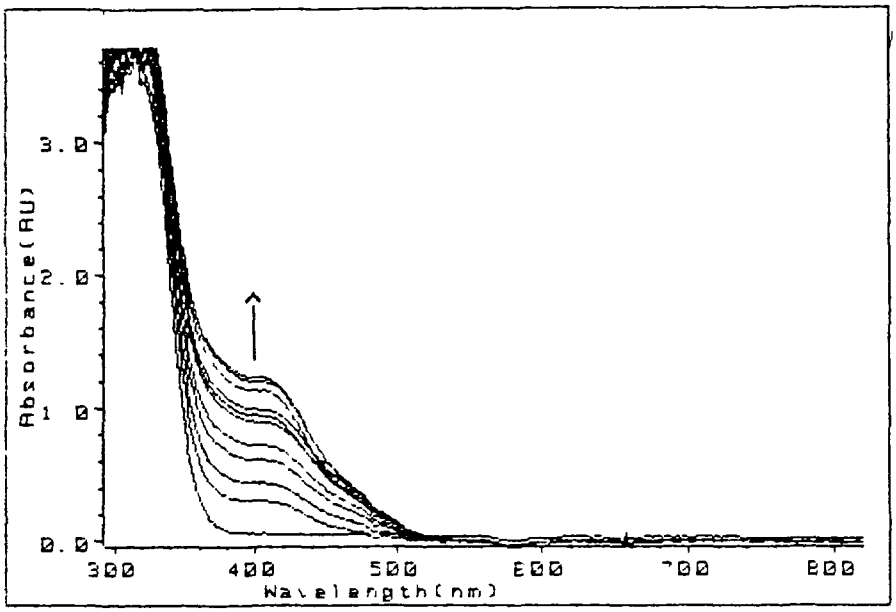

3.3.3.1 Reaction rates of $Cr(CO)_5$(toluene) with pyridine ligands

The rates of reaction of monomeric and polymeric pyridine ligands with the pentacarbonyl toluene complex (Reaction 3.3 3.1) were determined for comparsion with the reaction of the $ArCr(CO)_2$(toluene) complex with similiar ligands As with the manganese and chromium tricarbonyl systems (Sections 3 3 1 and 3 3.2) the polymeric pyridine ligands were in the form of poly(styrene-co-4-vinylpyridine)

$$Cr(CO)_5(toluene) + pyridine \longrightarrow Cr(CO)_5(pyridine) \qquad 3\,3\,3.1$$

pyridine = monomeric or polymeric pyridine ligands

As can be seen from the second order rate constants determined for Reaction 3 3 3 1 (Table 3 3 3 1), the rates of reaction are higher for the copolymers than for the free pyridine in solution

---

Table 3.3.3.1: Second order rate constants for the reaction of $Cr(CO)_5$(toluene) with various pyridine ligands

---

Ligand	k_2 $dm^3mol^{-1}s^{-1}$
pyridine	$0\,75 \times 10^5$
4-mepyridine	$0\,92 \times 10^5$
5 1 copol	$0\,96 \times 10^5$
10 1 copol	$1\,44 \times 10^5$
30 1 copol	$1\,07 \times 10^5$
40 1 copol	$3\,52 \times 10^5$

4-mepyridine = 4-methylpyridine, copol = poly(styrene-co-4-vinylpyridine)

The second order rate constants determined follow the same trend as observed in the $MeCpMn(CO)_3$ system As can be seen from Table 3 3 3 1 the 30 1 copolymer does not fit into the trend, but its rate of reaction with the pentacarbonyl complex is faster than the free pyridine and the 5 1 copolymer, so it probably can be accommodated within experimental error Changing the electronic nature of the pyridine (reaction with 4-methylpyridine) appears to enhance the rate constant but not to the same degree as the polymeric ligands A similiar trend was observed in the manganese system where the 4-methylpyridine complex had a higher rate of formation while in the $ArCr(CO)_3$ the presence of the methyl group on the pyridine ligand did not appear to affect the rate of formation of the dicarbonyl pyridine complex (Table 3 3 3 2)

Table 3.3.3.2: Rates of reaction of pyridine and 4-methylpyridine with the primary photoproducts

	k_2 $dm^3mol^{-1}s^{-1}$	
Primary photopdt	Pyridine	Mepyridine
$MeCpMn(CO)_2(tol)$	$0\,90 \times 10^3$	$1\,29 \times 10^3$
$ArCr(CO)_2$(toluene)	$8\,33 \times 10^5$	$8\,30 \times 10^5$
$Cr(CO)_5$(toluene)	$7\,50 \times 10^4$	$9\,15 \times 10^4$

Thus in the chromium hexacarbonyl system as was observed in the manganese system we see an interaction of the pentacarbonyl fragment with the polymer backbone as well as with the pendant nitrogen atom

Tables 3 3 3 3 - 3 3 3 7 and Figures 3 3 3 2 - 3 3 3 6 give the experimental data used in determining the second order rate constants for the reaction of the pentacarbonyl fragment with the various pyridine ligands.

Table 3.3.3.3 and Figure 3.3.3.2: Second order rate constant for the reaction of $Cr(CO)_5$(toluene) with pyridine

---

[pyridine]	$k_{obs}s^{-1}$
0 63 x 10^{-2} M	607.1
1 35 x 10^{-2} M	1199 7
1 63 x 10^{-2} M	1177 3
3 35 x 10^{-2} M	2202 1
6 27 x 10^{-2} M	4000 3

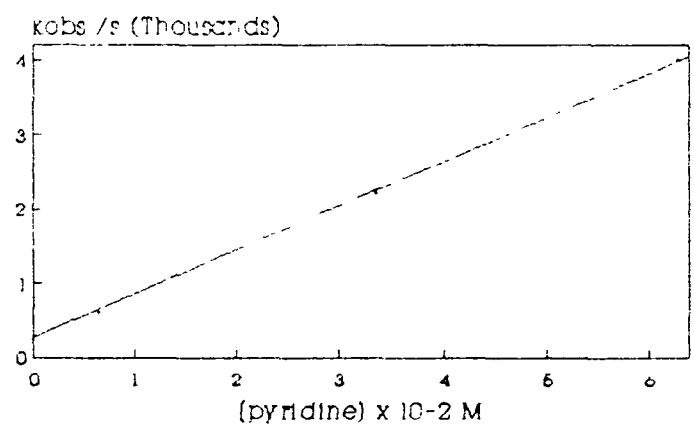

Slope = 7 50 ± 0 46 x 10^4 $dm^3mol^{-1}s^{-1}$

Intercept = 42 24 ± 207 0 s^{-1}

Correlation coefficient= 0 99441

Table 3.3.3.4 and Figure 3.3.3.3: Second order rate constant for the reaction of $Cr(CO)_5$(toluene) with 5 1 poly(styrene-co-4-vinylpyridine)

[pyridine]	$k_{obs}s^{-1}$
0 35 x 10^{-2} M	576
1 11 x 10^{-2} M	944 7
2 15 x 10^{-2} M	2004 5
3 70 x 10^{-2} M	3460 9
5 47 x 10^{-2} M	5232 4
6 66 x 10^{-2} M	6521 6

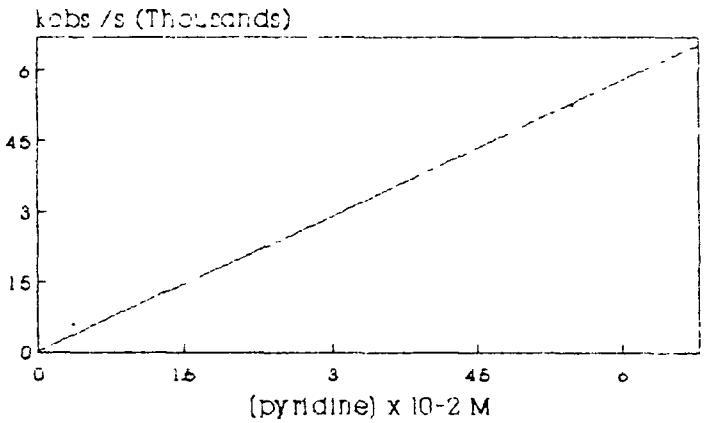

Slope = 9 55 ± 0 31 x 10^4 $dm^3mol^{-1}s^{-1}$

Intercept = 29 67 ± 170 s^{-1}

Correlation coefficient = 0 99796

Table 3.3.3.5 and Figure 3 3 3.4: Second order rate constant for the reaction of $Cr(CO)_5$(toluene) with 10 1 poly(styrene-co-4-vinylpyridine

[pyridine]	$k_{obs}s^{-1}$
0 53 x 10^{-2} M	941 72
1 02 x 10^{-2} M	1945 0
1 57 x 10^{-2} M	2253 6
2 06 x 10^{-2} M	2931 6
2 67 x 10^{-2} M	4277.0

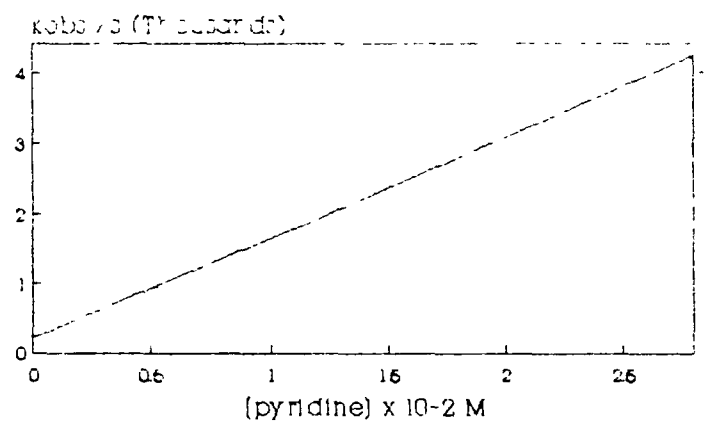

Slope = 1 44 ± 0.16 x 10^5 $dm^3mol^{-1}s^{-1}$

Intercept = 209.71 ± 276 1 s^{-1}

Correlation coefficient = 0 9812

Table 3.3.36 and Figure 3.3.3.5: Second order rate constant for the reaction of $Cr(CO)_5$(toluene) with 30.1 poly(styrene-co-4-vinylpyridine)

[pyridine]	$k_{obs}s^{-1}$
4.25×10^{-3} M	532.04
8.83×10^{-3} M	1259.0
1.46×10^{-2} M	1563.8
1.90×10^{-2} M	2269.6
2.50×10^{-2} M	2926.3

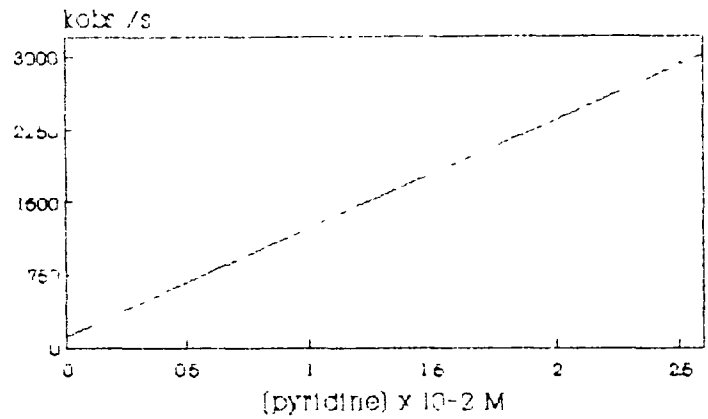

Slope = 1.07 ± 0.07 x 10^5 $dm^3mol^{-1}s^{-1}$

Intercept = 143.12 ± 134.20 s^{-1}

Correlation coefficient = 0.99202

Table 3.3.37 and Figure 3.3.3.6: Second order rate constant for the reaction of $Cr(CO)_5$(toluene) with 40.1 poly(styrene-co-4-vinylpyridine)

[pyridine]	$k_{obs}s^{-1}$
1.64×10^{-3} M	703.78
4.39×10^{-3} M	1763.2
8.92×10^{-3} M	3321.5
1.29×10^{-2} M	4415.5
1.80×10^{-2} M	6612.5

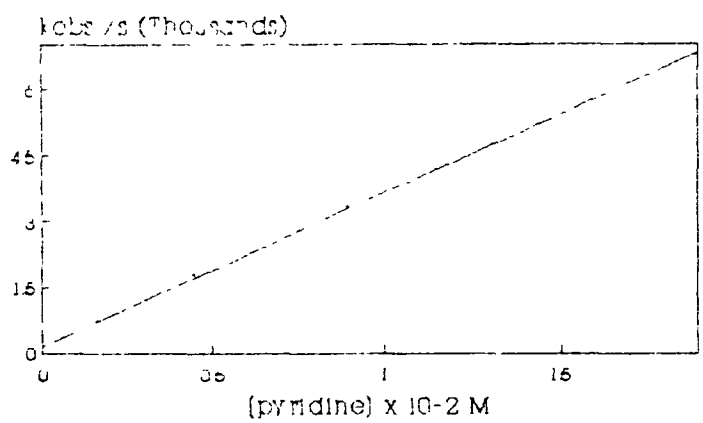

Slope = 3.52 ± 0.14 x 10^5 $dm^3mol^{-1}s^{-1}$

Intercept = 138.94 ± 179.71 s^{-1}

Correlation coefficient = 0.99772

3.3.3.2 Activation parameters for the reaction of $Cr(CO)_5$(toluene) with the various pyridine ligands

The activation parameters for the reaction of the pentacarbonyl complex with both monomeric and polymeric pyridine ligands were determined and are summarised in Table 3 3 3 8 As with the $MeCpMn(CO)_2$(toluene) and $ArCr(CO)_2$(toluene) complexes, k_2 was used in determining the activation parameters for the reaction of the free pyridine ligands with the pentacarbonyl fragment, whereas k_{obs} was used in the calculations for the polymeric ligands

The activation parameters were determined to confirm that the quicker reaction rate for the polymeric ligands with the pentacarbonyl complex was not because of a difference in the activation energy of the reaction, but was a result of an interaction between the pentacarbonyl fragment and the polymer backbone, as was the case in the reaction of the $MeCpMn(CO)_2$(toluene) complex with the pyridine ligands The activation parameters for all three systems ($MeCpMn(CO)_3$, $ArCr(CO)_3$, and $Cr(CO)_6$) could then be compared

As can be seen from Table 3 3 3 8 the activation parameters determined for the reaction of the pentacarbonyl complex are quite similiar for all the pyridine ligands implying that the trend observed is not a result of a difference in these parameters The energies of activation (E_{act}) are relatively low and within experimental error of each other The highly negative $\Delta S^{\ddagger}$ values imply an associative process, the degree of associativity is increased for the polymeric ligands. The Gibbs free energy ($\Delta G^{\ddagger}$) is similiar for the reaction of the free pyridine ligands which is lower than that recorded for the polymeric ligands The polymeric ligands all have similiar $\Delta G^{\ddagger}$ values

Table 3.3.3.8. Summary of activation parameters for the reaction of the $Cr(CO)_5$(toluene) complex with the various pyridine ligands

Ligand	E_{act} kJmol^{-1}	$\Delta H^{\ddagger}$ kJmol^{-1}	$\Delta S^{\ddagger}$ Jmol^{-1}K^{-1}	$\Delta G^{\ddagger}$ kJmol^{-1}
Pyridine	32 90	30 44	-46 23	44 22
Mepyridine	33 99	31 28	-42 44	43 93
5 1 copol	29 61	27 11	-94 42	55 25
10 1 copol	33 29	30 89	-79 71	54 64
30 1 copol	38 40	35 81	-61 96	54 27
40 1 copol	32 60	30 10	-77 77	53 28

The experimental data used in the determination of the activation parameters is given in Tables 3 3 3.9-3 3 3 14 and shown graphically in Figures 3 3 3 7-3 3 3 12

Table 3.3 3.9: Experimental data for the determination of the activation parameters for the reaction of $Cr(CO)_5$(toluene) with pyridine [pyridine] = $4\ 21 \times 10^{-2}$ M

T K	$1/TK \times 10^{-3}$	$k_2 \times 10^5$ M	Ln k_2	Lnk_2/T
293	3 41	0 93	11 44	5 76
297	3 37	1 13	11 64	5 94
303	3 30	1 29	11 77	6 05
308	3 25	1 52	11 93	6 20
314	3 18	2 13	12 27	6 52
319	3 13	2 73	12 52	6 75
325	3 08	3 59	12 79	7 01

Arrhenius Plot

Slope = -3956 6 ± 265 83

Intercept = 24 89 ± 0 08

Correlation coefficient = 0 9889

E_{act} = 32 90 ± 2 21 kJmol^{-1}

Eyring Plot

Slope = -3661 7 ± 265 49

Intercept = 18 20 ± 0 08

Correlation coefficient = 0 98711

$\Delta H^{\ddagger}$ = 30 44 ± 2 21 kJmol^{-1}

$\Delta S^{\ddagger}$ = -46 22 ± 0 6 Jmol^{-1}K^{-1}

Figure 3.3 3.7: Arrhenius (a) and Eyring (b) plots for the reaction of $Cr(CO)_5$(toluene) with pyridine

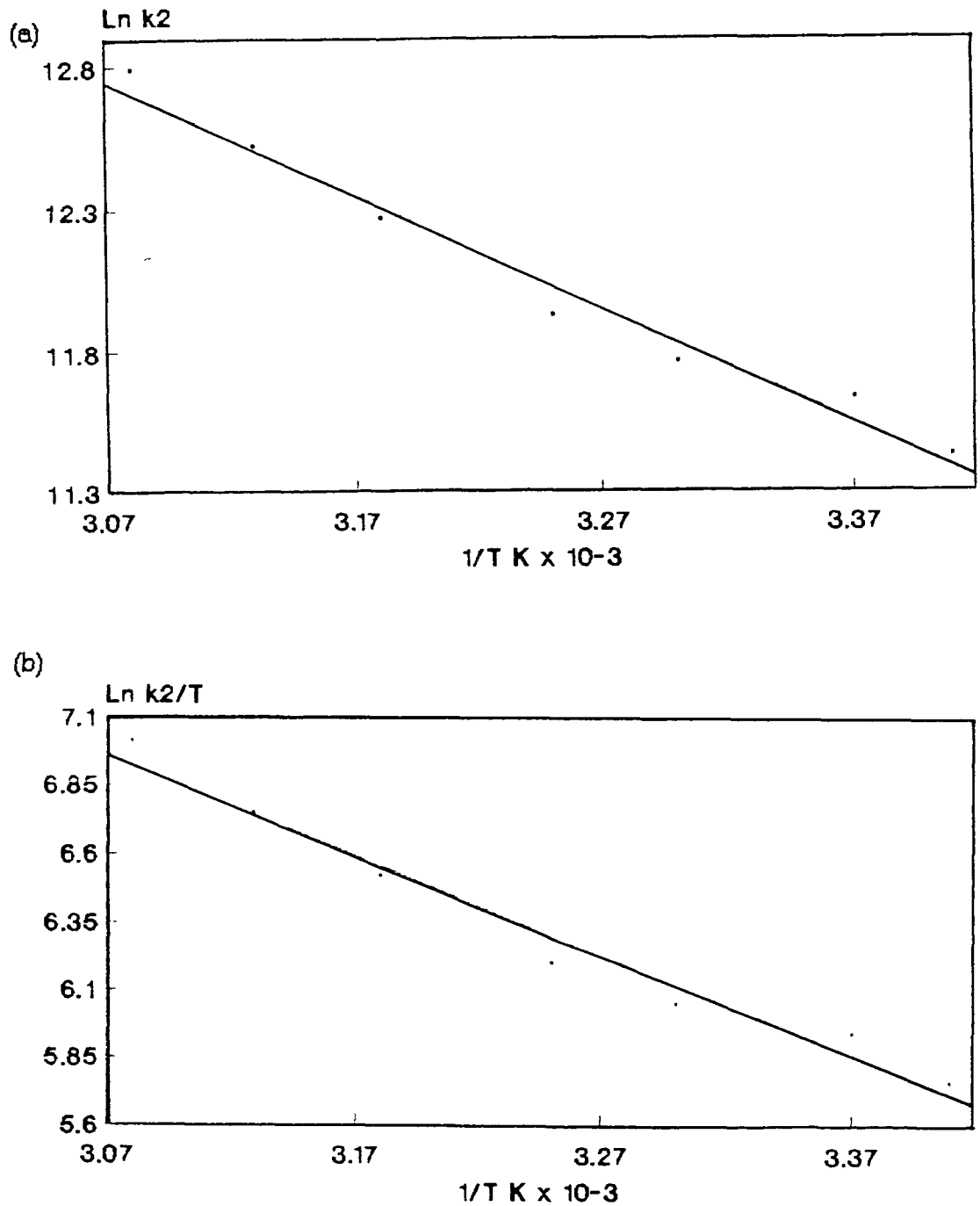

Table 3 3.3.10 Experimental data for the determination of the activation parameters for the reaction of $Cr(CO)_5$(toluene) with 4-methylpyridine [mepyridine] = $2\,64 \times 10^{-2}$ M

T K	$1/T\,K \times 10^{-3}$	k_2	Ln k_2	Lnk_2/T
290	3 45	2082 38	11 28	5 61
297	3 37	3152 10	11 69	6 00
303	3 30	4248 46	11 99	6 27
308	3 25	5552 69	12 26	6 53
314	3 18	6344 27	12 39	6 64
319	3 13	7646 78	12 58	6 81
324	3 09	9906 10	12 84	7 05

Arrhenius Plot

Slope = -4088 2 ± 218 53

Intercept = 25 45 ± 0 07

Correlation coefficient = 0 99293

E_{act} = 33 99 ± 1 82 kJmol^{-1}

Eyring Plot

Slope = -3762 6 ± 217 23

Intercept = 18 66 ± 0 07

Correlation coefficient = 0 99177

$\Delta H^{\ddagger}$ = 31 28 ± 1 81 kJmol^{-1}

$\Delta S^{\ddagger}$ = -42.44 ± 0 58 Jmol^{-1}K^{-1}

Figure 3.3.3.8: Arrhenius (a) and Eyring (b) plots for the reaction of $Cr(CO)_5$(toluene) with 4-methylpyridine

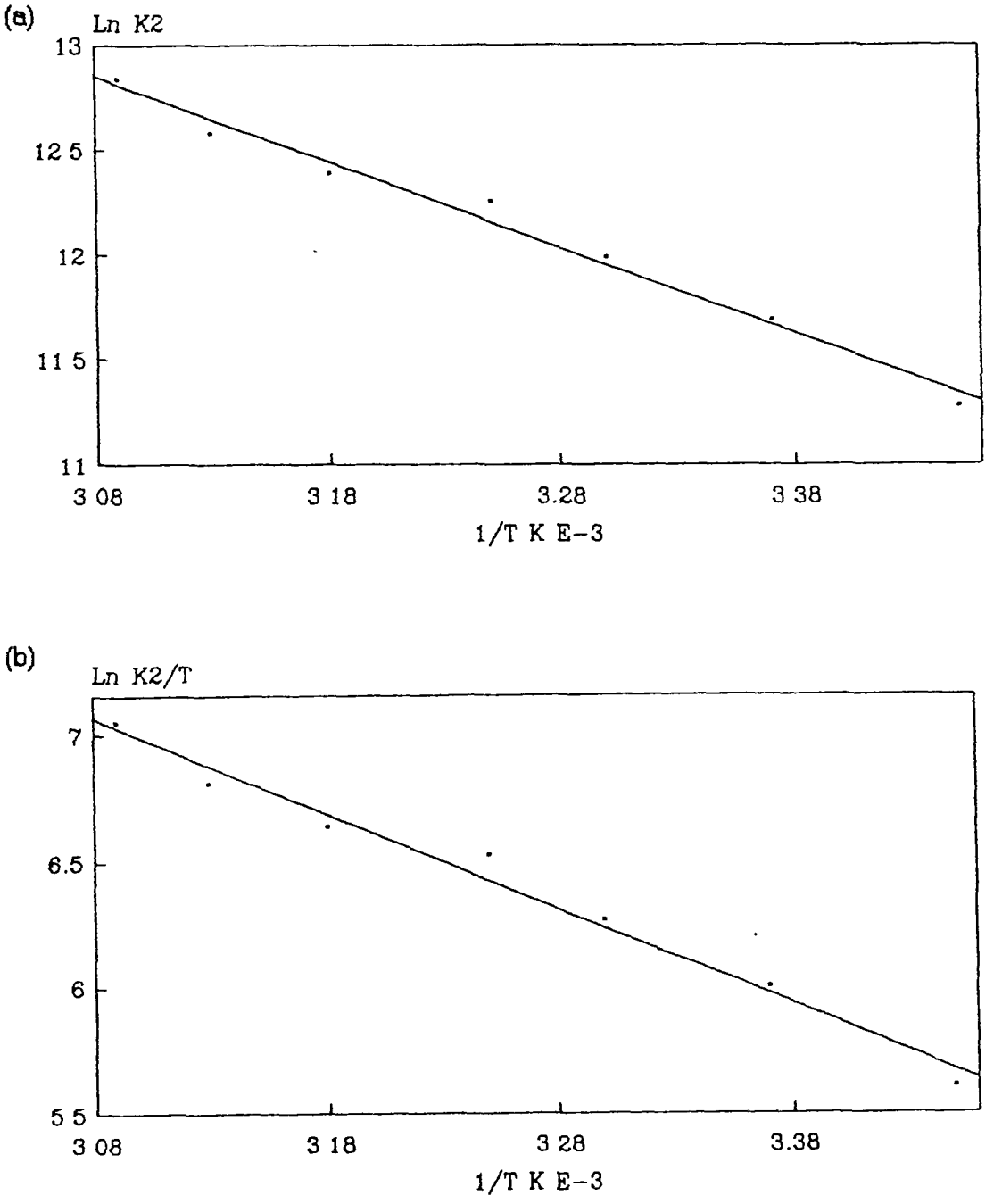

Table 3.3.3.11. Experimental data for the determination of the activation parameters for the reaction of $Cr(CO)_5$(toluene) with 5 1 poly(styrene-co-4-vinylpyridine) [pyridine] = 1 21 x 10^{-2} M

T K	1/T K x 10^{-3}	k_{obs} s^{-1}	Ln k_{obs}	Lnk_{obs}/T
292	3 42	1042 71	6 95	1 27
297	3 37	1226 55	7 11	1 42
304	3 29	1519 75	7 33	1 61
309	3 24	2026 44	7 61	1 88
315	3 17	2500 28	7 82	2 07
324	3 09	3320 92	8 11	2 33

Arrhenius Plot

Slope = -3561 9 ± 139 47

Intercept = 19 11 ± 0 04

Correlation coefficient = 0 99695

E_{act} = 29 61 ± 1 16 kJmol^{-1}

Eyring Plot

Slope = -3260 3 ± 145 02

Intercept = 12.40 ± 0 04

Correlation coefficient = 0 99607

$\Delta H^{\ddagger}$ = 27.11 ± 1 21 kJmol^{-1}

$\Delta S^{\ddagger}$ = -94 42 ± 0 58 Jmol^{-1}K^{-1}

Figure 3.3.3.9: Arrhenius (a) and Eyring (b) plots for the reaction of $Cr(CO)_5$(toluene) with 5 1 poly(styrene-co-4-vinylpyridine)

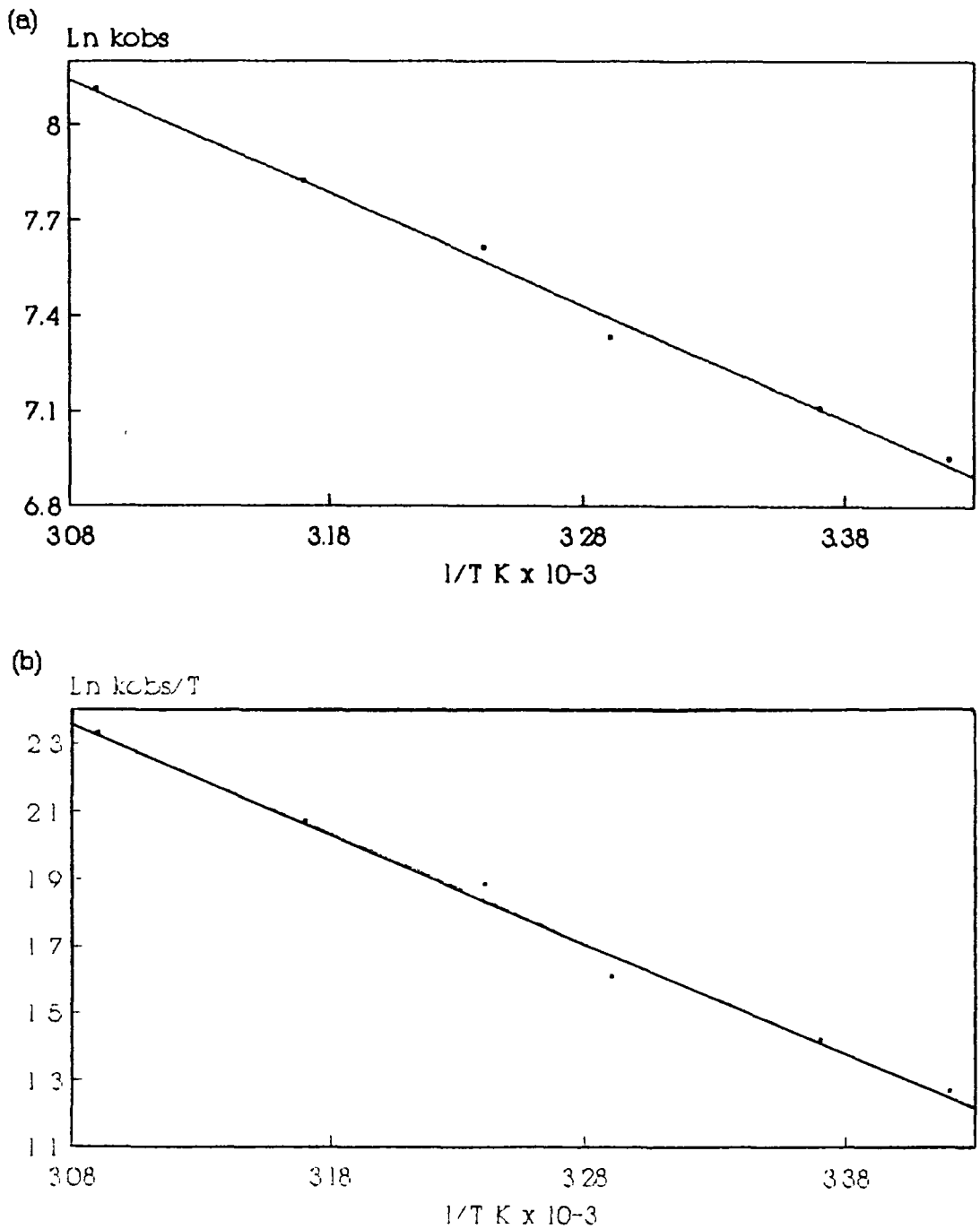

Table 3.3 3.12: Experimental data for the determination of the activation parameters for the reaction of $Cr(CO)_5$(toluene) with 10 1 poly(styrene-co-4-vinylpyridine [pyridine] = 1 01 x 10^{-2} M

T K	1/T K x 10^{-3}	k_{obs} s^{-1}	Ln k_{obs}	Lnk_{obs}/T
291	3 44	1256 60	7 14	1 46
298	3 36	1481 17	7 30	1 60
303	3 30	1956 87	7 58	1 87
308	3 25	2571 96	7 85	2 12
312	3 21	3154 34	8 06	2 31
318	3 14	3548 37	8 17	2 41
324	3 09	5054 40	8 53	2 75

Arrhenius Plot

Slope = -4004 3 ± 276 6

Intercept = 20 84 ± 0 08

Correlation coefficient = 0 98828

E_{act} = 33 29 ± 2 30 kJmol^{-1}

Eyring Plot

Slope = -3715 8 ± 264 88

Intercept = 14 17 ± 0 08

Correlation coefficient = 0 98753

$\Delta H^{\ddagger}$ = 30 89 ± 2 20 kJmol^{-1}

$\Delta S^{\ddagger}$ = -79.71 ± 0 67 Jmol^{-1}K^{-1}

Figure 3 3 3.10. Arrhenius (a) and Eyring (b) plots for the reaction of $Cr(CO)_5$(toluene) with 10 1 poly(styrene-co-4-vinylpyridine)

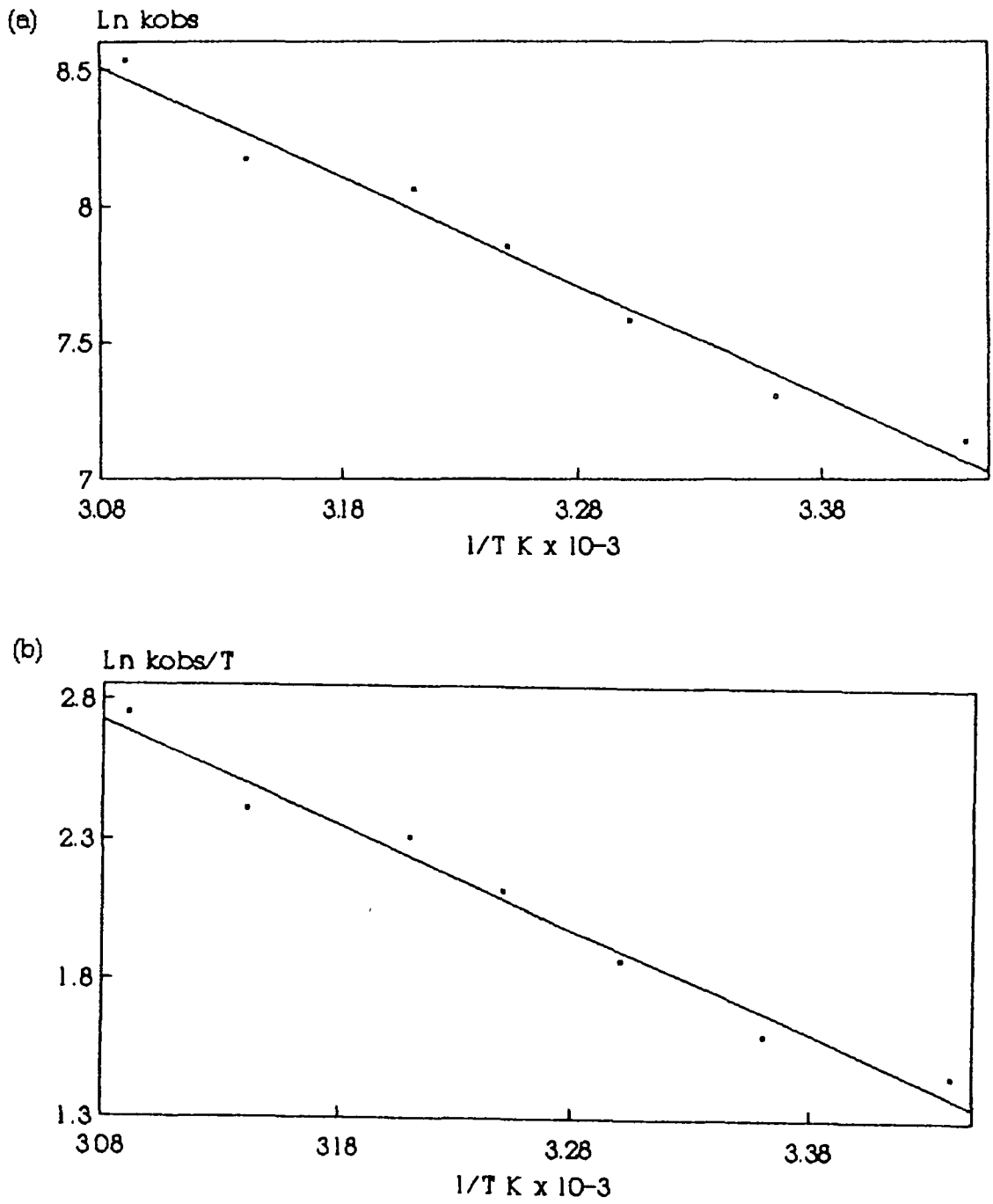

Table 3 3.3.13. Expenmental data for the determination of the activation parameters for the reaction of $Cr(CO)_5$(toluene) with 30 1 poly(styrene-co-4-vinylpyridine) [pyridine] = 1 81 x 10^{-2} M

T K	1/T K x 10^{-3}	$k_{obs}s^{-1}$	Ln k_{obs}	Lnk_{obs}/T
292	3 42	1361 22	7 22	1 54
299	3 34	2074 08	7 64	1 94
303	3 30	2572 36	7 85	2 14
308	3 25	3008 41	8 01	2 28
313	3 19	4249 81	8 35	2 61
318	3 14	5142 13	8 55	2 78
324	3 09	6311 35	8 75	2 97

Arrhenius Plot

Slope = -4618 9 ± 121 49

Intercept = 23 05 ± 0 03

Correlation coefficient = 0 99827

E_{act} = 38 40 ± 1 01 kJmol^{-1}

Eyring Plot

Slope = -4306 8 ± 134 34

Intercept = 16 31 ± 0 04

Correlation coefficient = 0 99758

$\Delta H^{\ddagger}$ = 35.81 ± 1 12 kJmol^{-1}

$\Delta S^{\ddagger}$ = -61 96 ± 0 33 Jmol^{-1}K^{-1}

Figure 3.3 3.11: Arrhenius (a) and Eyring (b) plots for the reaction of $Cr(CO)_5$(toluene) with 30 1 poly(styrene-co-4-vinylpyridine)

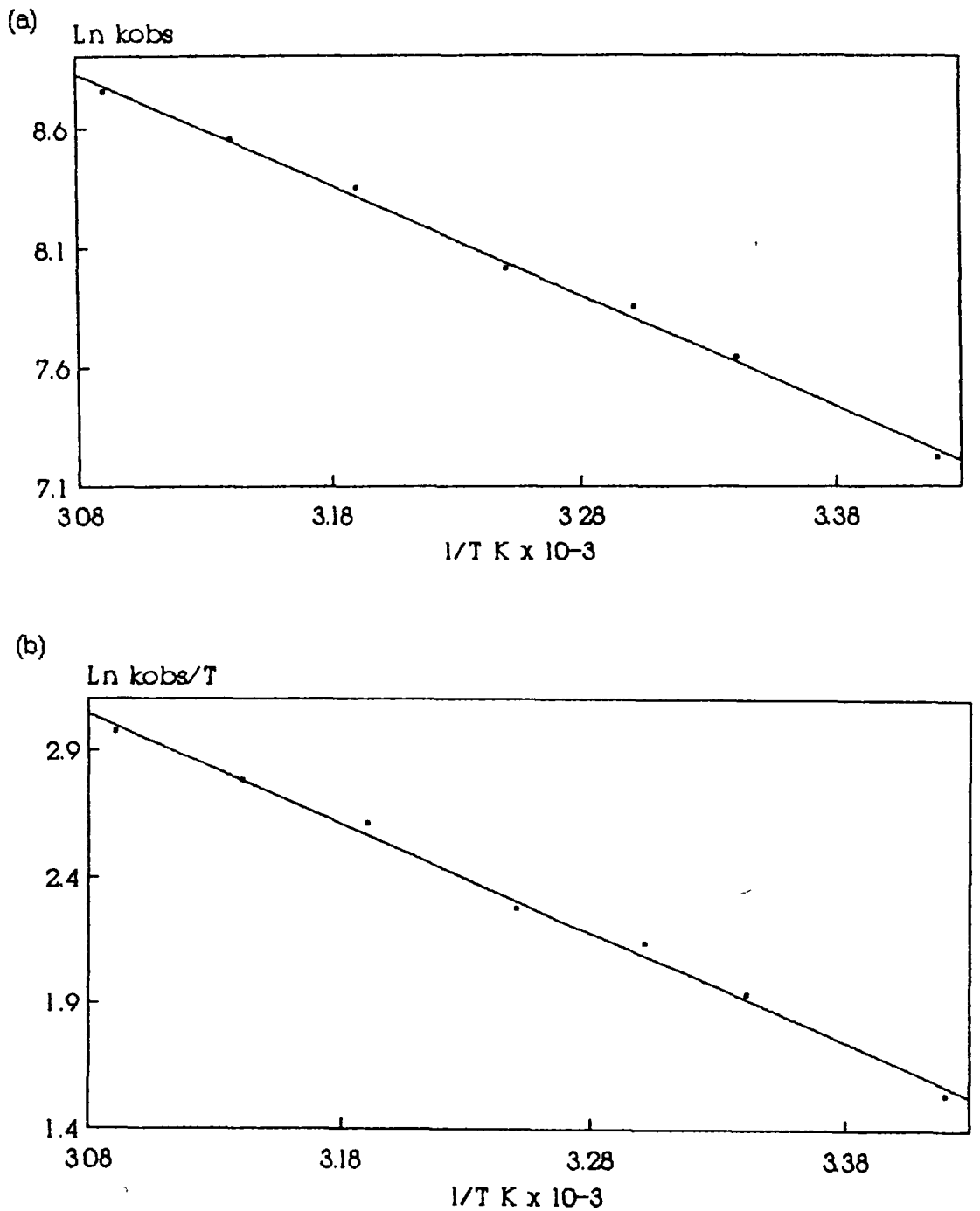

Table 3.3.3.14.Expenmental data for the determination of the activation parameters for the reaction of $Cr(CO)_5$(toluene) with 40 1 poly(styrene-co-4-vinylpyridine) [pyridine] = 8 92 x 10^{-3} M

T K	1/T x 10^{-3}	$k_{obs}s^{-1}$	Ln k_{obs}	Lnk_{obs}/T
297	3 37	2817 91	7 94	2 25
303	3 30	3528 61	8 17	2 45
307	3 26	4016 76	8 30	2 57
313	3 19	5221 81	8 56	2 81
317	3 15	6232 40	8 74	2 98
325	3 08	8891 43	9 09	3 31

Arrhenius Plot

Slope = -3921 1 ± 189 25

Intercept = 21 11 ± 0 04

Correlation coefficient = 0 99537

E_{act} = 32 60 ± 1 57 kJmol^{-1}

Eyring Plot

Slope = -3620 6 ± 199 32

Intercept = 14 41 ± 0 04

Correlation coefficient = 0 99399

$\Delta H^{\ddagger}$ = 30 10 ± 1 66 kJmol^{-1}

$\Delta S^{\ddagger}$ = -77 77 ± 0 33 Jmol^{-1}J^{-1}

Figure 3.3.3.12: Arrhenius (a) and Eyring (b) plots for the reaction of $Cr(CO)_5$(toluene) with 40:1 poly(styrene-co-4-vinylpyridine).

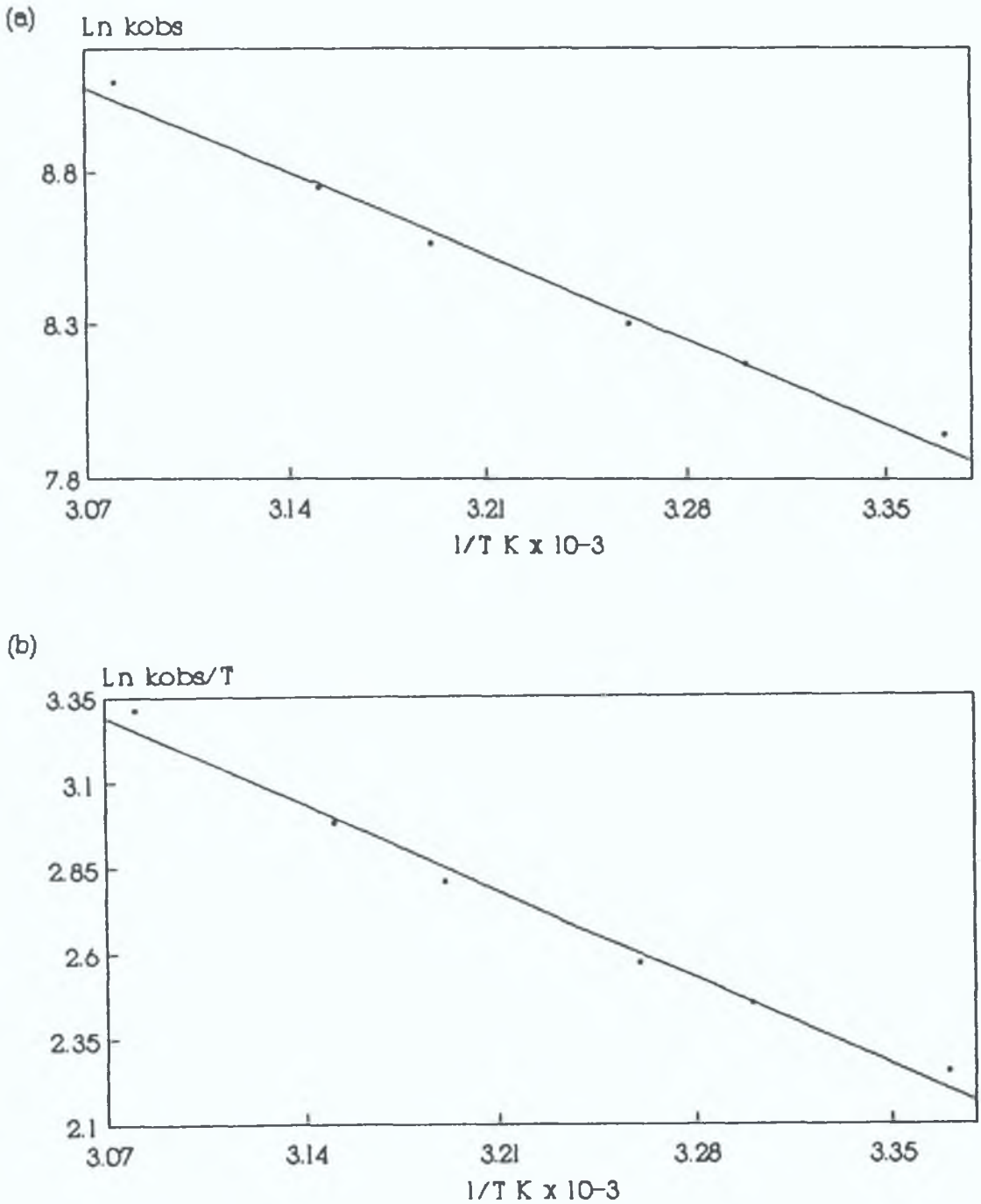

3.3 3 3 Summary

The reaction kinetics of $Cr(CO)_6$ in the presence of both monomeric and polymeric pyridine ligands were investigated using flash photolysis in room temperature toluene solution These experiments were carried out to investigate the trends observed in the reaction rates of the $MeCpMn(CO)_2$(toluene) and $ArCr(CO)_2$(toluene) with the various pyridine ligands

The second order rate constants determined for the reaction of the $Cr(CO)_5$(toluene) complex with the various pyridine ligands follow the same trend as observed in the manganese system Thus in the chromium hexacarbonyl system we are also detecting an interaction of the pentacarbonyl fragment with the polymer backbone as well as with the pendant nitrogen atoms (Scheme 3 3.3 2).

The activation parameters for the reaction of the $Cr(CO)_5$(toluene) complex with the monomeric and polymeric ligands are quite similiar to those for the same reaction with the $ArCr(CO)_2$(toluene) species This would seem to imply that the different trends observed in the reaction rates between the $MeCpMn(CO)_3$ and $ArCr(CO)_3$ systems is not a result of a difference in the Gibbs free energy of activation because of the different metal centre

The reason the "polymer effect" observed in the manganese tricarbonyl and chromium hexacarbonyl systems does not occur in the arene chromium tricarbonyl system could be because of steric hindrance, the arene ring is larger than the cyclopentadienly ring As both ring systems sit above the metal, the large polymer molecules are hindered in gaining access to the metal centre in the case of the arene system Thus the observed increase in the rate constants recorded for the $MeCpMn(CO)_2$(toluene) and

$Cr(CO)_5$(toluene) fragments due to the interaction of the solvent complexes with the polymer backbone does not occur in the $ArCr(CO)_3$ system

---

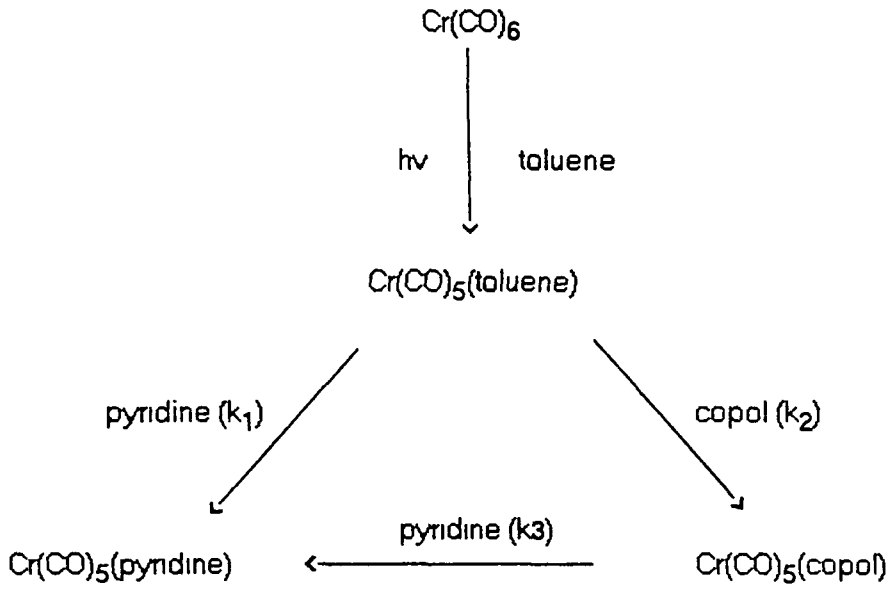

copol = poly(styrene-co-4-vinylpyridine), pyridine = pendant nitrogen on copolymer backbone

Scheme 3.3.3.2

As with the manganese system the rate law corresponding to the mechanism in Scheme 3 3 3 2 was determined by assuming a steady state concentration of the pentacarbonyl copolymer complex Therefore the rate law is,

$$d[Cr(CO)_5(pyridine)]/dt = [Cr(CO)_5(toluene)](k_1[pyridine] + k_2[copol])$$

Therefore in terms of the pseudo-first-order rate constant k_{obs}, this equation may be written as,

$$k_{obs} = (k_1[\text{pyridine}] + k_2[\text{polymer}])$$

3.3.4 Conclusion

Photolysis of the isoelectronic $LM(CO)_3$ (LM = MeCpMn or ArCr) in low temperature argon and methane matrices and alkane solvents have shown loss of CO as the primary photoprocess In our studies on the solution photochemistry of these compounds in toluene, loss of CO has also been observed as the primary photoreaction The resultant unsaturated $LM(CO)_2$ species coordinates to a solvent molecule (Reactions 3 3 4 1-3 3 4 2)

$$LM(CO)_3 \xrightarrow{h\nu} LM(CO)_2 + CO \qquad 3.3.4.1$$

$$LM(CO)_2 + \text{toluene} \longrightarrow LM(CO)_2(\text{toluene}) \qquad 3.3.4.2$$

In the $MeCpMn(CO)_3$ system the $MeCpMn(CO)_2$(toluene) fragment does not react further to form a dinuclear species as was observed for $MeCpMn(CO)_2$(cyclohexane) [12] Therefore the only species observed on the flash photolysis of $MeCpMn(CO)_3$ in toluene is the primary photoproduct $MeCpMn(CO)_2$(toluene) In the investigation of the $ArCr(CO)_3$ system in toluene the primary photoproduct $ArCr(CO)_2$(toluene) was observed to react with the parent complex to form the dinuclear species $Ar_2Cr_2(CO)_5$ (Reaction 3 3 4 3)

$$ArCr(CO)_2(toluene) + ArCr(CO)_3 \longrightarrow Ar_2Cr_2(CO)_5 \qquad 3.3.4.3$$

Loss of the arene ligand has also been reported to result upon the photolysis of $ArCr(CO)_3$ [14] These results were reported for expenments where the photolysis was carried out in the presence of ^{14}C labelled CO and arene group Incorporation of both carbonyl and arene ligands was recorded The loss of the arene ligand was reported to be inhibited in the presence of CO implying that it occurs *via* the dicarbonyl complex In the examination of the photolysis of $ArCr(CO)_3$ in toluene arene exchange was also observed However it is proposed that the exchange process occurs via an η^4 ring slippage interaction rather than the dicarbonyl complex as previously reported [22]

The reactivity of the coordinatively unsaturated $LM(CO)_2$(toluene) complexes towards monomeric and polymeric pyridine ligands was investigated by measuring the reaction kinetics and activation parameters for the reaction The $MeCpMn(CO)_2$(toluene) fragment was observed to have a higher rate of reaction with the polymeric ligands than with the free pyridine This increase in the observed rate constants is probably a result of an interaction of the dicarbonyl complex with the polymer backbone as well as with the pendant nitrogen atoms

The results recorded for the $ArCr(CO)_2$(toluene) complex were the opposite of those observed for the manganese system The monomenc pyridine complex had a higher rate of reaction than the polymeric ligands with the dicarbonyl toluene complex The lower reaction rates for the polymeric ligands is probably a result of steric hindrance caused by the presence of the arene group which prevents access to the metal centre

The activation parmeters for the reactions in the $MeCpMn(CO)_3$ and $ArCr(CO)_3$ systems were investigated to confirm that the trends observed were not a result of a difference in the Gibbs free energy of activation for the reactions The reaction of the $Cr(CO)_5$(toluene) species with the pyridine ligands was investigated to see if the different trends observed between the manganese and chromium tricarbonyl systems was a result of the metal centre This was discounted as the reaction rates observed for the pentacarbonyl complex followed the same trend as was observed for the manganese dicarbonyl fragment.

In general the $ArCr(CO)_2$(toluene) complex is the more reactive It reacts with the pyridine ligands two orders of magnitude quicker than the $MeCpMn(CO)_2$(toluene) species The activation energies for the formation of $ArCr(CO)_2$(pyridine) complexes are on average 15 $kJmol^{-1}$ lower than the corresponding manganese complex. This may partially account for the differences in reactivity The large negative $\Delta S^{\ddagger}$ values for both metal systems indicate the associative character of the rate determining step However there is a large error inherent in the $\Delta S^{\ddagger}$ value which means no definite conclusions can be made Wrighton and Hill [30] observed a trend in reactivity of the $LM(CO)_2$(matrix) species which appeared to correlate with the electron density on the metal atom They suggested that the reactivity differences may be a result of the smaller size of the chromium atom which leads to higher electron density on the metal atom and thus increased reactivity

3.4 References

1 J.K. Ruff, *Inorg Chem.*, **10**, 409, (1971)

2 R.B King, R.N Kapoor, M.S Suran, and P.N Kapoor, *Inorg Chem.*, **10**, 1851, (1971).

3 W Strohmeier and K Gerlach, *Z Naturforsch.*, **15b**, 675, (1960)

4 W Strohmeier, J F Guttenberger, and H Hellman, *Z Naturforsch.*, **19b**, 353, (1964)

5 W Strohmeier and J K Guttenberger, *Chem Ber.*, **97**, 1871, (1964)

6 W Strohmeier and C Barbeau, *Z Naturforsch.*, **17b**, 848, (1962).

7 M L Ziegler and R K Sheline, *Inorg Chem.*, **4**, 1230, (1965).

8 E O Fischer and M Herberhold, *Experimenta Suppl.*, **9**, 259, (1964)

9 W Strohmeier and D von Hobe, *Z Phys Chem.*, **34**, 393, (1962)

10 P J Giordano and M S Wrighton, *Inorg Chem.*, **16**, 160, (1977)

11 M Herberhold, W Kremnitz, H Trampisch, R B Hitam, A J Rest and D J Taylor, *J Chem Soc, Dalton Trans.*, 1261, (1982)

12 B S Creaven, A J Dixon, J M Kelly, C Long, and M Poliakoff, *Organometallics*, **6**, 2600, (1987)

13 J K Klassen, M Selke, A A Sorenson, and G K Young, *J Amer Chem Soc.*, **112**, 1267, (1990)

14 W Strohmeier and D von Hobe, *Z Naturforsch.*, **18b**, 981, (1963)

15 (a) B M Yavorskii, N K Baranetskaya, V N Trembovler, and N K Setkina, *Doklady Akad Nauk S S R.*, **207**, 1147, (1972)

(b) B M Yavorskii, V N Trembovler, N K Setkina, N K Baranetskaya, G B Zaslavskaya, and M G Evdokimora, *Russ. J Phys Chem.*, **3**, 1231, (1974)

(c) B M Yavorskii, V N Trembovler, N K Setkina, N K Baranetskaya, and G B Zaslavskaya, *Doklady Akad Nauk S S R.*, **218**, 1153, (1974)

16 V.N. Trembovler, N K Baranetskaya, N V Fok, G B Zaslavskaya, B M Yavorskii, and N K Setkina, *J Organomet Chem.*, **117**, 339, (1976)

17 M Cais, M Kaftory, D H Kohn, and D Tatarsky, *J Organomet Chem.*, **184**, 103, (1979)

18 M S Wrighton and D S Ginley, *J Amer Chem Soc.*, **97**, 4246, (1975)

19 J Nasielski and O Densioff, *J Organomet Chem*, 102, 65, (1975)

20 M S Wrighton, *Chem Revs* 74, 401, (1974)

21 M S. Wrighton and J L Haverty, *Z Naturforsch*, 30b, 254, (1975)

22 A Gilbert, J M Kelly, M Budzwait and E K von Gustorf, *Z Naturforsch* 31b, 1091, (1976)

23 C H Bamford, K G Al-Lamee, and C J Konstantinov, *J Chem Soc, Faraday Trans*, 73, 1406, (1977)

24 W Strohmeier and E H Staricco, *Z Phys Chem*, 38, 315, (1963)

25 (a) T G Traylor, K J Stewart and M J Goldberg, *J Amer Chem Soc*, 106, 4445, (1984)

(b) T G Traylor and K.J. Stewart, *J Amer Chem Soc*, 108, 6977, (1986)

26 R.N Perutz and J J Turner, *J Amer Chem. Soc*, 97, 4791, (1975)

27 (a) J D Simon and K S Peters, *Chem Phys Lett*, 98, 53, (1983)

(b) J D Simon and X Xie, *J Phys Chem*, 90, 6751, (1986)

(c) J D Simon and X Xie, *J Phys Chem*, 91, 5538, (1987)

(d) J D Simon and X Xie, *J Phys Chem*, 93, 291, (1989)

28 A.J Rest, J R. Sodeau, and D J Taylor, *J Chem Soc, Dalton Trans*, 651, (1978)

29 (a) P S Braterman and J D Black, *J Organomet Chem*, 39, C3, (1972)

(b) J D Black, M J Boylan, and P S Braterman, *J Chem Soc, Dalton Trans*, 673, (1981)

30 R.H Hill and M S Wrighton, *Organometallics*, 6, 632, (1987).

31 J C Gjaldbek, *Acta Chem Scand*, 6, 623, (1952)

32 B S Creaven, Ph D Thesis, Dublin City University, (1989)

33 R.M Kolodziej and A J Lees, *Organometallics*, 5, 450, (1986).

34 H B Abrahamson and M S Wrighton, *Inorg Chem*, 17, 3385, (1978)

35 G Russell, Ph D Thesis, Dublin City University, (1990)

36 M Lyons and C Long, Results to be published

37 (a) W J Moore, "Physical Chemistry", Longman, New York, (1978)

(b)H E Avery, "Basic Reaction Kinetics and Mechanisms", MacMillan, London, (1986)

38 G L Geoffroy and M S Wrighton, "Organometallic Photochemistry", Academic Press, New York, (1979)

39 For example. (a) J Nasielski, P Kirsh, and L Wipulte-Steiner, *J Organomet Chem*, **29**, 269, (1971)

(b) J M. Kelly, H Herman, and E K von Gustorf, *J Chem Soc. Chem Commun*, 105, (1973)

(c) A J Lees and A W Adamson, *Inorg Chem*, 20, 4381, (1981)

(d) J M Kelly, C Long, and R Bonneau, *J Phys Chem*, **87**, 3344, (1983).

(e) S.P Church, F W. Grevels, H Herman, and K Schnaffer, *Inorg Chem*, **24**, 418, (1985)

(f) S Oishi, *Organometallics* 7, 363, (1988)

Chapter 4

Flash Photolysis of Polystyrene Anchored Chromium Tricarbonyl

4 1 Introduction to polymer-bound metal carbonyl complexes

Polymer-bound metal carbonyl compounds have an important role to play in many organometallic catalytic systems [1] These polymer-bound metal carbonyls exhibit the unique selectivity and reactivity of their homogeneous counterparts even under mild conditions The ease of separation from the products is increased thus facilitating the recycling of the catalysts Other advantages reported for polymer-bound systems include enhanced hydrogenation activity of immobilised titanocene [2] and $[Ir(CO)Cl(PPh_3)_2]$ [3], greater positional selectivity in both hydrogenations [2,3] and hydroformylations [4], and increased selectivity based on substrate size considerations [3]

Several methods can be used to activate the catalyst, for instance polymer-supported organometallic complexes can be photoactivated to generate catalytically active intermediates which remain immobilised to the resin bed [5] The generation of coordinatively unsaturated metal complexes play a fundamental role in many organometallic and catalytic systems [6] These systems can be generated by thermal, photochemical, or electrochemical means [6,7]

A wide range of catalytic uses for polymer-supported metal carbonyl complexes have been reported Moffat in 1970 reported the catalysis of hydroformylation reactions utilising a poly-2-vinylpyridine/$Co_2(CO)_8$ system [8] He also emphasised the use of this system as a "catalyst reservoir" suitable for the release of small amounts of cobalt carbonyl under hydroformylation conditions, followed by its uptake after completion of the reactions [9]

Several workers have investigated the coordination of phosphine ligands to rhodium complexes Manassen has described the catalysis of hydroformylation and hydrogenations using polymeric rhodium complexes [10] The catalysis of hydrosilation, hydrogenation, and hydroformylation reactions has been described by Capka *et al* [11] also by employing rhodium complexes coordinatively bonded to polymeric phosphine ligands

Pittman and his fellow workers have carried out comparison studies on hydroformylation reactions catalysed by polymer attached and homogeneous rhodium carbonyl complexes [12] They reported enhanced selectivity for the polymer-supported catalyst

There have also been studies carried out on polymeric chromium complexes Cross-linked polystyrene anchored-$Cr(CO)_3$ moieties have been used in selective methyl sorbate hydrogenations [1]

Fahey demonstrated that polyenes can be hydrogenated to their corresponding monenes with remarkably high selectivity using $(PPh_3)_2RuCl_2(CO)_2$ [13] Pittman anchored this catalyst to a polymeric support and essentially confirmed Fahey's results [14]

Pittman and Smith [15] reported examples of sequential multistep organic reactions by binding two catalysts $[(PPh_3)_2Ni(CO)_2]$ for cyclooligomerisation and $[(PPh_3)_3RhCl]$ for hydroformylation to the same crosslinked polystyrene resin Cyclooligomerisation of butadiene to 1,5-cyclooctadiene, 1,5,9-cyclododecatriene, and 4-vinlycyclohexane by the supported nickel carbonyl catalyst occurred first This was followed by the selective hydroformylation of the exocyclic double bond of the vinylcyclohexane species catalysed by the bound rhodium complex Similar results were obtained when the

catalysts were attached to separate polymeric resins and mixed in the reactor Interaction of the two catalysts with each other was prevented by the polymer supports to which they were anchored

Another possible use of organometallic polymers involves their use in preparing highly dispersed metal or metal oxides within polymer films [16] By decomposing an organometallic moiety which is chemically attached along the polymer chain one might be able to prepare tiny metal or metal oxide particles within the polymer matrix Dispersions of oxides are of great importance for practical applications They are encountered in paints, fillers, soils, magnetic tapes, and corrosion products [17]

Organometallic complexes with catalytic activity have been incorporated into polymers in a variety of ways Most often a preformed polymer is functionalised so that a catalytic complex can be attached This may be carried out by derivatising the polymer with a ligand which in turn is used to bind the metal [4] Examples include the preparation of chloromethylated styrene resins followed by treatment with metal carbonyl anions to give σ-bonded transition metal to polymer linkages (Scheme 4 1 1) [18]

Phosphine linkages are the most widely used means of attaching metal complexes to the polymer backbone Phosphines may be introduced by reacting chloromethylated resins with $LiPR_2$ as described by Evans et al [19] They reacted lithium diphenylphoside (i e. $Li^+PPh_2^-$) with linear and crosslinked chloromethylated polstyrene to give polymers (I) and (II) according to Scheme 4 1 2 Functionalised polymers have also been prepared using brominated polystyrene (Scheme 4 1 2)

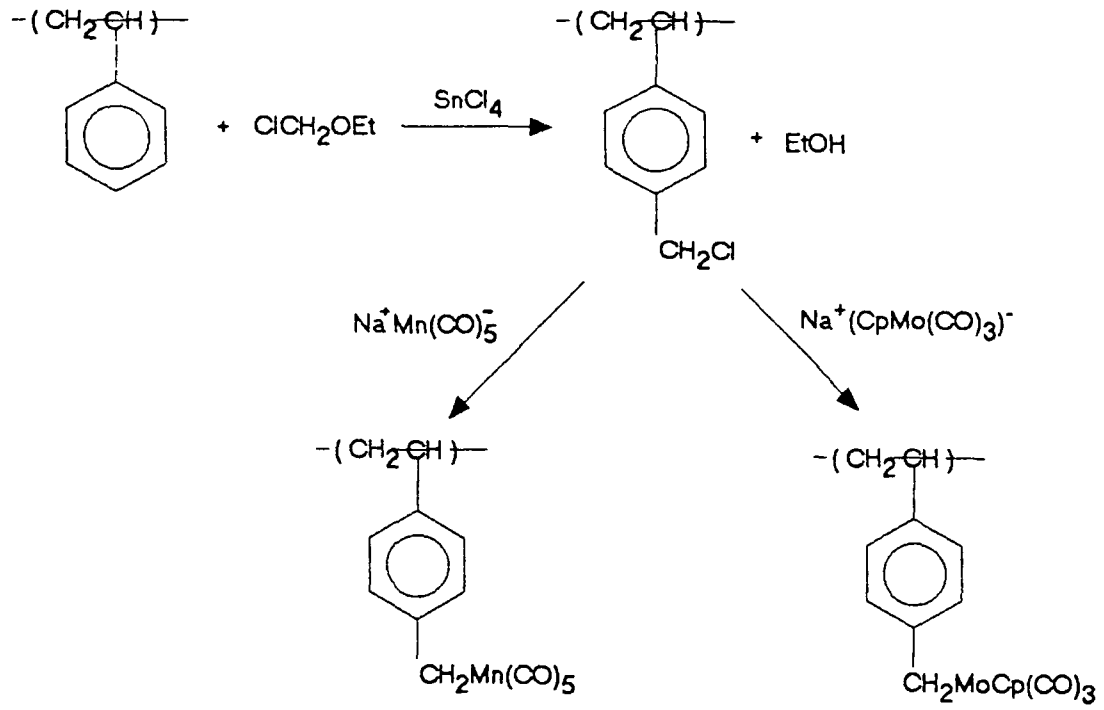

Scheme 4.1.1

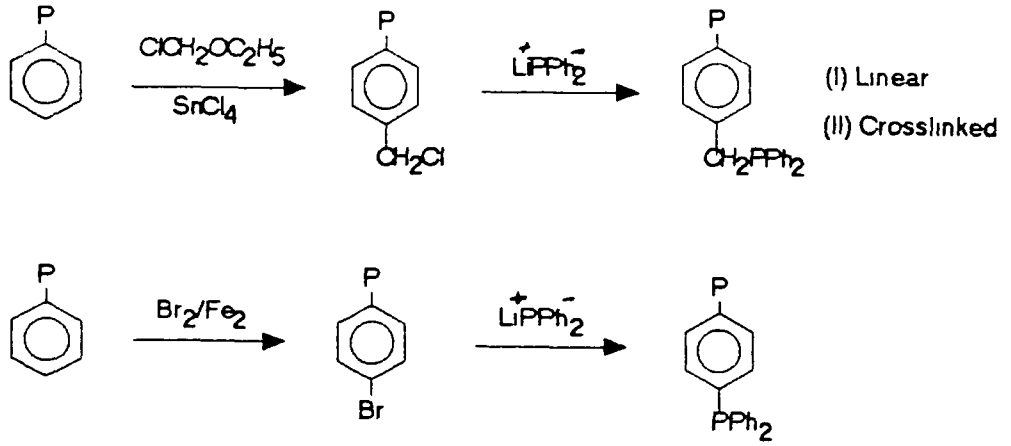

Scheme 4.1.2

The metal carbonyl complexes are then anchored on the polymer backbone using ligand replacement reactions Most commonly carbonyl substitution or phosphine exchange reactions are employed Ligands can be replaced either thermally or photochemically [19] Scheme 4 1 3 [4] illustrates several ligand replacement reactions used to prepare polymer-anchored metal carbonyls

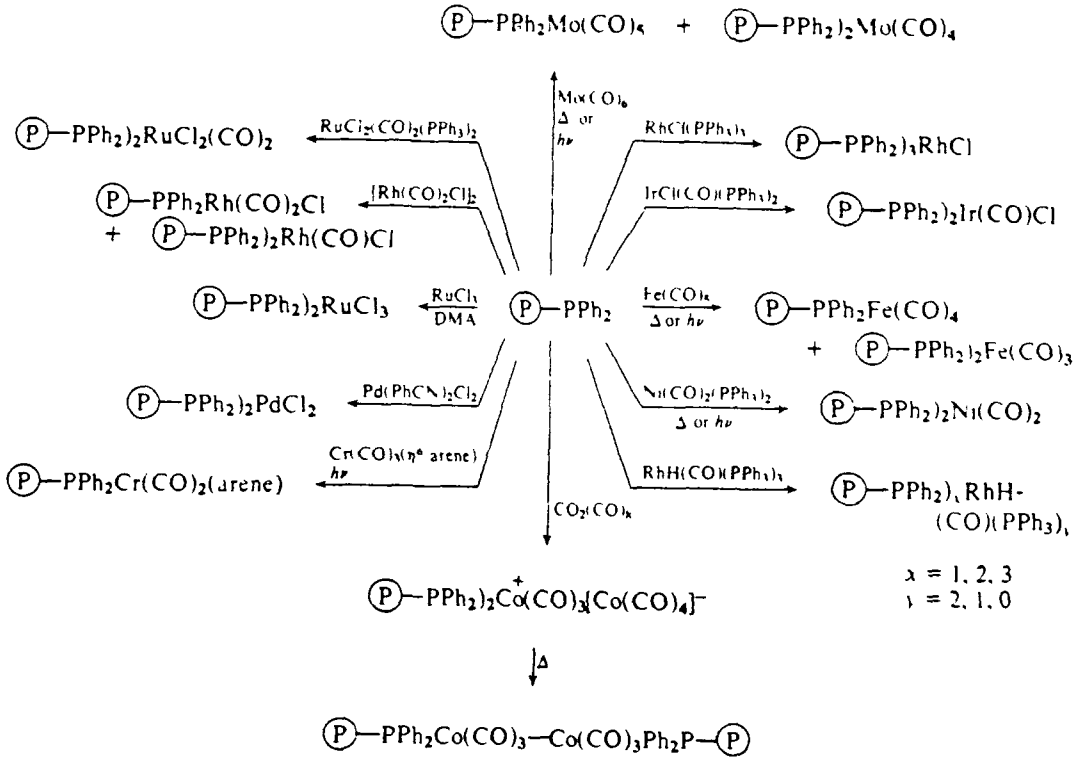

Scheme 4.1 3

Tatarsky *et al.* [20] reported the anchoring of arene chromium complexes through a photochemical ligand substitution reaction in which one of the CO groups is replaced by a phosphine ligand covalently bound to the polymer (Reaction 4 1 1) Thus preventing leaching of the Cr moiety into solution in the course of the catalytic reaction, which would occur if the $Cr(CO)_3$ group was attached directly to the phenyl rings of the polymer support

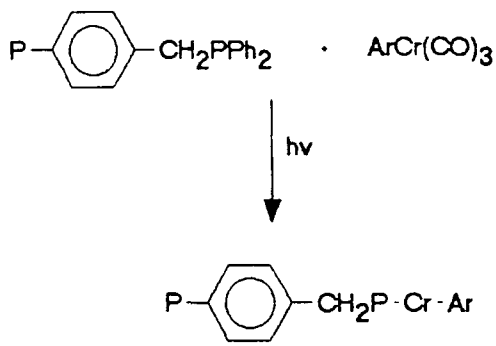

411

Polymers do not always require functional modification to provide ligands to bind metal complexes The metal carbonyl can complex directly with the polymer An example of this is the reaction of $Cr(CO)_6$ with polystyrene [1,21] Polystyrene anchored $Cr(CO)_3$ units can be prepared by refluxing $Cr(CO)_6$ with polystyrene in dimethoxyethane according to Reaction 4 1 2

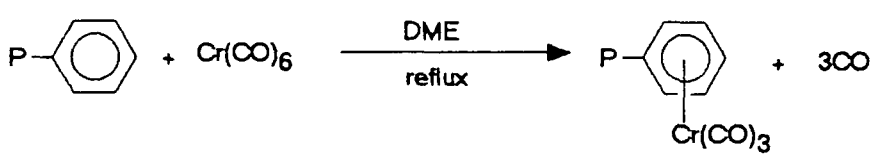

412

Metal pentacarbonyl complexes of 2- and 4- polyvinylpyridine have been prepared by reacting homopolyvinylpyridine or a vinylpyridine copolymer with $M(CO)_5$ (M = Cr, Mo, or

W), generated *in situ* either photochemically or from some labile complex such as $M(CO)_5(EtOH)$, to give polymers of the form $M(CO)_5(P(4\text{-}VP))$ or $M(CO)_5(P(2\text{-}VP))$ [22]

Another synthetic approach to construct polymer-bound metal carbonyls involves the preparation of a monomer, which contains the ligand or the ligand-metal complex The monomer is then polymerised to generate the appropriate resin This method has several advantages over anchoring the metal carbonyl directly to the polymer First, the concentration of the monomer can be controlled and polymers containing a wide range of ligand concentrations can be prepared Secondly, the nature of of the polymer matrix can be varied depending on the comonomer Third, the degree of cross-linking can be systematically varied, and finally distribution of ligand or metal complex throughout the resin beads is assured at the microstructure level There are also problems associated with this approach Monomers containing transition metal complexes may undergo undesirable reactions with radical, basic or acidic initiators which preclude optimum polymerisation behaviour [4]

A variety of organometalic vinyl monomers have been synthesied and both homo- and copolymerised [23] Examples include (1) η^5-vinylcyclopentadienyl-manganese tricarbonyl, (2) η^5-vinylcyclopentadienylchromiumdicarbonylnitrosyl, (3) η^5-vinylcyclopentadienyltungstenmethyltricarbonyl, (4) η^6-styrenechromium-tricarbonyl

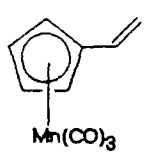

(1)

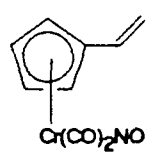

(2)

(3)

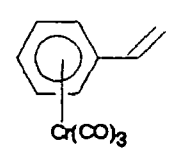

(4)

Pittman and Marlin [24] described the preparation of the monomer η^6-2-phenylethylacrylatechromiumtricarbonyl (PEAC) and its subsequent copolymerisation with styrene, methyl acrylate, acrylonitrile and 2-phenylethyl acrylate The PEAC monomer was prepared as in Scheme 4 1 4 [24] and was then readily copolymerised (Reaction 4 1 3)

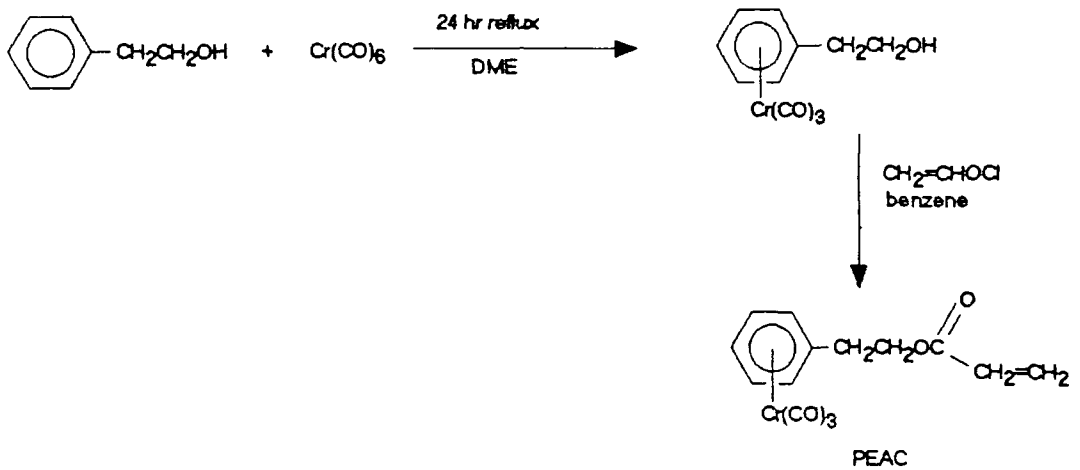

Scheme 4 1.4

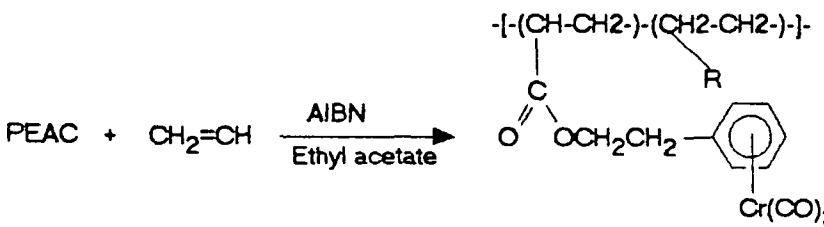

4 1 3

R = C_6H_6, $-COOCH_3$, CN, $-COOCH_2CH_2C_6H_5$, AIBN = azobisisobutyronitrile

Kelly and Long [22], in their preparation of copolymers of $M(CO)_5$(vinylpyridine) (M = Cr, Mo, W) with vinylpyridine, styrene, or methyl methyacrylate, first prepared the monomer

complex and then caused it to copolymense with the other vinyl monomers The monomers were prepared as in Scheme 4 1 5

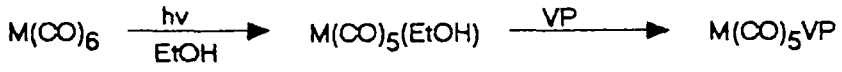

Scheme 4.1.5

Vinylpyridine copolymers of the complexes resulting from Scheme 4.1 5 were formed by heating vinylpyndine solutions of the metal complexes with free-radical initiator AIBN at 80°C [22]

Having previously investigated the photochemistry of $ArCr(CO)_3$ in cyclohexane [25] and in toluene as part of this thesis, we were interested in the photochemistry of the polystyrene-anchored chromium tricarbonyl complex. It was hoped to simplify the photochemistry of the $ArCr(CO)_3$ complex by anchoring it on a polymeric support The lifetime of the highly reactive intermediates generated on flash photolysis should be increased by attaching them to a polymer backbone Also formation of the dinuclear species which poisons the catalyst may be prevented by the rigid polymer supports As well as improving the recovery of catalysts different polymer supports could also be used to improve the solubility of the metal complexes in more freely available solvents and possibly lead on to the photochemistry of such compounds in water

4.2 Results and Discussion

Polymer-anchored chromium tricarbonyl was prepared by refluxing polystyrene with chromium hexacarbonyl in dimethoxyethane. Four polymers with different loadings of styrene to chromium tricarbonyl units were prepared (31, 61, 81, 1001). The photochemistry of these polymers was investigated by flash photolysis in room temperature toluene solutions. As similar results were obtained for the different loading polymers they are taken together in this section. Expermental difficulties were encountered in working with these polymer systems, because of the high extinction coefficient of $ArCr(CO)_3$ the resulting concentration of the metal complex in solution was low. Therefore any impurities in the polymer matrix or particulate matter remaining as a result of the method of preparation of the polymer-anchored species will have a profound effect on the results obtained.

Figure 4.2.1 shows the UV/vis spectrum of polymer-anchored-$Cr(CO)_3$ in toluene, the changes that occur in the spectrum during the course of the experiment can be seen (i.e. the system is not very reversible under an argon atmosphere). The spectrum is identical to that of $ArCr(CO)_3$ recorded in toluene (Figure 3.3.2.1).

On the flash photolysis of polymer-anchored chromium tricarbonyl in toluene three transient species were observed.

Figure 4 2.1: UV/vis spectrum of polymer-anchored-$Cr(CO)_3$ in toluene

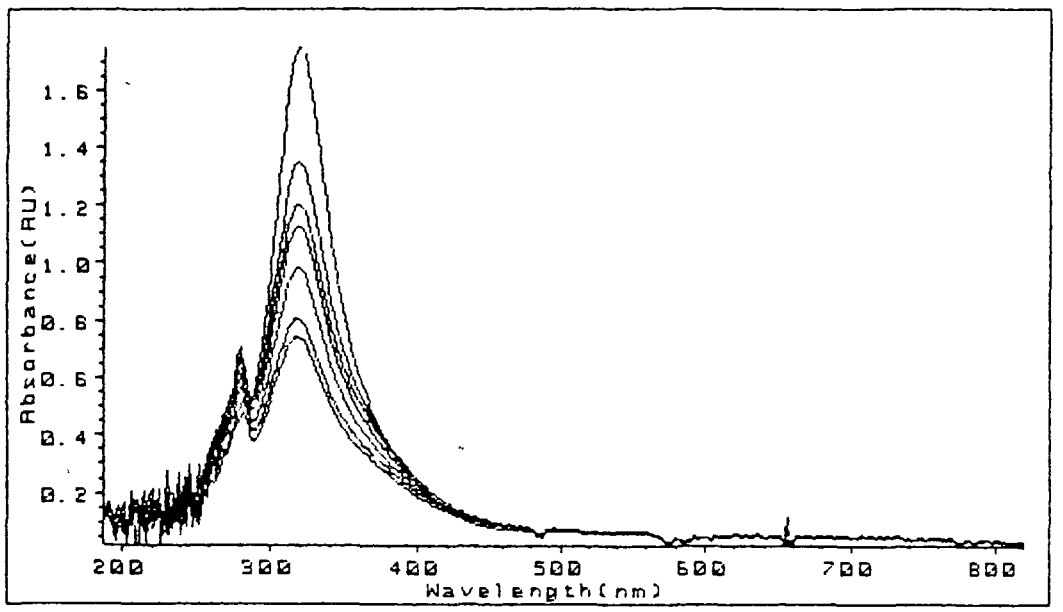

4.2.1 Primary photoproduct

The UV/vis difference spectrum of the first observed species recorded under an argon atmosphere is shown in Figure 4 2 2 The spectra were recorded at the time of the flash and 640 μs after the flash. As with the $ArCr(CO)_3$ system, the λ_{max} is at 400 nm, the depression centred at 335 nm is a result of a depletion of the parent complex, a second specis can be seen growing in around 500 nm From comparison of the spectra recorded with the $ArCr(CO)_3$ system it can be assumed that this first observed species is the dicarbonyl complex. However unlike the $ArCr(CO)_3$ system, in the polymer system two species were observed decaying at 400 nm, the decay of the of dicarbonyl solvent complex was followed by a slower decay of a second species Figure 4 2 3 shows the trace recorded for the decay of the two species

Figure 4.2.2: Transient UV/vis difference spectrum of the first observed species

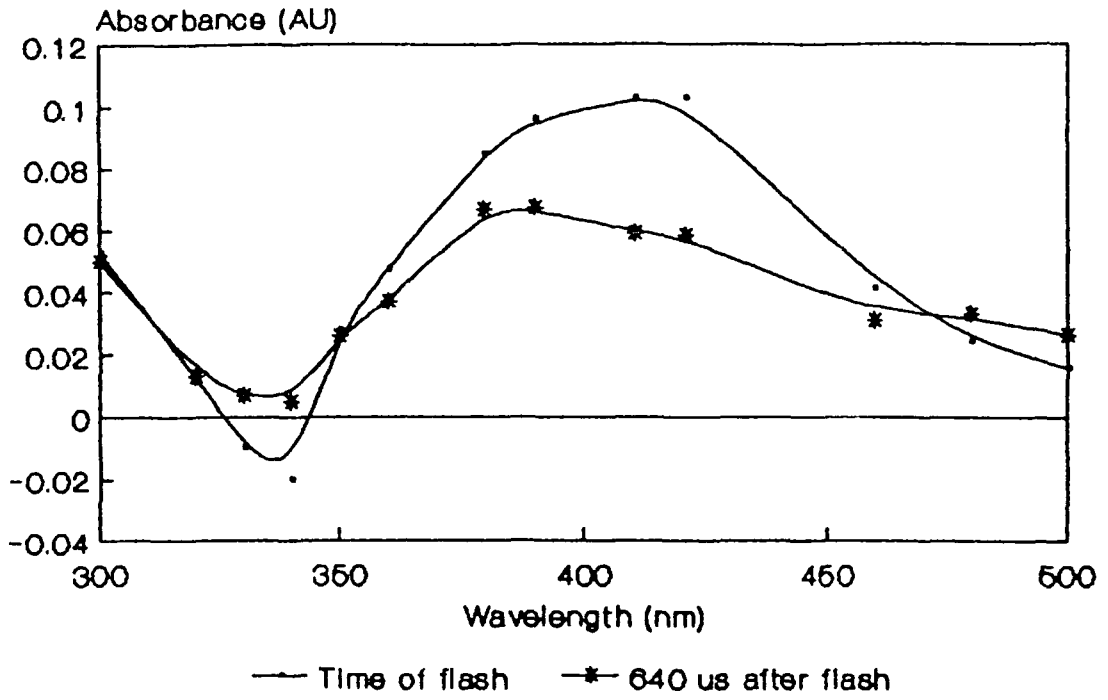

As with the other systems investigated the effect of saturating the solution with CO was examined This was carried out to confirm that the primary photoproduct was loss of CO, if this is the case its yield would be unaffected by the addition of CO and its lifetime decreased because the back reaction of the photolytically formed species is favoured by the presence of CO in solution Figure 4 2 4 shows the effect of CO on the initially formed species as can be seen from the recorded oscilloscope traces the conecentration of the species formed was not affected by the presence of CO in solution The rate of decay of this first formed species or the second decay is unaffected by the presence of CO (Figure 4 2 4 and Table 4 2 1) Although the system does appear to be more reversible as the residual absorbance is lower.

Figure 4 2 3. (a) the initial quick decay of the dicarbonyl solvent complex followed by (b) a second slower decay (see Section 5 2 1 for explanation of the axes)

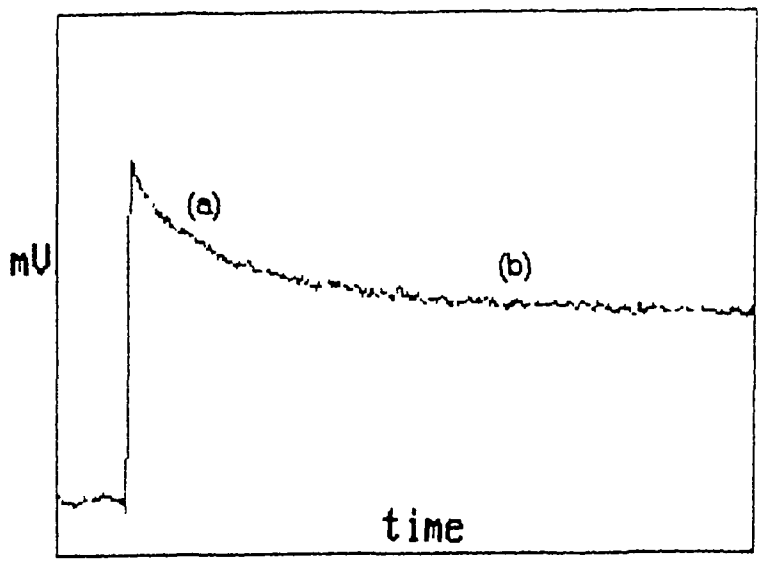

Figure 4.2.4: The effect of CO on the decay of the two species observed at 400 nm

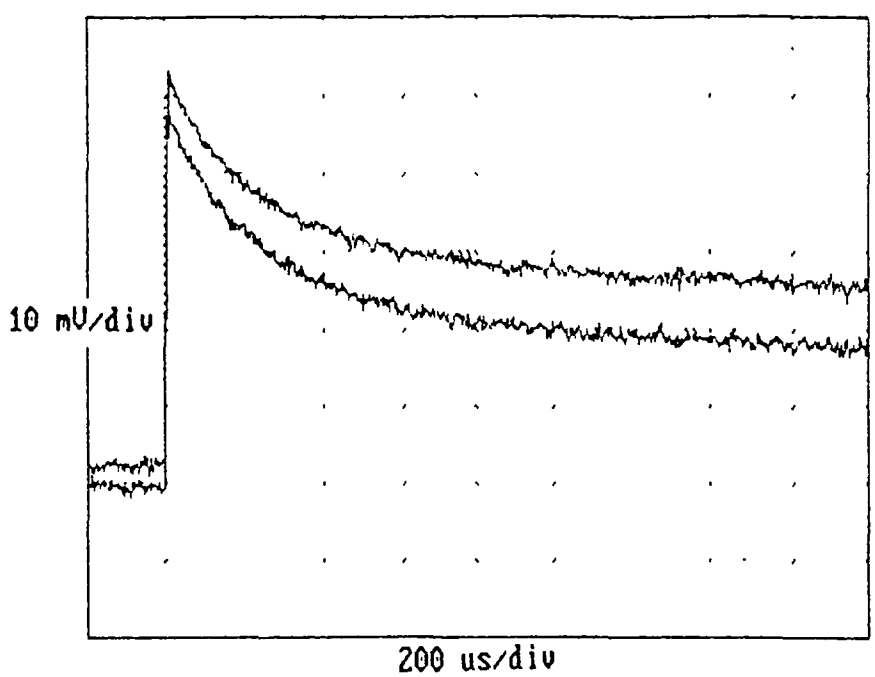

Table 4.2.1: The effect of CO on the k_{obs} value for the decay of the dicarbonyl complex and the second species

(a) 3 1 Poly(Styrene-$Cr(CO)_3$)

$[ArCr(CO)_3] = 3.48 \times 10^{-4}$ M

[CO] dm^3mol^{-1}	$k_{obs}(1)$	$k_{obs}(2)$
0	7430 s^{-1}	281s^{-1}
1.88×10^{-3}	7820 s^{-1}	169s^{-1}
3.77×10^{-3}	6880 s^{-1}	243s^{-1}
5.66×10^{-3}	6950 s^{-1}	202s^{-1}
7.53×10^{-3}	8140 s^{-1}	312s^{-1}

(b) 6 1 Poly(Styrene-$Cr(CO)_3$)

$[ArCr(CO)_3] = 2.57 \times 10^{-4}$ M

[CO] dm^3mol^{-1}	$k_{obs}(1)$	$k_{obs}(2)$
0	8050 s^{-1}	139s^{-1}
1.88×10^{-3}	7470 s^{-1}	203s^{-1}
3.77×10^{-3}	9290 s^{-1}	133s^{-1}
5.66×10^{-3}	8230 s^{-1}	315s^{-1}
7.53×10^{-3}	8530 s^{-1}	303s^{-1}

(c) 8 1 Poly(Styrene-$Cr(CO)_3$)

$[ArCr(CO)_3] = 2.57 \times 10^{-4}$ M

[CO] dm^3mol^{-1}	$k_{obs}(1)$	$k_{obs}(2)$
0	4880 s^{-1}	105s^{-1}
1.88×10^{-3}	4860 s^{-1}	113s^{-1}
3.77×10^{-3}	4960 s^{-1}	130s^{-1}
5.66×10^{-3}	5660 s^{-1}	153s^{-1}
7.53×10^{-3}	4720 s^{-1}	201s^{-1}

(d) 100 1 Poly(Sytrene-$Cr(CO)_3$)

$[ArCr(CO)_3] = 2.82 \times 10^{-4}$ M

[CO] dm^3mol^{-1}	$k_{obs}(1)$	$k_{obs}(2)$
0	5390 s^{-1}	138s^{-1}
1.88×10^{-3}	3680 s^{-1}	157s^{-1}
3.77×10^{-3}	4840 s^{-1}	184s^{-1}
5.66×10^{-3}	4320s^{-1}	167s^{-1}
7.53×10^{-3}	4520 s^{-1}	490s^{-1}

From Table 4 2 1 one can see that saturating the solution with CO has little to no effect on the rate of decay of either of the species It may be that the primary photoproduct is a mixture of a solvent complex (the fast decay) and a dicarbonyl polymer species (the slower decay) Access of the CO to solvent complex may be prevented by the large polymer molecules in solution while the dicarbonyl polymer species may preferentially react further with the polymer backbone to carry out arene group exchange along the polymer

4.2 2 Effect of parent concentration on the primary photoproduct

Increasing the concentration of the polystyrene anchored chromium tricarbonyl complex in solution results in an increase in the concentration of the dicarbonyl complex formed. However the effect of increased parent concentration on the rate of decay of the dicarbonyl complex is not very clear (Table 4 2 2)

In the case of the higher loading polymers (3 1, 6 1, 8 1) increasing parent concentration gives a resultant increase in the decay of the dicarbonyl complex. Although there is not a definite trend, in most cases the lowest concentration of parent has the lowest value of k_{obs} for the decay, and the highest concentration has the highest value The rate of decay of the dicarbonyl complex in the 100 1 polymer appears to be unaffected by the concentration of parent in the solution. Therefore it would appear that the dicarbonyl complex generated in the higher loading polymers reacts further with unphotolysed tricarbonyl units to possibly form a dinuclear species Whereas in the 100 1 polymer no further reaction appears to take place, this is probably because the chromium units are on average going to be further apart in the lower loading polymer

As can be seen from Table 4 2 2 the decay of the longer lived species in all cases does not depend on the concentration of the parent in solution

Table 4 2.2: Effect of parent concentration on the rate of decay of the dicarbonyl complex

(a) 3 1 P(Sty-$Cr(CO)_3$)

[P(Sty-$Cr(CO)_3$]	$k_{obs}(1)$	$k_{obs}(2)$
2 94 x 10^{-4} M	6050s^{-1}	116s^{-1}
3 48 x 10^{-4} M	7430s^{-1}	281s^{-1}
3 96 x 10^{-4} M	6100s^{-1}	86 s^{-1}
4 75 x 10^{-4} M	9030s^{-1}	119s^{-1}

(b) 6 1 P(Sty-$Cr(CO)_3$)

[P(Sty-$Cr(CO)_3$]	$k_{obs}(1)$	$k_{obs}(2)$
0 98 x 10^{-4} M	3980s^{-1}	267s^{-1}
2 09 x 10^{-4} M	5950s^{-1}	74s^{-1}
2 57 x 10^{-4} M	7480s^{-1}	99s^{-1}
2 89 x 10^{-4} M	7060s^{-1}	62s^{-1}
3 44 x 10^{-4} M	8050s^{-1}	139s^{-1}

(c) 8.1 P(Sty-$Cr(CO)_3$)

[P(Sty-$Cr(CO)_3$]	$k_{obs}(1)$	$k_{obs}(2)$
2 38 x 10^{-4} M	5970s^{-1}	204s^{-1}
2 57 x 10^{-4} M	4880s^{-1}	105s^{-1}
2 61 x 10^{-4} M	8940s^{-1}	25s^{-1}
4 28 x 10^{-4} M	8790s^{-1}	181s^{-1}

(d) 100 1 P(Sty-$Cr(CO)_3$)

[P(Sty-$Cr(CO)_3$]	$k_{obs}(1)$	$k_{obs}(2)$
2 08 x 10^{-4} M	3365s^{-1}	2 4s^{-1}
2 82 x 10^{-4} M	5390s^{-1}	138s^{-1}
3 34 x 10^{-4} M	5870s^{-1}	83s^{-1}
4 07 x 10^{-4} M	3330s^{-1}	78s^{-1}

4 2 3 Effect of power of the laser on the concentration of the primary phtoproduct

To determine if the primary photoproduct was formed as a result of a single photon excitation of the parent polymer tricarbonyl complex An experiment was carried out whereby the relative power of the laser was varied and the initial absorbance of the dicarbonyl complex was recorded For the four polymer complexes the formation of the dicarbonyl complex was seen to vary linearly with the laser power (Figures 4 2 5–4 2 8), charactenstic of a single photon event

---

Figure 4.2.5: Plot of relative laser power versus concentration of primary photoproduct for 3 1 P(Styrene-$Cr(CO)_3$)

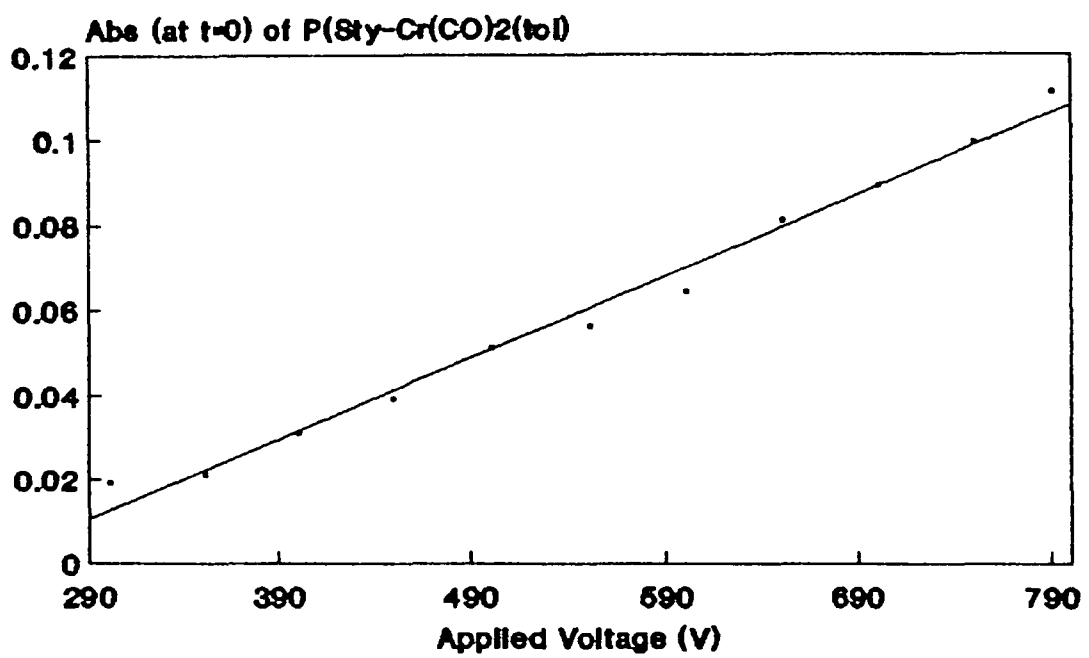

Figure 4 2.6. Plot of relative laser power versus concentration of primary photoproduct for 6 1 P(Styrene-$Cr(CO)_3$)

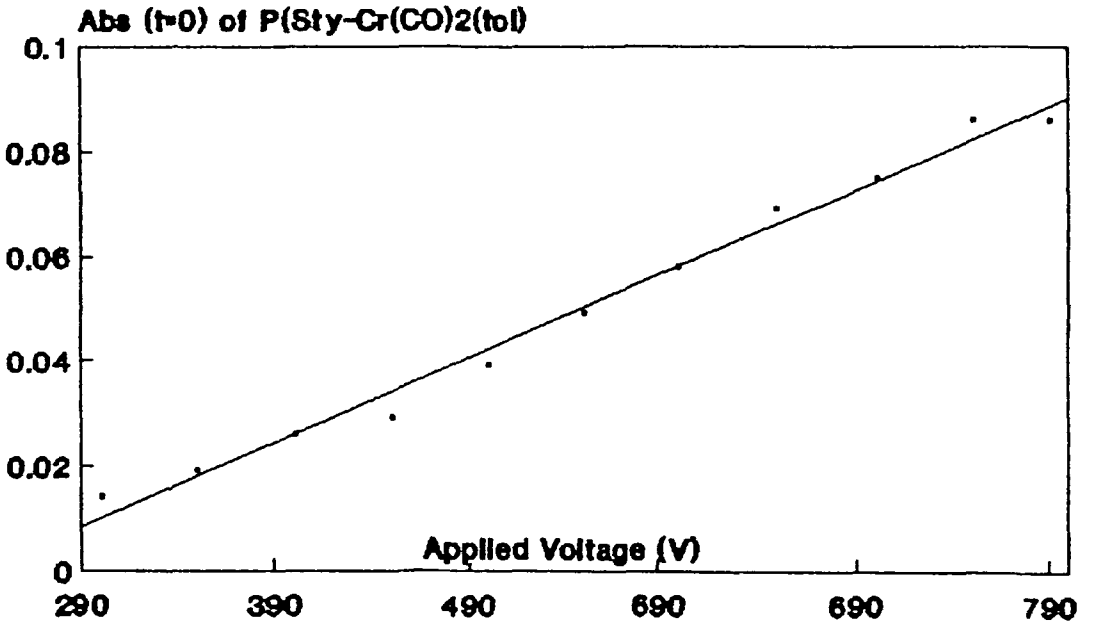

Figure 4 2.7: Plot of relative laser power versus concentration of primary photoproduct for 8 1 P(Styrene-$Cr(CO)_3$)

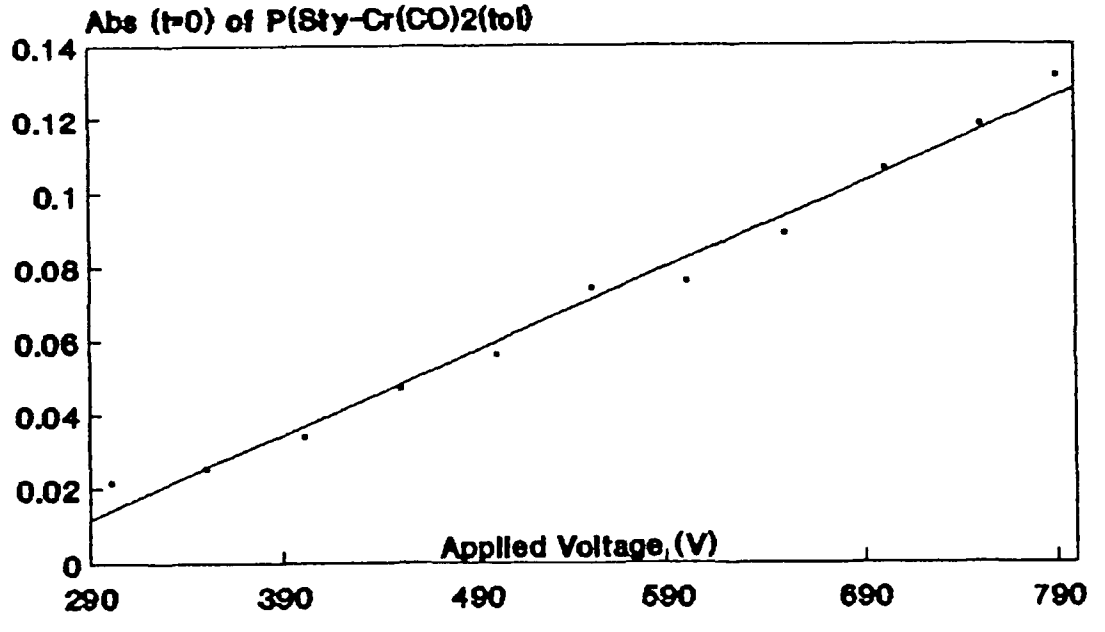

Figure 4 2 8: Plot of relative laser power versus concentration of primary photoproduct for 100 1 P(Styrene-$Cr(CO)_3$)

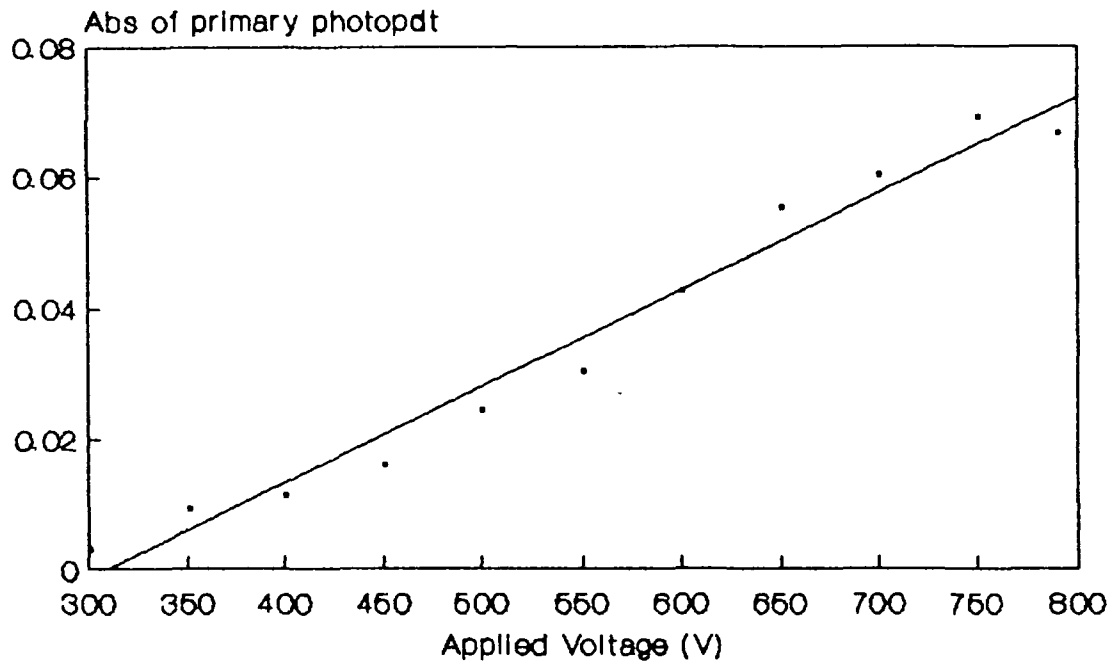

4 2 4 Formation of the second transient species

On flash photolysis of the higher-loading polymers (3 1, 6 1, 8 1) a second species was observed growing in on the same timescale as the decay of the dicarbonyl complex In the transient UV/vis difference spectrum (Figure 4 2 2) this species can be seen best at 500 nm, although this is not necessarily the λ_{max} of the complex, at this wavelength absorbance arising from the primary photoproduct is low In the case of the 100 1 polymer the grow-in of this second species was not observed

4.2 5 Effect of parent concentration and CO on the rate of formation of the second transient species.

The formation of this second species was observed at 500 nm and on the same timescale as the decay of the primary photoproduct The transients recorded for the formation of this species proved to be very noisy and irreproducible Nevertheless, in general, it appeared that the rate of formation of this species depended on the concentration of the parent complex in solution (Table 4 2 3)

As can be seen from Table 4.2 3 in general as the concentration of parent in solution is increased the rate of formation of this second species also increases Also at low concentrations of the polymer-bound parent complex its formation is not detected This would imply that the formation of this second species involves a reaction with the parent complex. In CO saturated solution the formation of this second transient species appears to be reduced, as can be seen from the overlayed oscilloscope traces in Figure 4 2 9 recorded under argon and carbon monoxide atmospheres This would seem to imply that the formation of this second species is *via* the dicarbonyl fragment, as under a CO atmosphere the lifetime of the dicarbonyl fragment is greatly reduced Therefore, allied

with the fact that its rate of formation is also related to the concentration of parent in solution, what is probably been observed is the formation of a dinuclear species on the polymer backbone (Reaction 4 2 1) The metal centres could be either on the same or different polymer coils

Table 4 2.3. Effect of parent concentration on formation of the second transient species

(a) 3 1 P(Styrene-$Cr(CO)_3$)

[P(Sty-$Cr(CO)_3$]	k_{obs} s^{-1}
0 98 x 10^{-4} M	—
2 68 x 10^{-4} M	7928
2 97 x 10^{-4} M	8898
3 96 x 10^{-4} M	5599
4 75 x 10^{-4} M	9581

(b) 6.1 P(Styrene-$Cr(CO)_3$)

[P(Sty-$Cr(CO)_3$]	k_{obs} s^{-1}
0 61 x 10^{-4} M	—
2 89 x 10^{-4} M	7154
3 06 x 10^{-4} M	8497
3 14 x 10^{-4} M	9995
4 36 x 10^{-4} M	8053

(c) 8 1P(Styrene-$Cr(CO)_3$)

[P(Sty-$Cr(CO)_3$]	k_{obs} s^{-1}
0 98 x 10^{-4} M	—
2 37 x 10^{-4} M	6495
2 61 x 10^{-4} M	6547
4 28 x 10^{-4} M	9372

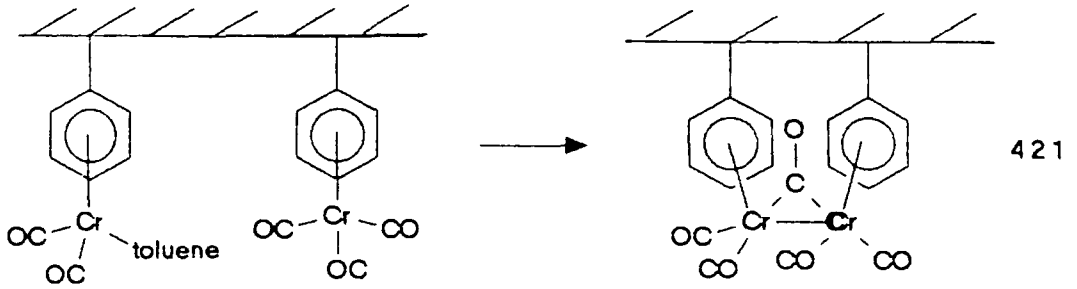

421

Figure 4 2.9: Effect of CO on the formation of the dinuclear species; trace recorded under (a) argon atmosphere (b) CO atmosphere

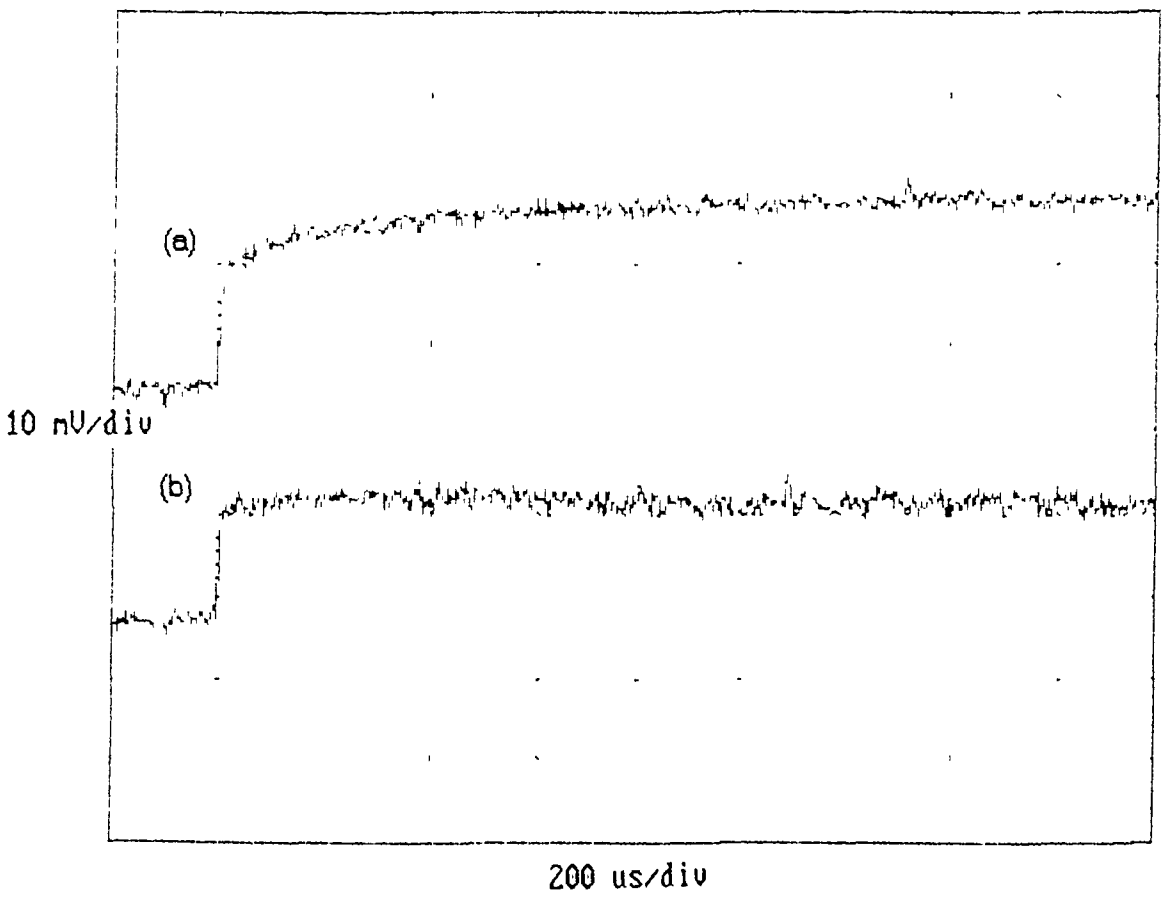

4 2 6 Formation of the third transient species

A third species was observed growing in at longer timescales The rate of formation of this species was on the same timescale as the decay recorded for the polymer dicarbonyl species (Figure 4 2 3) Figure 4 2 10 shows the trace recorded for the formation of this species Initially we see depletion of the parent complex followed by the grow in of this third complex Figure 4 2 11 shows the transient UV/vis difference spectrum recorded, the spectrum is similar to that of the dicarbonyl complex, depletion of the parent on the flash can be seen at 330 nm, broad maximum absorbance centred at 380 nm 340 nm proved to be the most suitable wavelength for analysis of this species

---

Figure 4 2 10 Oscilloscope trace recorded for the formation of the third species (see Section 5 2 1 for explanation of axes)

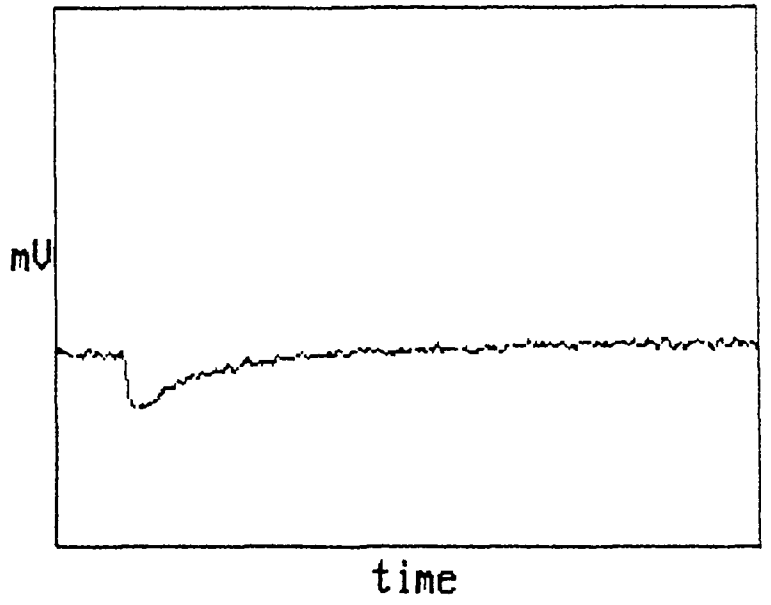

Figure 4 2 12 Transient UV/vis difference spectrum recorded for the third species

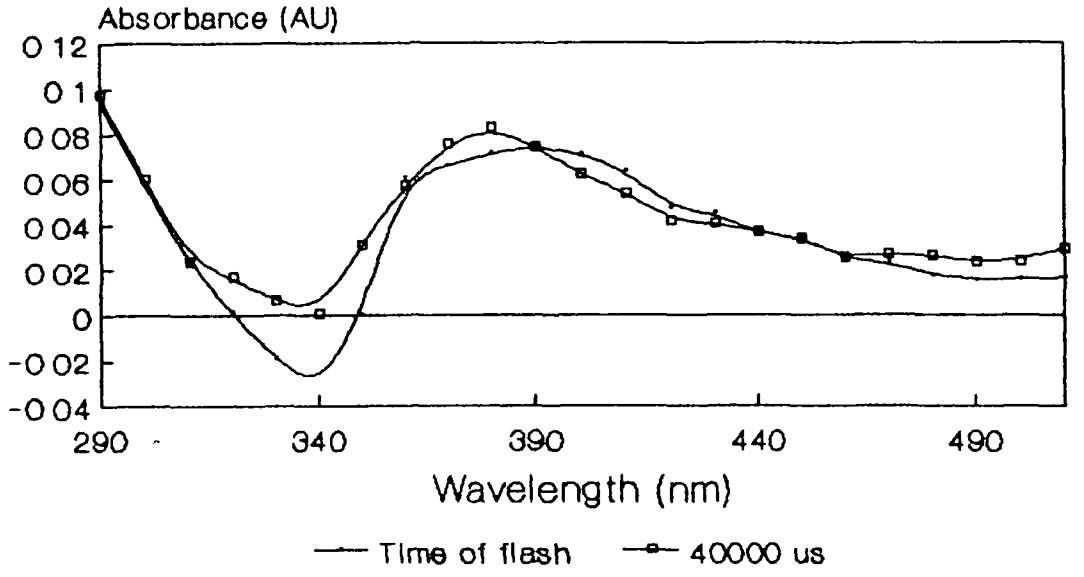

4 2 7 Effect of parent concentration on the rate of formation of the third transient species

The effect of increasing the concentration of the parent in solution on k_{obs} for the formation of the third species was investigated The results are summarised in Table 4 2 4

As can be seen from Table 4 2 4 the concentration of the parent complex in solution does not appear to have an effect on the rate of formation of this third species Therefore this transient species is not formed as a result of a reaction involving the parent complex

Table 4 2 4 Effect of parent concentration on the formation of the third species

(a) 3 1 P(Sty-Cr(CO)$_3$)

[P(Sty-Cr(CO)$_3$]	k_{obs}
2 37 x 10^{-4} M	297 s^{-1}
2 97 x 10^{-4} M	303 s^{-1}
3 96 x 10^{-4} M	216 s^{-1}
4 75 x 10^{-4} M	206 s^{-1}

(b) 6 1 P(Sty-Cr(CO)$_3$)

[P(Sty-Cr(CO)$_3$]	k_{obs}
2 09 x 10^{-4} M	150 s^{-1}
2 89 x 10^{-4} M	139 s^{-1}
3 06 x 10^{-4} M	205 s^{-1}
3 14 x 10^{-4} M	199 s^{-1}
4 36 x 10^{-4} M	139 s^{-1}

(c) 8 1 P(Sty-Cr(CO)$_3$)

[P(Sty-Cr(CO)$_3$]	k_{obs}
2 37 x 10^{-4} M	226 s^{-1}
2 61 x 10^{-4} M	308 s^{-1}
3 51 x 10^{-4} M	281 s^{-1}
4 28 x 10^{-4} M	216 s^{-1}

(c) 100 1 P(Sty-Cr(CO)$_3$)

[P(Sty-Cr(CO)$_3$]	k_{obs}
2 08 x 10^{-4} M	261 s^{-1}
2 82 x 10^{-4} M	167 s^{-1}
3 34 x 10^{-4} M	188 s^{-1}
4 07 x 10^{-4} M	240 s^{-1}

4 2 8 Effect of CO on the formation of the third transient species

The effect of CO on the formation of the third species was investigated by observing the rates of formation at various concentrations of CO in solution The results recorded are given in Table 4 2 5

From Table 4 2 5 it can be seen that increasing the concentration of CO in the solution gives a resultant increase in the rate of formation of this species In the three lower loading polymers (6 1, 8 1, and 100 1) the effect is more pronounced than in the 3 1 polymer This third species is probably an arene exchange product along the polymer backbone, resulting in regeneration of the parent complex The oscilloscope trace recorded for this species (Figure 4 2 10) initially shows depletion of the parent complex followed by a grow in to the baseline recorded for the parent absorption The final stage in the arene exchange reaction is the dicarbonyl η^4 complex going to the tricarbonyl η^6 complex the rate of conversion of these species would be enhanced by the presence of CO in solution

Table 4 2 5 Effect of CO on the formation of the third observed transient species

(a) 3 1 P(Sty-Cr(CO)$_3$)

[P(Sty-Cr(CO)$_3$)] = 2 94 x 10^{-4} M

[CO]dm^{3}mol^{-1}	k_{obs}
0	147 s^{-1}
1 88 x 10^{-3}	152 s^{-1}
3 77 x 10^{-3}	235 s^{-1}
5 65 x 10^{-3}	297 s^{-1}
7 53 x 10^{-3}	358 s^{-1}

(b) 6 1 P(Sty-Cr(CO)$_3$)

[P(Sty-Cr(CO)$_3$)] = 3 14 x 10^{-4} M

[CO]dm^{3}mol^{-1}	k_{obs}
0	199 s^{-1}
1 88 x 10^{-3}	360 s^{-1}
3 77 x 10^{-3}	454 s^{-1}
5 65 x 10^{-3}	506 s^{-1}
7 53 x 10^{-3}	654 s^{-1}

(c) 8 1 P(Sty-Cr(CO)$_3$)

[P(Sty-Cr(CO)$_3$)] = 2 61 x 10^{-4} M

[CO]dm^{3}mol^{-1}	k_{obs}
0	110 s^{-1}
1 88 x 10^{-3}	307 s^{-1}
3 77 x 10^{-3}	389 s^{-1}
7 53 x 10^{-3}	616 s^{-1}

(d) 100 1 P(Sty-Cr(CO)$_3$)

[P(Sty-Cr(CO)$_3$)] = 3 34 x 10^{-4} M

[CO]dm^{3}mol^{-1}	k_{obs}
0	188 s^{-1}
1 88 x 10^{-3}	385 s^{-1}
3 77 x 10^{-3}	376 s^{-1}
7 53 x 10^{-3}	610 s-1

4 2 9 Summary

On flash photolysis of polystyrene-anchored chromium tricarbonyl in toluene (355 nm excitation), the formation of three transient species were observed The first of these is a dicarbonyl complex followed by the formation of the dinuclear species and an arene exchange product. Scheme 4 2 1 summarises a possible mechanism for the formation of these species

From Scheme 4 2 1 on flash photolysis as well as the major primary photoproduct solvent complex (A), one also gets formation of a minor photoproduct (B), where the polymer-bound dicarbonyl species forms an η^2 interaction with an arene on the polymer backbone The solvent complex can then react with an unphotolysed tricarbonyl unit on the polymer to form a dinuclear species The dicarbonyl η^2 polymer species (B) rearranges to form two η^4 interactions on the polymer support, this complex then picks up a CO molecule and displaces the first arene group (i e the $Cr(CO)_3$ unit moves along the polymer backbone)

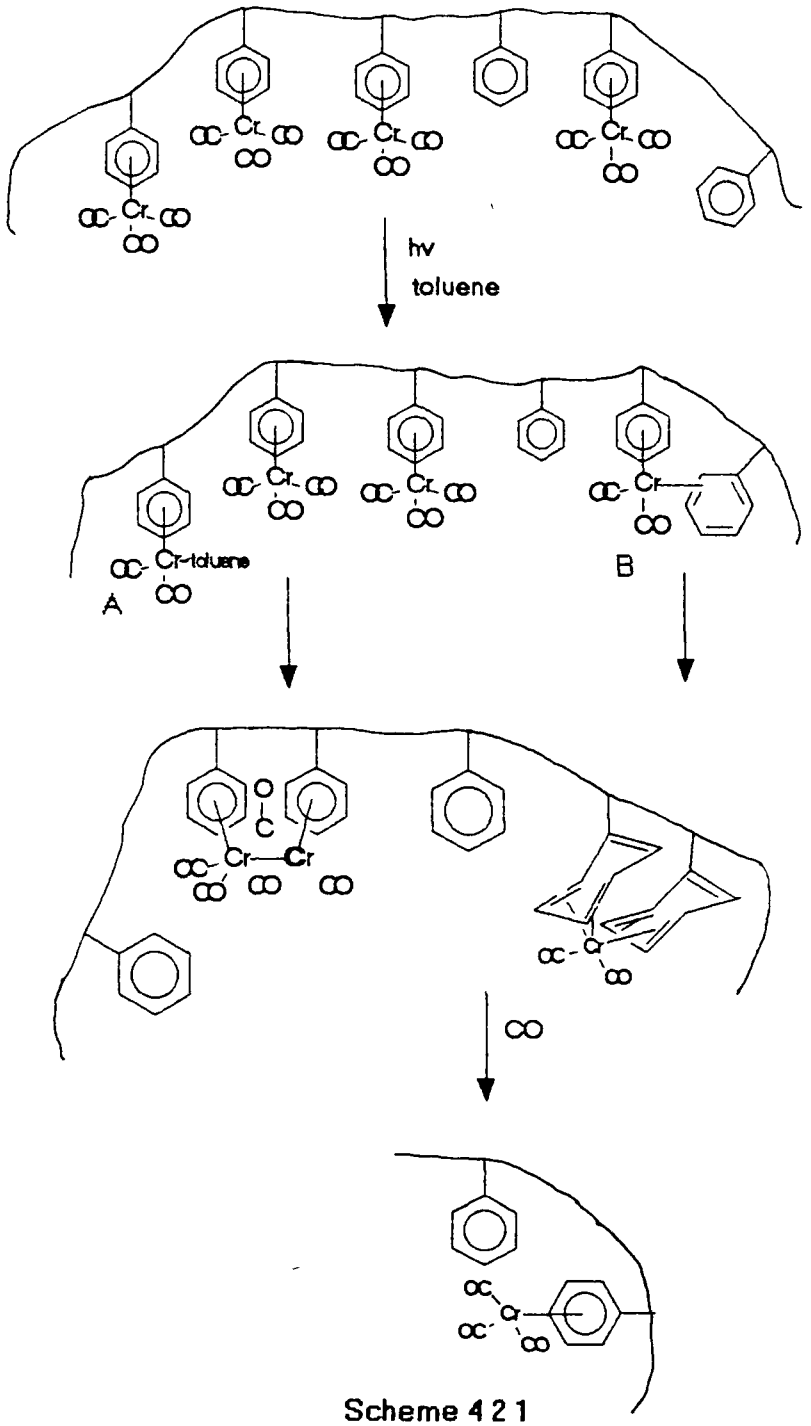

Scheme 4 2 1

4 2 10 Flash photolysis of polystyrene-anchored chromium tricarbonyl in toluene in the presence of pyridine

As with the other systems investigated ($MeCpMn(CO)_3$, $ArCr(CO)_3$ and $Cr(CO)_6$) the reaction of the primary photoproduct with both free and polymeric pyridine ligands was examined It was thought possible that by photolysing the polymer-bound chromium complex in the presence of the polymeric pyridine ligands one would form a double membrane which could be then opened by photolysing at a different wavelength (Scheme 4 2 2)

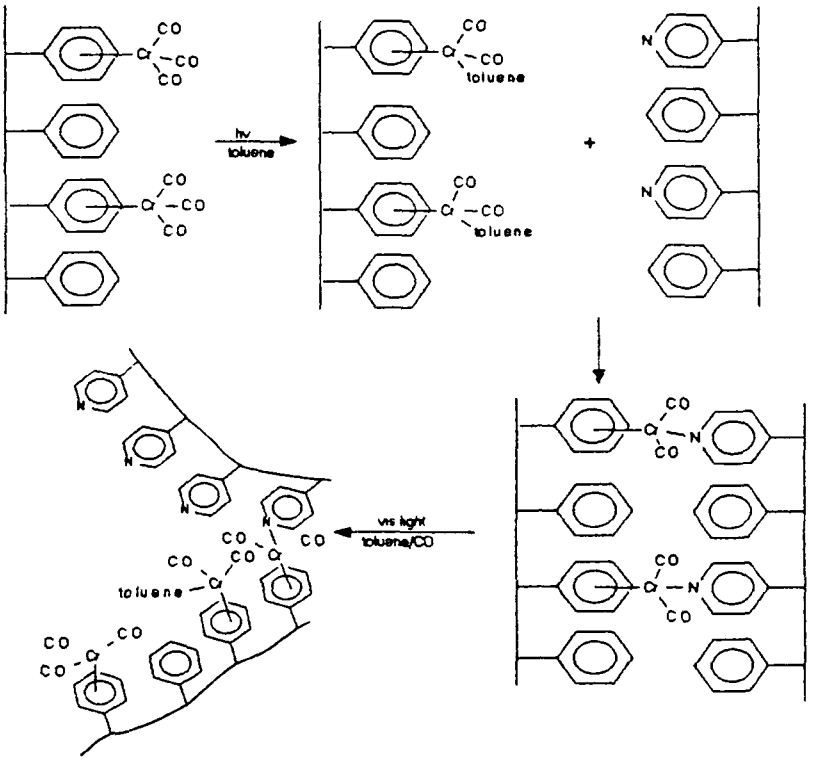

Scheme 4 2 2

Therefore the reaction kinetics and activation parameters for the reaction of the polymer-bound dicarbonyl complex with the various pyridine ligands were investigated The second order rate constants determined for the reaction of the polymer-bound dicarbonyl species with the pyridine ligands are given in Table 4 2 6

Table 4 2 6 Second order rate constant for the reaction of the various P(Styrene-$Cr(CO)_2$(toluene) complexes with pyridine

---

Polymer	$k_2 dm^3 mol^{-1} s^{-1}$
3 1	$3\,25 \times 10^5$
6 1	$3\,49 \times 10^5$
8 1	$3\,50 \times 10^5$
100 1	$3\,63 \times 10^5$

3 1 6 1 8 1,100 1 = P(Styrene-$Cr(CO)_3$)

As can be seen from Table 4 2 6 all the rate constants determined are practically the same The different loadings of chromium tricarbonyl units on the polymer backbone does not appear to affect the rate of reaction with the pyridine ligand The rates determined are lower than for the similar reaction of the $ArCr(CO)_2$(toluene) species with pyridine, which was determined to be $8\,33 \times 10^5$ $dm^3 mol^{-1} s^{-1}$ This difference is probably a result of the effect of the polymer coils in solution slightly hindering the reaction possibly by increased viscosity

The reaction rates for the reaction of the polymeric pyridine ligands with the polymer-bound dicarbonyl chromium complex were not determined as reproducible data was not forthcoming from the flash photolysis experiments The two polymer complexes did not appear to interact in solution i e two large molecules trying to gain access to a relatively small reaction centre Long time prepatative photolysis of the polymer-bound chromium tricarbonyl complex in the presence of the polymeric pyridine ligands also failed to yield the desired product.

Tables 4 2 7-4 2 10 and Figures 4 2 12-4 2 15 give the experimental data for the determination of the second order rate constants for the reaction of P(Styrene-$Cr(CO)_2$(toluene)) with pyridine

---

Table 4 2 7 and Figure 4 2 12 Second order rate constant for the reaction of 3 1 P(Styrene-$Cr(CO)_2$(toluene)) with pyridine

---

[pyridine]	$k_{obs}s^{-1}$
2 50 x 10^{-2} M	5666
4 06 x 10^{-2} M	9080
5 92 x 10^{-2} M	16268
6 55 x 10^{-2} M	18535

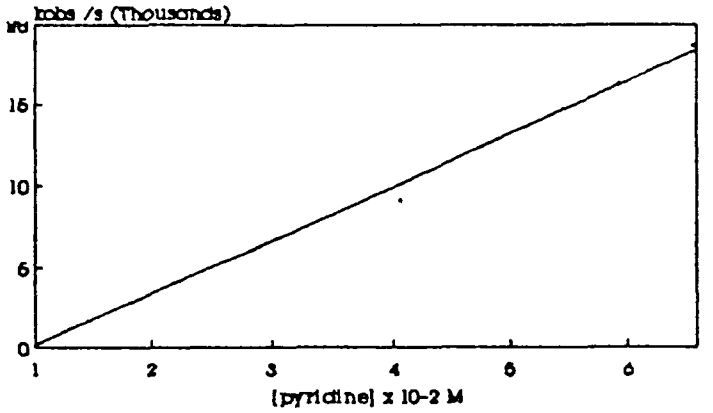

Slope = 3 25 ± 0 28 x 10^5 $dm^3mol^{-1}s^{-1}$

Intercept = -3090 7 ± 887 8 s^{-1}

Correlation coefficient = 0 99274

Table 4 2 8 and Figure 4 2 13 Second order rate constant for the reaction of 6 1 P(Styrene-$Cr(CO)_2$(toluene)) with pyridine

[pyridine]	$k_{obs}s^{-1}$
1 53 x 10^{-2} M	5500
3 53 x 10^{-2} M	12032
5 23 x 10^{-2} M	17422
7 03 x 10^{-2} M	24811
8 63 x 10^{-2} M	30010

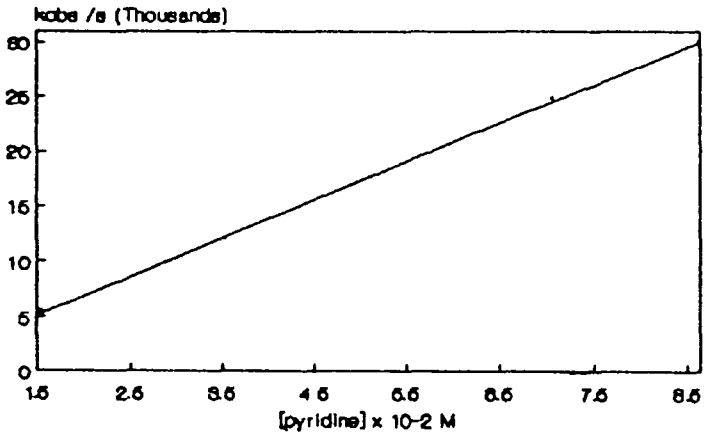

Slope = 3 49 ± 0 15 x 10^5 $dm^3mol^{-1}s^{-1}$

Intercept = -157 ± 503 s^{-1}

Correlation coefficient = 0 99901

Table 4 2 9 and Figure 4 2 14 Second order rate constant for the reaction of 8 1 P(Styrene-$Cr(CO)_2$(toluene)) with pyridine

[pyridine]	$k_{obs}s^{-1}$
1 64 x 10^{-2} M	4632
3 64 x 10^{-2} M	10769
5 34 x 10^{-2} M	15753
7 38 x 10^{-2} M	25773
9 61 x 10^{-2} M	31597

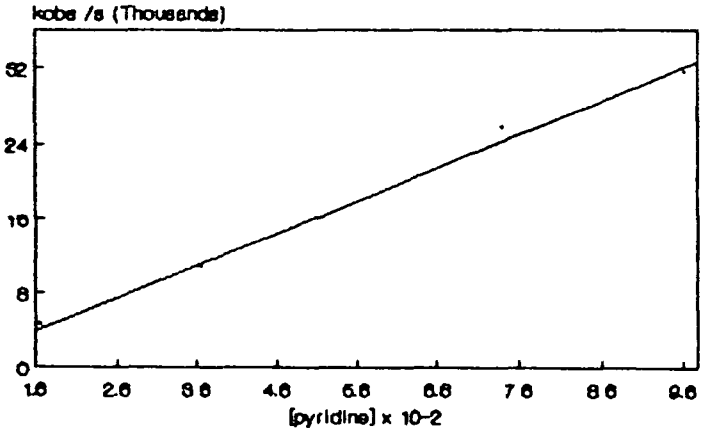

Slope = 3 50 ± 0 2 x 10^5 $dm^3mol^{-1}s^{-1}$

Intercept = -1637 ± 1256 s^{-1}

Correlation coefficient = 0 99506

Table 4 2 10 and Figure 4 2 15 Second order rate constant for the reaction of 100 1 P(Styrene-$Cr(CO)_2$(toluene)) with pyridine

[pyridine]	$k_{obs}s^{-1}$
$2\ 33 \times 10^{-2}$ M	8959
$5\ 84 \times 10^{-2}$ M	18796
$8\ 67 \times 10^{-2}$ M	29850
$9\ 90 \times 10^{-2}$ M	37028

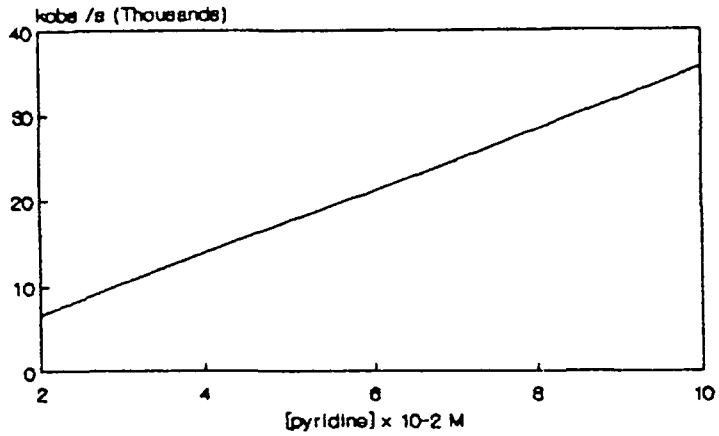

Slope = $3\ 63 \pm 0\ 35 \times 10^5\ dm^3mol^{-1}s^{-1}$

Intercept = $-635\ 7 \pm 2045\ s^{-1}$

Correlation coefficient = 0 9908

4 2 11 Activation parameters for the reaction of P(Styrene-$Cr(CO)_2$(toluene)) with pyridine

The activation parameters for the reaction of the polymer-bound dicarbonyl complex with pyridine were determined using the Arrhenius and Eyring equations as described in Section 3 3 1 4 The parameters determined are summarised in Table 4 2 11 The experimental data is given in Tables 4 2 12-4 2 15 and Figures 4 2 16-4 2 19

Table 4 2 11 Activation parameters determined for the reaction of the different P(Styrene-$Cr(CO)_2$(toluene)) complexes with pyridine

(a)

Polymer	E_{act}kJmol^{-1}	$\Delta H^{\ddagger}$kJmol^{-1}	$\Delta S^{\ddagger}$Jmol^{-1}K^{-1}	$\Delta G^{\ddagger}$kJmol^{-1}
3 1	40 73	38 09	-15 80	42 80
6 1	36 68	34 18	-23 13	41 07
8 1	40 84	38 14	-10 73	41 34
100 1	29 90	27 46	-44 84	40 82

(b) Activation parameters for the reaction of Ar$Cr(CO)_2$(toluene) with pyridine

E_{act}kJmol^{-1}	$\Delta H^{\ddagger}$kJmol^{-1}	$\Delta S^{\ddagger}$Jmol^{-1}K^{-1}	$\Delta G^{\ddagger}$kJmol^{-1}
35 61	32 98	-18 15	38 39

The activation parameters determined for the reaction of the various polymer-anchored chromium complexes with pyridine are all quite similar The activation energies are practically identical for the higher loading polymers (3 1 6 1, and 8 1), while the 100 1 polymer has a slightly lower value The negative value of $\Delta S^{\ddagger}$ in all cases indicates the associative nature of the reactions The Gibbs free energy ($\Delta G^{\ddagger}$) of each reaction is the same indicating that the different loadings of chromium units on the polymer backbone does not directly affect the formation of the pyridine complex. From Table 4 2 11 (b) we can see that the activation parameters determined for the reaction of Ar$Cr(CO)_2$(toluene) with pyridine (Section 3 3 2 10) are more or less the same as those determined for the

reaction of the polymer-bound species Therefore it can be concluded that there are no major differences in the activation parameters for the reaction with pyridine, when the chromium tricarbonyl unit is anchored on a polymer support or is free in solution

---

Table 4 2 12 Experimental data for the determination of the activation parameters for the reaction of 3 1 P(Styrene-$Cr(CO)_2$(toluene)) with pyridine [pyridine] = 6 85 x 10^{-2} M

T K	1/T K x 10^{-3}	k_2	Ln k_2	Ln k_2/T
288	3 47	94674	11 46	5 80
293	3 41	172829	12 06	6 38
300	3 33	201359	12 21	6 51
305	3 28	302689	12 62	6 90
309	3 24	399909	12 90	7 17
313	3 19	464070	13 05	7 30
318	3 14	538255	13 20	7 43
325	3 08	676145	13 42	7 64

Arrhenius Plot

Slope = -4899 2 ± 370

Intercept = 28 62 ± 0 13

Correlation coefficient = 0 9834

E_{act} = 40 73 ± 3 1 kJmol^{-1}

Eyring Plot

Slope = -4580 9 ± 368

Intercept = 21 86 ± 0 13

Correlation coefficient = 0 9881

$\Delta H^{\ddagger}$ = 38 09 ± 3 1 kJmol^{-1}

$\Delta S^{\ddagger}$ = -15 80 ± 1 1 Jmol^{-1}K^{-1}

Figure 4 2 16 Arrhenius (a) and Eyring (b) plots for the reaction of 3 1 P(Styrene-$Cr(CO)_2$(toluene)) with pyridine

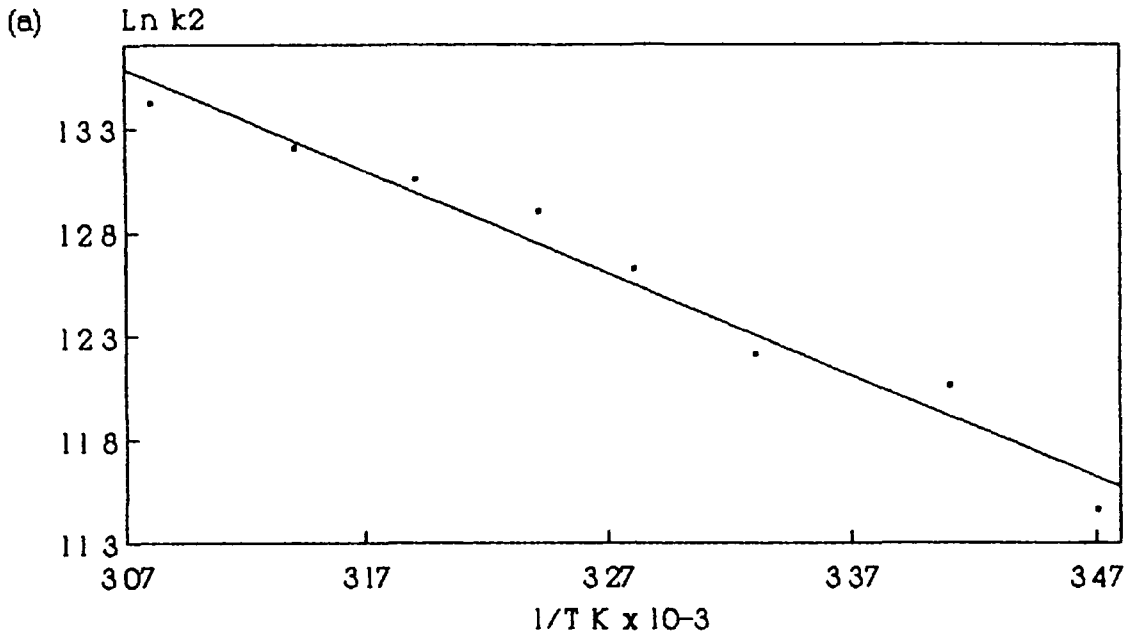

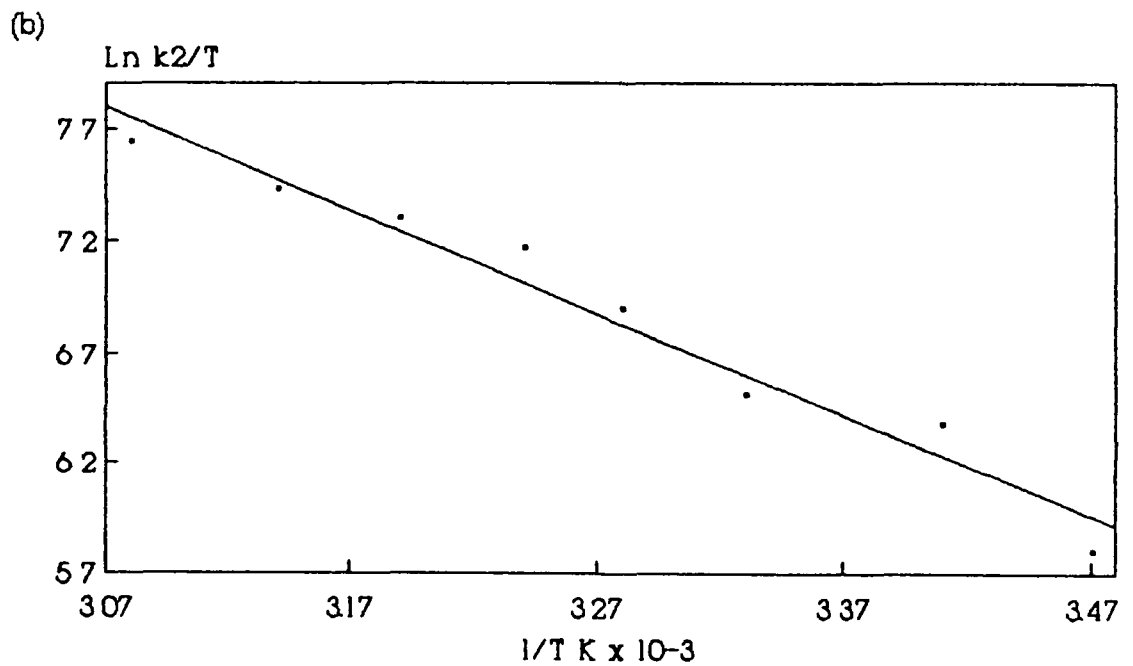

Table 4 2 13 Experimental data for determing the activation parameters for the reaction of 6 1 P(Styrene-$Cr(CO)_2$(toluene)) with pyridine [pyridine] = 5 23 x 10^{-2} M

T K	1/T K x 10^{-3}	k_2 x 10^5	Ln k_2	Ln k_2/T
291	3 44	2 56	12 45	6 78
298	3 36	4 32	12 98	7 28
303	3 30	4 93	13 11	7 39
309	3 24	6 10	13 32	7 59
313	3 19	8 38	13 64	7 89
318	3 14	1 07	13 88	8 12
324	3 09	1 23	14 02	8 24

Arrhenius Plot

Slope = -4411 4 ± 241 7

Intercept = 27 69 ± 0 07

Correlation coefficient = 0 9926

E_{act} = 36 68 ± 2 0 kJmol^{-1}

Eyring Plot

Slope = -4110 6 ± 237 4

Intercept = 20 98 ± 0 07

Correlation coefficient = 0 9918

$\Delta H^{\#}$ = 34 18 ± 2 0 kJmol^{-1}

$\Delta S^{\#}$ = -23 13 ± 0 62 Jmol^{-1}K^{-1}

Figure 4 2 17 Arrhenius (a) and Eyring (b) plots for the reaction of 6 1 P(Styrene-$Cr(CO)_2$(toluene)) with pyridine

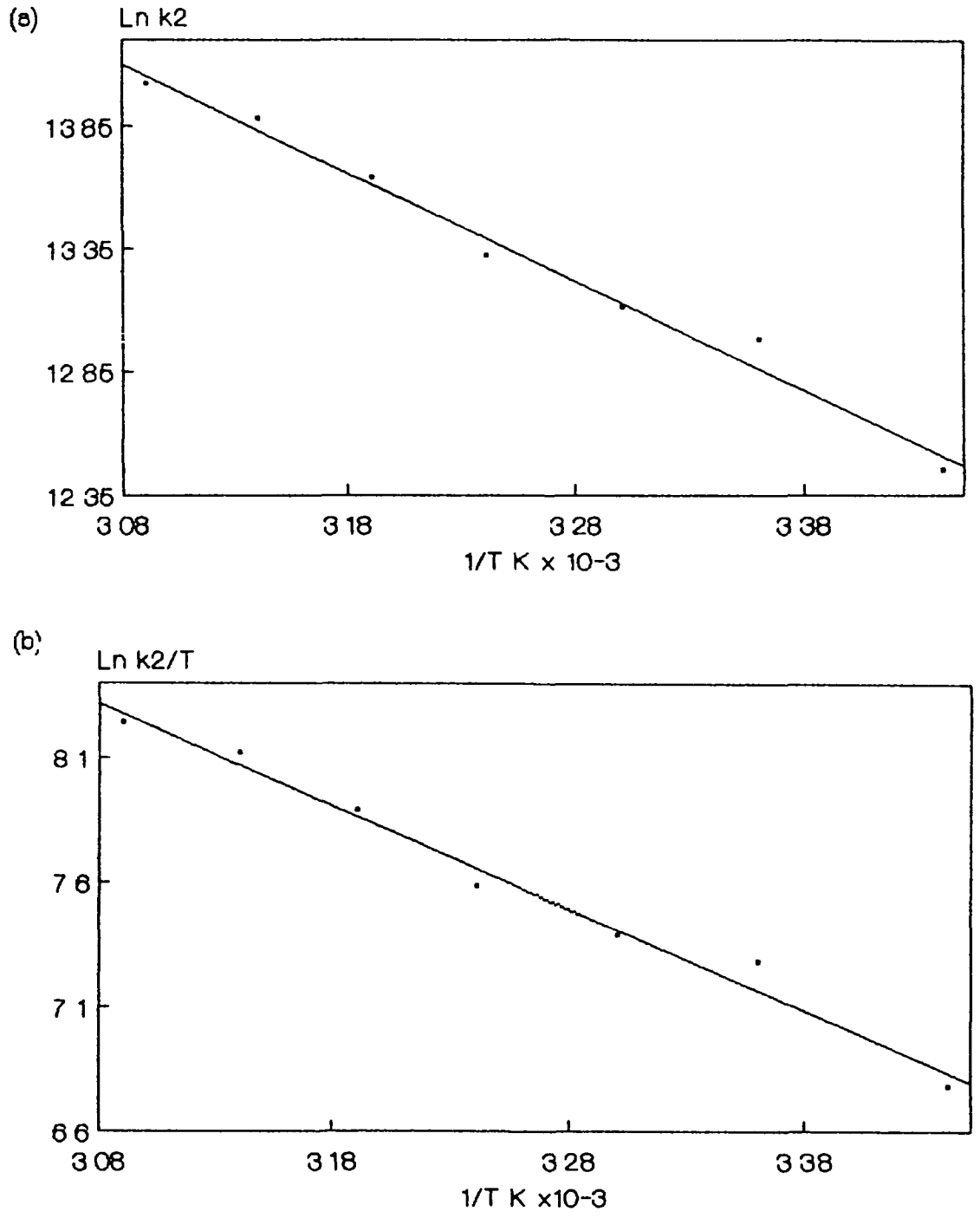

Table 4 2 14 Experimental data for determining the activation parameters for the reaction of 8 1 P(Styrene-$Cr(CO)_2$(toluene)) with pyridine [pyridine] = 5 31 x 10^{-2} M

T K	1/T KE-3	k_2	Ln k_2	Lnk_2/T
291	3 44	2 22 x 10^5	12 31	6 64
298	3 36	3 57 x 10^5	12 79	7 09
303	3 30	4 96 x 10^5	13 11	7 40
308	3 25	5 87 x 10^5	13 28	7 55
313	3 19	7 36 x 10^5	13 51	7 76
318	3 14	1 02 x 10^6	13 84	8 08
324	3 09	1 31 x 10^6	14 09	8 30

Arrhenius Plot

Slope = -4911 9 ± 175

Intercept = 29 25 ± 0 05

Correlation coefficient = 0 9968

E_{act} = 40 84 ± 1 45 kJmol^{-1}

Eyring Plot

Slope = -4587 8 ± 177

Intercept = 22 47 ± 0 05

Correlation coefficient = 0 9963

$\Delta H^{\ddagger}$ = 38 14 ± 1 47 kJmol^{-1}

$\Delta S^{\ddagger}$ = -10 73 ± 0 42 Jmol^{-1}K^{-1}

Figure 4.2.18: Arrhenius (a) and Eyring (b) plots for the reaction of 8:1 P(Styrene-$Cr(CO)_2$(toluene)) with pyridine.

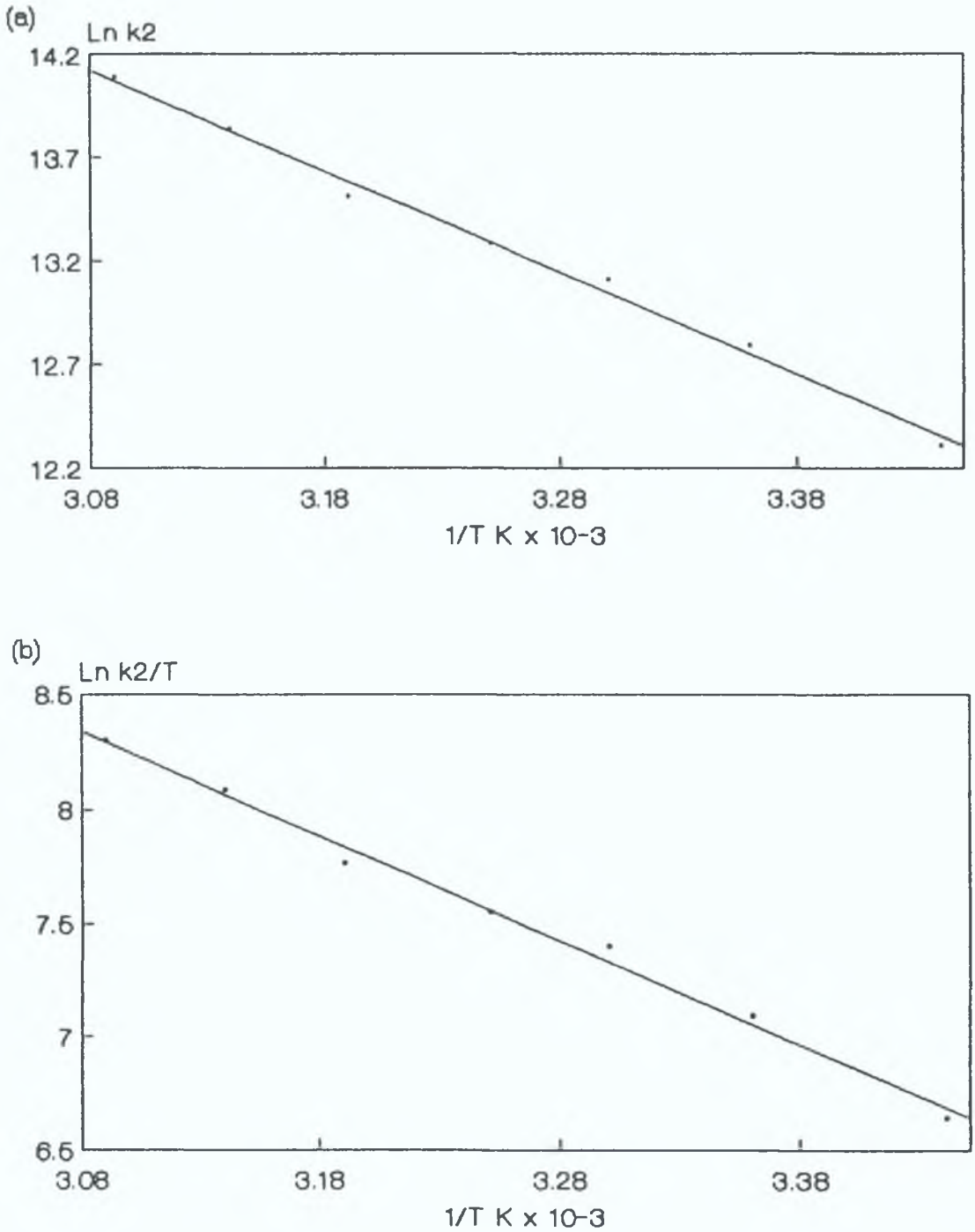

Table 4 2 15 Experimental data for the determination of the activation parameters for the reaction of 100 1 P(Styrene-$Cr(CO)_2$(toluene) with pyridine [pyridine] = $5\ 84 \times 10^{-2}$ M

T K	$1/T \times 10^{-3}$	k2	Ln k2	Ln k2/T
298	3 36	$4\ 25 \times 10^{5}$	12 96	7 26
304	3 29	$5\ 38 \times 10^{5}$	13 20	7 48
309	3 24	$6\ 88 \times 10^{5}$	13 44	7 71
314	3 18	$8\ 10 \times 10^{5}$	13 60	7 86
319	3 13	$1\ 02 \times 10^{6}$	13 84	8 07
324	3 09	$1\ 08 \times 10^{6}$	13 90	8 12

Arrhenius Plot

Slope = -3596 9 ± 168 9

Intercept = 25 05 ± 0 04

Correlation coefficient = 0 9956

E_{act} = 29 90 ± 1 4 kJmol^{-1}

Eyring Plot

Slope = -3302 8 ± 168 6

Intercept = 18 37 ± 0 04

Correlation coefficient = 0 99483

$\Delta H^{\#}$ = 27 46 ± 1 4 kJmol^{-1}

$\Delta S^{\#}$ = -44 84 ± 0 32 Jmol^{-1}K^{-1}

Figure 4 2 19 Arrhenius (a) and Eyring (b) plots for the reaction of 100 1 P(Styrene-$Cr(CO)_2$(toluene) with pyridine

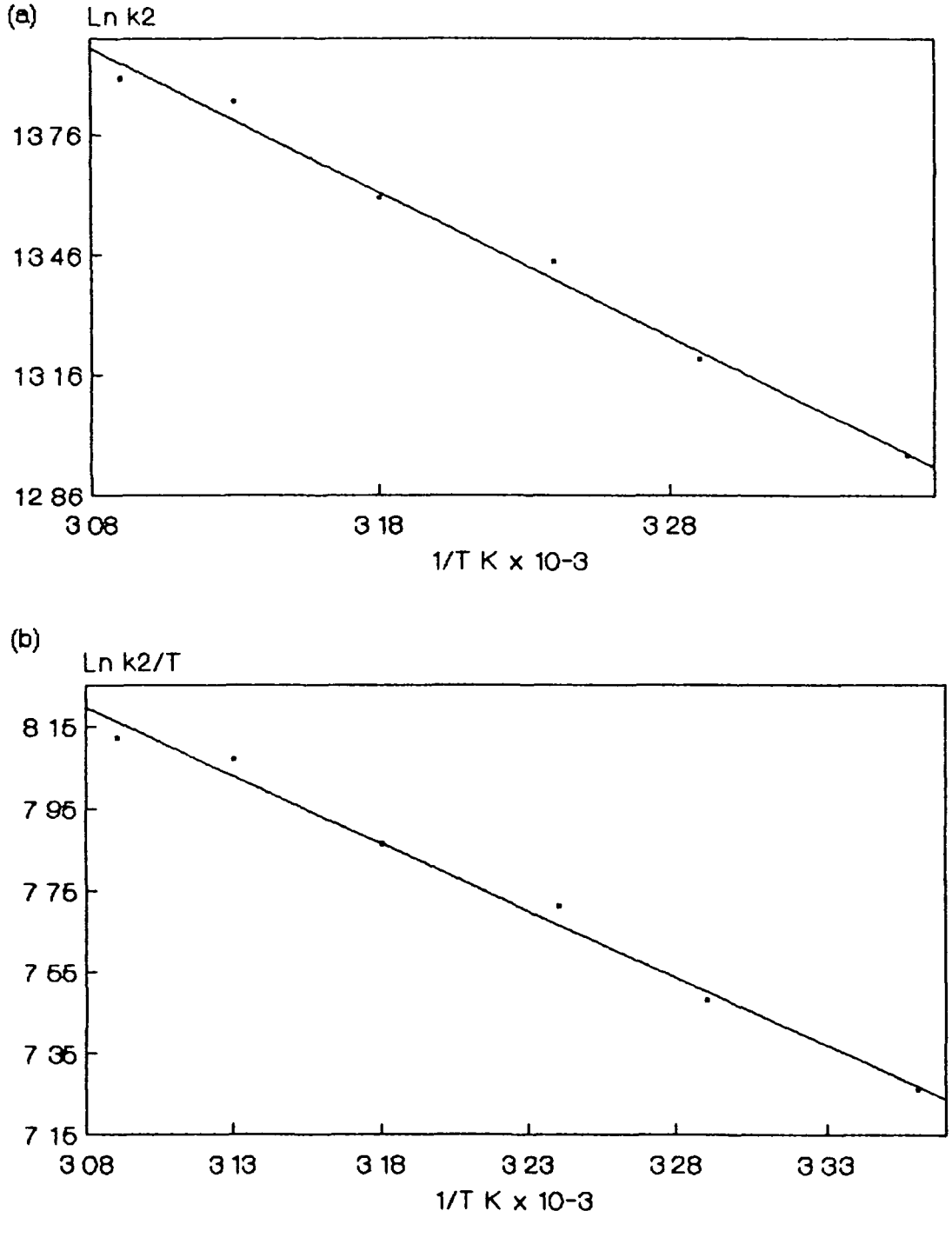

4 3 Conclusion

The flash photolysis of polymer-bound chromium tricarbonyl in toluene at room temperature was investigated On photolysis three transient species were observed, the primary photoproduct appeared to be a mixture of a dicarbonyl solvent complex and a dicarbonyl η^2 polymer complex The solvent complex, which had a faster decay rate than the polymer complex, appeared to react with unphotolysed tricarbonyl units on the polymer backbone to form the dinuclear species P(Styrene-$Cr_2(CO)_5$) (in the case of the higher loading polymers only) This dinuclear species was not formed in the 100 1 polymer system probably because the chromium units on the polymer backbone are further apart making access by the dicarbonyl fragment difficult

Saturating the solution with CO had no effect on the rate of decay of the primary photoproduct Although the presence of CO in solution does hinder the formation of the dinuclear species the solvent complex binds with CO in preference to the unphotolysed parent molecule The rate of formation of the arene exchange product is enhanced in a CO saturated solution, this is possibly because the final stage of arene exchange along the polymer backbone involves binding of a CO molecule to reform the parent tricarbonyl

The second order rate constants determined for the reaction of the polymer-bound dicarbonyl complexes with pyridine are identical for the different polymers but are lower than the rate of the same reaction involving the $ArCr(CO)_3$ species This is probably because of hindrance from the polymer coils in solution The activation parameters determined for the reaction with pyridine are practically the same for the different polymers and compare well to those determined for the $ArCr(CO)_2$(toluene) complex This implies that there is no change in the energy of activation between the reaction of

the polymer-anchored chromium and the $ArCr(CO)_2$(toluene) species with the pyridine ligand

Comparing the photochemistry of the polymer-anchored chromium tricarbonyl complexes with that of the $ArCr(CO)_3$ species one can see slight differences between the systems In the free chromium system there is only formation of the dicarbonyl solvent fragment as the primary photoproduct whereas in the polymer-bound species there is also a dicarbonyl polymer complex formed To prevent the formation of the dinuclear species the loading of styrene to chromium units on the backbone must be low (i e 100 1) There is very little difference between the reaction of the polymer-bound and free $ArCr(CO)_3$ complexes with pyridine, the rates are slightly lower but the activation parameters are the same

The results obtained for the photochemistry of these polymer systems proved difficult to reproduce because of particulate matter in the systems, therefore the general trends were recorded and discussed

4 4 References

1 C U Pittman, Jr , B T Kim, and W M Douglas, *J Org Chem*, **40**, 590, (1975)

2 R H Grubbs and L C Kroll, *J Amer Chem Soc* 93, 3062, (1971)

3 R H Grubbs, C Gibbons, L C Kroll, W D Bonds, Jr , and C H Brubaker, Jr , *J Amer Chem Soc*, 95, 2373, (1973)

4 For example see C U Pittman Jr in "Comprehensive Organometallic Chemistry", eds Wilkinson, Stone, and Abel, Pergamon Press, Oxford, Ch 55, 553, (1982)

5 (a) R.D Sanner, R G Austin, M S Wrighton, W D Honnick, and C U Pittman, Jr *Adv Chem Ser.*, **184**, 13 (1980)

(b) R.D Sanner R.G Austin, M S Wrighton, W D Honnick, and C U Pittman, Jr., *Inorg Chem.*, **18** 928 (1979)

(c) C U Pittman, Jr., W D Honnick, M S Wrighton, R D Sanner, and R G Austin in "Fundamental Research in Homogeneous Catalysis," ed M Tsutsui Plenum, New York, **3**, 603, (1979)

6 H Nagorashi, M J Mirbach and M F Mirbach, *J Organomet Chem.*, **297**, 171, (1985)

7 M.A. de Paoli, *J Macromol Sci Chem.*, **16** 152, (1981)

8 A.J Moffat, *J Catal.*, 18 193, (1970)

9 A.J Moffat, *J Catal.*, **19**, 322, (1970)

10 J Manassen, *Isr J Chem.*, **8**, 5 (1970)

11 M Capka, P Svoboda, M Corny, and J Hetflejs, *Tetrahedron Lett.*, 4787, (1971)

12 (a) C U Pittman, Jr., W D Honnick, and J J Yang, *J Org Chem* 45, 684, (1980)

(b) C U Pittman, Jr., and H Hirao, *J Org Chem.*, 43 640, (1978)

13 (a) D R Fahey, *J Org Chem.*, 38 80, (1973)

(b) D R Fahey, *J Org Chem.*, 38, 3343, (1973)

14 C U Pittman, Jr., L.R. Smith, and R.M Hanes, *J Amer Chem Soc.*, **97**, 1742, (1975)

15 C U Pittman, Jr and L R Smith *J Amer Chem Soc.*, **97** 1749, (1975)

16 C U Pittman, Jr and M D Rausch *Pure and Appl Chem.*, **58**, 617, (1986)

17 J Lyklema, *Chemistry and Industry*, 741, (1987)

18 C U Pittman, Jr and R F Felis, *J Organomet Chem.*, 72, 389, (1974)

19 G O Evans, C U Pittman, R McMillan, R.T Beach, and R Jones, *J Organomet Chem.*, **67**, 295, (1974)

20 D Tatarsky D H Kohn, and M Cais *J Polym Sci, Polym Chem Ed*, **18**, 1387 (1980)

21 (a) M D Rausch, G A Moser E J Zaiko, and A L Lipman Jr, *J Organomet Chem*, 23, 185, (1970)

(b) C U Pittman, Jr, P L Grube, O E Ayers, S D McManus, M D Rausch, and G.A. Moser, *J Polym Sci, Polym Chem Ed*, **10**, 379 (1972)

22 J M Kelly and C Long, *J Organomet Chem*, **235**, 315, (1982)

23 C U Pittman, Jr, "Organometallic Reactions and Synthesis", ed E I Becker and M Tsutsui Plenum, New York, **6**, 1, (1977)

24 C U Pittman, Jr and G V Marlin, *J Polym Sci, Polym Chem Ed*, **11**, 2753, (1973)

25 B S Creaven, Ph D Thesis, Dublin City University, (1989)

Chapter 5

Experimental Section

5 1 Materials

Methylcyclopentadienyl manganese tricarbonyl ((MeCp)Mn(CO)$_3$) supplied by Strem Chemicals, styrene supplied by Merck and 4-Vinylpyridine supplied by Riedel de Haen were distilled under reduced pressure and stored at -30^{o}C until required Methyl methacrylate supplied by Riedal de Haen, pyridine (gold label) obtained from Aldrich, benzene chromiun tricarbonyl (ArCr(CO)$_3$) and chromium hexacarbonyl supplied by Strem Chemicals were used without further purification Azoisobutyronitrile (AIBN) from Merck was recrystallised from anhydrous methanol and stored at 4^{o}C until required Chloroform used in casting films was reagent grade Anhydrous toluene (99%+) with a water content < 0 005% supplied by Aldnch was used in the laser flash photolysis expenments 1,2-Dimethoxyethane from Riedel-de Haen was refluxed and distilled from lithium aluminium hydride prior to use Argon, nitrogen, and carbon monoxide gases supplied by Insh Industnal Gases Ltd (IIG) were used without further purification

5 2 Equipment

Infrared spectra were recorded on a Perkin-Elmer 983G grating spectrometer with an internal polystyrene spectrum as calibration The instrument is fitted with presample chopping and so compensates for sample emission, important in variable temperature analysis Peak maxima are accurate to ± 3 cm^{-1}

A variable temperature infrared Specac model 2100 solids sample holder (Figure 5 2 1) in conjunction with a Specac model 20100 automatic temperature controller was used for low temperature infrared studies Liquid nitrogen was used as a coolant.

A Hewlett-Packard 8452A diode array spectrometer was used to record UV/visible spectra, peak positions are accurate to ± 2 nm For low temperature UV/visible studies the Specac sample holder was fitted with quartz windows (Figure 5 2 1)

Figure 5 2 1 Sample holder used for low temperature studies

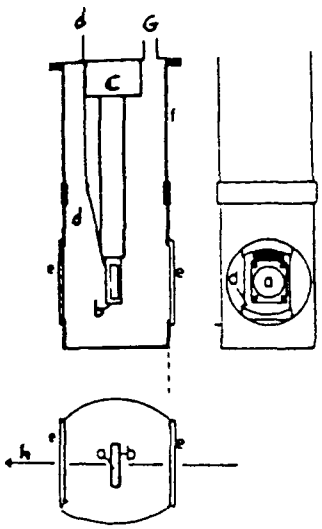

(a) sapphire disc
(b) disc support
(c) liquid nitrogen port
(d) thermocouple
(e) outer cell windows (NaCl)
(f) vacuum jacket
(g) to vacuum
(h) path of monitoring IR beam or photolysis beam

Thermogravimetric data was recorded using a Stanton Redcroft TG-750 instrument A platinum crucible was used All thermal analysis was carried out under a flowing nitrogen atmosphere (15 mLmin^{-1})

For centrifuging a Sorval RC-5B refrigerated superspeed centrifuge was used

An Oriel 100 W short arc high pressure mercury lamp was used for low temperature photolysis experiments

5 2 1 Laser Flash Photolysis

A schematic diagram of the flash photolysis instrumentation is given in Figure 5 2 2 The excitation source is a Q-switched Nd-YAG (neodymium doped yttrium aluminium garnet) laser (Spectron Laser Systems), which operates at 1064 nm but can be frequency doubled or tripled or quadrupled to generate a second, third, or fourth harmonic frequency at 532, 355, and 266 nm respectively The power of the laser pulse can be varied by applying different voltages across the amplifier flash tube At 355 nm, the power output was typically 30–40 mJ The pulse time varies from 5 to 10 ns The circular laser pulse (ca. 4 mm in diameter) is directed via two Pellin-Broca prisms onto the sample cuvette When the pulse passes through the power meter, situated after the second prism and before the sample holder, the oscilloscope is triggered The monitoring light source was an Applied Photophysics 40804, air cooled 275 watt xenon arc lamp arranged to be at right angles to the laser beam A UV filter (cut-off at 400 or 345 nm) was placed between the xenon arc lamp and the sample holder to prevent photolysis of the sample by the monitoring beam The output of the lamp is focussed on the front surface of the sample cuvette and the emerging beam is focussed through two circular lens onto the slit of an F/3 4 monochromator supplied by Applied photophysics The light detector was a Hamamatzu 5 stage photomultiplier which was operated at 850 volts The signal output was connected via a variable load resistor to the transient analyser, a Philips PM 3311 oscilloscope, later replaced by a Hewlett Packard 54510A model The oscilloscope is partially controlled by an Olivetti PCS 286 computer connected by an IEEE interface

A basic outline of the program which allows the kinetic traces to be recorded stored and analysed is given below

An experiment is one of monitoring absorbance changes Laser flash photolysis produces a transient species whose absorbance is recorded as a function of time Initially Io the amount of light being transmitted through the solution before the laser flash, is recorded This is achieved by recording the voltage corresponding to that light detected by the photomultiplier tube when the shutter is open, less the voltage generated by stray light I_0 is directly proportional to this voltage The laser is fired when the shutter is open Firing the laser triggers the oscilloscope Thus the resulting trace shows the change in voltage with time which corresponds to the change in optical density as species are formed or decay A typical trace is shown in Figure 5 2 3 The trace is then stored with the timebase and voltage settings of the oscilloscope This stored data can then be used to calculate I_t the amount of light being transmitted at any time t An absorbance spectrum of the transient species is obtained by recording transient signals at different monitoring wavelengths The absorbance readings can then be calculated at any time after the flash The oscilloscope is set at a delay to enable the absorbance (corresponding to the absorbance of the parent material at that wavelength) to be recorded before the laser pulse A transient difference spectrum is then obtained from a plot of absorbance versus wavelength

Printer
Transient
digitiser
Monochrom
P M
Computer
Sample
Plotter
Power supply
Pulsing
unit

Figure 5 2 2 Schematic diagram of the Laser Flash Photolysis system

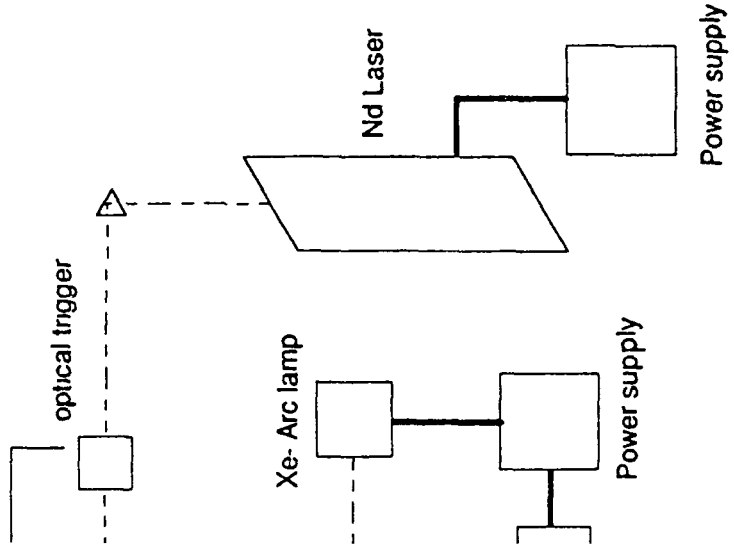

Figure 5 2 3 Typical traces recorded by the oscilloscope (a) shows the decay of one species and (b) shows the grow-in of a second species

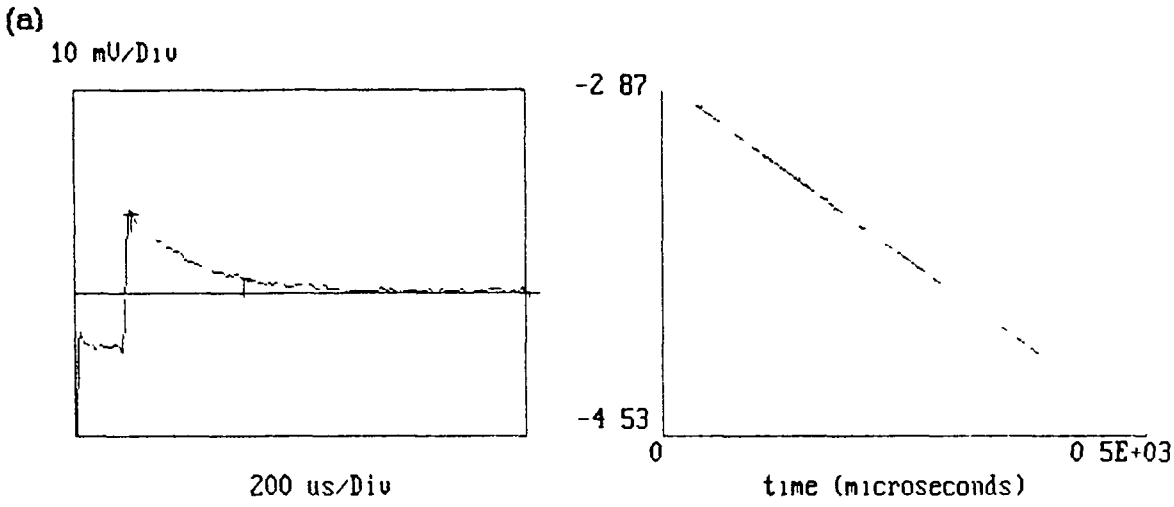

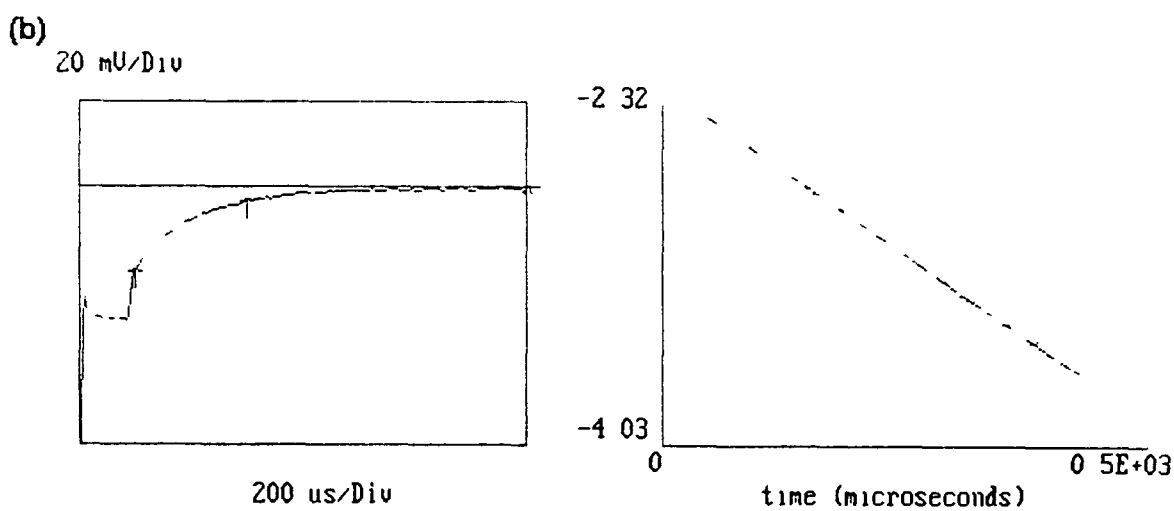

5 3 Procedures

5 3 1 Preparation of sample for laser flash photolysis experiments

Samples of $MeCpMn(CO)_3$, $ArCr(CO)_3$, $Cr(CO)_6$, and the polymer-bound $Cr(CO)_3$ in toluene for flash photolysis were prepared, so that the absorbance of the sample at the wavelength of excitation (355 nm) was between 0 6 and 1 0 absorbance units (AU) Samples were degassed by three cycles of a freeze-pump-thaw procedure followed by a liquid pumping phase in a specially designed degassing bulb attached to a fluorescence cell Argon or CO to a pressure of one atmosphere was then added depending on requirements The concentration of the carbonyl compound in solution can be determined from UV/vis absorption by utilising its known extinction coefficient at its wavelength of maximum absorption

For Arrhenius experiments, the sample cell was immersed in a thermostated water bath and allowed to equilibrate I_0 was measured at the monitoring wavelength and the system readied for analysis prior to the sample being heated so that the transient data could be recorded immediately on removing the cell from the water bath The sample was heated from room temperature to 50°C, a transient being recorded for analysis every 5°C

5 3 2 Synthesis of microcapsules

Outlined here is a general method for the synthesis of microcapsules The metal carbonyl was dissolved in an organic solvent (n-hexane) to form a dilute solution This solution was then mechanically dispersed in water to create an emulsion To this

emulsion a 10% solution of monomer, azoisobotyronitrile (AIBN), and surfactant (SDS) were added N_2 was bubbled through the reaction mixture, it was then heated to 80°C and maintained at that temperature until polymensation was complete (4 hrs) The product was centrifuged and then freeze dried

Formation of the microcapsules proved to be a very difficult and irreproducible process Despite using several different methods of adding the ingredients, different heating rates, and several initiators a reproducible and high yield could not be achieved

The best method for producing microcapsules is described here 2 mL of a 1 1 mixture of $MeCpMn(CO)_3$ (6 24 mmol) and n-Hexane was dispersed in 600 mL of Milli-Q H_2O using a mechanical stirrer The solution was degassed by purging with N_2 The temperature was increased to 80°C, 0 49 mmol of the monomer (methyl methacrylate), 1% AIBN and 0 05% surfactant (sodium dodecyl sulphate) were added The reaction mixture was kept at *ca* 80°C for 4 hours After polymensation was complete the solution was allowed to cool and then centrifuged at 9220g for 20 mins The pellet was washed in petroleum ether, to remove any $MeCpMn(CO)_3$ that was not encapsulated, and recentrifuged The residue was then freeze dried

5 3 2 1 Evidence for the existance of microcapsules

The characteristic tricarbonyl bands were present at 2011 and 1914 cm^{-1} in the infra red spectrum, bands for polymethylmethacrylate were also observed (band at 1721 cm^{-1} in Figure 5 3 1) Microscopic examination (mag 10x0 25) showed spherical shaped objects with debris attached to the side of the sphere Thermogravimetric analysis of the microcapsules revealed one clear weight transition This is a result of the breakdown of

the microcapsule and release of the metal carbonyl species compared to the TGA of the bulk polymer where this weight change is not present (Figure 5 3 2)

Figure 5 3 1 Infrared spectrum of the microcapsulated metal carbonyls

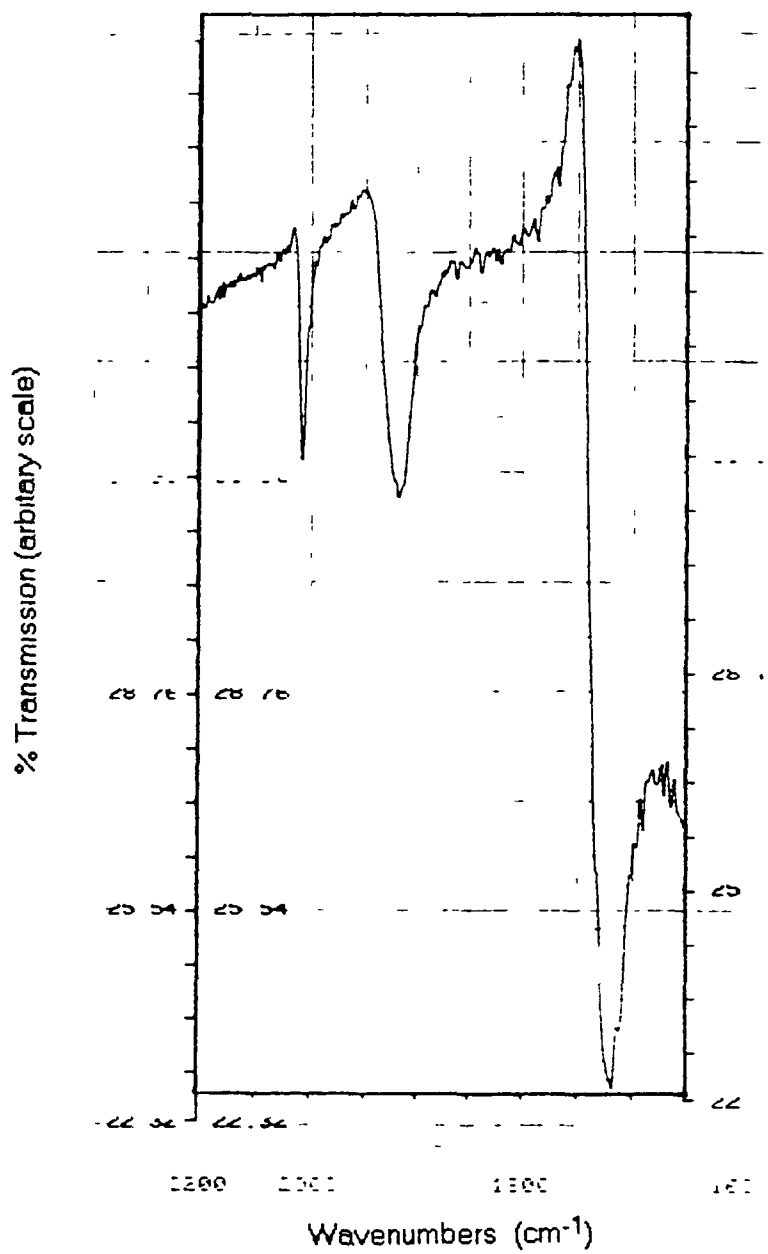

Figure 5 3 2 (a) TGA trace of microcapsulated metal carbonyl (b) TGA of polymethylmethacrylate Heating rate $5^{o}C\ min^{-1}$

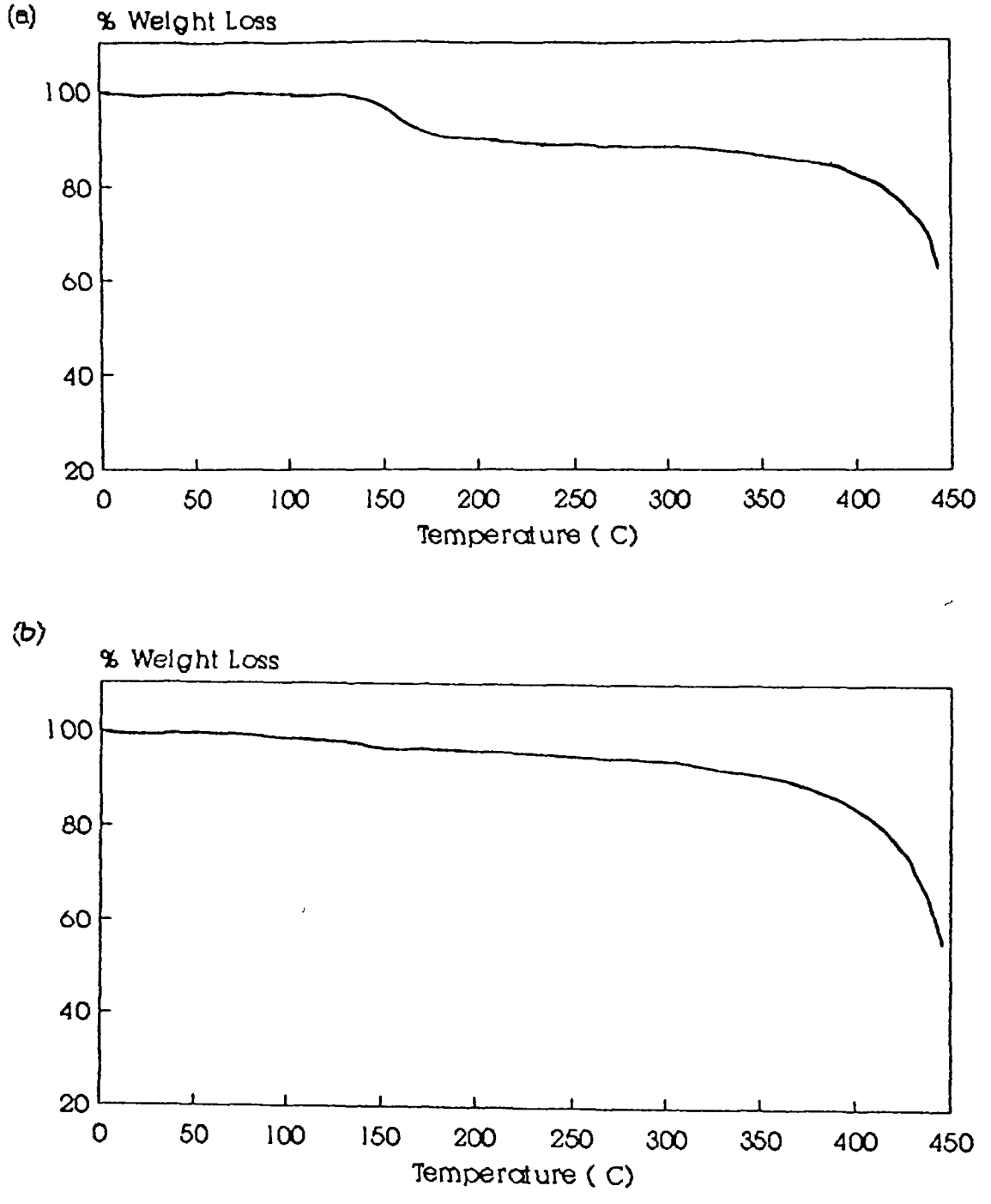

5 3 3 Casting of Films for Photolysis

(i) Films of the microcapsules were cast from a suspension of the microcapsule in n-Hexane The suspension was cast on a sapphire disk and the solvent was allowed to evaporate, leaving the microcapsules on the disk The disk was then photolysed at room temperature

(ii) The polymer films for low temperature photolysis were cast on a sapphire disk from a solution of the polymer and $MeCpMn(CO)_3$ or $ArCr(CO)_3$ (20 1 by weight) in chloroform The disk was allowed to dry overnight in the dark. Any remaining solvent was removed under reduced pressure Sapphire disks were used because of their robustness and resistance to thermal shock.

5 3 4 Synthesis of Polymers and Copolymers

Polystyrene and polymethylmethacrylate were prepared by free radical bulk polymerisation A mixture of the required monomer (styrene or methylmethacrylate) and initiator (AIBN) was purged for 20 mins with nitrogen gas The mixture was brought to 70-80^{o}C for 2hours with constant stirring until polymensation was complete The resulting glassy material was dissolved in the minimum volume of chloroform and precipitated into a large excess of petroleum ether The polymeric material was collected by filtration, washed with petroleum ether and dried under reduced pressure overnight Copolymers of styrene 4-vinylpyridine were prepared in the same manner except that different mole ratios of styrene to 4-vinylpyridine were added to the polymensation mixture These copolymers were prepared in 5 1, 10 1, 20 1, 30 1, and 40 1 mole ratios of styrene to 4-vinylpyridine The % nitrogen content was determined by microanalysis carried out by

UCD microanalytical laboratory. The % nitrogen for each polymer is listed in Table 5.3.1. From the microanalysis values the nitrogen content per gram of each polymer was determined.

Table 5.3.1: Nitrogen content of the various copolymers

Copolymer	% Nitrogen
5:1	2.29
10:1	1.09
20:1	0.85
30:1	0.42
40:1	0.31

5.3.5 Preparation of polystyrene-anchored chromium tricarbonyl

Polystyrene-anchored chromium tricarbonyl was prepared as described in the literature [1,2]. Polystyrene was refluxed in dimethoxyethane with $Cr(CO)_6$. After refluxing the mixture the solvent was removed under reduced pressure. The resulting green glassy type material was dissolved in the minimun amount of chloroform and precipitated into a large excess of petroleum ether.The olive coloured polymeric material was collected by filtration and dried under reduced pressure overnight. The polymer was characterised

by its infrared and UV/vis spectra (Figures 5 3 3 and 5 3 4) Terminal carbonyl stretching frequencies were found at 1975 and 1870 cm^{-1}, aromatic C-H stretch at 3019 cm^{-1} and aliphatic C-H stretch at 2919 cm^{-1}, the λ_{max} recorded in toluene was at 320 nm this is similiar to the unbound $ArCr(CO)_3$ complex in toluene

Figure 5 3 3 Infrared spectrum of the polystyrene-anchored chromium tricarbonyl complex

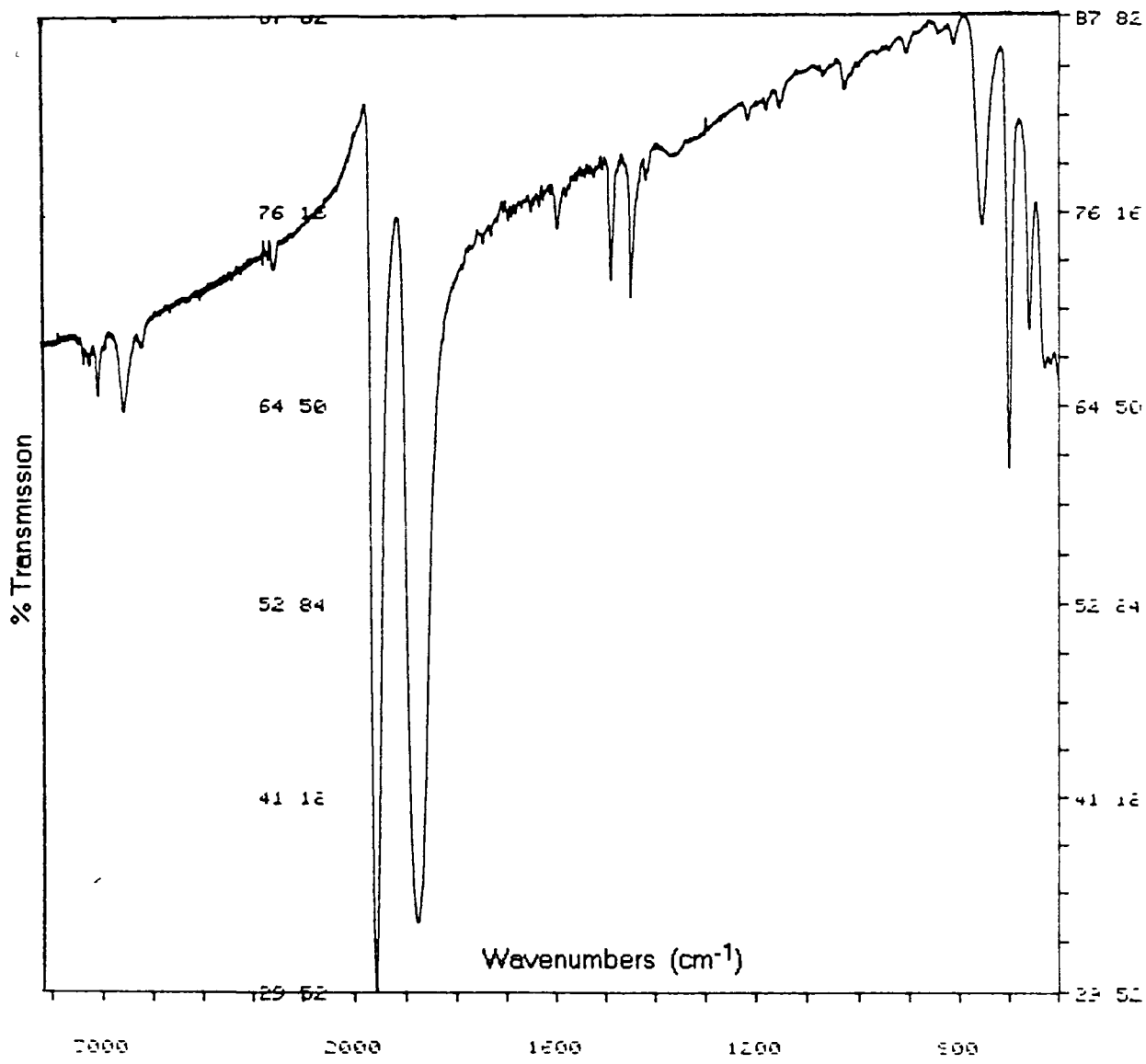

Figure 5 3 4 UV/vis spectrum of the polystyrene-anchored chromium tricarbonyl complex

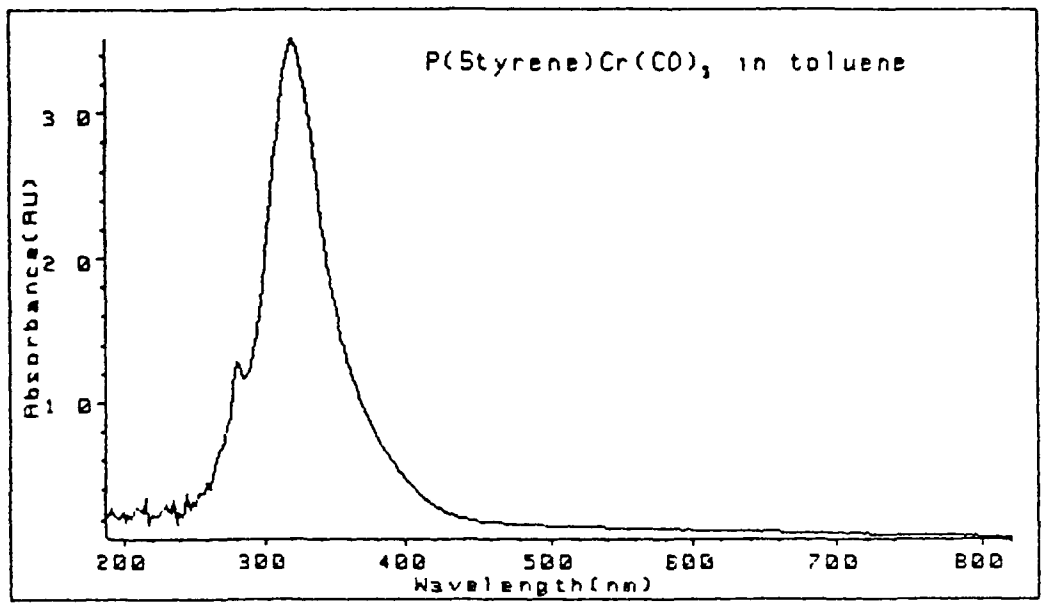

Different loadings of chromium tricarbonyl on the polymer backbone were achieved by changing the stoichiometry of the reaction mixture and the reflux time see Table 5 3 2

The amount of chromium tricarbonyl anchored on the polymer was determined from the extinction co-efficient of $ArCr(CO)_3$ A known amount of polymer was weighed out and dissolved in toluene the absorbance at 354 nm was read and from this the concentration of $ArCr(CO)_3$ present was determined Which can then be used to work out the loading of the $ArCr(CO)_3$ units on the polymer backbone

Table 5 3 2 Weights of reactants used in the preparation of various loadings of the polymer-anchored chromium tricarbonyl complex

Loading	Wgt. PS	Wgt $Cr(CO)_6$	Reflux time	Solvent
3 1	2g	2g	48 hrs	150 mls
6 1	2g	1g	36 hrs	150 mls
8 1	1g	0 25g	24 hrs	60 mls
100 1	2 5g	0 25g	24 hrs	100 mls

Solvent = dimethoxyethane

Loading = Loading of styrene to $ArCr(CO)_3$ units on the polymer backbone

5 3 6 Determination of solubility of CO in toluene

Solubility of CO in toluene at 25^0 expressed in mole fraction = $7\ 98 \times 10^{-4}$ [3]

1 Litre of toluene = 867g, 1 mole of toluene = 92 07g

=> 9 42 moles/Litre

$$\frac{\text{\# moles of CO}}{\text{\# moles of CO + \# moles of toluene}} = 7\ 98 \times 10^{-4}$$

$$\Rightarrow x = (7\ 98 \times 10^{-4})x + ((7\ 98 \times 10^{-4})(9\ 42)) \qquad \{x = \text{\# moles of CO}\}$$

$$\Rightarrow x = (7\ 98 \times 10^{-4})x + 7\ 52 \times 10^{-3}$$

$\Rightarrow (x - (7.98 \times 10^{-4})x) = 7.52 \times 10^{-3}$

$\Rightarrow x(1 - 7.98 \times 10^{-4}) = 7.52 \times 10^{-3}$

$$\Rightarrow x = \frac{7.52 \times 10^{-3}}{1 - 7.98 \times 10^{-4}}$$

$\Rightarrow x = 7.53 \times 10^{-3}$ moles of CO / Litre of toluene at 1 atms

5 3 7 Determination of extinction coefficients

5 3.7 1 Extinction coefficient of $MeCpMn(CO)_3$ in toluene at 354 nm

The extinction coefficient was determined from a plot of concentration of $MeCpMn(CO)_3$ versus optical density at 354 nm (Table 5 3 3 and Figure 5 3 5)

Table 5 3 3 and Figure 5 3 5 Experimental data for the determination of the extinction coefficient of $MeCpMn(CO)_3$ at 354 nm in toluene

---

$[MeCpMn(CO)_3]$	OD at 354 nm
0	0
$0\,5 \times 10^{-3}$ M	0 291 AU
$1\,0\,10^{-3}$ M	0 614 AU
$1\,5\,10^{-3}$ M	0 919 AU
$2\,0\,10^{-3}$ M	1 261 AU
$2\,5\,10^{-3}$ M	1 557 AU

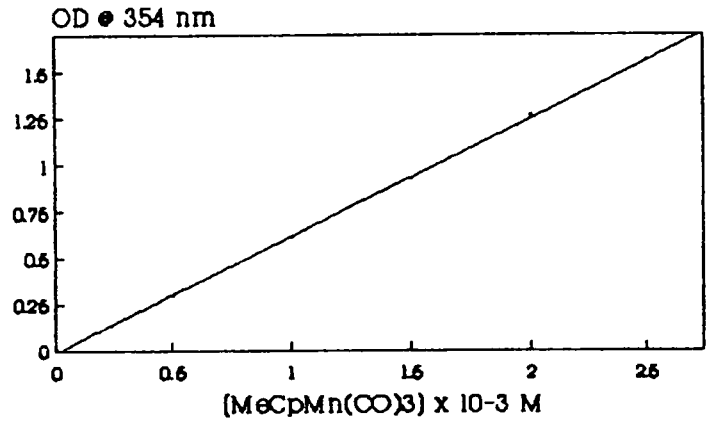

Slope = 628 54 ± 6 25 $dm^3mol^{-1}cm^{-1}$

Intercept = 0 01 ± 0 01

Correlation coefficient = 0 9998

---

5 3 7 2 Extinction coefficient of $ArCr(CO)_3$ at 354 nm in toluene

The experimental data for the determination of the extinction coefficient of $ArCr(CO)_3$ in toluene at 354 nm is given in Table 5 3 4 and Figure 5 3 6

Table 5 3 4 and Figure 5 3.6

$[ArCr(CO)_3]$	OD at 354 nm
0	0
3.0×10^{-4} M	0 867 AU
6.0×10^{-4} M	1 858 AU
$9.0\ 10^{-4}$ M	2 686 AU

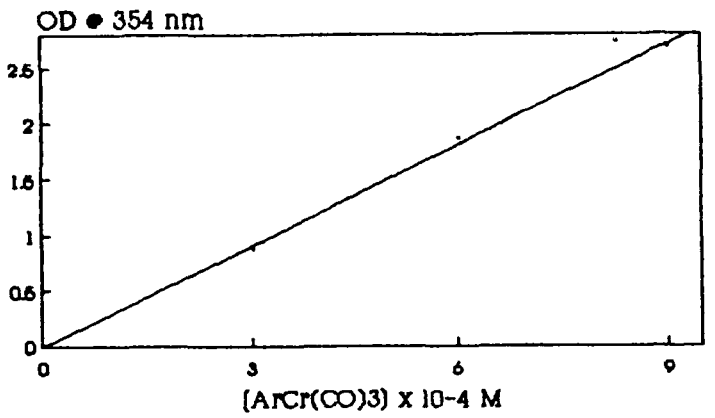

Slope = 3016 4 ± 70 81 $dm^3mol^{-1}cm^{-1}$

Intercept = -4 68 ± 0 05

Correlation coefficient = 0 99945

---

5 3 8 Determination of activation parameters

The activation parameters were calculated from the Arrhenius and Eyring equations [4]

The Arrhenius equation is given by

$$Lnk_{obs} = -E_{act}/(RT) + Ln(A)$$

T = Temperature in Kelvin

E_{act} = Activation energy in Jmol-1

R = Universal gas constant

A = Frequency factor

Therefore a plot of Ln k_{obs} versus 1/T should give a straight line of slope $-E_{act}/R$.

The Eyring equation is given by

$Ln(k_{obs}/T) = -(\Delta H^{\ddagger}/RT) + (\Delta S^{\ddagger}/R) + Ln(K/h)$

$\Delta H^{\ddagger}$ = enthalpy change of activation

$\Delta S^{\ddagger}$ = entropy change of activation

K = Boltzman constant

h = Planck constant

Therefore a plot of $Ln(k_{obs}/T)$ versus 1/T gives a slope of $-\Delta H^{\ddagger}/R$ and an intercept of $\Delta S^{\ddagger}/R + Ln(K/h)$

5 4 References

1 C U Pittman, Jr, B T Kim, and W M Douglas, *J Org Chem*, **40**, 590, (1975)

2 (a) M D Rausch, G.A. Moser, E J Zaiko, and A.L. Lipman, Jr, *J Organomet Chem*, 23, 185, (1970)

(b) C U Pittman, Jr, P L Grube, O E Ayers, S D McManus, M D Rausch, and G.A. Moser, *J Polym Sci, Polym Chem Ed*, 10, 379, (1972)

3 J C Gjaldbek, *Acta Chem Scand*, 6, 623, (1952)

4 (a) W J Moore, "Physical Chemistry", Longman, New York, (1978)

(b)H E Avery, "Basic Reaction Kinetics and Mechanisms", MacMillan, London, (1986)